VOLUME 81 JANUARY 27, 1977 NUMBER 2

JPCHAx

THE JOURNAL OF PHYSICAL CHEMISTRY

PUBLISHED BIWEEKLY BY THE AMERICAN CHEMICAL SOCIETY

THE JOURNAL OF

PHYSICAL CHEMISTRY

Published by the
AMERICAN CHEMICAL SOCIETY
BOOKS AND JOURNALS DIVISION

D. H. Michael Bowen, Director

Marjorie Laflin, Assistant to the Director

Editorial Department: Charles R. Bertsch, Head; Marianne C. Brogan, Associate Head; Celia B. McFarland, Joseph E. Yurvati, Assistant Editors

Magazine and Production Department: Bacil Guiley, Head

Research and Development Department: Seldon W. Terrant, Head

Advertising Office: Centcom, Ltd., 50 W. State St., Westport, Conn. 06880.

Published biweekly by the American Chemical Society at 20th and Northampton Sts., Easton, Pennsylvania 18042. Second class postage paid at Washington, D.C. and at additional mailing offices.

Editorial Information

Instructions for authors are printed in the first issue of each volume. Please conform to these instructions when submitting manuscripts.

Manuscripts for publication should be submitted to *The Journal of Physical Chemistry*, Department of Chemistry, University of Minnesota, Minneapolis, Minn. 55455. Correspondence regarding **accepted papers and proofs** should be directed to the Editorial Department at the ACS Easton address.

Page charges of $60.00 per page are assessed for papers published in this journal. Ability to pay does not affect acceptance or scheduling of papers.

Bulk reprints or photocopies of individual articles are available. For information write to Business Operations, Books and Journals Division at the ACS Washington address.

Requests for **permission to reprint** should be directed to Permissions, Books and Journals Division at the ACS Washington address. The American Chemical Society and its Editors assume no responsibility for the statements and opinions advanced by contributors.

Subscription and Business Information

1977 Subscription rates—including surface postage

	U.S.	PUAS	Canada, Foreign
Member	$24.00	$33.00	$34.00
Nonmember	96.00	105.00	106.00
Supplementary material	15.00	19.00	20.00

Air mail and air freight rates are available from Membership & Subscription Services, at the ACS Columbus address.

New and renewal subscriptions should be sent with payment to the Office of the Controller at the ACS Washington address. **Changes of address** must include both old and new addresses with ZIP code and a recent mailing label. Send all address changes to the ACS Columbus address. Please allow six weeks for change to become effective. **Claims for missing numbers** will not be allowed if loss was due to failure of notice of change of address to be received in the time specified; if claim is dated (a) North America—more than 90 days beyond issue date, (b) all other foreign—more than 1 year beyond issue date; or if the reason given is "missing from files". Hard copy claims are handled at the ACS Columbus address.

Microfiche subscriptions are available at the same rates but are mailed first class to U.S. subscribers, air mail to the rest of the world. Direct all inquiries to Special Issues Sales, at the ACS Washington address or call (202) 872-4554. **Single issues** in hard copy and/or microfiche are available from Special Issues Sales at the ACS Washington address. Current year $4.75. Back issue rates available from Special Issues Sales. **Back volumes** are available in hard copy and/or microform. Write to Special Issues Sales at the ACS Washington address for further information. **Microfilm** editions of ACS periodical publications are available from volume 1 to the present. For further information, contact Special Issues Sales at the ACS Washington address. **Supplementary material** mentioned in the journal appears in the microfilm edition. Single copies may be ordered directly from Business Operations, Books and Journals Division, at the ACS Washington address.

	U.S.	PUAS, Canada	Other Foreign
Microfiche	$2.50	$3.00	$3.50
Photocopy			
1–7 pages	4.00	5.50	7.00
8–20 pages	5.00	6.50	8.00

Orders over 20 pages are available only on microfiche, 4 × 6 in., 24X, negative, silver halide. Orders must state photocopy or microfiche if both are available. Full bibliographic citation including names of all authors and prepayment are required. Prices are subject to change.

American Chemical Society
1155 16th Street, N.W.
Washington, D.C. 20036
(202) 872-4600

Member & Subscription Services
American Chemical Society
P.O. Box 3337
Columbus, Ohio 43210
(614) 421-7230

Editorial Department
American Chemical Society
20th and Northampton Sts.
Easton, Pennsylvania 18042
(215) 258-9111

Notice to Authors last printed in the issue of January 13, 1977

THE JOURNAL OF

PHYSICAL CHEMISTRY

Volume 81, Number 2 January 27, 1977

JPCHAx 81(2) 93–186 (1977)

ISSN 0022-3654

p,p'-Di-n-heptyl

COMMUNICATIONS TO THE EDITOR

■ Supplementary and/or miniprint material for this paper is available separately (consult the masthead page for ordering information); it will also appear following the paper in the microfilm edition of this journal.

* In papers with more than one author, the asterisk indicates the name of the author to whom inquiries about the paper should be addressed.

AUTHOR INDEX

THE JOURNAL OF
PHYSICAL CHEMISTRY

VOLUME 81, NUMBER 2 JANUARY 27, 1977

Decay Kinetics of the Photochemical Hydrated Electron[1]

L. I. Grossweiner* and J. F. Baugher

Biophysics Laboratory, Department of Physics, Illinois Institute of Technology, Chicago, Illinois 60616 *(Received June 23, 1976)*

Publication costs assisted by the National Institutes of Health and the U.S. Energy Research and Development Administration

A model is proposed for the decay of hydrated electrons generated by photoionization of inorganic anions and aromatic solutes, in which the electron diffuses through a considerable volume of the medium before recombining with its radical coproduct, during which time it may react with scavengers or electrons and radicals generated in other geminate pairs. The analysis based on diffusional recombination theory leads to a new decay function in good agreement with electron decays observed by 265-nm laser flash photolysis of aqueous I^-, $Fe(CN)_6^{4-}$, tryptophan, and tyrosine. The dependence of the electron lifetimes on scavenger concentration and the initial electron concentration are in quantitative agreement with the theory, where the latter is developed in terms of a time-dependent rate constant to include the bimolecular electron–electron and electron–radical reactions. The recombination lifetimes are $\sim 10^4$ times longer than predicted by the Noyes recombination theory and comparable to those deduced in the earlier photochemical scavenging experiments of Stein and co-workers. It is proposed that the initial separation of the hydrated electron and radical supresses fast "Noyes type" recombination and permits the electron to enter a regime in which diffusion-limited back reactions with the original radical remain probable in the absence of high scavenger concentrations.

Introduction

The generation of hydrated electrons by ultraviolet flash photolysis of inorganic anions and aromatic molecules in aqueous solution was demonstrated many years ago.[2-4] The hydrated electron was identified by its characteristic red absorption band, the quenching action of electrophilic agents such as O_2 and N_2O, and the observation of appropriate counterradical spectra, e.g., I_2^- from I^-[5] and the phenoxyl radical from phenol.[6] The detailed analysis of the electron decay kinetics was not feasible in this early work because the flash lamp durations were comparable to the electron lifetimes. However, it was assumed that the reactions of the photochemical hydrated electron are similar to the radiolysis hydrated electron, i.e., competition between the bimolecular ($e_{aq}^- + e_{aq}^-$) reaction and the pseudo-first-order reactions with available scavengers including the original photolyte. In addition, bimolecular back reactions are possible between the electron and its radical coproduct which would not be easily separated from ($e_{aq}^- + e_{aq}^-$). The tacit assumption that the reactions of the "long time" photochemical electron are identical with the hydrated electron generated by water radiolysis was questioned in recent work of Bryant et al.[7] where it was observed that electrons generated by 265-nm laser photolysis of inorganic anions and aromatic amino acids decay faster than can be explained by the ($e_{aq}^- + e_{aq}^-$) and scavenger reactions in the bulk. It was proposed that the hydrated electron and its radical coproduct form a loosely bound complex of ~ 1 μs duration in which the back reaction competes with separation into the free species. The "loose complex" model is consistent with the significant loss of electrons during the time period from about 50 ns to 1 μs, the approximately exponential time dependence during the initial decay stage, the comparable activation energy for the observed decay rate with that for "inverse viscosity" of water, and the similarity of the initial and "long time" electron absorption spectra.

Prior to these flash photolysis studies, Stein and his colleagues proposed that hydrated electrons are generated from aqueous I^-[8-10] and phenolate[11] ions based on steady

irradiation quantum yields in the presence of electron scavengers. The quantum yield of electron scavenging was found to obey the square-root concentration dependence predicted by the Noyes theory of diffusive recombination,[12-14] in which the geminate coproducts escaping primary recombination undergo secondary diffusive recombination in competition with scavenging in the "cage" and diffusive separation into the bulk. According to Noyes, the efficiency of scavenger action is given by

$$\int_0^\infty h(t')[1 - e^{-k_s(S)t'}]\,dt'$$

where $h(t)$ is the probability (per s) that a radical pair generated at $t = 0$ (or interacting at $t = 0$ without reaction) recombines at time t, k_s is the bimolecular rate constant for the scavenging reaction, and (S) is the bulk scavenger concentration. The choice of $h(t)$ based on the random walk of a particle in three dimensions:

$$h(t) = (a/t^{3/2})e^{-\pi a^2/\beta'^2 t} \tag{1}$$

leads to the approximate solution

$$\gamma = \gamma_r + 2a\Gamma[\pi k_s(S)]^{1/2} \tag{2}$$

where γ is the total quantum yield for electron scavenging, γ_r is the "residual yield" for the scavenging of electrons that escape recombination at low scavenger concentrations, and Γ is the quantum yield for generation of the geminate radicals. The parameter β' is the total probability for recombination of the geminate pair

$$\beta' = \int_0^\infty h(t')\,dt' \tag{3}$$

and is related to the photochemical quantum yields by: $\beta' = 1 - \gamma_r/\Gamma$. Jortner et al.[8] obtained the exact solution of (1):

$$\gamma = \Gamma[1 - \beta' e^{-(2a/\beta')[\pi k_s(S)]^{1/2}}] \tag{4}$$

which reduces to (2) at low scavenger concentrations.

The functional dependence predicted by (2) or (4) was found for various photolytes (I^-, Br^-, $Fe(CN)_6^{4-}$, phenolate) in the presence of electron scavengers (H^+, N_2O, O_2, $H_2PO_4^-$, acetone) with approximately correct relative values of k_s from system to system.[8-11,15-17] However, the parameter $2a(\pi k_s)^{1/2}$ ranges from 2 to 60 $M^{-1/2}$, which is much too large to be consistent with the Noyes theory of diffusive displacements.[18] These results imply values of $a \simeq 10^{-4}$ $s^{1/2}$ and "cage" lifetimes $\sim 10^{-6}$ s, while the Noyes theory leads to $a < 10^{-6}$ and lifetimes $<10^{-10}$ s. Nevertheless, there has been no apparent explanation for the discrepancy excluding the total inapplicability of the diffusive recombination theory. Dainton and Logan[19] proposed an alternative mechanism in which the rapid reaction of the photoelectron with a scavenger may not permit adequate time for the formation of the ionic atmosphere of the electron, leading to a decreased rate constant for scavenging by charged solutes at high solute concentrations. However, this model does not explain the concentration dependence of scavenging quantum yields observed by Stein and co-workers.

Electron Decay Theory

The photochemical scavenging studies and laser flash photolysis measurements provide different probes of the same photochemical process; i.e., competition between the fast back reaction of the electron with its radical coproduct and the bimolecular reactions of the electron with an initially randomly dispersed, scavenging solute. Accordingly, the probability that an electron survives both decay process from $t = 0$ to $t = t$ is given by

$$p(t) = e^{-k_s(S)t}[1 - \int_0^t h(t')\,dt'] \tag{5}$$

We proceed formally by substituting $h(t)$ of (1) leading to the decay function

$$p(t) = e^{-k_s(S)t}[1 - \beta' \text{ erfc } (a/\beta')(\pi/t)^{1/2}] \tag{6}$$

where erfc $x = (2/\pi^{1/2}) \int_x^\infty e^{-x^2}\,dx$. The expansion: erfc $x = 1 - (2x/\pi^{1/2})[1 - x^2/3 + x^4/10 - ...]$ leads to an approximate form of (6) valid for $t >> \pi a^2/\beta'^2$:

$$p(t) \simeq e^{-k_s(S)t}[1 - \beta' + 2a/t^{1/2}] \tag{7}$$

These equations predict that the electron decay function is the product of the exponential rate as determined by reactions with scavenger S (which may be the photolyte) modulated by a scavenger-independent term related to the diffusive recombination of the geminate pair. Although the decay predicted by (6) is nonexponential, the mean electron lifetime can be defined as

$$\bar{t} = \int_0^\infty t\,dp / \int_0^\infty dp \tag{8}$$

The integrations in (8) are easily carried out using (1), (5), and the approximation of (7) for the $[1 - \int_0^t h(t')\,dt']$ term in dp leading to

$$\bar{t} = \frac{a[\pi/k_s(S)]^{1/2}[1 + e^{-(2a/\beta')[\pi k_s(S)]^{1/2}}] + (1 - \beta')/k_s(S)}{2a[\pi k_s(S)]^{1/2} + \beta' e^{-(2a/\beta')[\pi k_s(S)]^{1/2}} + (1 - \beta')}$$

[Formally, each of the 6 integrals in (8) is a Laplace transform L_p with $p = k_s(S)$.] In comparing the predicted dependence of $\bar{t}$ on (S) with experimental data it is convenient to use the reciprocal form:

$$1/\bar{t} = k_s(S) \times \frac{\beta' e^{-(2a/\beta')[\pi k_s(S)]^{1/2}} + 2a[\pi k(S)]^{1/2} + (1 - \beta')}{a[\pi k_s(S)]^{1/2}[1 + e^{-(2a/\beta')[\pi k_s(S)]^{1/2}}] + (1 - \beta')} \tag{9}$$

The probability that a geminate pair eventually recombines is also of interest. Since $(\gamma - \gamma_r)/\Gamma$ is the probability for scavenging and γ_r/Γ is the probability that the electron escapes both recombination and scavenging, the recombination p_r follows from (4) as

$$p_r = \beta' e^{-2(a/\beta')[\pi k_s(S)]^{1/2}} \tag{10}$$

Alternatively, the same result can be calculated directly from

$$p_r = \int_0^\infty h(t) e^{-k_s(S)t}\,dt$$

The attempt to calculate $\bar{t}$ in the absence of scavengers by substituting (1) in (8) leads to a divergent integral. This result is not surprising because $h(t)$ is based on random walk in three dimensions, in which there is a finite probability that two particles executing independent steps will never meet.[20] Nevertheless, the mean electron lifetime in the absence of scavengers can be estimated as the time required for $h(t)$ to fall from the maximum value $h(t^*)$ to $h(t^*)/e \equiv h(t')$. Direct differentiation of (1) leads to

$$t^* = (2\pi/3)(a/\beta')^2$$
$$t' \simeq 9.18(a/\beta')^2 \tag{11}$$

For example, if a/β' equals 10^{-6}, 10^{-5}, or 10^{-4} $s^{1/2}$, the corresponding electron lifetimes are 10^{-11}, 10^{-9}, and 10^{-7} s, respectively. Alternatively, the mean lifetime may be defined as the time required for the integrated probability of recombination to attain half the maximum value. Taking $\int_0^{t'} h(t)\,dt = \beta'/2$ gives

$$t'' \simeq 13.8(a/\beta')^2 \quad (12)$$

The electron decay function (5) can be related to a time-dependent scavenging rate constant k_t by differentiation:

$$\frac{dp}{dt} = -\left[k_s(S) + \frac{h(t)}{1 - \int_0^t h(t')\,dt'}\right] p(t)$$

i.e.

$$k_t \simeq k_s(S) + \frac{h(t)}{1 - \int_0^t h(t')\,dt'} \quad (13)$$

For the case where $t \gg \pi a^2/\beta'^2$:

$$k_t \simeq k_s(S) + \frac{1}{2t + (t^{3/2}/a)(1 - \beta')} \quad (14)$$

The integrated solution (6) is preferable to (14) because it can be compared directly to experimental data over the full decay period. However, the neglect of reactions between electrons generated in different pairs cannot be strictly correct. The bimolecular contribution to electron decay may be estimated for the case of high recombination probability by substituting the binomial expansion of (14) into the differential rate equation:

$$-d(e_{aq}^-)/dt = k_t(e_{aq}^-) + k'(e_{aq}^-)^2 \quad (15)$$

leading to the integrated solution for the case where $\gamma \equiv (1 - \beta')/2a \ll t^{1/2}$:

$$(e_{aq}^-)/(e_{aq}^-)_0 = \left\{(t_0/t)^{1/2} e^{-k_s(S)t + \gamma t^{1/2}}\right\} / \left\{ e^{-k_s(S)t_0 + \gamma t_0^{1/2}} + k'(e_{aq}^-)_0 e^{\gamma^2/4k_s(S)} \times [\pi t_0/k_s(S)]^{1/2}[\mathrm{erf}\, x - \mathrm{erf}\, x_0]\right\} \quad (16)$$

where $x \equiv [k_s(S)t]^{1/2} - \gamma/[4k_s(S)]^{1/2}$ and t_0 is an arbitrary starting time corresponding to $(e_{aq}^-)_0$. A reduced form of (16) for low scavenger concentrations and high recombination probability is:

$$(e_{aq}^-)/(e_{aq}^-)_0 = \frac{(t_0/t)^{1/2}}{1 + 2k'(e_{aq}^-)_0 t_0[(t/t_0)^{1/2} - 1]} \quad (17)$$

which predicts the dependence of the decay halftime on $(e_{aq}^-)_0$ as

$$k'(e_{aq}^-)_0 t_{1/2} + [1/(4t_0)^{1/2} - k'(e_{aq}^-)_0 t_0^{1/2}] t_{1/2}^{1/2} = 1 \quad (18)$$

Comparing (17) with (7) for low initial electron yields indicates $t_0 \simeq 4a^2$, consistent with $\int_{t_0}^{\infty} a/t^{3/2}\,dt = 1$. Although (17) is not applicable for the initial decay period where $t \lesssim t_0$, it has the merit of predicting a weak dependence on $t_{1/2}$ on the initial electron yield in agreement with experimental results (see below).

Comparison of Theory and Experiment

The electron decay curves were obtained by laser photolysis of various solutes at 265 nm with photoelectric monitoring of the absorption at 650 nm, following the general procedures of Bryant et al.[7] and Baugher and Grossweiner.[21] The initial electron yields were kept below 10 μM to minimize the bimolecular $(e_{aq}^- + e_{aq}^-)$ reaction with $k' = 1.1 \times 10^{10}$ M^{-1} s^{-1}.[22] In addition, the photolysis yield was kept as low as feasible for reliable data, typically 1–3% of the initial solute. The applicability of (6) was determined by taking $p(t) = (e_{aq}^-)/(e_{aq}^-)_0$ where $(e_{aq}^-)_0$ is the extrapolated electron yield immediately after the 17-ns laser flash. The analysis was carried out by taking the literature value of k_s and dividing the experimental values of $p(t)$ by $e^{k_s(S)t}$ in order to obtain $[1 - \beta'\,\mathrm{erfc}\,(a/\beta')(\pi/t)^{1/2}]$ at each point. The initial fit was made by taking $\beta' = 1$ leading to a value of a at each point. The predicted decay curve was determined using the average value $\bar{a}$. The sensitivity of $p(t)$ to $\bar{a}$ is indicated in Figure 1 in which the experimental points were obtained with 330 μM tryptophan (aq). The agreement is quite good for $\bar{a} = 2.5 \times 10^{-4}$ $s^{1/2}$ from 50 ns to about 2 μs, after which the electron decays more rapidly than predicted. The initial electron yield was 6 μM in this case, so that the expected decay halftime from $(e_{aq}^- + e_{aq}^-)$ or $(e_{aq}^-$ + radical) reactions coupled with the pseudo-first-order reaction of the electron with tryptophan based on $k_s = 3.6 \times 10^8$ M^{-1} s^{-1} [22] is approximately 4 μs. In contrast, the observed decay halftime is 1 μs, in agreement with (6) for the selected values of β' and $\bar{a}$.

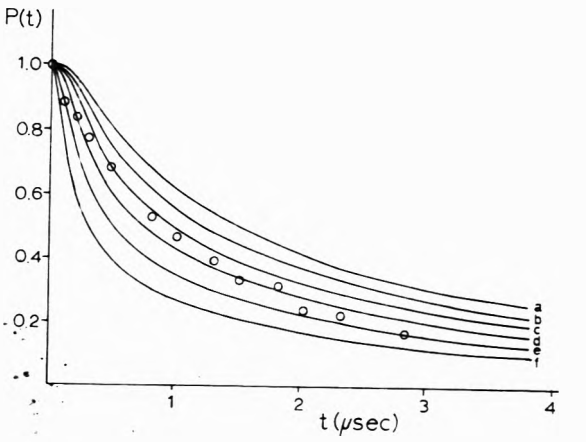

Figure 1. Comparison of eq 6 with electron decay after 265-nm laser photolysis of aqueous 330 μM tryptophan. The lines are calculated for $\beta' = 1$, $k_s = 3.6 \times 10^8$, and for following values of $\bar{a}$: (a) 4×10^{-4}; (b) 3.5×10^{-4}; (c) 3.0×10^{-4}; (d) 2.5×10^{-4}; (e) 2.0×10^{-4}; (f) 1.5×10^{-4}.

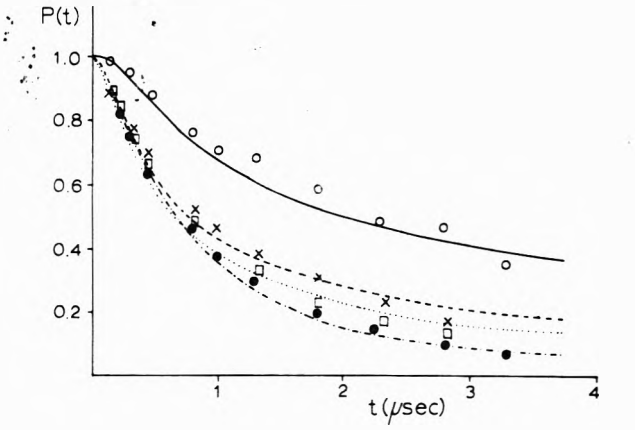

Figure 2. Comparison of eq 6 with electron decay after 265-nm laser photolysis of aqueous tryptophan at different initial concentrations: (O) 71 μM; (×) 330 μM; (□) 568 μM; (●) 1500 μM. The $\bar{a}$ values are in Table I.

Results obtained with other tryptophan concentrations from 0.07 to 1.5 mM are shown in Figure 2. The "best fit" value of $\bar{a}$ is $3.0 \pm 0.5 \times 10^{-4}$ based on $\beta' = 1$. A further test of the theory was made by comparing (9) with the observed dependence of $\bar{t}$ on tryptophan concentration. The experimental value of $\bar{t}$ was taken as $t_{1/2}/0.693$ which corresponds to the decay time constant for a purely first-order process. The results are plotted in Figure 3 as $1/\bar{t}$ vs. $(S)^{1/2}$ where the solid line is the theoretical prediction based on $\bar{a} = 3.0 \times 10^{-4}$ and $k_s = 3.6 \times 10^8$. The

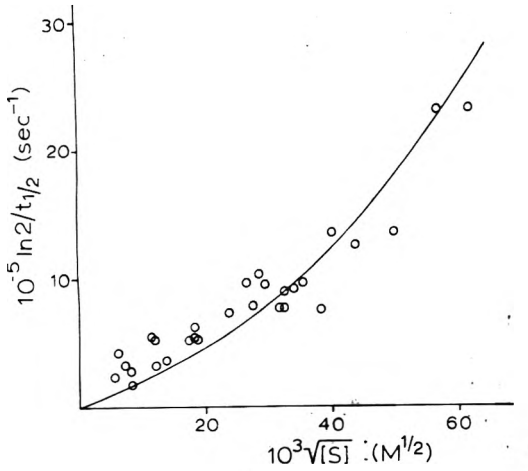

Figure 3. Dependence of experimental electron decay lifetimes on square-root tryptophan concentration. The solid line is based on eq 9 for $\beta' = 1$, $k_s = 3.6 \times 10^8$, and $\bar{a} = 3.0 \times 10^{-4}$.

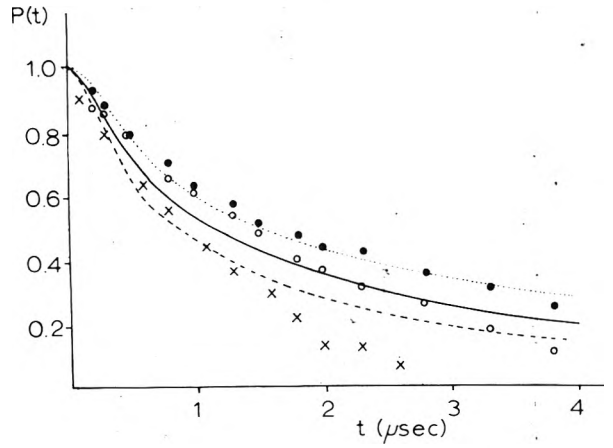

Figure 4. Comparison of eq 6 with electron decay after 265-nm laser photolysis of: 350 μM tryptophan at pH 10.9 (●, dotted line); 1560 μM aqueous tyrosine (×, dashed line); 1300 μM tyrosine at pH 11.0 (○, solid line). The lines are calculated with eq 6 using $\bar{a}$ values in Table I.

agreement is considered as quite good in view of the fact that no arbitrary fitting parameters were used and a wide range of tryptophan concentrations was employed. It is interesting to note that the parameter $(2a/\beta')(\pi k_s)^{1/2}$ for this case is $\sim$20 M$^{-1/2}$ comparable to the magnitudes obtained with the photochemical scavenging technique and external scavengers.

The selection of $\beta' = 1$ requires justification. In terms of steady irradiation quantum yields: $\beta' = 1 - \gamma_r/\Gamma$, where Γ was determined as 0.10 for aqueous tryptophan by laser flash photolysis.[21] (The higher values of 0.25 reported in ref 7 were shown to be due to the saturation of the $Fe(CN)_6^{4-}$ actinometer at the high laser intensities employed.[21] Lachish et al.[23] confirm that photoionization of $Fe(CN)_6^{4-}$ is monophotonic, but propose a biphotonic photoionization process for aqueous tryptophan, in disagreement with Bent and Hayon[24] and ref 21.) Taking $\gamma_r = 0.0003$ based on 280-nm irradiation of air-free tryptophan at pH 4.5[25] gives $\beta' = 0.997$. Several other runs with aromatic solutes are shown in Figure 4 applicable for different values of k_s: 350 μM tryptophan at pH 10.9 ($k_s = 1.3 \times 10^8$); 1560 μM aqueous tyrosine ($k_s = 1.6 \times 10^8$); 1300 μM tyrosine at pH 11.0 ($k_s = 9.6 \times 10^7$). In each case good agreement with (6) obtains with $\bar{a} = (3.4 - 4.1) \times 10^{-4}$ and $\beta' = 1$. As shown below, the fitting procedure is not sensitive to β' to the extent that smaller β' values are compensated by higher values of a. The results for $\beta' = 1$ are summarized in Table I.

TABLE I: Summary of Electron Decay Results

Photolyte	pH	$(e_{aq}^-)_0$, μM	$10^4\bar{a}$,[a] s$^{1/2}$
71 μM tryptophan	Aq	2.8	4.1
132 μM tryptophan	Aq	4.7	2.8
330 μM tryptophan	Aq	6.4	2.5
568 μM tryptophan	Aq	7.9	2.5
1500 μM tryptophan	Aq	7.1	3.4
350 μM tryptophan	10.9	5.8	3.5
1560 μM tyrosine	Aq	3.2	4.1
1300 μM tyrosine	11.0	10.7	3.4
0.2 M I^-	Aq	11.3	4.2
660 μM $Fe(CN)_6^{4-}$	Aq	7.4	5.8

[a] Based on eq 6 with $\beta' = 1$.

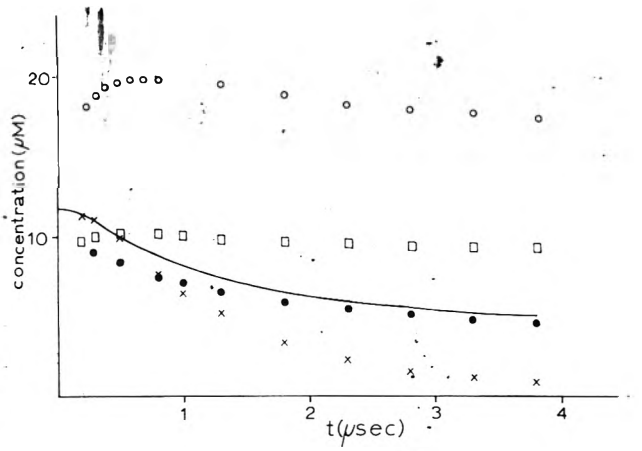

Figure 5. Electron and I_2^- decay after 265-nm laser photolysis of 0.2 M aqueous I^-: (●) I_2^-, N_2 saturated; (□) I_2^-, O_2 saturated; (○) I_2^-, N_2O saturated; (×) e_{aq}^-, N_2 saturated. The line is calculated with eq 6 for $\beta' = 1$ and $\bar{a} = 4.2 \times 10^{-4}$.

Photoionization of aqueous I^- presents an interesting contrast to the aromatic solutes because the electron is essentially nonreactive toward the photolyte with $k(e_{aq}^- + I^-) < 2.5 \times 10^5$ M^{-1} s^{-1}.[26] It has been shown that the long-lived I_2^- radical (λ_{max} 380–385 nm) is generated by flash photolysis of aqueous I^-[27] and I^- in ethanol.[28,29] Typical laser photolysis data for 0.2 M I^- (aq) in Figure 5 show that the electron and I_2^- radical decay together during the initial decay stage in N_2 saturated solution. [The I_2^- decay has been corrected for the overlapping e_{aq}^- absorption based on ϵ_{I_2} (380 nm) = 1.4×10^4 M^{-1} cm^{-1}[27,30] and $\epsilon_{e_{aq}^-}$ (380 nm) = 1.7×10^3 M^{-1} cm^{-1}.[31]] The long lifetime of I_2^- under O_2 saturation is a consequence of the suppression of recombination by electron scavenging. The I_2^- yield doubles in N_2O-saturated solutions because of the fast reactions: $e_{aq}^- + N_2O + H^+ \rightarrow N_2 + OH\cdot$; $OH\cdot + I^- \rightarrow I + OH^-$; $I + I^- \rightleftharpoons I_2^-$, where the I_2^- equilibrium constant of 1.2×10^4 M^{-1}[27] ensures that all I atoms are converted to I_2^- within 10^{-9} s. The calculated electron decay curve based on (6) with $\bar{a} = 4.3 \times 10^{-4}$ and $\beta' = 1$ fits only the initial decay stage because of competition from $(e_{aq}^- + e_{aq}^-)$ at the high initial electron yield.

The electron decay observed after laser photolysis of 0.66 M $Fe(CN)_6^{4-}$ in Figure 6 is in good agreement with (6). This case provides a good test of (18) for predicting the dependence of the decay half-time on $(e_{aq}^-)_0$ since $k[e_{aq}^- + Fe(CN)_6^{4-}] < 10^5$.[22] The data up to moderately high $(e_{aq}^-)_0$ in Figure 7 are in good agreement with (18) for $t_0 = 0.75$ μs. The discrepancy at very high $(e_{aq}^-)_0$ probably results from the short electron lifetimes which invalidate the approximations employed to simplify (16). This value of t_0 was selected to fit at $(e_{aq}^-)_0 = 0$ and leads to $a = 4.3 \times 10^{-4}$ based on $t_0 = 4a^2$, compared with $\bar{a} = 5.8 \times 10^{-4}$ from the decay function. In the case of tryptophan

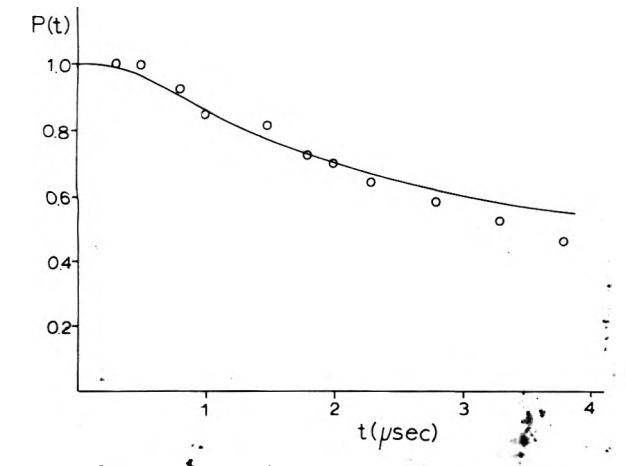

Figure 6. Comparison of eq 6 with electron decay after 265-nm laser photolysis of aqueous 0.66 M $K_4Fe(CN)_6^{4-}$. The line is calculated for $\beta' = 1$ and $\bar{a} = 5.8 \times 10^{-4}$.

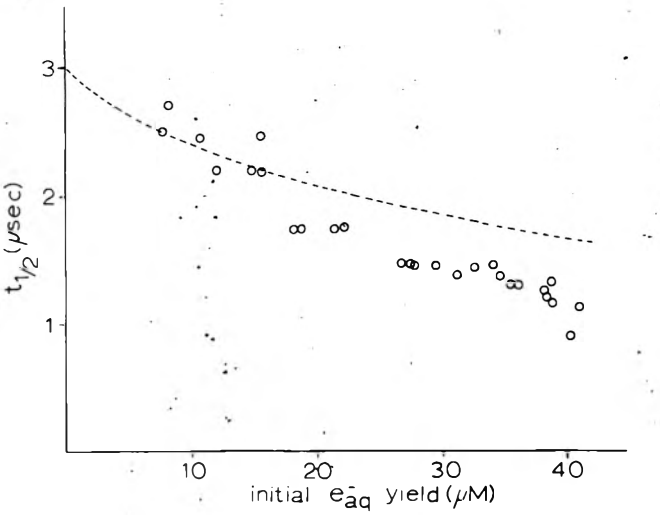

Figure 7. Dependence of experimental electron decay half-time on initial electron yield from 0.66 M $Fe(CN)_6^{4-}$. The dashed line is based on eq 18 for $\beta' = 1$ and $t_0 = 0.75$ μs.

photolysis, recent work[21] has shown that (17) is in satisfactory agreement with the electron decay lifetimes at high initial yields and low solute concentrations and that (18) predicts the dependence of the decay lifetime on initial (e_{aq}^-) for those conditions.

The $\bar{a}$ values have been calculated in this work for $\beta' = 1$, although the reported scavenging quantum yields lead to lower values varying with the excitation wavelength. However, the shape of $p(t)$ is not sensitive to the value of β' with an appropriate change of a. The exact relationship for equivalence depends on the decay time according to

$$a(\beta' = 1) = (a/\beta')(k/\pi)^{1/2} \operatorname{erfc}^{-1} [\beta' \operatorname{erfc} (\pi/k)^{1/2}]$$

where the time is expressed in the reduced units: $t \equiv (a/\beta')^2 k$. It is found by direct numerical calculation that the value of $a(\beta' = 1)$ is approximately constant for the time range of interest ($2 < k < 10$) for $0.2 < \beta' < 1$. An empirical relationship accurate to 10% for this range of parameters is

$$a(\beta' = 1) \simeq a/\beta'^{3/2} \qquad (19)$$

The early scavenging results led to $\beta' = 0.75$ and $a = 1.2 \times 10^{-4}$ for I^- photolysis at 254 nm in the presence of N_2O.[9] The application of (19) gives $\bar{a}(\beta' = 1) \simeq 2 \times 10^{-4}$ which is somewhat lower than deduced from the electron decay data in Figure 5. Similarly, steady state photolysis of phenolate anion at 254 nm in the presence of N_2O and 1 M CH_3OH to scavenge OH radicals gave $\beta' = 0.38$ and $a = 1.5 \times 10^{-4}$ corresponding to $a(\beta' = 1) \simeq 6 \times 10^{-4}$.[11] In the case of tyrosinate at pH 11 the decay curves in Figure 3 lead to $\bar{a} = 3.5 \times 10^{-4}$. It should be noted that the a values derived from scavenging experiments based on (2) or (4) may reflect experimental errors in the determination of β'. Nevertheless, the agreement between the two types of experiments is sufficiently good to demonstrate that the present theory is consistent with the earlier work.

Discussion

The comparison of experimental results with the theory in Figures 1–7 provides good evidence for the validity of (5) as the correct decay function for hydrated electrons generated by photolysis of inorganic anions and aromatic molecules. While this equation does not describe a specific physical model, the agreement strongly suggests that the electron migrates a considerable distance from the radical prior to recombination, during which time it is free to react with accessible scavengers. This picture differs from the usual interpretation of diffusional reactions where it is assumed that a separation of about 10 Å leads to a negligible probability for recombination. The significantly larger displacements and longer recombination lifetimes deduced from both the present data and the earlier photochemical scavenging experiments are not compatible with the original Noyes theory. However, $h(t)$ may be considered as a semiempirical diffusion function in which the parameter a is not related directly to the microscopic models of Noyes.[13,14]

In contrast to photochemical bond splitting reactions in the gas phase, it appears likely that the initial displacement of the electron from the radical is sufficiently large that "Noyes type" recombination within 10^{-10} s is inefficient. Dainton and Logan[19] estimate ~10 Å for I^- photolysis. Furthermore, the observation of the "long time" radical spectra within 10^{-8} s after laser photolysis with both aromatic solutes[7,21] and inorganic anions (this work) indicates that the separation is at least a full hydration layer prior to this time. The activation energy required for reorganization of the hydration sheath of the electron probably acts also to inhibit "Noyes type" recombination, as evidenced by the rapid increase of initial electron yields with temperature.[19,24] The electron should be free to migrate through the medium until it reacts with the original radical, a radical or electron generated in another pair, or a scavenger. However, the last process may be very inefficient in the absence of external scavengers such as H^+, O_2, or N_2O. For example, the reactivity of e_{aq}^- with I^- or $Fe(CN)_6^{4-}$ is negligible compared with I_2^- and $Fe(CN)_6^{3-}$, respectively.[22,26] In the case of tryptophan, $k(e_{aq}^- + \text{Trp}) = 3.6 \times 10^8$ may be compared with $\sim 3 \times 10^{10}$ from diffusion-limited reaction theory,[32] indicating that only about 1 in 80 encounters leads to scavenging of the electron. Thus, the electron has considerable time to "find" its radical coproduct even at relatively high solute concentrations. For example, taking $\bar{a} = 3 \times 10^{-4}$ from the aqueous tryptophan data, (11) leads to a mean recombination lifetime of 8×10^{-7} s and equating to the scavenging lifetime $1/k_s(S)$ gives 3.5 mM as the tryptophan concentration at which scavenging and recombination are equally probable. When the initial photolysis yields are very high, it is possible that the electron will encounter the radical from another pair or another electron. This corresponds to the case of bimolecular reactions as treated by means of the time-dependent rate constant in (15). The deviations of the observed electron decay rates from the predictions of (6)

at long decay times in Figures 1, 4, and 5 probably are due to the onset of such bimolecular processes.

In connection with pulse radiolysis studies on frozen aqueous media containing high salt concentrations, Buxton et al.[33] derived an expression for the decay of the solvated electrons by substituting the time-dependent rate constant derived from diffusion theory[14] into (15) with $k' = 0$. The integrated result can be expressed as

$$p(t) = e^{-k_s(S)t} e^{-k_s^2(S)t^{1/2}/2(\pi D)^{3/2}}$$

which like (7) comprises the product of an exponential decay term and a function decreasing with $t^{1/2}$. Although their data are in good agreement with this result, it is surprising that the scavenger concentration (S) appears in the term related to pairwise recombination. The fit of (6) to the Buxton data for the decay of electrons after pulse radiolysis of 10 M OH^- containing 0.02 M CrO_4^{2-} at 200 K was found to be equally good, with $\bar{a} = 6.5 \times 10^{-4}$ $s^{1/2}$ and $\beta' = 1$. This case applies to the generation of an initially random distribution of electrons and radicals in the frozen medium which alters to the steady state concentration gradients when the electrons diffuse to the scavenger ions, while in the aqueous photoionization process each electron is initially associated with its radical coproduct in the presence of a random distribution of scavengers. However, Noyes[14] has demonstrated that the development of the time-dependent rate constant based on specific molecular pairs is equivalent to the concentration gradient approach, suggesting the present analysis may be equally applicable to the case of frozen systems.

In summary, the theory is in good agreement with the functional shape of the observed electron decays and the dependence of the decay lifetimes on scavenger concentration and the initial electron yield. Only two parameters a and β' are required to fit a wide range of experimental parameters, neither of which is sensitive to the specific photolyzed solute. It is not apparent why the same $h(t)$ function as derived originally for diffusional recombination should be applicable to the slower decay of photoelectrons with a scale change about 10^2 in the a parameter. The contradiction is resolved by postulating two recombination regimes, the first corresponding to displacements up to about 10 Å and recombination lifetimes $\lesssim 10^{-10}$ s and the other applicable to those initial products which escape "Noyes type" recombination and are free to diffuse for relatively long distances, corresponding to recombination lifetimes $\sim 10^{-6}$ s. The second regime would only be significant when the initial displacement and/or hydration inhibit immediate recombination (on the time scale of the present experiments) and where scavenging by the original solute or added scavengers does not completely suppress the back reaction. Furthermore, the initial concentration of geminate pairs should not be so high that bimolecular processes control. All of these criteria appear to be reasonable for the photoionization of the inorganic anions and aromatic molecules as investigated in the present work. However, they may be totally inapplicable to other systems, e.g., photodissociation of molecular iodine in hydrocarbon solvents where the minimum root-mean-square displacement distance was estimated as 0.4 Å.[13] Recently, Stevens and Williams[34] estimated the diffusive displacement parameters for the quenching of anthracene fluorescence by oxygen in various hydrocarbon solvents as ~2 Å. It is not really known why photoionization in aqueous media should differ so significantly from these cases. Picosecond flash photolysis studies will be required to provide direct information about the first time regime of the photoionization process.

References and Notes

(1) Work supported by ERDA Contract No. E(11-1)-2217 and PHS Grant No. GM-20117. This is COO-2217-17.
(2) L. I. Grossweiner and H. I. Joschek, *Adv. Chem. Ser.*, **No. 50**, 279 (1965).
(3) L. I. Grossweiner, "Energetics and Mechanisms in Radiation Biology", G. O. Phillips, Ed., Academic Press, New York, N.Y., 1968, p 303.
(4) G. Stein, "Actions Chimiques et Biologiques des Radiations", Vol. 13, M. Haissinsky, Ed., Masson et Cie, Paris, 1969, p 119.
(5) M. S. Matheson, W. A. Mulac, and J. Rabani, *J. Phys. Chem.*, **67**, 2613 (1963).
(6) L. I. Grossweiner, G. W. Swenson, and E. F. Zwicker, *Science*, **141**, 805 (1963).
(7) F. D. Bryant, R. Santus, and L. I. Grossweiner, *J. Phys. Chem.*, **79**, 2711 (1975).
(8) J. Jortner, M. Ottolenghi, and G. Stein, *J. Phys. Chem.*, **66**, 2029 (1962).
(9) J. Jortner, M. Ottolenghi, and G. Stein, *J. Phys. Chem.*, **66**, 2037 (1962).
(10) J. Jortner, M. Ottolenghi, and G. Stein, *J. Phys. Chem.*, **66**, 2042 (1962).
(11) J. Jortner, M. Ottolenghi, and G. Stein, *J. Am. Chem. Soc.*, **85**, 2712 (1963).
(12) R. M. Noyes, *J. Am. Chem. Soc.*, **77**, 2042 (1955).
(13) R. M. Noyes, *J. Am. Chem. Soc.*, **78**, 5486 (1956).
(14) R. M. Noyes, *Prog. React. Kinet.*, **1**, 129 (1961).
(15) J. Jortner, M. Ottolenghi, and G. Stein, *J. Chem. Phys.*, **37**, 2488 (1962).
(16) J. Jortner, M. Ottolenghi, and G. Stein, *J. Phys. Chem.*, **68**, 247 (1964).
(17) M. Shirom and G. Stein, *J. Chem. Phys.*, **55**, 3372 (1971).
(18) F. S. Dainton and P. Fowler, *Proc. R. Soc. London, Ser. A*, **287**, 312 (1965).
(19) F. S. Dainton and S. R. Logan, *Proc. R. Soc. London, Ser. A*, **287**, 281 (1965).
(20) W. Feller, "An Introduction to Probability Theory and Its Applications", Vol. I, Wiley, New York, N.Y., 1950.
(21) J. F. Baugher and L. I. Grossweiner, *J. Phys. Chem.*, submitted for publication.
(22) M. Anbar, M. Bambenek, and A. B. Ross, *Natl. Stand. Ref. Data Ser., Natl. Bur. Stand.*, **No. 43**, (1973).
(23) U. Lachish, A. Shafferman, and G. Stein, *J. Chem. Phys.*, **64**, 4205 (1976).
(24) D. V. Bent and E. Hayon, *J. Am. Chem. Soc.*, **97**, 2599, 2612 (1975).
(25) Yu. A. Vladimirov, D. I. Roshchupkin, and E. E. Fesenko, *Photochem. Photobiol.*, **11**, 227 (1970).
(26) A. B. Ross, *Natl. Stand. Ref. Data Ser., Natl. Bur. Stand.*, Supplement **No. 43**, (1975).
(27) L. I. Grossweiner and M. S. Matheson, *J. Phys. Chem.*, **61**, 1089 (1957).
(28) F. H. Edgecombe and R. G. W. Norrish, *Proc. R. Soc. London, Ser. A*, **253**, 154 (1959).
(29) G. Dobson and L. I. Grossweiner, *Radiat. Res.*, **23**, 290 (1964).
(30) J. K. Thomas, *Trans. Faraday Soc.*, **61**, 702 (1965).
(31) E. M. Fielden and E. J. Hart, *Trans. Faraday Soc.*, **63**, 2975 (1967).
(32) P. Debye, *Trans. Electrochem. Soc.*, **82**, 265 (1942).
(33) G. V. Buxton, F. C. R. Cattell, and F. S. Dainton, *J. Chem. Soc., Faraday Trans. 1*, **71**, 115 (1975).
(34) B. Stevens and R. R. Williams, *Chem. Phys. Lett.*, **36**, 100 (1975).

Pulse Radiolysis Studies of Zn^+ Reactions[1]

Joseph Rabani,*[2] W. A. Mulac, and Max S. Matheson

Chemistry Division, Argonne National Laboratory, Argonne, Illinois 60439 *(Received July 12, 1975)*

Publication costs assisted by Argonne National Laboratory

The chemical reactivity of Zn^+ toward a number of radicals and molecules was determined using the technique of pulse radiolysis to produce Zn^+ in aqueous solutions containing $ZnSO_4$ and one or more of the following: H_2, methanol, 2-propanol, 2-methyl-2-propanol, N_2O, H_2O_2, H^+, and sodium formate. The following rate constants were measured, all in units M^{-1} s^{-1}: $k(Zn^+ + Zn^+) = (3.5 \pm 1.0) \times 10^8$, $-d(Zn^+)/dt = 2k(Zn^+)^2$; $k(Zn^+ + H) = (1.9 \pm 0.5) \times 10^9$; $k(Zn^+ + CH_2OH) = (2.5 \pm 0.3) \times 10^9$; $k(Zn^+ + (CH_3)_2COH) = (1.3 \pm 0.25) \times 10^9$; $k(Zn^+ + N_2O) = (1.6 \pm 0.15) \times 10^7$, assuming 0.02 M N_2O/atm; $k(Zn^+ + H_2O_2) = (2.45 \pm 0.2) \times 10^9$; $k(Zn^+ + CO_2^-) \simeq 4 \times 10^9$; $k(Zn^+ +$ acetone$) < 10^8$ and maybe much smaller; $k(CO_2^- + Zn^{2+}) < 2 \times 10^4$; $k(e_{aq}^- + Zn^{2+}) = (9.5 \pm 0.3) \times 10^8 \times 10^{-2.04\mu^{1/2}/(1+\mu^{1/2})}$; where μ is the ionic strength due to $ZnSO_4$, $MgSO_4$, or $MnSO_4$ in the range 0–0.2 M. A number of extinction coefficients at 310 nm were determined: $\epsilon_{Zn^+} = 13\,000 \pm 1\,000$, $\epsilon_{CH_2OH} = 270 \pm 15$, $\epsilon_{(CH_3)_2COH} = 353 \pm 15$, and $\epsilon_{CH_2C(CH_3)_2OH} < 10$ M^{-1} cm^{-1}. Except for ϵ_{Zn^+} these agree with previously published values. Our measurements of the rate constants for two alcohol radicals reacting also agree with earlier results: $k(CH_2OH + CH_2OH) = (1.5 \pm 0.1) \times 10^9$ and $k((CH_3)_2COH + (CH_3)_2COH) = (6.5 \pm 0.5) \times 10^8$. The Zn^+ reactions and the relation of this work to earlier work are discussed. Atomically dispersed Zn^0, from $Zn^+ + Zn^+$, reacts with water at pH 3 in less than 1 s.

Introduction

We are investigating a number of aqueous inorganic solutions which, if combined with suitable photosensitizers, might store solar energy. Further, we are using radiation chemistry, particularly pulse radiolysis, for the preliminary investigation of these systems, since the oxidation and reduction chemistry of the selected solutions can be studied in simplified form in the absence of sensitizers. The data accumulated in the preliminary studies should make possible the selection of the most promising systems for further photochemical investigations.

We have chosen Zn^{2+} as one possible reducible component of several redox pairs for the following reasons. (a) Peled and Czapski[3] reported a relatively high yield of H_2 in the γ irradiation of $ZnSO_4$. Although we were unable to obtain as high yields as they reported, we have found that, when $MnSO_4$ is also present, H_2 forms with $G > 1$. This indicated some of the reduced zinc escaped reoxidation by the oxidized species and reacted with water to form H_2. Fixation of H_2 may be very useful.[4] (b) The behavior of Zn^{2+} can be related to that of several similar ions, for which considerable information is already known.[5,6] (c) Some work on the radiation chemistry of Zn^{2+} has already been reported.[5]

Although the radiation chemistry of Zn^{2+} has previously been studied, we found we needed much more information on the behavior of the reduced species, Zn^+. In this paper we summarize our results on the chemical behavior of Zn^+.

Experimental Section

The Argonne ARCO electron linac was used with standard pulse radiolysis techniques involving photomultiplier detection.[7] Electron pulse duration varied between 4 and 40 ns. A xenon or mercury–xenon lamp, 450 W, served as the source of analyzing light, and a pulsed xenon lamp was used for measurement of e_{aq}^- rate constants at 600 nm. Unless otherwise stated, scattered light was less than 0.5% and was ignored. Cell lengths were 5 or 1 cm with one light pass. Cell filling techniques and pressurized cells have been previously described.[8] Temperature was 22 ± 1 °C.

The kinetic data were either scanned from a smooth trace of the Polaroid picture by an automatic curve follower (Hewlett-Packard Type No. F3B), digitized into a 400-channel analyzer, and transmitted to a Xerox Sigma 5 computer; or the photomultiplier output was digitized in a Biomation 8100 transient recorder in conjunction with a backoff circuit and then transmitted to the computer.

Dosimetry was carried out with a 0.5 mM $K_4Fe(CN)_6$ (Fluka, puriss.) solution saturated with 0.1 atm of N_2O (Liquid Carbonic, 99.9% purity). The optical density was measured at 420 nm ($\epsilon = 1000$ M^{-1} cm^{-1} for ferricyanide) or at 436 nm ($\epsilon = 717$ M^{-1} cm^{-1}). G(ferricyanide) = 5.4 was assumed.

Unless otherwise stated the $ZnSO_4$ was Baker Analyzed twice recrystallized from cold water. $ZnSO_4$ 99.999% pure from Apache Chemicals was used without further purification in some experiments and yielded the same results. Fisher certified 2-methyl-2-propanol was recrystallized 20 times. $MgSO_4$, NaCl, 2-propanol, and acetone free methanol (Mallinckrodt, AR), $HClO_4$ (G. Frederick Smith Chemical Co., 70%, double vacuum distilled), and argon (Matheson 99.998% pure) were used as received. Water was triply distilled.

Unless otherwise stated, the error limits reflect the maximum deviations in the data. Error limits of constants derived from curve fittings reflect the limits in which the constants can be still considered in agreement with the data.

Results and Discussion

The Extinction Coefficient of Zn^+. The extinction coefficient of Zn^+ at 310 nm, $\epsilon_{Zn^+}^{310}$, needed for optical observation of Zn^+, was determined in solutions containing 2–10 mM $ZnSO_4$ plus 2–20 mM of one of the following: methanol, 2-propanol, or 2-methyl-2-propanol. λ_{max} for Zn^+ is 300 ± 3 nm. Our first step was a careful redetermination of the extinction coefficients of the radicals derived from the above alcohols in solutions containing the given alcohol and saturated at 0.05 atm of N_2O. In these solutions OH radicals produced by reactions 1 and 2 react rapidly with

$$H_2O \rightsquigarrow e_{aq}^-, OH, H, H_2O_2, H_2, H_3O^+, OH^- \quad (1)$$

$$e_{aq}^- + N_2O \rightarrow N_2 + OH + OH^- \quad k_2 = 8 \times 10^9\ M^{-1}\ s^{-1}\ ^9 \quad (2)$$

$$OH + RH_2 \rightarrow H_2O + \dot{R}H \quad (3)$$

the alcohols, RH_2, in reaction 3. The H atoms reacted less rapidly with RH_2 or combined. $k_3 = 9 \times 10^8$, 2×10^9, and

TABLE I: Reactivity of e_{aq}^- toward Zn^{2+} in 0.05 M CH_3OH Solutions[a]

$[ZnSO_4]$, mM	Additive, in mM	k_6[b]	$k_6{}^0$[c]
2.03[d]		6.35 ± 0.1	9.4
2.08		6.20 ± 0.1	9.2
10	$MgSO_4$, 40	2.3 ± 0.05	9.7
5.9	$MnSO_4$,[e] 38	2.4 ± 0.1	9.6
10	$MnSO_4$,[e] 40	2.3 ± 0.1	9.7

[a] Measured at 600 nm with pulsed lamp and 5-cm light path. (1.5 μM e_{aq}^- per pulse.) Units of k_6 are 10^8 M^{-1} s^{-1}. [b] Each value is an average of at least three determinations. Error limits show maximum deviation. Results are corrected using data from control experiments. [c] At $\mu = 0$, calculated from the formula $\log k_6{}^0/k_6{}^\mu = 2.04\mu^{1/2}/(1 + \mu^{1/2})$. [d] Not recrystallized. [e] The same solutions in the absence of $ZnSO_4$ gave $k(e_{aq}^- + Mn^{2+}) = 2.0 \times 10^7$ M^{-1} s^{-1}. The values of k_6 have been corrected for this reaction.

$$H + RH_2 \rightarrow H_2 + \dot{R}H \quad (4)$$

$$H + H \rightarrow H_2 \qquad k_5 = 1.3 \times 10^{10}\ M^{-1}\ s^{-1}\ [10] \quad (5)$$

5×10^8 M^{-1} s^{-1}, respectively,[11] for methanol, 2-propanol, and 2-methyl-2-propanol, and in the same order $k_4 = 3 \times 10^6$, 8×10^7, and 1.5×10^5 M^{-1} s^{-1}.[10] With these rate constants we could calculate the fraction of H atoms ($G_H = 0.6$) which reacted during the pulse and resolution time (0.5 μs). Comparing initial absorptions in the alcohol–N_2O solutions with those observed in the ferrocyanide dosimeter, and assuming the same G values for primary radicals, we determined $\epsilon^{310}_{CH_2OH} = 270 \pm 15$, $\epsilon^{310}_{CH_2C(CH_3)_2OH} < 10$, and $\epsilon^{310}_{(CH_3)_2COH} = 353 \pm 15$ M^{-1} cm^{-1} in agreement with earlier results. For each alcohol more than one type of radical is formed,[12] but the radicals indicated by the ϵ subscripts comprise >85% of the radicals in each case and all absorption has been assigned to them. In the above experiments each experiment produced 18 μM radicals.

In pulse irradiated solutions containing sufficient $ZnSO_4$ and alcohol the "initial" absorption is due to both Zn^+ and $\dot{R}H$. Taking the primary G values the same as in the dosimeter and correcting for incomplete radical scavenging when necessary, we determined $\epsilon^{310}_{Zn^+} = 1.30 \times 10^4$ M^{-1} cm^{-1} (maximum deviation 0.1×10^4) as the average of 25 independent experiments. This is considerably higher than previously reported.[5a,b] We also found, see below, that the reactivity of e_{aq}^- toward Zn^{2+} is considerably lower than earlier reported.[9] The error in some of the earlier values of $\epsilon^{310}_{Zn^+}$ may have resulted from incomplete scavenging of e_{aq}^- by Zn^{2+}.

The Reactivity of Zn^{2+} toward e_{aq}^-. The initial absorbances in dilute $ZnSO_4$ solutions were considerably smaller than predicted by previously reported values for k_6, therefore we reinvestigated this reaction. The results

$$e_{aq}^- + Zn^{2+} \rightarrow Zn^+ \quad (6)$$

in Table I have been corrected for competing reactions of e_{aq}^-, using data from control experiments. As noted above k_6 is considerably smaller than previously reported.[9] The effect of ionic strength, μ, is in good agreement with the relation, $\log k_6{}^0/k_6{}^\mu = 2.04\mu^{1/2}/(1 + \mu^{1/2})$, yielding 9.5×10^8 M^{-1} s^{-1} for $k_6{}^0$ calculated at zero ionic strength.

The Reaction of Zn^+ with N_2O. Solutions containing 0.1 M $ZnSO_4$ and 0.1 M 2-methyl-2-propanol saturated with 0.3 or 1.0 atm of N_2O were pulse irradiated (5 μM radicals per pulse). The optical absorption formed decayed to zero after the pulse by a pseudo-first-order process. With 0.3 atm of N_2O $D_0{}^{310}$ was 0.044 corresponding to an initial 0.67 μM Zn^+ accompanied by 3.9 μM $\dot{R}H$. Under these conditions, as later discussion shows, reactions 7–10 contributed only about 4% to the initial decay of Zn^+.

$$Zn^+ + Zn^+ \rightarrow Zn^0 + Zn^{2+} \quad (7)$$

$$Zn^+ + H_2O_2 \rightarrow Zn^{2+} + OH + OH^- \quad (8)$$

$$Zn^+ + RH \xrightarrow{H^+} Zn^{2+} + RH_2 \quad (9)$$

or

$$\rightarrow ZnRH^+$$

$$Zn^+ + H \rightarrow ZnH^+ \text{ (or } Zn^0 + H^+\text{) (or } Zn^{2+} + H^-\text{)} \quad (10)$$

Assuming the solubility of N_2O is 0.02 M/atm, experiments with 0.3 and 1.0 atm N_2O gave $k_{11} = 1.75 \times 10^7$ and 1.44×10^7 M^{-1} s^{-1}, respectively, in agreement with previous work.[5c]

$$Zn^+ + N_2O \xrightarrow{H_2O} Zn^{2+} + N_2 + OH + OH^- \quad (11)$$

or[5d,e]

$$\rightarrow ZnO^+ + N_2$$

The Reaction of Zn^+ with H_2O_2. To measure k_8 solutions containing 20 mM 2-propanol, 10 mM $ZnSO_4$, and 68 or 183 μM H_2O_2 were pulse irradiated to yield 4.6 μM radicals. The decay of Zn^+ at 310 nm was strictly first order and proportional to $[H_2O_2]$. After correcting for reactions 7 and 9 (contributing <5% to the Zn^+ decay), we obtained $k_8 = (2.45 \pm 0.2) \times 10^9$ M^{-1} s^{-1}. This value is slightly higher than that previously reported,[5c] but the difference is within the accuracy generally attributed to such measurements. Special care was taken to determine H_2O_2 concentrations before and after these irradiations. No change in concentration was found. The H_2O_2 reaction with I^- was used for analysis, taking $\epsilon^{350}_{I_3^-} = 26000$ M^{-1} cm^{-1}. The solutions were prepared and argon bubbled through them less than 20 min before the measurements.

The Reaction of $Zn^+ + Zn^+$. Ideally one would prefer to study $Zn^+ + Zn^+$ in a solution wherein this reaction was the predominant mode of decay. We were unable to devise such a solution. To establish our results more securely we investigated this reaction in two different systems: one in which H_2 converts OH to H; and one in which alcohol converts OH to alcohol radicals. Both H and alcohol radicals react with Zn^+.

Zn^+ in Solutions Equilibrated with 107 atm of H_2. In these experiments with about 0.08 M H_2, OH conversion to H has a half-life of about 0.1 μs, and reactions 7, 8, and 10 must be considered in the decay of Zn^+ radical ions. H atoms react principally by reactions 5 and 10. Reaction 12 is relatively slow, and is followed rapidly by (13). The

$$H + H_2O_2 \rightarrow H_2O + OH \qquad k_{12} = 6.0 \times 10^7\ M^{-1}\ s^{-1} \quad (12)$$

$$OH + H_2 \rightarrow H_2O + H \quad (13)$$

net effect of this cycle is the reaction of H_2O_2 and H_2 to form water. In any case (12) is not important in the time range where Zn^+ absorbance is significant. Reaction 8 followed rapidly by (13) produces H atoms at the expense of Zn^+.

In previously unirradiated 10 mM solution of twice recrystallized $ZnSO_4$ (neutral prior to irradiation) Zn^+ decay was first order suggesting reaction with impurities. Preirradiation at low dose rates (γ rays at 7.5 krads/min for 10 min or 75 electron pulses of 500 krads) slowed the Zn^+ decay. After preirradiation the decay was second order with respect to initial radical concentrations, but more complex during the course of an individual experiment. Taking D_∞ (D_t = absorbance at time t) to best fit the data (D_∞ experimental was zero), the second-order expression $S = (d/dt)(D_t - D_\infty)^{-1}$ was systematically higher for the

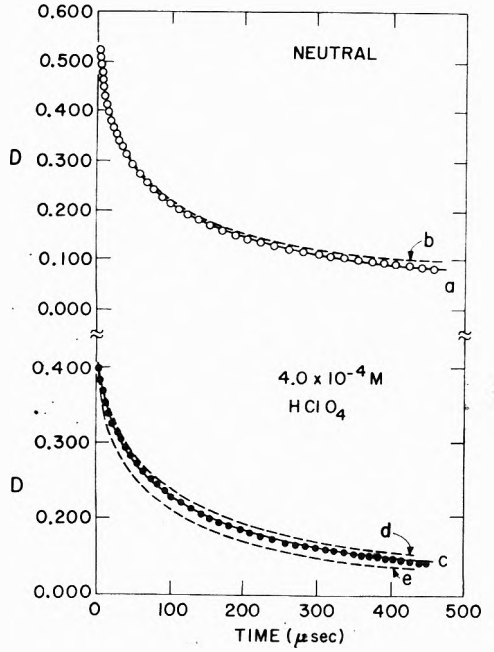

Figure 1. The decay of Zn^+ in the presence of 107 atm of H_2 and 10 mM $ZnSO_4$, 5-cm light path, 40-ns pulse. Time zero is the beginning of the electron pulse. Circles are experimental measurements: (O) neutral pH; (●) 0.4 mM $HClO_4$ present. Lines are computed with the aid of the Schmidt–Jonah–Hamilton program.[13,14] The values $k_5 = 1.5 \times 10^{10}$ M^{-1} s^{-1}, $k_8 = 2.45 \times 10^9$ M^{-1} s^{-1}, $k_{12} = 6.0 \times 10^7$ M^{-1} s^{-1}, and $G_{H_2O_2} = 0.75$ were used in all five computations. For curves a and b we used $G(Zn^+) = 2.5$ and $G(H) = 3.3$. For curve a the dose was 2.0×10^{20} eV l^{-1}, and $k_7 = 3.1 \times 10^8$ and $k_{10} = 2.4 \times 10^9$ M^{-1} s^{-1} were taken. For curve b, k_7 was taken as 2.0×10^8 M^{-1} s^{-1} and $k_{10} = 3.75 \times 10^9$ M^{-1} s^{-1}. The dose had to be adjusted to 2.1×10^{20} in order to obtain a fit with the initial stage of the decay in b. For curve c we used the same parameters as for curve a, except that $G(Zn^+) = 1.53$ and $G(H) = 4.37$ were taken. $G(Zn^+)$ was adjusted to obtain a fit with the experimental initial absorption. For curve d we used $G(Zn^+) = 1.55$, $G(H) = 4.35$, 1.92×10^{20} eV l^{-1}, $k_7 = 3.8 \times 10^8$ M^{-1} s^{-1}, and $k_{10} = 1.5 \times 10^9$ M^{-1} s^{-1}. For curve e, parameters were the same as for curve b except that $G(Zn^+) = 1.42$ and $G(H) = 4.48$ were used.

intial portion of the decay. S decreased if initial portions of the decay curve were excluded. Thus several reactions are involved. If reaction 10 were unimportant, then initially S would be about equal to $2k_7/(\epsilon^{310}_{Zn^+}l)$ (where l is the light path), but would increase with time as reaction 8 became relatively more important. Further, we were unable to fit our results without including reaction 7. For example, reaction 5 is known to be very fast[10] and in the absence of (7) unreacted Zn^+ remains after the H atoms have reacted. In our computations the H_2O_2 present was insufficient to remove this unreacted Zn^+. This would have yielded a small, long-lived absorption, contrary to experimental observations.

We carried out computations with Schmidt's program[13] as modified by Jonah and Hamilton[14] including reactions 5, 7, 8, and 10 and the unimportant reaction 12 to determine which values of k_5, k_7, and k_{10} would best fit our experimental results. k_5 has been determined within a relatively small range.[10] The initial concentration of Zn^+ was obtained from the initial absorbance and $\epsilon^{310}_{Zn^+}$, and this through known G values gave the initial concentrations of other species. k_8 and k_{12} are known. The optical density was calculated as a function of time and compared with experiment. The kind of fit obtained can be seen in Figure 1.

A procedure was developed to conserve computer time. The essence of our treatment involved was the following: (1) Finding in neutral solutions the combinations of k_7 and k_{10} which for several values of k_5 gave the best fit at long

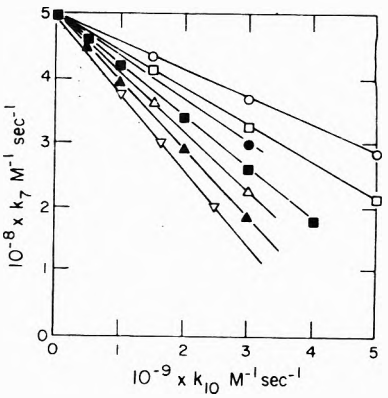

Figure 2. The combinations of k_7 and k_{10} which correspond to $S(0.170, 3300) = 2.0 \times 10^4$ s^{-1} for several fixed values of k_5. Computations carried out according to procedures used for Figure 1, neutral solutions, using the same G values and reaction rate constants (other than k_7, k_5, and k_{10}). The values of $10^{-10}k_5$ were: (O) 4.0, (□) 2.5, (●) 2.0, (■) 1.5, (△) 1.25, (▲) 1.0, (▽) 0.78. Note that the point at $k_{10} = 0$ is independent of the value of k_5 chosen.

TABLE II: Consistent Values of k_5, k_7, and k_{10}

	k_7[b]		k_{10}[c]	
k_5[a]	Neutral	Acid	Neutral	Acid
0.78	3.0	3.1	1.6	1.55
1.0	2.9	3.1	2.0	1.85
1.5	2.5	3.1	3.1	2.4
2.5	2.2	2.6	4.8	4.1

[a] Units 10^{10} M^{-1} s^{-1}. Although $k_5 = 0.78 \times 10^{10}$ M^{-1} s^{-1} apparently gives the best agreement with the data, we do not consider our results as an independent estimate of k_5. [b] Units 10^8 M^{-1} s^{-1}. [c] Units 10^9 M^{-1} s^{-1}.

times ($D < 0.170$ and t out to 3300 μs) where (7) and (8) are relatively more important (Figure 2); (2) Finding which of the combinations from step 1 best fit the data in neutral solution, where $[Zn^+] \simeq [H]$, and at early times (2–470 μs) where H atom reactions are very important; (3) Finding (simultaneously with step 2) which combinations from step 1 best fit the data in 0.4 mM $HClO_4$ solution, where $[Zn^+] \simeq 0.5$ [H] owing to partial capture of e_{aq}^- by H^+, and at early times (2–470 μs) so that H atom reactions are even more important. The results in neutral and acid solutions for several values of k_5 are give in Table II. The consistency between results in neutral and acid solutions supports the reliability of the rate constant determinations.

If the average of listed values,[10] 1.0×10^{10}, is taken for k_5, then from Table II, $k_7 = 3.0 \times 10^8$ and $k_{10} = 1.9 \times 10^9$ M^{-1} s^{-1}. If k_5 is revised Table II provides for the revision of k_7 and k_{10}. The error limits for k_7 and k_{10} which result from errors in other rate constants and in G values and from scatter of the data are estimated as ±20%. This is in addition to the uncertainty from errors in k_5. In any case k_7 cannot be less than 2×10^8 as the computed absorbance left at 3300 μs would be much higher than observed, and it cannot be greater than 5×10^8 or k_{10} must be omitted with a resulting decay very close to simple second order contrary to experiment.

Since interfering impurities were reduced by preirradiation which produces H_2O_2 ($G \simeq 0.75$) and H^+ (the latter corresponding to Zn^0 formed), the effects of possible unreduced impurities and residual H_2O_2 and H^+ must be considered. In one test a pulse fourfold smaller than the standard 40-ns pulse left S essentially unchanged, indicating no appreciable effects from these species. In another test 20 very small pulses (10^{-7} M Zn^+/pulse) were given before and after each standard pulse to destroy residual H_2O_2 from the previous standard pulse. Assigning the

TABLE III: Decay of Zn^+ in the Presence of Alcohols[a]

Alcohol, concn, mM	$[ZnSO_4]$,[b] mM	D_0[c]	Fraction[d]	$10^2 D_\infty$[c,e]	$10^{-4}(d/dt)\cdot(D - D_\infty^c)^{-1}$	Rel pulse intensity	$[HClO_4]$, mM
2-Propanol, 20	10	0.66	0.92	−2.8	4.47	A	0
2-Propanol, 20	10	0.168	0.91	−0.78	4.75[f]	0.25 A	0
2-Propanol, 100	10	0.181	0.92	−0.89	4.47[f]	0.25 A	0
2-Propanol, 20	10	0.433	0.88	−2.5	7.1	A	0.3
2-Propanol, 20	10	0.331	0.91	−2.0	9.9	A	0.6
2-Propanol, 20	10	0.209	0.86	−1.5	14.5	A	1.2
2-Propanol, 20	10[g]	0.210	0.86	−1.4	4.58[f]	0.24 B	0
2-Propanol, 20	10[g]	0.89[h]	0.90	−6.0	4.63	B	0
2-Propanol, 20	200[i]	0.95[h]	0.91	−6.6	4.9	B	0
2-Propanol, 20	200[i]	0.87[h]	0.90	−6.2	5.4	B	1.0
2-Propanol, 20	200[i]	0.74	0.93	−5.0	5.3	0.78 B	0
2-Propanol, 20	200[i]	0.193	0.84	−1.7	5.5[f]	0.20 B	0
2-Propanol, 20	200[i]	0.185	0.88	−3.3	6.9[j,f]	0.20 B	0
Methanol, 25	2	0.485[k]	0.88	−2.0	6.5	C	0
Methanol, 25	100	0.68	0.89	−3.0	5.1	C	0
Methanol, 25	100[l]	0.69	0.93	−5.2	5.7	C	0
Methanol, 200	5	0.38	0.92	−0.95	6.4	D	0
Methanol, 200	5	0.087	0.93	−0.1	7.2[f]	0.20 D	0
Methanol, 200	5	0.178	0.91	−1.9	22[m]	D	0
Methanol, 200	5	0.020	0.86	+0.12	26[n]	D	0
2-Methyl-2-propanol,[o] 10	10	0.572	0.91	−3.0	4.4	A	0
2-Methyl-2-propanol,[o] 10	10	0.606	0.98	−1.9	4.6	A	0
2-Methyl-2-propanol,[o] 10	10	0.151	0.86	−0.7	4.5[f]	0.25 A	0
2-Methyl-2-propanol,[o] 50	10	0.153	0.84	−0.9	4.4[f]	0.25 A	0
2-Methyl-2-propanol,[o] 10	10	0.320	0.92	−2.5	6.3	A	0.3
2-Methyl-2-propanol,[o] 10	10	0.220	0.92	−2.4	8.3	A	0.6
2-Methyl-2-propanol,[o] 10	10	0.144	0.93	−2.0	12.1	A	1.2

[a] Each value is an average of at least three runs. 5-cm cell, 40-ns pulses, initially neutral solutions were used unless otherwise stated. All the experiments were carried out at 310 nm. [b] Recrystallized twice, unless otherwise stated (see Experimental Section). [c] Optical density extrapolated (using the second-order rate law) to the end of the electron pulse. The extrapolation added about 10% to the highest measured optical density. [d] The fraction of absorbance that decayed away during the time of the measurements. The measured optical absorption always decayed back to zero within 1–5 ms. [e] The final optical density which was assumed in order to force the results into a precise second-order fit. [f] 10-ns pulse. [g] 0.2 M $MgSO_4$ present. [h] 2-cm cell. Optical densities normalized to 5 cm. [i] 99.999% pure. Not recrystallized. [j] 30 pulses (0.78 B) were given prior to the test pulse. [k] Incomplete scavenging of e_{aq}^- by the $ZnSO_4$. [l] In the presence of 0.30 mM acetone. [m] In the presence of 0.02 atm of N_2O. [n] In the presence of 0.05 atm of N_2O. [o] There was an initial relatively fast decay (5–15% of the initial absorption) which we attribute to a reaction between Zn^+ and H atoms. D_0 is the initial optical density, before this decay took place. D_∞^c and $(d/dt)(D - D_\infty^c)^{-1}$ were calculated with the exclusion of the initial decay.

decay to $Zn^+ + H_2O_2$ alone, the average of six traces for small pulses just preceding the standard pulses gave $[H_2O_2] = (6.3 \pm 2) \times 10^{-8}$ M, and since (7) and (10) are important, $[H_2O_2]$ is actually about zero. These traces include any impurity reactions, which therefore are negligible also. In 0.4 mM $HClO_4$ solutions this procedure gave $[H_2O_2] \leq (2 \pm 1) \times 10^{-7}$ M, corresponding to about 1.5×10^{-7} or ~6% of the H_2O_2 initially formed by a standard pulse.

A neutral solution preirradiated with γ rays in a pressure cell showed a loss of light transmission. This remaining transmission was reduced a further 52% by 15 pulses of 40 ns at one pulse every 2 s. Neither pulses of 10 or 40 ns a few minutes apart nor the very small pulses had an appreciable long time effect on the transmission. The loss of transmission, which reached a fairly constant level during the irradiations, was due to turbidity from Zn^0 formed, and such turbidity was not formed in acid solutions, at least by pulses of electrons. The neutral solution pressure cell subject to the series of irradiations was opened and the solution analyzed for turbidity and H_2O_2 within 20 min of the last irradiation. No turbidity was found indicating Zn^0 had reacted with O_2, and the expected product is H_2O_2 from the dismutation of $HO_2 + O_2^-$.[15] The iodide technique[16] gave $(7.8 \pm 1) \times 10^{-7}$ and $(6.0 \pm 1) \times 10^{-7}$ M H_2O_2 in the irradiated neutral and acid solutions, respectively. Electrical balance requires $[Zn^0]$ equal to one-half the $[H^+]$ formed, so the maximum $[H^+]$ produced after irradiation would be 1.5 and 1.2 μM, respectively, for the neutral and 0.4 mM $HClO_4$ solutions. As was noted an approximately constant turbidity level was reached, suggesting Zn^0 was reacting with H^+ or water to give H_2, thus limiting both the Zn^0 and H^+. The pH of the "neutral" solution was measured as ≥5.4 at the end of the irradiation. Perhaps some Zn^+ reacted with impurities at the beginning of the irradiation or CO_2 dissolved in the solution during measurement. Even pH 5.4 would not significantly affect our results.

Zn^+ in Solutions of Alcohols. Buxton and Sellers[5a] observed that the second-order rate constants for decay of Zn^+ (and some similar ions) depended on the OH scavenger present, being lowest when 2-propanol or 2-methyl-2-propanol were used. As the initial concentrations of Zn^+ and RH are about equal in such solutions, the second-order behavior of Zn^+ decay may be attributed to the parallel reactions 7, 9, 14, plus 8. In 2-propanol, 2-methyl-2-propanol, or methanol we indeed found Zn^+ disappearance second order. Although actual optical densities decayed to zero, we found a small negative D_∞ required for best second-order fits of data. This requirement indicates a small deviation from second order, perhaps owing to reaction 8. Typical results are shown in Table III.

$$RH + RH \rightarrow RH_2 + R \text{ or } (RH)_2 \qquad (14)$$

In 2-methyl-2-propanol solutions H atoms disappear mostly by reactions 5 and 10, since this alcohol is relatively unreactive toward H atoms. However, in 2-propanol or 0.2 M methanol solutions under our conditions H atoms more rapidly abstract H from RH_2. Thus, in acid 2-propanol solutions (Table III) RH is increased and Zn^+

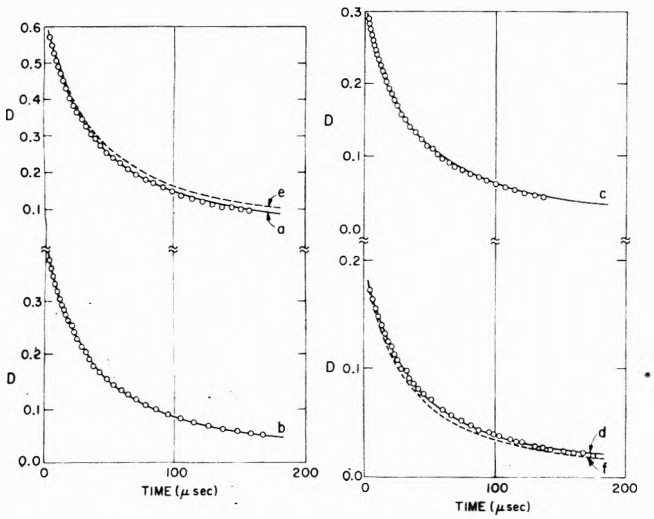

Figure 3. Decay of Zn^+ at 310 nm in the presence of 20 mM 2-propanol, 10 mM $ZnSO_4$ (recrystallized), and 2.2×10^{20} eV l^{-1} (40-ns pulse). The curves were computed taking $G_{H_2O_2} = 0.6$, $k_{14} = 6.5 \times 10^8$ M^{-1} s^{-1}, and $k_8 = 2.45 \times 10^9$ M^{-1} s^{-1}. H atoms ($G_H = 0.6$) were assumed to react with 2-propanol instantaneously ($k_4 = 7 \times 10^7$ M^{-1} s^{-1} for 2-propanol[10]). The curves were computed. Circles are experimental points. (a) Solution was neutral before the pulse. $G(RH) = 3.35$, $G(Zn^+) = 2.65$, $k_7 = 4.5 \times 10^8$, and $k_9 = 1.3 \times 10^9$ M^{-1} s^{-1} were used for the computations. Precisely the same curve was obtained using $k_7 = 3.5 \times 10^8$ and $k_9 = 1.5 \times 10^9$ M^{-1} s^{-1}. (b) 0.3 mM $HClO_4$ present. $G(RH) = 4.4$, $G(Zn^+) = 1.6$, $k_7 = 4.5 \times 10^8$, and $k_9 = 1.3 \times 10^9$ M^{-1} s^{-1} were used for the computation. (c) 0.6 mM $HClO_4$ present. $G(RH) = 4.8$, $G(Zn^+) = 1.2$, $k_7 = 4.5 \times 10^8$, and $k_9 = 1.3 \times 10^9$ M^{-1} s^{-1} used for the computation. (d) 1.2 mM $HClO_4$ present. $G(RH) = 5.32$, $G(Zn^+) = 0.68$, $k_7 = 4.5 \times 10^8$, and $k_9 = 1.3 \times 10^9$ M^{-1} s^{-1} were used for the computation. Curve (e) same as (a) but $k_7 = 3.5 \times 10^8$ M^{-1} s^{-1}. Curve (f) same as (d) but $k_7 = 3.5 \times 10^8$ and $k_9 = 1.5 \times 10^9$ M^{-1} s^{-1} were chosen.

decreased, since H^+ competes with Zn^{2+} for e_{aq}^- forming H atoms. The strong effect of $HClO_4$ can only be accounted for if most Zn^+ reacts with RH. N_2O was added to methanol instead of H^+ introducing reaction 11, which was assumed to be followed by instantaneous formation of RH. For computations in Schmidt's program[13] we used reactions 8 and 9 plus, where appropriate, (11) in methanol and (5) and (10) in 2-methyl-2-propanol. We could not fit the data unless (7) was included. The fit for 2-propanol is shown in Figure 3. Best fits for 2-propanol were obtained with $k_7 = 4.5 \times 10^8$ and $k_9 = 1.3 \times 10^9$ M^{-1} s^{-1}. The decay of optical absorption at 310 nm (same pulse intensity as Figure 3) in 0.02 M 2-propanol saturated with 0.05 atm of N_2O gave $k_{14} = (6.5 \pm 0.5) \times 10^8$ M^{-1} s^{-1} in agreement with Simic, Neta, and Hayon.[17]

Figure 3 shows appreciable changes in k_7 and k_9 do not fit the data. For $k_7 = 3.5 \times 10^8$ and $k_9 = 1.3 \times 10^9$ the decay is too slow (3e), and, although the pair 3.5×10^8 and 1.5×10^9 do fit the data in neutral solutions, they do not fit the data from acid solution (3f). Indeed, in 1.2 mM $HClO_4$ reaction 7 can almost be neglected, so that the computed decay is governed by (8) and especially (9), and only k_9 is unknown.

After considering possible errors in G values and rate constants, we conclude from results in 10 mM $ZnSO_4$ plus 20 mM 2-propanol solutions that $k_7 = (4.5 \pm 1.5) \times 10^8$ and $k_9 = (1.3 \pm 0.25) \times 10^9$ M^{-1} s^{-1}. Although this result for k_7 is higher than in H_2 solutions, the error limits overlap for the two values. The difference seems to be systematic rather than random.

Acetone is a common impurity in alcohols, therefore, we tested the reactivity of acetone toward Zn^+. Adding 0.3 mM acetone to a solution containing 100 mM $ZnSO_4$ and 25 mM methanol did not change either the initial absorbance or the decay kinetics (Table III). The methanol used was "acetone free". The decay of e_{aq}^- in aqueous solutions of 2-propanol or 2-methyl-2-propanol set respective upper limits for acetone of 0.004 or 0.0007% in the alcohol. Decreasing the dose four-fivefold had little or no effects on $(d/dt)(D - D_\infty{}^c)^{-1}$, confirming the lack of acetone or other impurity effect.

The data for neutral 2-methyl-2-propanol solution were fit with $k_5 = 1.3 \times 10^{10}$, $k_7 = 4 \times 10^8$, $k_9 = (1.0 \pm 0.3) \times 10^9$, $k_{14} = 6.5 \times 10^8$,[17] and $k_{10} = 2.8 \times 10^9$ M^{-1} s^{-1}. (This is *not* an independent determination of k_{10}.) Reaction 15

$$RH + H \rightarrow RH_2 \qquad (15)$$

is probably diffusion-controlled but was neglected owing to the small yield of H atoms. The acid 2-methyl-2-propanol data are qualitatively in agreement with those from the 2-propanol system, however, precise values of k_5, k_{10}, and k_{15} are required to estimate k_7 independently.

Next we come to the methanol results. For methanol k_{14} was redetermined in agreement with previous work[17] as $(1.5 \pm 0.1) \times 10^9$ M^{-1} s^{-1} in aqueous methanol saturated with 0.05 atm of N_2O. Computations were made on solutions containing 0.2 M CH_3OH and 5 mM $ZnSO_4$ in the presence and absence of 0.02 atm of N_2O, for which G values were taken as $G_{OH} = G_e = 2.7$, $G_H = 0.6$, and $G_{H_2O_2} = 0.5$. This latter value was taken since methanol and ethanol react similarly.[18] In the absence of N_2O the 40-ns pulse gave an initial pH of 5.5 and some e_{aq}^- react with H^+, so $G(Zn^+) = 2.4$ and $G(H) = 0.8$ were taken. Using our measured rate constants for k_8, k_{11}, and k_{14}, a best fit was obtained with $k_7 = 4.5 \times 10^8$ and $k_9 = 2.5 \times 10^9$ M^{-1} s^{-1}. Although other combinations fit the data reasonably well in the absence of N_2O, only this pair also fit the data in the presence of N_2O (higher $[RH]/[Zn^+]$ ratio) where the computations are very sensitive to the value of k_9 and less so to k_7. Error limits are estimated as 20% for k_9 and 40% for k_7. The 2-propanol results are considered more accurate than those with methanol, because reaction 9 is more important in methanol and because the H^+ used in 2-propanol does not react with Zn^+ while N_2O used in methanol does. Considering all systems we believe most weight should be given to the H_2 system in averaging k_7, and we have done so.

Zn^+ in Formate Solutions. In 10 mM sodium formate plus 2 mM recrystallized $ZnSO_4$ solutions with 5–20 μM initial radical concentrations $S = 9.7 \times 10^4$ s^{-1}, corresponding to $k(Zn^+ + CO_2^-) \simeq 4 \times 10^9$ M^{-1} s^{-1} and to reaction 7 contributing ~10% to Zn^+ decay. In 0.5 M $ZnSO_4$ S decreased to 6.1×10^4 s^{-1}, apparently an ionic strength effect. In alcohols where reaction 9 involves a neutral radical no ionic strength effect was observed. No evidence for reaction 16 was found in 0.5 M $ZnSO_4$, setting a limit for $k_{16} < 2 \times 10^4$ M^{-1} s^{-1}.

$$CO_2^- + Zn^{2+} \rightarrow CO_2 + Zn^+ \qquad (16)$$

The Nature of Zn^+ Reactions. Baxendale and Dixon[6e] found no formaldehyde in γ irradiated 1 mM $ZnSO_4$ solutions containing 0.1 M methanol. Therefore, we conclude that the fast reaction 9 we have observed between CH_2OH and Zn^+ does not reduce Zn^+, but rather Zn^{2+} or $ZnRH^+$ is produced. If $ZnRH^+$ is formed, we expect it to be unstable (zinc alkyl compounds react with water)[19] and decompose to Zn^{2+} and RH_2 in a way similar to the decomposition reported for $CdRH^+$.[6h] Baxendale and Dixon also measured in their $ZnSO_4$–CH_3OH solution $G(H_2) = 1.57$, considerably greater than $G_H + G_{H_2} = 1.05$. One source of additional H_2 is reaction 7 followed by (17).

$$Zn^0 + 2H_2O \rightarrow H_2 + Zn^{2+} + 2OH^- \qquad (17)$$

Some H_2 must also come from reaction of e_{aq}^- + H^+, since $ZnSO_4$ solutions may be slightly acidic and if Zn^0 accumulates so must H^+.

Since electron transfer reactions of H are generally much slower than the corresponding e_{aq}^- reaction,[9,10] the rapid rate of reaction 10 suggests this does not involve direct electron transfer from H to Zn^+. Only the most electropositive elements form saline hydrides,[20] suggesting direct electron transfer from Zn^+ to H is also unlikely. ZnH^+ is the most likely product of (10) and maybe an intermediate in (17). ZnH^+ may react with H^+ or H_2O to yield Zn^{2+} + H_2. If Zn^0 were an intermediate in this reaction, it might react to yield e_{aq}^-, but this would mean reaction 7 is reversible, since e_{aq}^- reacts rapidly with Zn^{2+}. We found no evidence for this and estimate $k_7 > 10^7$, assuming Zn^0 remains atomically dispersed.

The overall reaction of Zn^0 with water is slow, and once Zn^0 aggregates form, they react with H_2O or 1 mM H^+ only in minutes or longer. However, since 1 mM $HClO_4$ reduces the turbidity formed, and since turbidity forms in seconds, we conclude that atomic Zn^0 reacts with H^+ in seconds or less. Thus, in 0.2 M $ZnSO_4$ plus 0.02 M 2-propanol, both at pH 3 and 5.5 (pH's before pulsing), a single 40-ns pulse irradiation produced no light scattering, but 30 pulses in 2 s produced 32% scatter in the acid and 50% in the near neutral. Turbidity reached a maximum in a few seconds. In this experiment 1 mM $HClO_4$ had very little effect on the initial $[Zn^+]$ or its decay. Treating light scattering as if it were absorbance, the turbidity partially decayed, after attaining a maximum, from 0.32 to 0.21 ($\tau_{1/2}$ = 1.5 s) at pH 5.5 and from 0.17 to 0.09 ($\tau_{1/2}$ = 2.7 s) at pH 3 and then remained constant for at least 1 min. The decay may correspond to the formation of larger Zn^0 particles, which are fewer in number and scatter less light.

Acknowledgment. We thank Don Ficht, Joseph Becker, and Lee Rawson for consistently excellent operation of the electron Linac. We are also grateful to Patricia Walsh and Robert Clarke for invaluable assistance.

References and Notes

(1) Work performed under the auspices of the U.S. Energy Research and Development Administration.
(2) On leave from the Department of Physical Chemistry, The Hebrew University of Jerusalem, Jerusalem, Israel.
(3) E. Peled and G. Czapski, *J. Phys. Chem.*, **74**, 2903 (1970).
(4) See, for example, "Hydrogen Energy", Parts A and B, T. N. Teziroglu, Ed., Plenum Press, New York, N.Y., 1975.
(5) (a) G. V. Buxton and R. M. Sellers, *J. Chem. Soc., Faraday Trans. 1*, **71**, 558 (1975); (b) J. H. Baxendale, E. M. Fielden, and J. P. Keene, *Proc. R. Soc. London, Ser. A*, **286**, 320 (1965); (c) D. Meyerstein and W. A. Mulac, *J. Phys. Chem.*, **72**, 784 (1968); **73**, 1091 (1969); (d) G. V. Buxton, F. Dainton, and D. R. McCracken, *J. Chem. Soc., Faraday Trans. 1*, **69**, 243 (1973); (e) G. V. Buxton, R. M. Sellers, and D. R. McCracken, *ibid.*, **72**, 1464 (1976).
(6) (a) M. Kelm, J. Lilie, A. Henglein, and E. Janata, *J. Phys. Chem.*, **78**, 882 (1974); (b) D. Meyerstein and W. A. Mulac, *Inorg. Chem.*, **9**, 1762 (1970); (c) J. H. Baxendale and R. S. Dixon, *Proc. Chem. Soc.*, 148 (1963); (d) M. Faraggi and J. Desalos, *Int. J. Radiat. Phys. Chem.*, **1**, 335 (1969); (e) J. H. Baxendale and R. S. Dixon, *Z. Phys. Chem. (Frankfurt am Main)*, **43**, 161 (1964); (f) P. S. Rao and E. Hayon, *J. Phys. Chem.*, **79**, 865 (1975); (g) A. Barkatt and J. Rabani, *ibid.*, **79**, 1359 (1975); (h) M. Kelm, J. Lilie, and A. Henglein, *J. Chem. Soc., Faraday Trans. 1*, **71**, 1132 (1975).
(7) M. S. Matheson and L. M. Dorfman, "Pulse Radiolysis", M.I.T. Press, Cambridge, Mass., 1969, Chapter 3.
(8) E. J. Hart and M. Anbar, "The Hydrated Electron", Wiley-Interscience, New York, N.Y., 1970, Chapter IX.
(9) M. Anbar, M. Bambenek, and A. B. Ross, *Natl. Stand. Ref. Data Ser., Natl. Bur. Stand.*, **No.** 43 (1973).
(10) M. Anbar, M. Bambenek, and A. B. Ross, *Natl. Stand. Ref. Data Ser., Natl. Bur. Stand.*, **No. 51** (1975).
(11) L. M. Dorfman and G. E. Adams, *Natl. Stand. Ref. Data Ser., Natl. Bur. Stand.*, **No.** 46 (1973).
(12) K.-D. Asmus, M. Mockel, and A. Henglein, *J. Phys. Chem.*, **77**, 1218 (1973).
(13) K. Schmidt, Argonne National Laboratory Reports ANL 7199 (April 1966) and ANL 7693 (March 1970).
(14) C. D. Jonah, private communication.
(15) (a) J. Rabani and S. O. Nielsen, *J. Phys. Chem.*, **73**, 3736 (1969); (b) D. Behar, G. Czapski, L. M. Dorfman, J. Rabani, and H. A. Schwarz, *J. Phys. Chem.*, **74**, 3209 (1970).
(16) C. J. Hochanadel, *J. Phys. Chem.*, **56**, 587 (1952).
(17) M. Simic, P. Neta, and E. Hayon, *J. Phys. Chem.*, **73**, 3794 (1969).
(18) J. D. Backhurst, G. R. A. Johnson, G. Scholes, and J. Weiss, *Nature (London)*, **183**, 176 (1959).
(19) F. A. Cotton and G. Wilkinson, "Advanced Inorganic Chemistry", Interscience, New York, N.Y., 1962, p 479.
(20) See, for example, T. Moeller, "Inorganic Chemistry", Wiley, London, 1952.

A Pulse Radiolysis Study of Aqueous Benzene Solutions[1]

S. Gordon,* K. H. Schmidt, and Edwin J. Hart

Chemistry Division, Argonne National Laboratory, Argonne, Illinois 60439 *(Received August 5, 1976)*

Publication costs assisted by Argonne National Laboratory

The reaction of the hydrated electron, the H atom, and the OH radical with benzene in aqueous solution, and the decay of the reaction products, have been studied and the data evaluated with the aid of computer model calculations. Our results are quantitatively consistent with the assumption that the reaction product of e_{aq}^- and benzene, $C_6H_6^-$, protonates rapidly on a microsecond timescale to form C_6H_7. We show that the spectra of the observed reaction products of e_{aq}^- and H, respectively, with benzene, are identical in shape and peak absorption, and that the two products have the same rate of decay. We measured the following rate constants (B = C_6H_6): $k_{e_{aq}^-+B} = 9 \times 10^6$ M^{-1} s^{-1} ± 5%, $k_{H+B} = 7.2 \times 10^8$ M^{-1} s^{-1} ± 5%, $k_{OH+B} = 7.75 \times 10^9$ M^{-1} s^{-1} ± 5%, $k_{BH+BH} = 8.7 \times 10^8$ M^{-1} s^{-1} ± 15%, $k_{BOH+BOH} = 4.6 \times 10^8$ M^{-1} s^{-1} ± 10%, with $\epsilon_{BH}^{312} = 3550 \pm 5\%$ and $\epsilon_{BOH}^{312} = 2100 \pm 5\%$. Reaction rates of e_{aq}^-, H, and OH with *tert*-butyl alcohol were also measured.

Introduction

Although the hydrated electron (e_{aq}^-) reacts with benzene in aqueous solution, no evidence for the transitory negative ion of benzene (B^-) has ever been observed in water or even in alcohols. Recently, however, an absorption band with a λ_{max} at 312 nm resulting from the pulse radiolysis of (0.35–1.01) × 10^{-2} M benzene in aqueous 2 M *tert*-butyl alcohol was assigned to B^-.[2] These authors (Marketos et al.) state that "our results do not conclusively prove the existence and reaction of B^-, but are entirely consistent with it." Arguments given in support of their assignment are the following: (a) The growing in of the

spectrum of B^- agreed "in rate" with the rate of disappearance of the e_{aq}^- spectrum. (b) There is no two-stage formation of C_6H_7. (c) If the assumption is made that protonation is so fast that B^- is not observed, then only 35–40% of the absorption expected (assuming it all due to BH and using the authors' value of the absorptivity for BH) is obtained. (d) The decay of an absorption of which 25% was due to the H and OH adducts and 75% attributed to B^- was twice as fast as that for the absorption where the H and OH adducts are the major species. (e) B^- has an absorption spectrum which differs with respect to shape and absorptivity from C_6H_7, although λ_{max} is essentially the same.

Since rapid protonation of B^- would also form C_6H_7 in an apparent one-stage process concurrent with the disappearance of e_{aq}^- (arguments a and b), our new experiments deal primarily with the quantitative aspects of arguments (c), (d), and (e) which provide the major support for the B^- assignment of the observed absorption. We confirm their findings that less C_6H_7 is formed in neutral and alkaline 2 M *tert*-butyl alcohol solutions than in acid solutions. However, after corrections are made for the reactions of e_{aq}^- and H with *tert*-butyl alcohol, as well as new determinations of the absorptivities of the transient species observed, the need for B^- vanishes.

Experimental Section

1. *Materials.* Zone refined 99.999% benzene (Litton Chemical Co., Inc.), reagent grade *tert*-butyl alcohol (Fisher and Mallinckrodt), and perchloric acid (Baker Analyzed Reagent 71.3%) were used without further purification. The Fisher *tert*-butyl alcohol, crystalline at room temperature, was much less reactive with e_{aq}^- than the Mallinckrodt product. However, successive fractionations of the Fisher product failed to diminish its reactivity. Nitrous oxide (Matheson Gas Products) was frozen out with liquid N_2, evacuated to remove noncondensables, refrozen, and repumped. Saturated solutions of this product were stored as air-free solutions in 100-ml syringes. Sodium hydroxide solutions were prepared from 20 M NaOH from which most of the Na_2CO_3 had precipitated (Baker Analyzed Reagent).

2. *Solutions.* Oxygen-free benzene solutions were prepared from triply distilled water at the desired concentrations and pH's by the mixing and injecting techniques previously described.[3,4] The O_2 concentration of the solutions was usually less than 10^{-6} M determined by gas chromatography. The benzene concentration was determined spectrophotometrically using $\epsilon^{264} = 180$ M cm^{-1}.[4] Wherever possible the measurement was made on the benzene solution after it had been transferred to the irradiation cell. Because C_6H_6 is volatile, serious errors in the C_6H_6 concentration may result unless care is exercised in the transfer and measurement of these solutions. Small volumes of stock oxygen-free solutions of 1 M NaOH, 2 M $HClO_4$, and 0.025 M N_2O were injected into the 100-ml syringes containing the benzene solutions. This procedure minimized impurity problems resulting from the preparation of the individual solutions when pH and other solution parameters were used. The various types of solutions used in our experiments are listed in Table I.

3. *Irradiation and Dosimetry.* The irradiation cells used have been previously described[5] (insert A of Figure IX.3, ref 5). These were irradiated from the side with the analyzing light going through the cell at right angles to the electron beam. The optical pathlength was 5 cm. The pulsed electron source used was an L band linear accelerator. The electron gun was gated to give pulses of electrons varying from 4 ns (~18 MeV) to 3 μs (12 MeV).

TABLE I: Solutions Used for the Experiments (Concentration and pH Values are Nominal)

Type (main radicals)	pH[a]	$[C_6H_6]$,[b] 10^{-3} M	[*t*-Bu-OH],[b] M	$[N_2O]$, 10^{-3} M	He
OH	7	0.25		1.0	(Degassed)
e_{aq}^-, OH	11	10			Satd
e_{aq}^-	11	10	2.0		Satd
H, OH	2	0.5,[c] 10[d]			Satd
H	2	0.5,[c] 10[d]	2.0		Satd

[a] Adjusted with $HClO_4$ for acid solutions and with NaOH for alkaline solutions. [b] Nominal concentration normally used unless stated differently in the text. [c] Used for measuring radical [C_6H_7 and/or C_6H_7O] buildup. [d] Used for measuring radical decay.

The irradiation cell was placed in a collimator and Faraday cup assembly described in a previous publication.[6] For the rate constant studies, doses between 0.6 and 6 krads were used. Transient spectra covering approximately 180 nm were obtained with single pulses of electrons using our streak camera-TV system.[7,8] For the spectral data, 0.25–1 μs pulses at doses of 6–20 krads were used. For dosimetry, the charge collected by the Faraday cup was measured by means of an integrating circuit consisting of a current-to-voltage amplifier, a voltage-to-frequency converter, and a counter. The calibration factor (dose/charge) was determined by two methods: (1) absorption of e_{aq}^- at 650 nm[9] and (2) absorption by $(CNS)_2^-$ at 470 nm.[10] In the latter case, we added N_2O to convert e_{aq}^- to OH. Using $G(e_{aq}^-) = 2.83$, $\epsilon_{e_{aq}^-}^{650} = 15\,780$,[6] $G(OH) = 2.75$,[11] $\epsilon_{(CNS)_2^-} = 7100$,[10] we obtained agreement within 1% between the two methods.

4. *Evaluation of Transients.* The transient absorption signals, measured by the photomultiplier method and obtained in the form of oscilloscope pictures, were scanned by our optical line follower interfaced with a Sigma 5 computer. First-order rates of formation or decay or second-order decay rate constants (as k/ϵ), respectively, were determined by means of a non-linear least-squares fitting program developed by C. Jonah at this laboratory.

In later experiments, the transient signals were stored and digitized in a Biomation Type 8100 transient recorder and the data directly transferred to the computer. The rate constants were then again determined by the above-mentioned program.

Results and Discussion

Our experiments were guided by the assumed reaction mechanism (B = C_6H_6)

$$e_{aq}^- + B \rightarrow B^- \quad (1)$$

$$\left.\begin{aligned} B^- + H^+ &\rightarrow BH \quad (2a)\\ B^- + H_2O &\rightarrow BH + OH^- \quad (2b)\end{aligned}\right\} \text{rapid protonation}$$

$$H + B \rightarrow BH \quad (3)$$

$$OH + B \rightarrow BOH \quad (4)$$

$$BH + BH \rightarrow \text{products} \quad (5)$$

$$BOH + BOH \rightarrow \text{products} \quad (6)$$

We redetermined the rate constants for these reactions, the absorptivity values for BH and BOH, and examined the experimental data with respect to their consistency with the above mechanism, i.e., the assumption that B^- protonates too rapidly (reactions 2a and 2b) to be observable on a microsecond time scale.

Five groups of experiments were carried out:

(1) Measurements with the streak camera-TV system to compare the spectra of BH and "B^-".

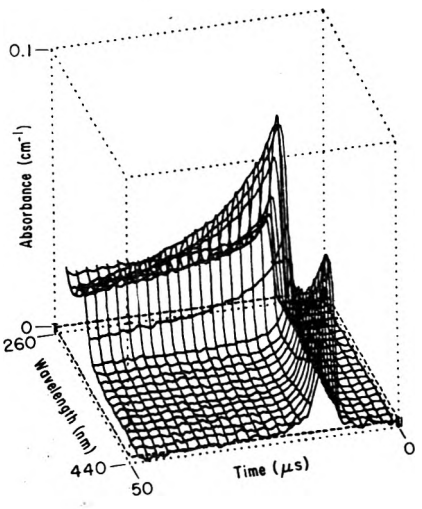

Figure 1. Three-dimensional computer plot of transient spectrum representing the reaction of e_{aq}^- with benzene (1.5×10^{-2} M C_6H_6, 10^{-3} M NaOH, 2 M *tert*-butyl alcohol, He saturated; pulse: 1 μs, ~9 krads).

(2) Rate constant determinations for the reactions 7–9 (C_4H_9OH = *tert*-butyl alcohol)

$$e_{aq}^- + C_4H_9OH \rightarrow \text{products} \quad (7)$$

$$H + C_4H_9OH \rightarrow C_4H_9O + H_2 \quad (8)$$

$$OH + C_4H_9OH \rightarrow C_4H_9O + H_2O \quad (9)$$

(3) Experiments to determine k_1 and k_3 through k_6.

(4) Experiments to determine ϵ_{BH} and ϵ_{BOH}, and to decide if the observed buildup of the absorption signal under various conditions is quantitatively consistent with these values and with the measured rate constants k_1, k_3, and k_4.

(5) Experiments to test if the amplitude and decay rate of the absorption signal observed under various conditions can be quantitatively described on the basis of our measured values of ϵ_{BH}, ϵ_{BOH}, k_5, and k_6. The latter two groups of experiments were evaluated with the aid of computer model calculations.

The results of the five groups of experiments will be described and discussed in the following sections. All error limits given represent 90% probability errors including random and possible systematic errors.

A. *Streak Camera Experiments.* With the streak camera technique, transient spectra were recorded for solutions of type (e_{aq}^-), (H), and (OH) (Table I), characterizing the reactions of e_{aq}^-, H, and OH, respectively, with benzene, and for solutions containing no benzene. Figure 1 shows a three-dimensional computer plot of a transient spectrum obtained with a 19-krad pulse in a type (e_{aq}^-) solution containing 0.015 M benzene. The figure illustrates the fast decaying e_{aq}^- peak at the longer wavelength and the slowly decaying "B^-" peak at about 312 nm. The benzene-free solution (not shown) displays only the e_{aq}^- absorption plus a small long-lived absorption component increasing with shorter wavelength (at 265 nm, about 10% of the C_6H_7 peak). The latter component is presumably due to radiation products of *tert*-butyl alcohol. Figure 2 shows the corresponding plot in acid solution (type (H)). The dose was 9.6 krads, and the benzene concentration 2.5×10^{-3} M. In this figure, the e_{aq}^- peak is absent. The benzene-free solution (not depicted) shows again only a small absorption signal increasing with shorter wavelength, with an amplitude of about 6% of the C_6H_7 peak at 265 nm. Figure 3 is the three-dimensional representation of the OH reaction with benzene. The solution was 1.2×10^{-2} M benzene, N_2O-saturated. The figure

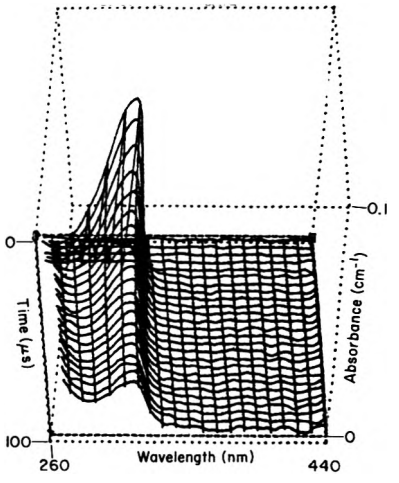

Figure 2. Three-dimensional computer plot of transient spectrum representing the reaction of H with benzene (2.5×10^{-3} M C_6H_6, 10^{-2} M $HClO_4$, 2 M *tert*-butyl alcohol, He saturated; pulse: 0.5 μs, 5.6 krads).

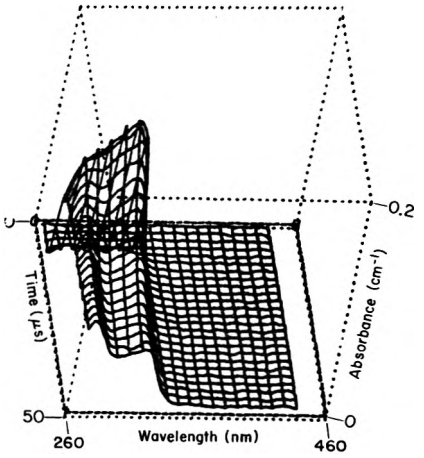

Figure 3. Three-dimensional computer plot of transient spectrum representing the reaction of OH with benzene (1.2×10^{-2} M C_6H_6, N_2O saturated; pulse: 0.25 μs, 5.4 krads).

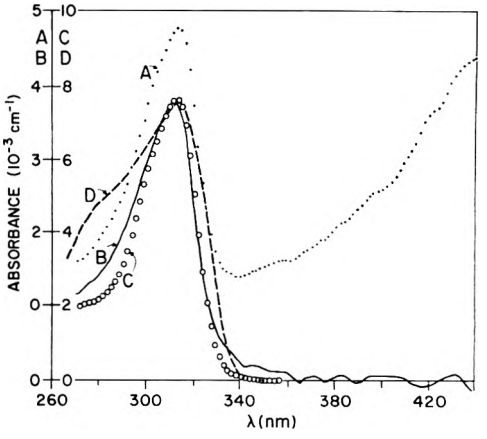

Figure 4. Comparison of the uncorrected spectrum of "B^-", BH, and BOH. (A) Same solution as in Figure 1, pulse: 9.7 krads, 0.6 μs after the pulse; (B) like curve A, but 11 μs after the pulse ("B^-" spectrum); (C) same solution as in Figure 2, 9.7 krads, 6 μs after the pulse (BH spectrum); (D) from experiment shown in Figure 3, 3 μs after pulse (BOH spectrum).

shows the C_6H_7O peak at 313 nm and a developing second peak below 275 nm (lower left corner or figure) which we tentatively ascribe to the $(BOH)_2$ absorption.[2] Figure 4 compares the spectra of "B^-" (curve B), BH (curve C), and BOH (curve D) (uncorrected for other products). The pulse doses used for these experiments were 9.1, 9.7 and 5.4 krads, respectively. Curve B was measured after the

TABLE II: Experimental Conditions for Measuring Various Rate Constants, and Results

Rate constant	Type of soln (main radicals)	Dose per pulse, krad	$[C_6H_6]$, 10^{-3} M	Species obsd	Wavelength nm	k(measd), M^{-1} s^{-1}
k_1	(e_{aq}^-, OH)	0.6	0.9–13.6	e_{aq}^-	600	$9.0 \times 10^6 \pm 5\%$
k_1'	(e_{aq}^-)	0.56	2.7–35	e_{aq}^-	600	$7.2 \times 10^6 \pm 10\%$
k_3	(H)	3.3	0.4–9.7	C_6H_7	312	$7.2 \times 10^8 \pm 5\%$
k_4	(OH)	1.4	0.035–0.5	C_6H_6OH	312	$7.75 \times 10^9 \pm 5\%$
k_5	(H)	0.8–5.1	3.2	C_6H_7	312	$8.7 \times 10^8 \pm 15\%$
k_6	(OH)	0.73–5.9	8.6	C_6H_6OH	312	$4.6 \times 10^8 \pm 10\%$[b]

[a] See Table I. [b] Rate constant corrected for contribution of C_6H_7 to decay signal.

decay of the e_{aq}^- absorption. The corresponding spectrum observed directly after the pulse, with a strong e_{aq}^- component, is represented by curve A. Curves B and C are identical within experimental errors except for a small deviation at the short wavelength end. Since the decay in this wavelength region is much slower than at the peak at 312 nm, as demonstrated by the three-dimensional representations, we ascribe the deviation to other products, an assumption which is also supported by the streak spectra of the blanks. We want to note at this point that we did not observe the increase of the BH absorption below 290 nm reported in ref 12 and quoted in ref 2 as a feature distinguishing it from the spectrum of "B^-". However, Sauer and Ward[12] based on similar arguments ascribe this increase to "either an absorption due to a product or the presence of another transient".

The practical identity of the "B^-" spectrum with the BH spectrum strongly indicates the identity of the respective species, and we, therefore, felt justified to proceed under this working hypothesis.

B. *Reaction Rates of the Radical Species with tert-Butyl Alcohol.* Since *tert*-butyl alcohol was used as an OH scavenger in the solutions of the types (e_{aq}^-) and (H), we considered it important to obtain reliable values for k_7, k_8, and k_9, as these constants were required for our computer model calculations.

k_7 was determined by observing the e_{aq}^- decay at 600 nm in a type (e_{aq}^-) solution (Table I) and plotting the decay rate vs. the *tert*-butyl alcohol concentration (0.5–2 M). We found that the value obtained for k_7 varied strongly not only with the brand of *tert*-butyl alcohol, but even with the individual bottle of the alcohol. Values ranged from $k_7 = 1.77 \times 10^4$ M^{-1} s^{-1} for a bottle of Fisher brand alcohol to $k_7 = 1.26 \times 10^5$ M^{-1} s^{-1} for a bottle of Mallinckrodt brand. From this we conclude that the measured rate constant essentially represents reactions of e_{aq}^- with impurities in the alcohol.

Our values are much lower than the only available literature value of $k_7 = 10^8$ M^{-1} s^{-1}.[13]

Whenever k_7 was needed later for the evaluation of an experiment, we used a value determined on the same day using the same batch of *tert*-butyl alcohol.

k_8 was determined by measuring the rate of formation of C_6H_7 at 312 nm as a function of *tert*-butyl alcohol concentration (0.5–2 M). The value of k_8 obtained by this method was in good agreement with one derived from a Stern–Volmer plot using the peak concentrations of C_6H_7. The average value is $k_8 = 1.45 \times 10^5$ M^{-1} s^{-1} ± 15%. Published values range from 0.8 to 1.7×10^5 M^{-1} s^{-1}.[14]

k_9 was determined by direct observation of the OH decay at 280 nm in a type (OH) solution (see Table I) as a function of [*t*-BuOH] at concentration of 0.5–2 M. Our rate constant of $k_9 = 7.55 \times 10^8$ M^{-1} s^{-1} ± 10% represents the only absolute determination. It is higher than the published values ranging from 4.2 to 6.3×10^8 M^{-1} s^{-1}.[15]

For determination of k_8 and k_9, we used the batch of *tert*-butyl alcohol with the lowest apparent e_{aq}^- rate constant and therefore, presumably, the purest alcohol available to us. However, previous experiments with other brands of *tert*-butyl alcohol had indicated little or no dependence of k_8 and k_9 on the brand of alcohol.

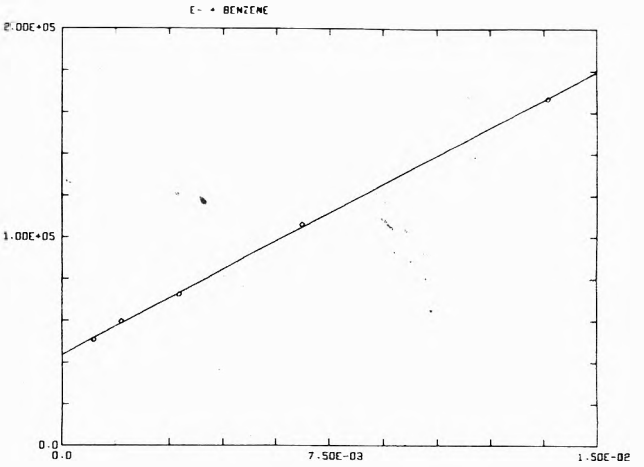

Figure 5. Plot of first-order decay rate of e_{aq}^- (s^{-1}) vs. benzene concentration (M), with best fitting straight line (aqueous benzene, 10^{-3} M NaOH, He saturated; pulse: 4 ns, 0.6 krad).

C. *Experiments to Determine k_1 and k_3–k_6.* Table II gives a summary of the experimental conditions used for measuring these rate constants, and the results obtained. k_1 was measured first in the absence of *tert*-butyl alcohol, the benzene itself serving as the OH scavenger. Figure 5 shows a computer plot of the measured pseudo-first-order decay rate of e_{aq}^- vs. $[C_6H_6]$, including the best fitting straight line. The intercept is caused by the reactions of e_{aq}^- with BOH and impurities, and a small second-order component. A similar plot, although with a greater intercept, was obtained for a solution also containing 2 M *tert*-butyl alcohol. However, the rate constant, k_1' was 20% smaller than k_1 (second line in Table II). This is presumably due to the partial solvation of the benzene molecules in *tert*-butyl alcohol.[16] Our value compares with previously reported values ranging from 0.7 to 1.4×10^7 M^{-1} s^{-1} (compiled in ref 2). The rate constants k_3 and k_4 were determined by plotting the first-order rate of formation of the H and OH adduct, respectively, vs. $[C_6H_6]$. The plot for the OH adduct is shown in Figure 6. Previously reported values for k_3 range from 5.3 to 11×10^8 M^{-1} s^{-1}.[15] k_5 and k_6 were calculated using the values k/ϵ obtained for several different pulse doses by means of the non-linear least-squares fitting program. Since k_6/ϵ decreased slightly with increasing dose, possibly due to a small pseudo-first-order component, the value extrapolated for infinite dose was assumed to be the true second-order decay constant. Furthermore, a correction of about 16% for the contribution of C_6H_7 to the decay signal, obtained by means of a computer model calculation, was applied to obtain the value listed in Table II. We used $\epsilon^{312}_{C_6H_7} = 3550$ and $\epsilon^{312}_{C_6H_7O^-} = 2100$ (see below).

Taking into account the different values of $\epsilon_{C_6H_7}$ used by various authors, our k_5 is in good agreement with the values reported in ref 2 ($k_5 = 1.25 \pm 0.22 \times 10^9$ M^{-1} s^{-1},

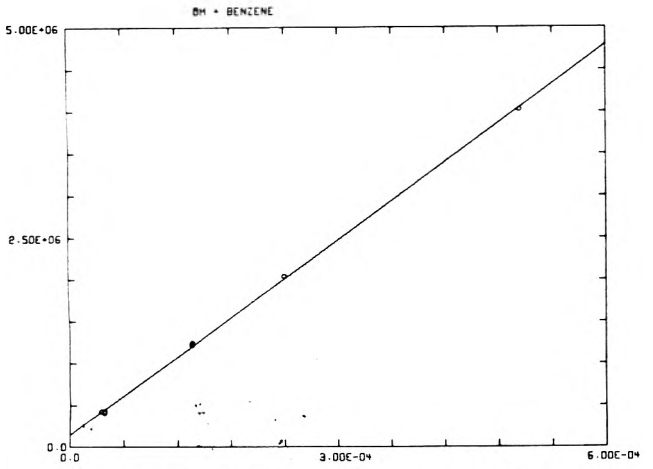

Figure 6. Plot of first-order rate of formation of C_6H_7O (s^{-1}) vs. benzene concentration (M) (aqueous benzene, 10^{-3} M N_2O; pulse: 10 ns, 1.4 krads).

$\epsilon^{311}_{C_6H_7}$ = 5350) and in ref 4 ($k_5 = 0.8 \pm 0.15 \times 10^9$ M^{-1} s^{-1}, $\epsilon^{311}_{C_6H_7}$ = 3300). On the same basis, the values for k_6 reported in ref 2 ($k_6 = 7.05 \pm 0.35 \times 10^8$ M^{-1} s^{-1}, $\epsilon^{313}_{C_6H_7O}$ = 4700) is 30% lower than our value. We have no explanation for this discrepancy.

D. *Computer Model Calculations.* The computer model calculations which were required to evaluate the last two groups of experiments were carried out on our Sigma 5 computer (Xerox Corp.) by means of slightly modified version (WR22) of our kinetic program WR20.[17]

For the reactions 1 and 3–9, we used our own rate constants. Reactions 2a and 2b were assumed to be instantaneous, i.e., the formation of BH from e_{aq}^- was written as

$$e_{aq}^- + B \rightarrow BH + OH^- \quad (1a)$$

and rate constant k_1 was used. Additional reactions taken into account were

$$e_{aq}^- + N_2O \rightarrow N_2 + OH + OH^- \quad k_{10} = 9.1 \times 10^9 \ M^{-1} s^{-1}\ ^{18} \quad (10)$$

$$e_{aq}^- + OH \rightarrow OH^- \quad k_{11} = 3 \times 10^{10} \ M^{-1} s \quad (11)$$

$$e_{aq}^- + e_{aq}^- \rightarrow H_2 + 2OH \quad k_{12} = 5 \times 10^9 \ M^{-1} s^{-1} \quad (12)$$

$$H + OH \rightarrow H_2O \quad k_{13} = 2 \times 10^{10} \ M^{-1} s^{-1} \quad (13)$$

$$H + H \rightarrow H_2 \quad k_{14} = 1 \times 10^{10} \ M^{-1} s^{-1} \quad (14)$$

$$OH + OH \rightarrow H_2O_2 \quad k_{15} = 4.5 \times 10^9 \ M^{-1} s^{-1} \quad (15)$$

$$e_{aq}^- + H^+ \rightarrow H \quad k_{16} = 2.2 \times 10^{10} \ M^{-1} s^{-1} \quad (16)$$

k_{11}–k_{16} are presumably "best" values taken from ref 14, 15, and 19. These values are not critical for our calculations. The G values (in particles/100 eV) used were: $G_{e_{aq}^-}$ = 2.85,[6] G_{OH} = 2.75,[11] and G_H = 0.55[11] for pH 7, $G_{e_{aq}^-} + G_H$ = 3.6 and G_{OH} = 2.85 for pH 2 (using the pH dependence of G values as summarized in ref 20).

For some of the experiments, the optical absorption signal (percent absorption vs. time) was calculated and compared with the measured oscilloscope trace. For later experiments, computer-produced plots of measured absorbance vs. time were compared with calculated absorbance curves. In all calculations, the dose actually used in the corresponding experiment was entered.

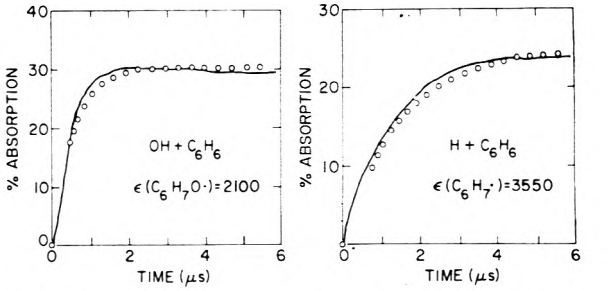

Figure 7. Measured (solid lines) and calculated (circles) absorption signals at 312 nm representing the formation of BOH (left plot) and BH (right plot). Solutions: type (OH) and (H), respectively, of Table I. Pulse: 40 ns, 2.7 krads. Parameters adjusted: $\epsilon_{C_6H_7}$ and $\epsilon_{C_6H_7O}$.

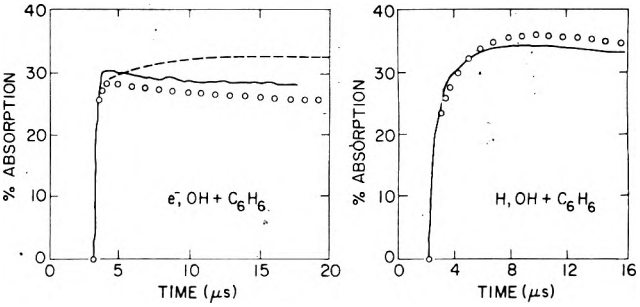

Figure 8. Measured (solid lines) and calculated (circles) absorption signals at 312 nm representing the combined formation of "B⁻" and BOH (left plot) and BH and BOH (right plot). Solutions: type (e_{aq}^-, OH) and (H, OH), respectively, of Table I. Pulse: 40 ns, approximately 2.8 krads. Parameters adjusted: k_{17} and k_{18} (left plot only). Dashed line: calculated without reactions 17 and 18.

E. *Experiments to Study the Buildup of "B⁻", BH, and BOH.* Figure 7 illustrates the results of experiments to determine ϵ_{BOH} and ϵ_{BH}. Solid lines represent the experimental curves; circles represent the computed curves. The left curve was obtained with a solution of type (OH) (Table I) and a 40-ns pulse of 2.7 krads; the right curve was obtained with a solution of type (H) at approximately the same dose. The wavelength was 312 nm in both cases. The parameters fitted were ϵ_{BOH} and ϵ_{BH}. Other parameters were *not* adjusted. We obtained ϵ^{312}_{BOH} = 2100 M^{-1} cm^{-1} and ϵ^{312}_{BH} = 3550 M^{-1} cm^{-1}. While the latter value is in fair agreement with the one reported in ref 4 (3300), it is much smaller than the one measured by Marketos et al.[2] (5350). Our ϵ_{BOH} is much lower than the earlier reported values (4700 and 3500 M^{-1} cm^{-1}).[2] To test our results we irradiated a solution of type (H, OH) with a similar dose, thereby producing about equal concentrations of BH and BOH. The calculated curve, based on our ϵ values, is in good agreement with the experimental curve (Figure 8, right plot). The left plot of Figure 8 represents the corresponding experiment in alkaline solution (type (e_{aq}^-, OH)), producing both "B⁻" and BOH. The dashed line was calculated using the reactions and parameters mentioned so far, plus a value of $\epsilon^{312}_{e_{aq}^-}$ = 770 measured by Michael and Hart[21] and approximately corresponding to other published values.[20] Identity of "B⁻" and BH was assumed for the calculation.

The dashed curve differs in shape from the experimental curve. However, if one makes the reasonable assumption that e_{aq}^- also reacts with the radicals BH and BOH:

$$e_{aq}^- + BH \rightarrow \text{products} \quad (17)$$

$$e_{aq}^- + BOH \rightarrow \text{products} \quad (18)$$

one obtains the correct signal shape by using $k_{17} = k_{18}$ =

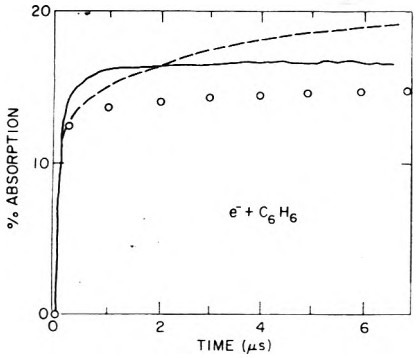

Figure 9. Measured (solid line) and calculated (circles) absorption signals at 312 nm representing the formation of "B^-". Solution: type (e_{aq}^-) of Table I. Pulse: 40 ns, 2.6 krads. Dashed line: calculated without reactions 17 and 18. Parameters adjusted: none.

6×10^9 M^{-1} s^{-1} (circles). This value was used in all subsequent calculations.

As a further test, an experimental curve obtained with a solution of type (e_{aq}^-) was compared with calculated curves in Figure 9. The dose was 2.6 krads. Again, the dashed line was calculated excluding reactions 17 and 18, the circles include these reactions. The agreement is only fair, but one has to consider that more than half of the hydrated electrons react with the *tert*-butyl alcohol which introduces a degree of uncertainty.

E. *Experiments to Study the Decay of "B⁻", BH, and BOH.* The results obtained so far are consistent with the assumption that "B^-" and BH are identical. Our last group of experiments was performed to compare the second-order decay rate constants of the two species. Preliminary experiments using solutions of type (e_{aq}^-) and (H) (Table I) seemed to confirm the result of Marketos et al.[2] that "B^-" decays faster than BH. However, since reactions of BH or "B^-" with radical products of *tert*-butyl alcohol very probably affect the decay rate of the species in question, we compared the decay rates in the corresponding solutions containing no *tert*-butyl alcohol, namely, solutions of the type (e_{aq}^-, OH) and (H, OH). The result is shown in Figure 10. The dose was about 1.7 krads, the pulse length 10 ns. The solid lines again represent the experimental curves. The dashed lines were calculated using all reactions and parameters discussed so far, including reactions 17 and 18. Whereas there is excellent agreement between the measured and calculated initial absorbance values (no parameter was adjusted), again confirming the consistency of our values for ϵ_{BH} and ϵ_{BOH}, the calculated decay rates are lower than the experimental ones. However, one can obtain good agreement for both experiments by adding the mixed decay reaction

$$BH + BOH \rightarrow \text{products} \qquad (19)$$

assuming a value of $k_{19} = 6 \times 10^9$ M^{-1} s^{-1}, lying between k_5 and k_6 (circles).

An estimate shows that in the two experiments, 2/3 of the initial signal amplitude is due to BH or "B^-", respectively, and that reaction 5 contributes about 60% to the initial signal decay rate. The comparison is therefore sufficiently sensitive to a possible difference between k_5 and $k_{(B^-+B^-)}$, and we regard this result as a further confirmation for the identity of "B^-" and BH.

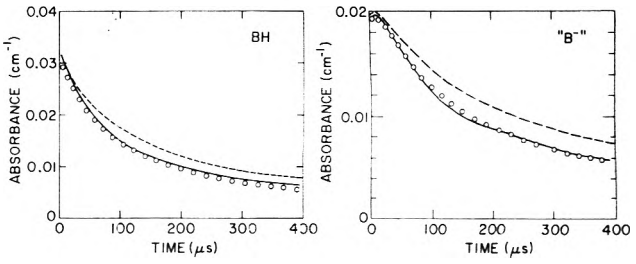

Figure 10. Comparison of the combined decay of BH and BOH (left plot) with that of "B^-" and BOH (right plot). Solutions: type (H, OH) and (e_{aq}^-, OH), respectively, of Table I. Pulse: 10 ns, 1.7 krads. Solid line: experimental curves measured at 312 nm. Calculated using all reactions except reaction 19 (dashed line). Calculated including reaction 19 (circles), with k_{19} tentatively adjusted to 6×10^8 M^{-1} s^{-1}.

F. *Relationship to Other Results.* Jonah[22] has studied solutions of benzene in methanol and ethanol on the picosecond time scale. He observed a prompt transient whose decay was unaffected by increasing the acid concentration. Trifunac[23] studied the ESR signal from pulsed aqueous benzene and found no signal attributable to B^- on the microsecond time scale. Both these results are consistent with our conclusions.

Acknowledgment. We thank W. A. Mulac for his technical assistance with the photomultiplier experiments, and Patricia D. Walsh and Robert M. Clarke for the preparation of the samples and the chemical analyses. We furthermore thank Charles D. Jonah for the use of his computer program, Donald T. Ficht, Lee R. Rawson, and Benno J. Naderer for operating the linac, and Steve G. Petrek for building the dosimeter circuitry.

References and Notes

(1) Work performed under the auspices of the USERDA.
(2) D. G. Marketos, A. Marketou-Mantaka, and G. Stein, *J. Phys. Chem.*, **78**, 1987 (1974).
(3) E. J. Hart, S. Gordon, and J. K. Thomas, *J. Phys. Chem.*, **68**, 1271 (1964).
(4) B. D. Michael and E. J. Hart, *J. Phys. Chem.*, **74**, 2878 (1970).
(5) E. J. Hart and M. Anbar, "The Hydrated Electron", Wiley-Interscience, New York, N.Y., 1970.
(6) B. D. Michael, E. J. Hart, and K. H. Schmidt, *J. Phys. Chem.*, **75**, 2798 (1971).
(7) S. Gordon, K. H. Schmidt, and J. E. Martin, *Rev. Sci. Instrum.*, **45**, 522 (1974).
(8) K. H. Schmidt, S. Gordon, and W. A. Mulac, *Rev. Sci. Instrum.*, **47**, 356 (1976).
(9) E. J. Hart and E. M. Fielden in "Manual on Radiation Dosimetry", N. W. Holm and R. J. Berry, Ed., Marcel Dekker, New York, N.Y., 1970, pp 331–335.
(10) E. M. Fielden and N. W. Holm in ref 9, pp 288–289.
(11) M. S. Matheson and L. M. Dorfman, "Pulse Radiolysis", M.I.T. Press, Cambridge, Mass., 1969, p 64.
(12) M. C. Sauer and B. Ward, *J. Phys. Chem.*, **71**, 3571 (1967).
(13) V. Gold and J. H. Rolston, *Chem. Commun.* **4**, 208 (1970).
(14) U.S. Department of Commerce, *Natl. Stand. Ref. Data Ser., Natl. Bur. Stand.*, **No. 51** (1975).
(15) U.S. Department of Commerce, *Natl. Stand. Ref. Data Ser., Natl. Bur. Stand.*, **No. 46** (1973).
(16) J. R. Miller, private communication.
(17) K. Schmidt, Argonne National Laboratory Reports, ANL-7199, April, 1966, and ANL-7693, March, 1970.
(18) B. Hickel and K. H. Schmidt, *J. Phys. Chem.*, **74**, 2470 (1970).
(19) U.S. Department of Commerce, *Natl. Stand. Ref. Data Ser., Natl. Bur. Stand.*, **No. 43** (1973).
(20) I. G. Draganic and Z. D. Draganic, "The Radiation Chemistry of Water", Academic Press, New York, N.Y., 1971, p 142.
(21) B. D. Michael and E. J. Hart, unpublished value.
(22) C. Jonah, private communication.
(23) A. Trifunac, private communication.

Low-Temperature Pulse Radiolysis and γ-Irradiated Matrix Studies of Dimer Anions of Olefin Derivatives

Shigeyoshi Arai,* Akira Kira, and Masashi Imamura

The Institute of Physical and Chemical Research, Wako-shi, Saitama 351, Japan *(Received August 16, 1976)*

Publication costs assisted by The Institute of Physical and Chemical Research

Intense IR absorptions were found for irradiated methyltetrahydrofuran solutions of various olefin derivatives using low-temperature pulse radiolysis and γ-irradiated matrix techniques. The compounds investigated were fumaronitrile, maleic anhydride, citraconic anhydride, dimethylmaleic anhydride, methyl vinyl ketone, acrolein, crotononitrile, methacrylonitrile, methyl acrylate, methyl methacrylate, and methyl crotonate. The IR absorptions increased gradually with time in pulse radiolysis and also increased by warming solutions via the γ-irradiated matrix method. The growth was always in parallel with the decay of the anion radical of each compound in both experiments. The IR absorptions, therefore, are concluded to be due to dimer anions produced by reactions of anion radicals with neutral parent molecules. Growth rates were determined from the formation curves of dimer anions. In many cases, IR spectra changed in shape by repeated warming and their peaks shifted to shorter wavelengths. These results are attributed to conformational changes of the dimer anions which occur in warmed solutions. Dimer anions were not observed for acrylamide, methacrylamide, 1,3-butadiene, and styrene, although their anion radicals were produced in irradiated solutions. The electron affinity of a functional group seems to be an important factor for dimer anion formation. Aromatic compounds such as phthalonitrile and phthalic anhydride did not form dimer anions under similar conditions.

Introduction

Cation radicals of aromatic hydrocarbons often react with their neutral parent molecules forming dimer cations. The formation was found first in the ESR study[1] of aromatic hydrocarbon cations prepared chemically using antimony pentachloride as an oxidant and methylene chloride as a solvent. Although several ESR studies[2-4] were published on dimer cations, a number of spectroscopic and kinetic data[5-15] have been compiled in γ-irradiated matrix and pulse radiolysis studies because radiolysis provides an excellent method for the preparation of cations of organic compounds.

Anion radicals of various organic compounds are also prepared easily in radiolysis. In contrast to dimer cations, however, several attempts[5,6,15-17] failed to observe organic dimer anions except for a few cases. An anthracene dimer anion[18] was formed by the dissociative attachment of a mobile electron to dianthracene in a rigid cage of 2-methyltetrahydrofuran (MTHF) at 77 K. The anthracene dimer anion was obviously metastable because it dissociated into anthracene and its anion radical when warmed slightly. An acetonitrile dimer anion[19] was detected using ESR in the upper crystalline phase of γ-irradiated acetonitrile at 77 K.

In the course of the study on radiation-induced polymerization of methyl methacrylate, we found that the dimer anion is produced spontaneously by the reaction between methyl methacrylate and its anion radical. Such dimer anions were observed for many other olefin derivatives. This paper presents their absorption spectra and kinetic behavior obtained from the low-temperature pulse radiolysis and γ-irradiated matrix method. The results provide useful information on the interaction between a charged species and a neutral molecule.

Experimental Section

All chemicals used here were of the purest grade commercially available. MTHF, maleic anhydride, citraconic anhydride (methylmaleic anhydride), acrolein, crotononitrile, methacrylamide, styrene, and phthalonitrile were purchased from Tokyo Kasei Kogyo. Fumaronitrile, methacrylonitrile, methyl acrylate, methyl methacrylate, methyl crotonate, acrylamide, and phthalic anhydride were from Wako Junyaku. Dimethylmaleic anhydride, methyl vinyl ketone, and 1,3-butadiene were from Aldrich Chemical Co., Mitsubishi Kasei Kogyo, and Takachiho Shoji, respectively. MTHF was fractionally distilled over metallic sodium; the middle fraction was stored in vacuo over sodium and potassium alloy. Volatile compounds of the solute chemicals were purified by vacuum distillation after dehydration with anhydrous calcium sulfate. The other chemicals were used without further purification. All sample solutions were prepared on a vacuum line.

The matrix technique used here was the same as described in previous papers.[14,15] A sample solution was sealed in a cell with an optical path of 1.5 mm, and irradiated with γ rays from ^{60}Co at a dose rate of 38 200 rads min^{-1}. The spectrum was measured on a Cary 14 RI. The solution was warmed in a simple way where it was drawn from liquid nitrogen for short time in a dewar vessel.

The procedures and apparatus of the low-temperature pulse radiolysis in our laboratory have been also described in previous papers.[20,21] Electron pulses from a Mitsubishi Van de Graaff accelerator were used at a suitable current in the range up to 200 mA. The accelerating energy was 2.6 MeV and the duration was selected among 0.5, 1, 2, and 5 μs. The low-temperature apparatus was essentially the same as employed in previous studies,[20,21] although newly constructed. The sample solution sealed in a cell was cooled by blowing cold nitrogen gas at a controlled flow rate. An analyzing light beam was passed once through the cell, where the optical path length was 10 mm. The temperature was monitored with a copper–constantan thermocouple attached to the outside of the cell. Temperatures measured preliminarily with thermocouples inserted into the solution and attached to the outside of the cell agreed with each other to within a few degrees.

Results and Discussion

MTHF was used as a solvent in both pulse and matrix experiments; its solution was a viscous liquid at 113 K and rigid glass at 77 K. It is well established[22] that a solute

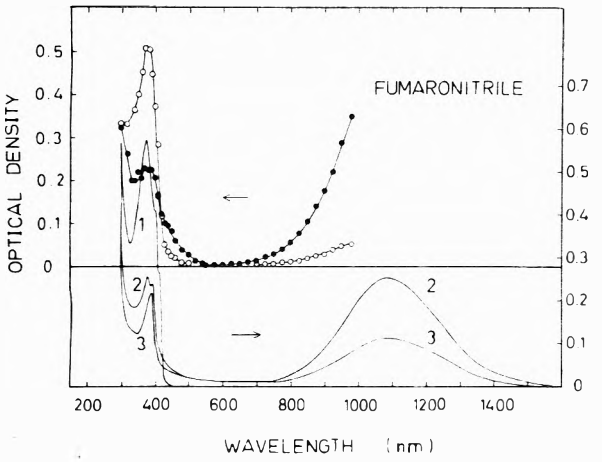

Figure 1. Spectra for irradiated fumaronitrile in MTHF solutions. Pulse radiolysis: 6.9 mol % fumaronitrile was irradiated at 113 K with 1-μs pulses at 100 mA: (circle) 30 μs after the pulse, (solid circle) 800 μs after the pulse. Matrix: 1.4 mol % fumaronitrile was irradiated at 77 K with γ rays to 1.9 × 10^5 rads: (spectrum 1) before warming, (spectrum 2) after warming, (spectrum 3) after warming further.

anion radical is produced in irradiated MTHF by the reaction of a mobile or solvated electron with a solute molecule. Absorption spectra of a number of anion radicals have been obtained successfully with the radiolysis of MTHF solutions at 77 K. Figure 1 shows absorption spectra determined at 30 and 800 μs after the pulse when a MTHF solution of 6.9 mol % fumaronitrile was irradiated at 113 K with electron pulses. The weak part of the early spectrum (500–700 nm) is excluded from the figure to avoid an overlap. Figure 1 also shows absorption spectra of a γ-irradiated solution of 1.4 mol % fumaronitrile before and after warming. The spectrum before warming has no absorption above 450 nm.

In dilute solutions below 0.4 mol % fumaronitrile, the rapid decay of the solvated electron was seen immediately after pulse irradiation at 113 K. The observed decrease of the decay rate with decreasing fumaronitrile concentration indicates that the solvated electron reacts directly with a fumaronitrile molecule. As shown in Figure 1, an intense absorption band with a peak at 380 nm appeared in the early spectrum of the pulse-irradiated solution or in the spectrum before warming the γ-irradiated solution. The 380-nm band was found to grow concurrently with the decay of the solvated electron in the pulse radiolysis of a 0.1 mol % solution. The rapid proton transfer from a solvent molecule to an anion radical does not occur in MTHF. The ion recombination is a slow process in MTHF at 113 K, because a styrene or 1,3-butadiene anion radical has a long lifetime under the same condition, as described later. Therefore, the 380-nm band produced from the solvated electron is assigned to a fumaronitrile anion radical itself. The broad IR band in Figure 1 always increased in parallel with a decrease of the 380-nm band in both pulse radiolysis and matrix experiments. The coincidence between growth and decay is demonstrated directly by oscilloscope traces of absorptions at 980 and 380 nm presented in Figure 2. Thus, the IR absorbing species must be produced from an anion radical of fumaronitrile. Both decay and growth fit a first-order rate law and give pseudo-first-order rate constants in Table I. The growth rate increased with increasing fumaronitrile concentration in dilute solutions below 1 mol %, as shown in Table I. From these results the IR absorbing speces is concluded to be a dimer anion produced by the following reaction

$$M^- + M \rightarrow M_2^- \qquad (1)$$

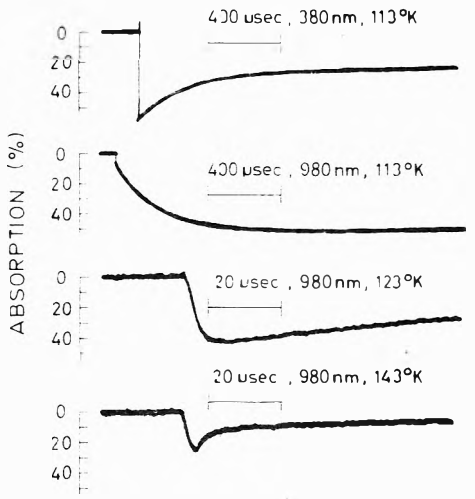

Figure 2. Oscilloscope traces of 380- and 980-nm absorptions at various temperatures. 7.2 mol % fumaronitrile in an MTHF solution was irradiated with 1-μs pulses at 100 mA.

TABLE I: Pseudo-First-Order Rate Constants of the Dimer Anion Formation at 113 K

Compound	Concn, mol %	k[solute],[a] s^{-1}
Fumaronitrile	0.17	4.9×10^3
	0.37	1.2×10^4
	0.77	2.3×10^4
	1.9	2.2×10^4
	6.9	4.2×10^3
	6.9	4.7×10^3 [b]
Maleic anhydride	2.1	5.6×10^3
	3.7	2.7×10^3
	6.4	1.6×10^3
Methyl vinyl ketone	9.7	2.4×10^4
Crotononitrile	8.3	5.8×10^4
Methyl acrylate	8.3	5.8×10^4
Methyl crotonate	9.4	5.4×10^3

[a] Pseudo-first-order rate constants, k[solute], were determined from formation curves of absorptions at 980 nm. [b] This value was determined from the decay curve of the 380-nm band due to a fumaronitrile anion radical.

where M represents a fumaronitrile molecule.

In contrast to dilute solutions, the growth rate of the dimer anion decreased with increasing fumaronitrile concentration in solutions above 1 mol %. This unusual concentration dependence probably results from an increase in viscosity by dissolving the solute at high concentrations. A small rise of temperature significantly increased both growth and decay rates of the dimer anion, as seen in Figure 2. The effect may be caused by a decrease in viscosity, rather than an increase in net reactivity.

The broad IR band is interpreted[23] in terms of an electronic transition between two charge-resonance states described by the following wave functions

$$\Phi(A^-)\Phi(B) + \Phi(A)\Phi(B^-) \rightarrow \Phi(A^-)\Phi(B) - \Phi(A)\Phi(B^-) \qquad (2)$$

where $\Phi(A^-)$ and $\Phi(B)$ represent the wave functions of an anion radical and a neutral molecule of fumaronitrile, respectively. Similar charge-resonance bands in the IR region have been observed for dimer cations of aromatic hydrocarbons. In the spectrum determined at 800 μs after the pulse, the absorption is very weak around 600 nm but increases again with decreasing wavelength. The absorption, at least in the region from 450 to 550 nm, is mainly caused by the dimer anion because it grows at the same rate that the absorption at 980 nm does. The UV band of the dimer anion can be ascribed to an electronic

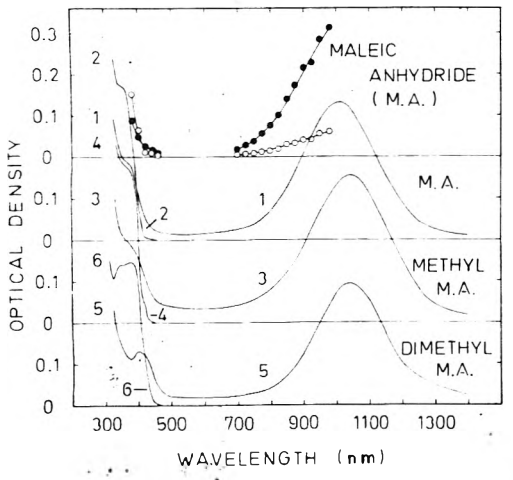

Figure 3. Spectra for irradiated maleic anhydride and its derivatives in MTHF solutions. Pulse radiolysis: 6.3 mol % maleic anhydride was irradiated at 113 K with 0.5-μs pulses at 120 mA: (circle) 75 μs after the pulse, (solid circle) 1.4 ms after the pulse. Matrix: 1.0 mol % maleic anhydride, 3.2 mol % methylmaleic anhydride, and 0.72 mol % dimethylmaleic anhydride were irradiated at 77 K with γ rays to 1.9 × 10^5 rads: (spectra 2, 4, and 6) before warming, (spectra 1, 3, and 5) after warming.

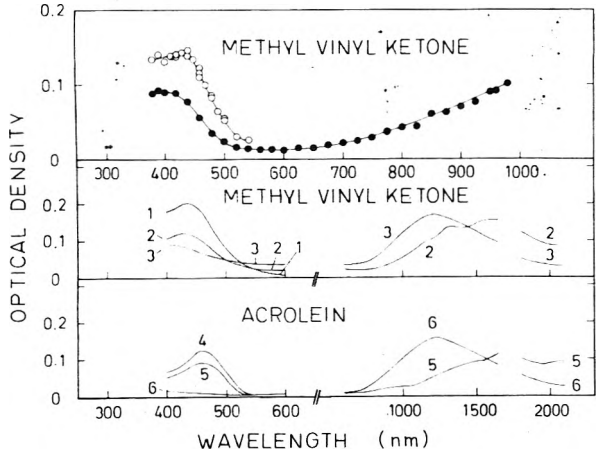

Figure 4. Spectra for irradiated methyl vinyl ketone and acrolein in MTHF solutions.[35] Pulse radiolysis: 9.7 mol % methyl vinyl ketone was irradiated at 113 K with 1-μs pulses at 80 mA: (circle) immediately after the pulse, (solid circle) 130 μs after the pulse. Matrix: 2.3 mol % methyl vinyl ketone and 1.6 mol % acrolein were irradiated at 77 K with γ rays to 1.9 × 10^5 rads: (spectra 1 and 4) before warming, (spectra 2 and 5) after warming, (spectra 3 and 6) after warming further.

transition between the two following states

$$\Phi(A^-)\Phi(B) + \Phi(A)\Phi(B^-) \rightarrow \Phi(A^-*)\Phi(B) + \Phi(A)\Phi(B^-*) \quad (3)$$

where $\Phi(A^-*)$ is the wave function of an excited fumaronitrile anion radical. The whole shape of the UV band could not be measured because another long-lived species absorbed below 400 nm; the species may be a neutral radical produced in radical processes.

Figures 3–6 present absorption spectra of irradiated MTHF solutions of various olefin derivatives. The results obtained with these compounds were almost similar to those of fumaronitrile. Intense UV bands due to anion radicals were observed in spectra determined immediately after the pulse or measured before warming solutions. However, there were no absorptions in the IR region. In parallel with the decay of UV bands in pulse-irradiated solutions or in warmed γ-irradiated solutions, broad bands appeared in the IR region. These bands are assigned to dimer anions of these compounds. Rate constants of the dimer anion formation are tabulated in Table I. These

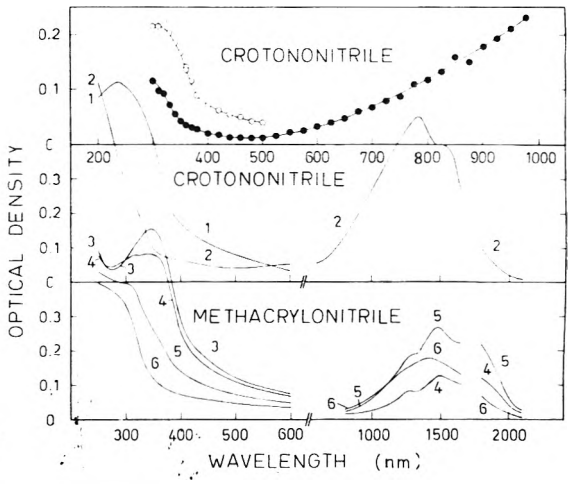

Figure 5. Spectra for irradiated crotononitrile and methacrylonitrile in MTHF solutions.[35] Pulse radiolysis: 9.1 mol % crotononitrile was irradiated at 113 K with 2-μs pulses at 100 mA: (circle) immediately after the pulse, (solid circle) at 35 μs after the pulse. Matrix: 1.6 mol % crotononitrile and 1.6 mol % methacrylonitrile were irradiated at 77 K with γ rays to 1.9 × 10^5 rads: (spectra 1 and 3) before warming, (spectra 2 and 4) after warming, (spectra 5 and 6) after the repetition of warming processes in the order.

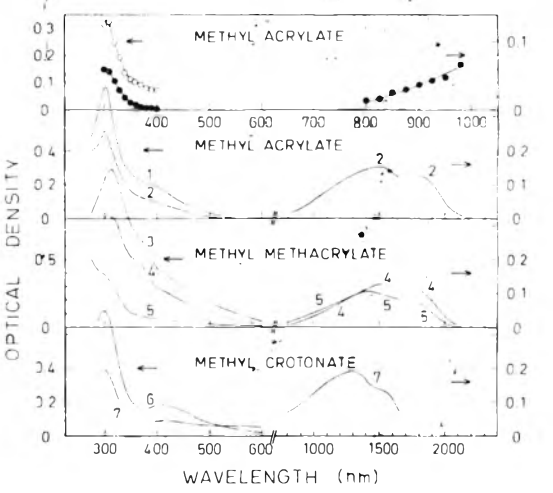

Figure 6. Spectra for irradiated methyl acrylate, methyl methacrylate, and methyl crotonate in MTHF solutions.[35] Pulse radiolysis: 8.3 mol % methyl acrylate was irradiated at 113 K with 0.5-μs pulses at 80 mA: (circle) immediately after the pulse, (solid circle) 80 μs after the pulse. Matrix: 1.1 mol % methyl acrylate and 2.0 mol % methyl crotonate were irradiated at 77 K with γ rays to 1.9 × 10^5 rads and 1.1 mol % methyl methacrylate to 3.8 × 10^5 rads: (spectra 1, 3, and 6) before warming, (spectra 2, 4, and 7) after warming, (spectrum 5) after warming further.

values are dispersed over a wide range. However, viscosities of solutions probably differ considerably owing to a large amount of solute, although MTHF has been used as a common solvent. It is important that all growth curves fit a first-order rate law.

A recent ESR study[24] has shown that the anion radical of maleic anhydride is formed upon irradiating its MTHF solutions at 77 K. The dimer anion produced from the anion radical has a broad band with a peak at 1000 nm. The introduction of one or two methyl groups to maleic anhydride scarcely changes the peak wavelength and shape of the IR band. This fact suggests that methyl groups do not affect appreciably the arrangement and interaction of the two component molecules. Methyl vinyl ketone and acrolein gave complicated IR spectra, when their solutions were warmed slightly for a short time. The spectra have several humps and main parts located at relatively long wavelengths. When the solutions were warmed further,

the spectra became smooth and the peaks shifted to about 1200 nm. We think that the former spectra are caused by several dimer anions with different conformations, which transform into the most stable one during repetitive warming processes.[15,25] Similar spectral changes were also observed for esters and nitriles, but not for fumaronitrile and maleic anhydride and its derivatives. By analogy with a dimer cation, the sandwich structure where two carbon–carbon π orbitals interact with each other seems plausible as the most stable dimer anion. However, it is difficult to obtain conclusive information from optical spectroscopy alone.

Unsuccessful results on other compounds may be worth describing because they provide suggestion on the formation of dimer anions. The pulse radiolysis of an MTHF solution of 13 mol % 1,3-butadiene at 113 K yielded a band with a peak at 390 nm, which corresponds to an anion radical of 1,3-butadiene.[26] Although the lifetime was longer than 200 μs, no absorption was observed in the range from 800 to 1000 nm, where the dimer anion, if produced, is expected to absorb. A pulse-irradiated MTHF solution of 3.6 mol % acrylamide showed a UV band with a peak at 300 nm, which agrees with that due to an acrylamide anion radical produced in an alkaline aqueous solution.[27,28] The lifetime was definitely longer than 400 μs at 113 K, although the absorption of another transient species made the determination of the lifetime difficult. However, no absorption attributable to its dimer anion was observed in both the visible and IR regions during and after the decay of the anion radical. The γ irradiation of an MTHF solution of 2 mol % methacrylamide at 77 K gave a spectrum with a peak at 320 nm. An IR absorption was not produced by warming the solution. The formation of a styrene anion radical in an irradiated solution was confirmed from the spectrum determined immediately after the pulse.[29] The anion radical decayed slowly over 10 ms at 113 K. However, an absorption assignable to the dimer anion did not appear in the solution, although the concentration was as high as 8 mol %. The pulse radiolysis of MTHF solutions of 1.9 mol % phthalonitrile and 1.9 mol % phthalic anhydride was carried out in expectation of the observation of aromatic dimer anions. However, we could not obtain any result indicating their formation, although their anion radicals were detected.

One of basic questions concerning a dimer anion is what kind of compounds produce dimer anions. Experimental results in this study suggest that the formation is favored in compounds with electron-withdrawing functional groups. Attractions of functional groups for electrons are reflected by the electric moments of benzene derivatives: 4.4 D for benzonitrile, 3.0 D for acetophenone, 2.8 D for benzaldehyde, 1.9 D for methyl benzoate, and 0 for benzene.[30] In fact, dimer anions of nitriles, ketone, aldehyde, and esters were formed successfully in both pulse radiolysis and matrix experiments. Radiation-induced polymerization of nitroethylene in an MTHF solution has been reported[31,32] to proceed via an anionic mechanism initiated by a nitroethylene anion radical. Shiga and Yamaoka[33] found the formation of nitroethylene dimer negative ions in the gas phase by the use of a mass spectrometer. A nitro group attracts electrons strongly, because the electric moment of nitrobenzene is 4.3 D. Therefore, nitroethylene dimer anions may be formed easily in MTHF, although the formation has not been tested in this study. Electron affinities of olefin derivatives are considered to be determined principally by functional groups. Lovelock[34] has measured affinities of various compounds for free electrons when that of chlorobenzene was taken as a standard: 1700 for diethyl maleate, 1500 for diethyl fumarate, 0.1 for ethyl acrylate, <0.01 for styrene, and <0.01 for cyclopentadiene. The values for diethyl maleate, ethyl acrylate, and cyclopentadiene may be applied approximately to maleic anhydride, methyl acrylate, and 1,3-butadiene, respectively. Affinities of styrene and 1,3-butadiene are very small and their dimer anions have not been observed. Although more studies are necessary for a conclusion, the electron affinity of a functional group seems to be an important factor for dimer anion formation.

Dimer anions of benzene derivatives were not formed, even if electron-withdrawing groups were introduced. Dimer anions of olefin derivatives were, however, formed spontaneously by reactions of anion radicals with neutral molecules. The dimer anions may play an important role in primary processes of anionic polymerization.

Acknowledgment. The authors wish to express their gratitude to Professor Hitoshi Yamaoka, Kyoto University, for his stimulating suggestions.

References and Notes

(1) I. C. Lewis and L. S. Singer, *J. Chem. Phys.*, **43**, 2712 (1965).
(2) O. Edlund, P. Kinell, A. Lund, and A. Shimizu, *J. Chem. Phys.*, **46**, 3679 (1967).
(3) O. Howarth and G. K. Fraenkel, *J. Am. Chem. Soc.*, **88**, 4514 (1966).
(4) O. Howarth and G. K. Fraenkel, *J. Chem. Phys.*, **52**, 6258 (1970).
(5) B. Badger and B. Brocklehurst, *Trans. Faraday Soc.*, **65**, 2576 (1968).
(6) B. Badger and B. Brocklehurst, *Trans. Faraday Soc.*, **65**, 2582 (1968).
(7) B. Badger and B. Brocklehurst, *Trans. Faraday Soc.*, **65**, 2588 (1968).
(8) B. Badger and B. Brocklehurst, *Trans. Faraday Soc.*, **66**, 2939 (1970).
(9) A. Kira, S. Arai, and M. Imamura, *J. Chem. Phys.*, **54**, 4890 (1971).
(10) A. Kira, S. Arai, and M. Imamura, *J. Phys. Chem.*, **76**, 1119 (1972).
(11) S. Arai, A. Kira, and M. Imamura, *J. Chem. Phys.*, **56**, 1777 (1972).
(12) M. A. J. Rodgers, *Chem. Phys. Lett.*, **9**, 107 (1971).
(13) M. A. J. Rodgers, *Trans. Faraday Soc. Faraday Trans. 1*, **68**, 1278 (1972).
(14) T. Shida and S. Iwata, *J. Am. Chem. Soc.*, **95**, 3473 (1973).
(15) A. Kira, M. Imamura, and T. Shida, *J. Phys. Chem.*, **80**, 1445 (1976).
(16) We have carried out the pulse radiolysis of several aromatic hydrocarbons in ethereal solutions. Results did not indicate the formation of their dimer anions.
(17) A. Ekstrom, *J. Phys. Chem.*, **74**, 1705 (1970); R. Brocklehurst, *ibid.*, **75**, 1177 (1971); A. Ekstrom, *ibid.*, **75**, 1178 (1971).
(18) T. Shida and S. Iwata, *J. Chem. Phys.*, **56**, 2858 (1972).
(19) E. D. Sprague, K. Takeda, and F. Williams, *Chem. Phys. Lett.*, **10**, 299 (1971).
(20) A. Kira, S. Arai, and M. Imamura, *Rep. Inst. Phys. Chem. Res.*, **47**, 139 (1971).
(21) S. Arai, M. Hoshino, and M. Imamura, *J. Phys. Chem.*, **79**, 702 (1975).
(22) W. H. Hamill, "Radical Ions", E. T. Kaiser and L. Kevan, Ed., Interscience, New York, N.Y., 1968, pp 321–416.
(23) A. Ishitani and S. Nagakura, *Mol. Phys.*, **12**, 1 (1976).
(24) M. Fukaya, H. Muto, K. Toriyama, and M. Iwasaki, *J. Phys. Chem.*, **80**, 728 (1976).
(25) R. E. Buhler and W. Funk, *J. Phys. Chem.*, **79**, 2098 (1975).
(26) T. Shida and W. H. Hamill, *J. Am. Chem. Soc.*, **88**, 5371 (1966).
(27) K. W. Chambers, E. Collison, and F. S. Dainton, *Trans. Faraday Soc.*, **66**, 142 (1970).
(28) A. J. Swallow, *Adv. Chem. Ser.*, **No. 82**, 499 (1968).
(29) J. P. Guarino and W. H. Hamill, *J. Am. Chem. Soc.*, **86**, 777 (1964).
(30) C. R. Noller, "Chemistry of Organic Compounds", W. B. Saunders, Philadelphia, Pa., 1965.
(31) H. Yamaoka, F. Williams, and K. Hayashi, *Trans. Faraday Soc.*, **63**, 376 (1967).
(32) H. Yamaoka, I. Obama, K. Hayashi, and S. Okamura, *J. Polym. Sci., A-1*, **8**, 495 (1970).
(33) T. Shiga and H. Yamaoka, *Bull. Chem. Soc. Jpn.*, **45**, 2065 (1972).
(34) J. E. Lovelock, *Nature (London)*, **189**, 729 (1961).
(35) A sharp IR absorption of MTHF prevented us from determining the spectra in the region from 1650 to 1800 nm.

The Charge Transfer to Solvent Spectrum of Iodide in Supercooled Water and Glass-Forming Aqueous Solutions

A. Barkatt and C. A. Angell*

Chemistry Department, Purdue University, West Lafayette, Indiana 47907 *(Received April 16, 1976)*

Publication costs assisted by the National Science Foundation

Measurements of the peak position and the line shape of the charge transfer to solvent (CTTS) band of aqueous I^- were carried out using thin samples squeezed between quartz disks. Results obtained in glass-forming aqueous magnesium acetate ($Mg(OAc)_2$) solutions show a temperature dependence similar to that observed in pure water above T_g, but below T_g both peak position and bandwidth suddenly become much less temperature dependent. This is a direct indication of the importance of configurational, as opposed to vibrational, degrees of freedom in accounting for temperature effects on CTTS transitions. In pure water supercooling to −31 °C was achieved. Below 0 °C, the temperature dependence of the energy of the transition deviates from linearity and becomes gradually smaller, and changes in bandwidth are arrested. These effects are discussed in terms of water structure in the supercooled region. Correlations of structural effects on CTTS with data concerning the absorption of the hydrated electron are discussed. Results are also given concerning the effects of solutes (e.g., I^-, OAc^-, Br^-) on the CTTS band. In particular, systematic observations were made on the line shape as a function of solute concentrations. The results are discussed using the physical picture of the diffuse model, attributing most structural effects to changes in the ground state energy.

Introduction

CTTS spectra, exhibited in the UV range by a number of anions, are associated with a transition from a ground state in which the negative charge resides mainly on the central ion surrounded by a solvation shell to an excited state in which negative charge is transferred to the solvating medium. The excited state can be regarded, in first approximation, as a combination of a neutral radical and a solvated electron. Since the ground state is a solvated ion its energy is considerably influenced by the solvent, although it is defined principally by the central ion. On the other hand, in defining the electronic excited state the solvent plays an integral part. Most spectroscopic transitions observed in solution are influenced to some extent by the solvent, especially in cases such as the symmetry-sensitive ligand field d–d transitions where the environment determines the symmetry of the field sensed by the ion. However, CTTS transitions constitute an unusually environment-sensitive class of transitions, and consequently are useful as probes of changes in solvent structure with temperature, pressure, or the addition of another solute or a cosolvent.

The dependence of CTTS spectra on environmental parameters shows many similarities to the behavior of transitions between energy levels of the solvated electron itself.[1,2] Indeed, the excited state of the CTTS transition closely approximates the structure of the solvated electron in its ground state, and data obtained for the energy levels of the solvated electron have played a major role in the development of models for CTTS transitions.

A comprehensive review of experimental findings and theoretical models for CTTS transitions was published by Blandamer and Fox.[1] Most studies have been concerned with solvent, second solute, and/or temperature effects on the position of the band maximum for the lower energy ($E_{max} \approx 226$ nm) of the two CTTS bands, with the aim of providing the empirical basis for a successful theoretical modeling of the transition. Unfortunately, despite the large amount of data on conventional solutions now available, the models so far proposed have been only moderately successful. Using a "polaron" model,[3] with rather crude approximations for the excited state, the value of E_{max} can be understood, but the temperature dependence is not properly accounted for. More recent models, "diffuse",[4] "confined",[5] and "configuration coordinate",[6] to be discussed later, have had interpretation of the temperature dependence as one of their primary concerns, but have also had only limited success.

The aims of the present investigation are twofold and self-reinforcing. In the first place we seek to sharpen the understanding of the nature and origin of the temperature dependence of the CTTS bands by extending their study to glass-forming solutions in which we can experimentally separate, by measurements above and below the glass transition temperature, the effects on dE_{max}/dT of purely vibrational from those of structural (configurational) expansion.[7] With the resultant clarification of the role of solution structure on the transition energy, we are then able to employ the structure sensitivity of the CTTS band transition to obtain some insight into structural ordering processes in water in the low-temperature supercooled regime in which recent thermodynamic and transport studies have revealed highly anomalous behavior.[8,9]

Experimental Section

The study of supercooled water requires small sample sizes, suggesting the use of thin aqueous layers enclosed between quartz surfaces for spectral studies. This is a method which was first developed by Fromherz and Menschick[10] in their pioneering work on CTTS spectra in high concentrations of aqueous halides. More recently it was considered preferable to carry out such studies in 0.1–1-cm cells and to observe only the low-energy tail of the band,[11] a method which cannot distinguish between shifts of the maximum and effects on the bandwidth. The use of thin samples makes it possible to extend the studies of solute effects on the entire band to the numerous cases of solutes with a significant absorption at high concentrations in the 200–250-nm range, such as the acetate ion, OAc^- (which was used in the present work to obtain

TABLE I: Values of E_{max} (20 °C) and Average dE_{max}/dT for Iodide in Water and Aqueous Solutions

Solution	T_g, °C	[I^-], M	E_{max} (20 °C), kcal mol^{-1}	Temp range, °C	Av dE_{max}/dT, kcal mol^{-1} deg^{-1}	Ref
Water		5×10^{-5}	126.40	1–91	0.0328	1
Water		4.28×10^{-5}	126.544	18–63	0.03320	12
Water		1×10^{-4}	126.590	12–69	0.0337	6
Water		2×10^{-5}	126.50 ± 0.03	20		This work
Water		0.1	126.54 ± 0.05	+40–0	0.033 ± 0.001	This work
				0 to −10	0.027 ± 0.003	This work
				−10 to −20	0.022 ± 0.003	This work
				−20 to −30	0.017 ± 0.005	This work
R = 14(3.105 M) $Mg(OAc)_2$	−81	0.1	130.11 ± 0.08	+20 to −81	0.035 ± 0.001	This work
				−81 to −132	0.005 ± 0.001	This work
R = 7(4.957 M) $Mg(OAc)_2$	−42	0.1	131.39 ± 0.06	+20 to −42	0.037 ± 0.001	This work
				−42 to −94	0.005 ± 0.001	This work
2 M Li_2SO_4		0.1	128.56 ± 0.04	20		This work
2 M Li_2SO_4		1×10^{-4}	128.47	20		1, 13
2 M $MgSO_4$		0.1	128.41 ± 0.04	20		This work
2 M $MgSO_4$		1×10^{-4}	128.36	20		1, 13
4 M NH_4Cl		0.1	127.31 ± 0.04	20		This work
4 M NH_4Cl		0.1	127.27	20		1, 13
4 M NH_4Br		0.1	126.60 ± 0.04	20		This work

glass-forming compositions), Br^-, and I^- itself.

Samples were prepared by placing a drop of the solution between two General Electric polished fused quartz disks (1 in. diameter, 1/8 in. thickness). These disks were mounted in a Perkin-Elmer liquid absorption cell holder. UV absorption spectra of iodide-containing solutions were obtained by means of a Cary 14R recording spectrophotometer operated at a scan speed of 0.5 nm/s. Temperature control was achieved by placing a 0.25-in. thick metal block between the disks and one side of the holder. This block consisted of a brass and copper plate of the same dimensions as the cell holder joined together by tin solder through which copper circulation tubes were passed, making it possible to cool the block by flowing through it dry nitrogen previously passed through a Dewar of liquid nitrogen, or to heat it with water pumped from a Haake FT constant temperature circulator. The other side of the quartz disks was always insulated and mechanically protected by a rubber O-ring pressed between the quartz and the cell holder. The temperature was monitored by means of a Cu–constantan thermocouple, epoxy-glued to the rim of the quartz disks at their junction. The reference solutions were contained in a similar setup without a temperature-control block. Cooling and heating of the samples were always carried out at a slow rate of ~1 deg/min to minimize temperature differences across the sample and between the sample and the thermocouple. Using this technique it was found possible to supercool aqueous 0.1 M NaI solution to −31 °C before freezing took place.

The thickness of the solution layer in the sample and reference cells was adjusted by tightening the screws of the cell holders. With samples consisting of 0.1 M NaI in water or aqueous solutions of various salts this thickness was adjusted to give an absorbance of 0.3–0.8 at the iodide peak wavelength (near 226 nm). Since Beer's law is still valid at this concentration range (see below), this corresponds to an optical path length of 2–6 μm and a total sample weight of 4–11 mg. The reference used with samples of NaI solutions in pure water was water, and the reference used with salt-containing solutions was an identical solution without iodide.

Acetate and bromide solutions have some background absorption in the spectral region of interest which had to be compensated in any samples containing $Mg(OAc)_2$ or NH_4Br. This was done by adjusting the thickness of the solution layer in the reference cell until the shape of the iodide spectrum (in particular, the ratio between the intensity of the absorbance at the 226-nm peak and the absorbances at the 193-nm peak and the 208-nm minimum between them) became identical with the line shape in pure water solution.

In the cases of samples containing high iodide concentrations, the solution layer was squeezed more tightly and peak absorbances as high as 3 were read using neutral density screens. In these cases especially it was found necessary to tighten the screws slowly and uniformly so as to prevent the formation of gaps in the solution film. When such gaps appear in the optical path the iodide spectrum disappears and is replaced by a weak, broad, and ill-defined reflection spectrum from the cavity between the wet quartz surfaces.

The spectra of samples containing low concentrations (≤0.05 M) of iodide were measured by using a 1-cm Pyrocell quartz cell against identical solutions without iodide. At iodide concentrations between 1×10^{-4} and 5×10^{-2} M NaI Pyrocell silica inserts were introduced into the sample (as well as the reference) cell to decrease the optical pathlength to 0.300–0.005 cm. All the determinations of peak absorbances were carried out with the quartz cell.

During all measurements both sample and reference compartments of the Cary 14R were purged with dry N_2 to prevent condensation and to make it possible to extend the short-wavelength limit of the measurements to 190 nm. Due to the small observed energy shifts, relative to the transition energy, being measured, and to the low signal-to-noise ratio of the spectrophotometer in the spectral region of interest, several spectra were recorded and analyzed to obtain each of the data points presented in the Results section. Each data point represents an average of n measurements, where $n = 20$ in the solute concentration effect studies, $n = 10$ in the temperature effect studies on water and $n = 5$ in the temperature effect studies on $Mg(OAc)_2$ solutions. All the chemicals used were Baker Analyzed reagents. Triply distilled or redistilled deionized water was employed.

Glass transition temperatures were measured by means of a Perkin-Elmer DSC-2 differential scanning calorimeter, operated at 10 deg/min, and the densities were obtained by weighing the solutions in 10-ml volumetric flask.

Results

1. *Solute Concentration Effects on the Iodide Peak Position.* The effect of increasing solute concentration on

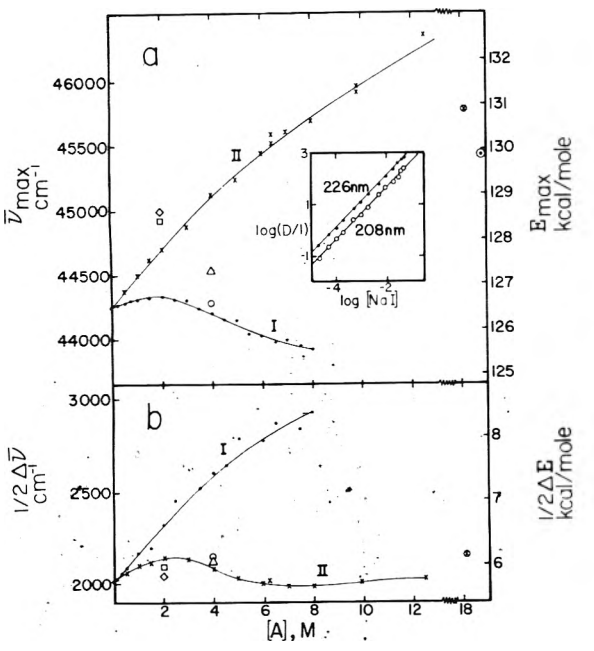

Figure 1. Solute concentration effects on the peak position (a) and the bandwidth (b) of the iodide absorption at 20 °C: (I,●) NaI, A = I^-; (⊖) KI crystals (ref 1 and 5); (II,×) $Mg(OAc)_2$, A = OAc^-; (⊗) dry 1:1 KOAc–$Ca(OAc)_2$ glass, A = OAc^-; (◇) Li_2SO_4, A = SO_4^{2-}; (□) $MgSO_4$, A = SO_4^{2-}; (△) NH_4Cl, A = Cl^-; (○) NH_4Br, A = Br^-. 0.1 M NaI present in all cases except I. Inset shows Beer's law test for the iodide absorption, 20 °C.

the position of the lower-energy component of the iodide CTTS doublet is shown in Figure 1a and Table I, using units of kilocalories per mole to accord with past practice.[1]

The results obtained for the dependence of the peak position on iodide concentration between 0.05 and 8.0 M NaI using the quartz disk "sandwich" method show a slight rise of E_{max} with [NaI] up to a maximum at 2 M NaI, followed by a decrease below the level of E_{max} in the case of [NaI] → 0. At a concentration of 0.05 M NaI, it was found possible to observe the peak position using both the quartz cell method, with a pathlength of 50 μm and a resulting E_{max} = 126.52 ± 0.03 kcal mol^{-1}, and the disk "sandwich" method, with pathlengths of 3–4 μm and E_{max} = 126.54 ± 0.05 kcal mol^{-1}. It is concluded that the reduction in pathlength involved in the disk method does not have a significant effect on E_{max}. Another conclusion, which is relevant to the temperature effect studies (see below), is that in 0.1 M NaI E_{max} shows only a very slight increase, of 0.04 kcal mol^{-1} (equivalent to a change of 1 deg in temperature), over its value in the case of [NaI] → 0.

The effects of other solutes were studied using the disk "sandwich" method. It can be seen that the energy of the transition considerably increases with increasing $Mg(OAc)_2$ concentration, and this increase goes on even at the highest $Mg(OAc)_2$ concentrations studied here. Higher concentrations, although available up to 4R,[15] could not be prepared in suitable thin films for study. A completely anhydrous acetate glass (1:1 KOAc–$Ca(OAc)_2$, which is 18.14 M in OAc^-)[14] containing NaI was more easily studied and yielded an E_{max} of 130.93 kcal mol^{-1} (Figure 1a). Although the accuracy in this case is lower than for the solutions due to the high background OAc^- absorption the E_{max} value is certainly lower than the last (12.5 M) solution value. The decrease is believed to be due primarily to the removal of H_2O dipoles rather than to the change of cations, implying the existence of a maximum in the E_{max} vs. concentration plot. An oppositely directed difference is found between the E_{max} value in the most concentrated NaI solutions and that in pure KI crystals[1,5] (see Figure 1a).

In order to compare the effects of iodide and acetate with those of other, previously studied, ions a few measurements were carried out on NH_4Br, NH_4Cl, $MgSO_4$, and Li_2SO_4, see Table I. These results show that the solute effect obtained using the disk method and 0.1 M NaI is almost identical with that observed previously[1,13] using 1-cm cells and 1 × 10^{-4} M KI for Li_2SO_4, $MgSO_4$, and NH_4Cl.

2. *Solute Concentration Effects on Bandwidth and Intensity.* The effect of increasing solute concentration on the bandwidth of the iodide absorption is shown in Figure 1b. In order to minimize the interference from the 193-nm iodide band and the background absorption of the solutes at low wavelength we measured the separation $^1/_2\Delta E$ between the peak energy and the energy at half-maximum on the low-energy side of the band. As discussed below, this may be slightly different from the correct half-width obtained by Gaussian resolution of the band but the difference between the two quantities is small and the solute effects measured here can be expected to be valid also for the correct ΔE.

From Figure 1b it can be seen that solute effects are generally small, ≤0.38 kcal mol^{-1} (6% of the bandwidth), except in the case of NaI. In all cases except >2 M $Mg(OAc)_2$ the addition of solutes increases the bandwidth. The order of the solutes with respect to the broadening, relative to $Mg(OAc)_2$ at the composition of comparison, is exactly the reverse of their effectiveness in shifting E_{max} to higher values, i.e., for broadening the order is NaI ≫ NH_4Br > NH_4Cl > $Mg(OAc)_2$ > $MgSO_4$ > Li_2SO_4. As in the case of the peak position measurements (see above), identical results were obtained for the bandwidths observed in 0.05 M NaI using the cell method and the disk method.

4 M NH_4Cl, 2 M $Mg(OAc)_2$, 2 M $MgSO_4$, and 2 M Li_2SO_4 cause a small (1–3%) reduction in the peak absorbance intensity of 0.005 M NaI, measured in the same quartz cell with a pathlength of 0.010 cm. Because of the smallness of the effect it is not given any further consideration.

More extensive measurements of the dependence of absorbance on concentration were carried out in the case of NaI itself since it was necessary to find out whether the Beer–Lambert law is valid in NaI solutions up to the concentration range of 0.05–0.1 M and thus is applicable to the determination of layer thicknesses in the disk "sandwich" setup. Using quartz cells, quartz inserts, and neutral density screens it was found that Beer's law is obeyed within ±5% over the entire concentration range studied here, 2 × 10^{-5} to 5 × 10^{-2} M NaI, both with respect to the absorbance at the 226-nm peak, with an ϵ_{226} of (13.8 ± 0.7) × 10^3 M^{-1} cm^{-1}, and with respect to the absorbance at the 208-nm minimum between the two peaks, with an ϵ_{208} of (4.3 ± 0.2) × 10^3 M^{-1} cm^{-1} (see Figure 1a, inset). These molar absorptivities, which are in good agreement with previous results,[1,6] could therefore be used in the determination of the thickness of layers of 0.05–0.1 M iodide between quartz disks.

On the other hand, the assumption that Beer's law still holds at very high iodide concentrations would lead to the conclusion that in 8 M NaI, where a peak absorbance of 3 was measured, the pathlength was 0.25 μm. In tests it was found impossible to compress films of 0.1 M Na to less than 0.5 μm, and it is therefore probable that a considerable negative deviation from Beer's law occurs at high iodide concentrations. The deviation may be connected

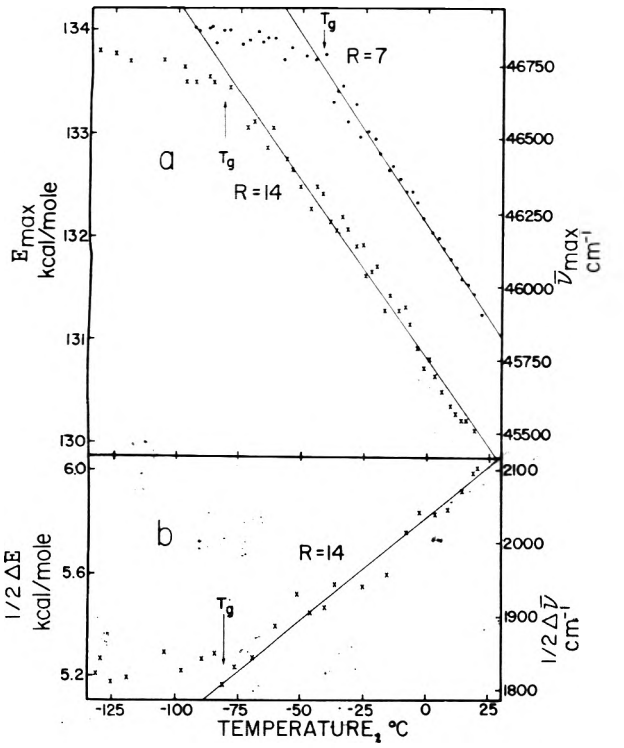

Figure 2. Temperature effects on the peak position (a) and the bandwidth (b) of 0.1 M NaI in R = 14 and R = 7 aqueous $Mg(OAc)_2$ solutions. T_g is the temperature of configurational arrest defined by differential scanning calorimetry measurements using scan rates of 10 deg min^{-1}.

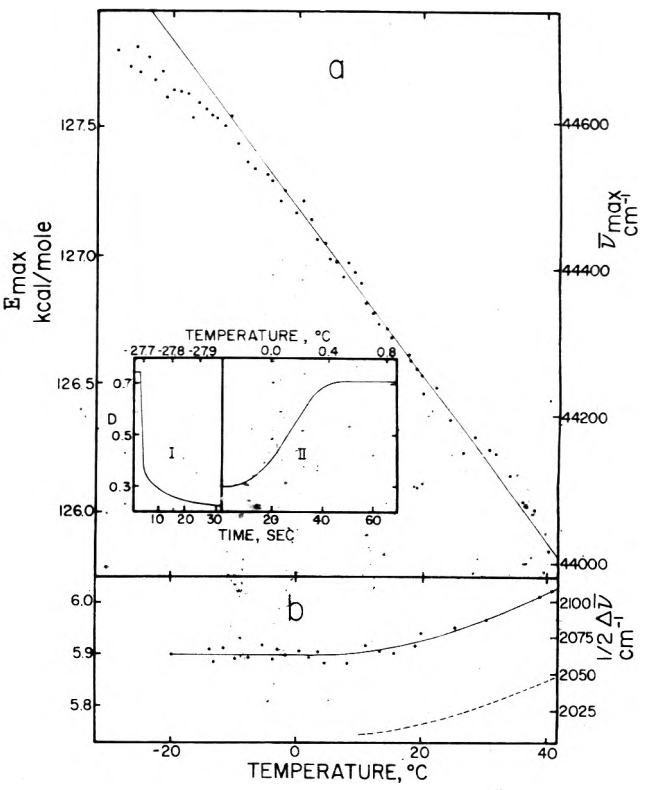

Figure 3. Temperature effects on the peak position (a) and the bandwidth (b) of 0.1 M NaI in water: (—) ref 6. Inset shows changes in the 225-nm absorbance during freezing and melting: (I) freezing upon cooling at 0.6 deg/min; (II) melting upon heating at 1.0 deg/min.

with increases in bandwidth observed above 0.5 M NaI. (A similar decrease in intensity takes place, as described above, to a much lesser extent with other solutes.)

3. *Temperature Effects. 0.1 M NaI in Aqueous $Mg(OAc)_2$ Solutions.* Measurements were carried out on two glass-forming compositions: R = 14 mol of H_2O/mol of $Mg(OAc)_2$ (3.150 M $Mg(OAc)_2$ at 20 °C, ρ = 1.224 g/ml) and R = 7 (4.957 M $Mg(OAc)_2$ at 20 °C, ρ = 1.332 g/ml). The results obtained for the peak position as a function of temperature (see Figure 2a and Table I) show that E_{max} increases linearly (within experimental error) with decreasing temperature, with a slope similar to dE_{max}/dT in water above 0 °C, though slightly higher the higher the $Mg(OAc)_2$ concentration. However, at a certain temperature, −79 ± 3 °C in R = 14 $Mg(OAc)_2$ and −41 ± 3 °C in R = 7 $Mg(OAc)_2$, the slope abruptly changes to a value almost an order of magnitude smaller. The temperatures at which the changes occur are very close to the known glass transition temperatures[15] which have been confirmed within ±1 deg in the present work using DTA and DSC techniques at heating rates of 10 deg/min (see Table I). Due to the limited accuracy of the spectral method, no effects of a changed rate of cooling (in our case, about 1 deg/min), or of differences between heating and cooling runs around T_g, were demonstrable.

Bandwidth measurements were carried out on the less concentrated, R = 14 solution for which the background acetate absorption was less troublesome. The results (see Figure 2b) show that the dependence of $^1/_2\Delta E$ on temperature is linear within experimental error, with a slope of 0.008 ± 0.001 kcal mol^{-1} deg^{-1}. The plot agains sharply breaks at T_g and $d(^1/_2\Delta E)/dT$ becomes very small (0.001 kcal mol^{-1} deg^{-1}) for lower T.

4. *Temperature Effects. 0.1 M NaI in Water.* The dependence of the peak position on temperature was studied using 2–6-μm films of 0.1 M NaI in liquid water between +40 and −30 °C. The results are presented in Figure 3a and Table I. Upon cooling the solution to a temperature between −15 and −31 °C, depending on the type of quartz used, the size of the sample and the presence of scratches or foreign particles, the solution suddenly freezes, as manifested by the disappearance of the iodide spectrum (see Figure 3a, inset), and its replacement by a weak, flat reflection spectrum from the ice layer. Such freezing was observed also in 1-μm films (with 0.3 M NaI to give sufficient absorption). Upon reheating, this spectrum remains unchanged up to a temperature of −0.1 ± 0.5 °C, where the iodide spectrum reappears (see Figure 3a, inset). This observation serves as a check of the temperature measurement. Both freezing and melting are completed with 40 s. The appearance of the iodide spectrum is therefore a very sensitive indicator of the phase transition.

The results obtained for the dependence of the peak position on temperature in the liquid during cooling and during heating runs are identical within experimental error. They show a linear dependence of E_{max} on T between 40 and 0 °C, with a slope equal to that obtained by previous workers.[1,6,12] However, a significant curvature is observed below −10 °C and between −20 and −30 °C the slope is found to be less than one-half its high temperature value.

The results obtained for the bandwidth as a function of temperature are higher by about 2.6% than those reported by Siano and Metzler[6] in the 10–40 °C range. This discrepancy is very probably due to the fact that the present results were obtained by direct measurements of the width of the lower-energy half of the band, while Siano and Metzler's results were obtained by a more accurate Gaussian analysis which eliminated interference from the 193-nm band and corrected for the very slight skew of the bandshape. However, it can be seen that the two sets of results show an almost identical temperature dependence. Upon extending the temperature range below 10 °C, we observed that the half-bandwidth levels off at about 5 °C

and retains a constant value of 5.90 ± 0.1 kcal mol^{-1} down to at least −20 °C.

Discussion

1. *Validity of Thin Film Spectra.* The discussion of this work should start with a brief reemphasis of the validity of our thin layer studies. Not only were E_{max} and $^1/_2\Delta E$ shown identical in 2–3-μm thin film and normal cell experiments for 0.05 M NaI (Results section) but also (a) complete agreement with previous data on dE_{max}/dT is obtained and (b) films as thin as 1 μ and containing 0.1–0.3 M NaI show completely normal freezing and remelting behavior. Clearly we are observing bulk solution properties unaffected by surface effects on solution structure.

2. *Models for the CTTS Transition, and the Temperature Dependence of the Transition Energy.* Toward the interpretation of CTTS spectra the present study introduces an important new element, viz., the separation of vibrational from structural effects on the temperature dependence of E_{max}. It will be appropriate therefore to consider first how our observations on this point can help refine concepts involved in models for the transition. The consistency of the model with observations on solutions will then be reviewed before its application to interpretation of the observations in supercooled water is considered.

All models for the transition have as a common concept the excitation of an electron originally located on the ion into a new orbital which extends, to a greater or lesser extent, over a region of solvent molecules surrounding the ion site. In accord with the Frank–Condon principle, the center-of-mass structure of the excited state is identical with that of the normal solvent cage of the iodide ion. The temperature dependence of the transition energy must therefore result from the effect of temperature on this structure and on the consequent change of ground state, and/or excited state, energies. According to the diffuse model,[4] which seems the best available at the moment, it is the change in ground state energy which is of primary importance.

The theoretical models differ primarily in the way in which the electron trapping potential established by the solvent cage is assessed, and in the extent to which the electron in the excited state is considered delocalized into the solvent. In all cases the "cage" or "cavity" radius is a critical parameter, and changes of the cavity radius with temperature must be invoked if the unusual magnitude of the CTTS energy temperature dependence is to be understood. That the latter concept provides an inadequate basis for discussion is demonstrated by the results shown in Figure 2, which we now discuss.

Figure 2 shows what is, with little doubt, true for all solution CTTS spectra, viz., that most (80%) of the temperature dependence of E_{max} vanishes when the solution passes into the glassy state below T_g.[16] The association of T_g with the "freezing" of the primary liquid structure and the loss of all except vibrational and weak, secondary structural, degrees of freedom is well understood by students of viscous liquids.[17-19] Figure 2 therefore shows that the temperature dependence of the CTTS spectra cannot be due to uniform expansion of the solvent cage since uniform expansion can only be achieved by anharmonic vibrations which are virtually unaffected by the occurrence of the glass transition.[17-19]

In the liquid as opposed to the glassy regime most expansion occurs by configurational rearrangements which, according to symmetry- and coordination number-sensitive spectroscopy and computer simulation studies,[20,21] usually produce both distortions to lower symmetry of existing coordination groups and introduction of new groups of lower coordination number. The higher the temperature the greater the range of sizes and distortions of the local coordination groups produced within the solvent and around any solute species. Distortion of a coordination shell should have qualitatively the same effect on the ground state energy as increase of its radius, hence the temperature dependence of the CTTS band maximum is best interpreted in terms of (a) increasing distortions from regular symmetry of existing solvent cages and (b) the generation of new solvent cages containing on the average fewer solvent dipoles to establish the electron trapping potential. These same factors are, of course, also responsible for the increased half-widths associated with decreasing E_{max} values. The oscillator strength $\int \epsilon_\nu \, d\nu$ remains approximately constant.

Similar considerations must apply to the effect of temperature on the solvated electron spectrum since the ground state for this transition is structurally similar to the excited state of the iodide CTTS transition. (The substitution of the neutral iodine radical in the latter case for the solvent cavity in the former case is of little consequence energetically.) The average radius for the charge distribution for e_{aq}^-, for instance, is estimated at 2.5–3.0 Å in the ground state,[22] while the radius of the excited state for the iodide CTTS spectrum should be $1.25r_i$ or 2.70 Å according to the diffuse model.[1] Unfortunately, while dE_{max}/dT for the solvated electron in certain liquids is known (and is large[23]), no data equivalent to our E_{max} vs. T measurement below T_g (temperature-independent site distribution) are available.[24]

3. *Solute Effects on E_{max} and $^1/_2\Delta E$.* Solute effects displayed in Figure 1 establish that the $Mg(OAc)_2$ solutions used for the dE_{max}/dT studies are representative of the general case. Figure 1 shows an order in the solute effectiveness in shifting E_{max} to higher values, $Li_2SO_4 > MgSO_4 > Mg(OAc)_2 \gg NH_4Cl > NH_4Br > NaI$, which is in agreement with previous results (for Li_2SO_4, $MgSO_4$, and NH_4Cl) and with the observation[17] that the solvent effect correlates with the "structure-making" character of the anions. The decrease in E_{max} produced by NaI in concentrations above 2 M is unusual but not unprecedented. N-*n*-Pr_4Cl has a similar maximum at 0.5 M, while N-*n*-$Pent_4Cl$ causes E_{max} to decrease below the pure water value even at the lowest concentrations.[1] A maximum may also exist in the $Mg(OAc)_2$–H_2O system at higher concentrations than those studied here (see below).

The solute effects are generally related to the temperature effects. Structure-making solvents, like temperature decreases, decrease the disorder in the solution permitting tighter binding of H_2O to I^- and thus smaller effective cavity radii. The analogy of solute and temperature effects extends to the relative half-width variations. The composition dependence of the half-width is particularly large in solutions of iodide itself. In this case the change is in the direction expected for a strong structure breaker—indeed, unusually pronounced increases in the diffusion coefficient of water, which depends on disorder, occur in the presence of iodide ion.[25] The bandwidth effect for I^- solutions, however, is so large compared with the other solutions examined that direct $I^- - I^-$ interactions must be suspected.

Very pronounced changes, including extrema in E_{max} and possibly in ΔE, must occur in solutions in the ultra-high concentration "hydrate melt" region where there are insufficient water molecules to provide even a single hydration shell since values for E_{max} in anhydrous acetate glasses (45 800 ± 500 cm^{-1}) are below the values observed

in the most concentrated solutions studied in this work (see Figure 1). This ultra-high concentration region warrants systematic investigation for the insight it should provide into the relation between electron trapping potentials and dipolar molecule coordination numbers.

The few available data for solute effects on the absorption spectra of e_{aq}^- show that 4.6 M $MgCl_2$, 12 M KF, and 15 M LiCl shift the e_{aq}^- absorption in the visible to higher spectra, and that these shifts (as well as shifts caused by a change of solvent[1,2,26]) have a linear correlation with the shifts to higher energies caused by the same solutes in the case of the iodide CTTS spectrum.[26]

4. *CTTS Transitions and Structuring in Supercooled Water.* Recently, studies of the physical properties of water have been extended into the metastable supercooled region with the finding that both thermodynamic and mass transport properties exhibit gross anomalies indicative of some sort of singularity at −45 °C (at 1 atm pressure).[8,9] Unfortunately, there is little direct structural information in the same temperature interval on which an interpretation of these anomalies can be based.

Figure 3 shows that, whereas E_{max} for the iodide CTTS spectrum in $Mg(OAc)_2$ solutions varies linearly with temperature over the entire temperature range down to T_g (Figure 2) departures from linearity become evident in water below about −10 °C. The decrease in slope becomes more pronounced with decreasing temperature down to the lowest temperature which could be studied before crystallization commenced, −31 °C. This unusual behavior, which reflects the temperature dependence of the CTTS transition ground state relative to a slowly varying[4] excited state, is consistent with the appearance of some constraint on the decrease in effective radius of the iodide coordination shell, (i.e., of the "cavity") in the anomalous region. A natural explanation would be the restriction on coordination sites imposed by the rapidly increasing rigidity of the water tetrahedral network. A terminal value of E_{max} at ~127.95 kcal mol^{-1} reached at −45 °C would not be inconsistent with the trend of the data. In this anomalous region the band half-width stabilizes, also indicative of the imposition of some specific distribution of iodide ion sites possessing uniform vibrational dynamics. Without more detailed quantitative and site-structure-dependent theoretical models for the transition, however, little more can be said.

It should be noted, in this connection, that the "configuration coordinate" model, adapted from solid state color center theory for solution studies by Siano and Metzler,[6] predicts a curvilinear half-width vs. temperature relation such as is observed above 10 °C. However, nothing in this theory limits this prediction to the case of iodide in pure water (in $Mg(OAc)_2$ solutions the observed dependence is almost prefectly linear). Furthermore an actual flattening out, as is observed below 0 °C, is not predicted under any circumstances.

It appears that behavior similar to that which we have observed for the CTTS transition in supercooled water may also be characteristic of the spectrum of the hydrated electron (the relation of which to the CTTS transition was referred to earlier). Although no spectra for e_{aq}^- are available below 4 °C an extrapolation of E_{max} based on the linear dE_{max}/dT observed for T = 4–90 °C[22] predicts that a value equal to that attributed to e_{aq}^- in amorphous ice, 46.1 kcal mol^{-1}, would be reached at only −67 °C. The latter energy was obtained by the dubious procedure of extrapolating data on methanol–H_2O glasses to 100% H_2O.[27] A more direct observation, which suggests an even higher temperature for the arrest of E_{max} on cooling, is that obtained from studies of Na deposition on vapor-deposited amorphous ice by Bennett, Mile, and Thomas.[28] These authors observed a rather flat absorption with a maximum between 40.8 and 48.5 kcal mol^{-1} deg^{-1}. This is supported by the observation that, in polycrystalline ice in which electrons can be trapped in very low yield, a band is observed with E_{max} between 44.7 and 46.1 kcal mol^{-1}.[29] The lower end of this range or the middle of the amorphous ice band would, according to extrapolations of the normal water data, be reached at −44.7 °C.

e_{aq}^- absorbs in the visible region of the spectrum, and it might be possible to conduct tests of its behavior in the temperature range 0 to −38 °C using emulsion techniques to suppress crystallization. The verification of CTTS-like anomalies in the anomalous temperature region would confirm in detail the close relation of the two phenomena and encourage the extension of CTTS studies to other vitreous and structurally interesting systems.

Acknowledgment. Support of this research by the National Science Foundation under Grant No. DMR 7302632A01 is gratefully acknowledged.

References and Notes

(1) M. J. Blandamer and M. F. Fox, *Chem. Rev.*, **70**, 59 (1970).
(2) M. F. Fox and E. Hayon, *Chem. Phys. Lett.*, **25**, 511 (1974).
(3) R. Platzman and J. Franck, *Z. Phys.*, **138**, 411 (1954).
(4) G. Stein and A. Treinin, *Trans. Faraday Soc.*, **55**, 1086, 1091 (1959).
(5) M. Smith and M. C. R. Symons *Discuss. Faraday Soc.*, **24**, 206 (1957); *Trans. Faraday Soc.*, **54**, 338, 346 (1958).
(6) D. B. Siano and D. E. Metzler, *J. Chem. Soc., Faraday Trans. 2*, **68**, 2042 (1972).
(7) J. Wong and C. A. Angell, *J. Non-Cryst. Solids*, **7**, 109 (1972).
(8) (a) C. A. Angell, J. Shuppert, and J. C. Tucker, *J. Phys. Chem.*, **77**, 3092 (1973); (b) D. H. Rasmussen and A. P. MacKenzie, *J. Chem. Phys.*, **59**, 5003 (1973).
(9) (a) J. Hallet, *Proc. Phys. Soc.*, **82**, 1046 (1963); (b) K. T. Gillen, D. C. Douglass, and M. J. R. Hoch, *J. Chem. Phys.*, **57**, 5117 (1972).
(10) H. Frommherz and W. Menschick, *Z. Phys. Chem. B*, **3**, 1 (1929); **7**, 439 (1930).
(11) D. Meyerstein and A. Treinin, *J. Phys. Chem.*, **66**, 446 (1962).
(12) M. J. Wooten, L. A. Dunn, C. E. Clarke, and H. S. Frank, *Nature (London), Phys. Sci.*, **23**, 138 (1971).
(13) G. Stein and A. Treinin, *Trans. Faraday Soc.*, **56**, 1393 (1960).
(14) J. A. Duffy and M. D. Ingram, *J. Am. Ceram. Soc.*, **52**, 224 (1969).
(15) C. A. Angell and E. J. Sare, *J. Chem. Phys.*, **52**, 1058 (1970); E. J. Sare, Ph.D. Thesis, Purdue University, 1971.
(16) A relatively large dE_{max}/dT above T_g and an arrest of the spectroscopic shift at T_g have been observed in the case of the $n \rightarrow \pi^*$ transition of NO_3^- in the KNO_3–$Ca(NO_3)_2$ glass-forming mixture.[7] These effects were associated with a dependence of E_{max} on the mutual arrangement and interactions between the cations (in particular, Ca^{2+}) and the nitrate anion. These considerations do not apply to most intramolecular transitions. In the case of CTTS the solvent is an integral part of both the ground and excited states. Accordingly, the dE_{max}/dT observed for aqueous iodide (0.033 kcal mol^{-1} deg^{-1}) is much larger than in the case of NO_3^- in KNO_3–$Ca(NO_3)_2$ (0.0138 kcal mol^{-1} deg^{-1}), which makes the arrest at T_g much more pronounced. Furthermore, CTTS transitions are allowed and the high molar absorptivity, 13 800 M^{-1} cm^{-1} in the case of iodide compared to 7 M^{-1} cm^{-1} for the nitrate $n \rightarrow \pi^*$ band, makes it possible to use iodide and other species with CTTS bands as probes, rather than major components in detecting T_g (and other structural changes) in a variety of solvents.
(17) W. Kauzmann, *Chem. Rev.*, **43**, 219 (1948).
(18) (a) M. Goldstein, *J. Chem. Phys.*, **51**, 3728 (1969); (b) *Trans. N.Y. Acad. Sci.*, in press. (Proceedings of the Workshop on the Glass Transition and Nature of the Glassy State, Dec, 1975.)
(19) C. A. Angell and W. Sichina, (Proceedings of the Workshop on the Glass Transition and Nature of the Glassy State, Dec, 1975) *Trans. N.Y. Acad. Sci.* (1976).
(20) W. E. Smith, J. Brynestad, and G. P. Smith, *J. Chem. Phys.*, **52**, 3890 (1970).
(21) (a) L. V. Woodcock, *Proc. R. Soc. London, Ser. A*, **328**, 83 (1972); (b) J. L. Finney, *ibid.*, **319**, 495 (1970).
(22) E. J. Hart and M. Anbar, "The Hydrated Electron", Wiley-Interscience, New York, N.Y., 1970, Chapter 3.
(23) S. Arai and M. C. Sauer, Jr., *J. Chem. Phys.*, **44**, 2297 (1966).
(24) dE_{max}/dT for the electron trapped in molecular glasses after irradiation at low temperatures has been measured during warm-up (H. Hase, T. Warashina, M. Noda, A. Namiki, and T. Higashimura, *J. Chem. Phys.*, **57**, 1039 (1972); L. Kevan, *Adv. Radiat. Chem.*, **4**, 256 (1974)), but this is not an equivalent experiment since thermal annealing with changes in the occupied trap distribution occurs. dE_{max}/dT may be almost as large as in the liquid state. The experiment more closely

related to our glass state observations would be to study the spectrum of the annealed irradiated glass on recooling, when dE_{max}/dT would be much smaller, and should be comparable to that in Figure 2 below T_g. As far as we know this experiment has not been done for a system whose liquid state spectral behavior is also known.
(25) G. Engel and H. G. Hertz, *Ber. Bunsenges. Phys. Chem.*, **72**, 808 (1968).
(26) M. Anbar and E. J. Hart, *J. Phys. Chem.*, **69**, 1244 (1965).
(27) B. G. Ershov and A. K. Pikaev, *Zh. Fiz. Khim.*, **42**, 2753 (1967); S. Ya. Pshezhetskii, "EPR of Free Radicals in Radiation Chemistry", Wiley, New York, N.Y., 1974, p 86.
(28) J. E. Bennett, B. Mile, and A. Thomas, *J. Chem. Soc. A*, 1393 (1967).
(29) L. Kevan in "Actions Chimiques et Biologiques des Radiations", M. Haissinsky, Ed., 13 eme serie, Masson, Paris, 1969.

Enthalpies of Mixing and Solution in Trialkylphosphate–Water Systems

A. S. Kertes* and L. Tsimering

Institute of Chemistry, The Hebrew University, Jerusalem, Israel *(Received June 9, 1976)*

Excess enthalpies of mixing at 25 °C of water with trimethyl-, triethyl- and tri-*n*-propylphosphate are negative and with tri-*n*-butylphosphate positive in the concentration range of complete mutual miscibility. Standard heats of solution of water in the esters is decreasingly negative with increasing chain length, becoming slightly positive for water in tributylphosphate. It is postulated that in the ester-rich region the donor strength of the phosphoryl oxygen is main factor for the trend observed. Calculations based on a model involving the lattice theory of mixtures and interchange enthalpies of interacting surfaces support the hypothesis. In dilute aqueous solutions, the trend of increasingly exothermic heats of solution with increasing chain length of the alkyl groups is explained as being due to hydrophobic stabilization of the water structure.

Interpretation of thermodynamic properties of binary mixtures of polar and self-associated liquids is often hampered by the fact that the molecules in the mixtures participate in several simultaneous interactions. The difficulties are illustrated, for example, by the limited applicability of the various statistical thermodynamic treatments based on the model of ideally associated liquids. The critical test for the validity of such models, which assume that the various homo- and hetero-associated species mix ideally, is usually restricted to the medium-domain composition, in the mole fraction range between 0.2 and 0.8. The predicted excess functions are frequently in a remarkably poor agreement with the experimental data at the two extremes of the mole fraction scale. The models usually fail to bring out the fine features of dilute solutions.

Properties of liquid mixtures in which water is one of the components are particularly interesting, and at the same time difficult for interpretation, due to the unique properties of water. Since most of such mixing data involves the whole composition range, but no sufficient data at low concentration ends, we have undertaken to investigate the composition dependence of the thermodynamic properties of such mixtures by measuring integral heats of solution in addition to those of mixing. The obtained data on the present binary systems of water and four trialkylphosphates show that the actual properties of the mixtures are far from simple, and that the oversimplifications inherent in the models advanced might be misleading in these complex systems if not checked against experimental data in the dilute solutions range.

In a different context, this report presents a part of a long-term project on a calorimetric investigation of the thermodynamics and thermochemistry of solvent extraction processes. This is the reason for selecting the homologous series of trialkylphosphates, when the highest member of the series, tri-*n*-butylphosphate, is widely used as a powerful extractant for inorganic compounds from aqueous solutions. As such, its interaction with water has received and continues to receive much attention since the formation of hydrated species affects the extractive capacity of the ester.

The polarity of the four esters investigated is essentially the same,[1] as is their donor strength expressed in donor numbers.[2] The experimentally determined dipole moments depend on the solvent employed, and range between 2.78 D for trimethyl- and 2.92 D for tributylphosphate in hexane at 20 °C, or between 3.02 D for trimethyl- and 3.10 D for tributylphosphate when carbon tetrachloride is the solvent. The dipole moments of the neat liquids at 25 °C are apparently the same for the four esters at a value of 3.21 ± 0.03 D. The differences in the donor numbers are equally insignificant, having the values of 23.0 for trimethyl- and 23.7 for tributylphosphate.

As the result of their relatively high dipole moments, trialkylphosphates associate through a system of dipole–dipole bonds. Spectral data suggest[3] that the extent of dimerization of the esters depends on the solvent employed, and increases with the chain length of the alkyl groups. In hexane at 25 °C, for example, dimerization constants of 0.7, 1.2, and 2.9 $dm^3\ mol^{-1}$ for triethyl-, tri-*n*-propyl-, and tri-*n*-butylphosphate, respectively, have been reported.[3] From recent heats of dilution data[4] of these three esters in isooctane at 25 °C, dimerization constants of 0.15, 0.13, and 0.21 $dm^3\ mol^{-1}$, respectively, have been calculated. The corresponding enthalpies of dimerization, −45.3, −36.7, and −27.5 kJ mol^{-1}, and entropies of dimerization, −167.7, −139.9, and −195.2 J mol^{-1} deg^{-1}, indicate a relatively strong dipole–dipole interaction. The favorable enthalpy changes are more than offset by unfavorable entropy changes during dimerization, thus yielding the small positive free energy changes. The large negative entropy changes reflect a restricted molecular arrangement needed for the dimerization, and the decreasing $-\Delta H(\text{dim})$ values with the alkyl chain length suggests some hindrance due to the bulkiness of the alkyl groups.

With the increase of the molecular weight of the esters their mutual solubilities with water decrease. At 25 °C, trimethyl- and triethylphosphate are miscible with water

in all proportions. Mutual solubilities of the higher members of the series, due most probably to steric shielding factors generally observed for homologous series, are very sensitive to temperature, exhibiting upper and lower critical temperatures.[5] In the tributylphosphate–water system a complete miscibility is reached around 260 °C, but a lower critical temperature could not be observed due to the freezing of the system.[6,7] On the mole fraction scale at 25 °C, the solubilities in this system are: ester in water $x = 2.87 \times 10^{-5}$, and water in ester $x = 0.515$,[6,8,9] when the volume change at the latter composition is less than 1%.[10] Solubilities in the tripropylphosphate system are slightly higher,[11] though that of water in the ester still corresponds roughly to a molar ratio of unity.[12] No precise numerical data are available, however.

The interaction between trialkylphosphates and water has been the subject of numerous investigations in the past when most of the information relates to the tributylphosphate.[1,3,4,13,14] There is enough spectral and other physicochemical evidence obtained under a wide variety of conditions for that system to show that the components are weakly interacting. It is fairly safe to assume that hydrogen bonding must be one of the major interactions between the components in these systems. As a result of such hydrogen bonding, the existence of a variety of ester hydrates has been suggested, when the hydrogen-bonded equimolar hydrate is probably the predominating species only under the experimental conditions of infinite water dilution. Spectral[3,14] and dielectric constant[3] measurements have shown that the stability of this hydrate and the energy of the hydrogen bond formed are practically independent of the length of the alkyl chains in the ester molecule, apparently in line with the essentially constant values of their dipole moment and donor number (vide supra). Under different experimental conditions, when the self-association of water must be considered, the nature of the possible interactions becomes an elusive matter, and the presence of discrete, stoichiometrically defined hydrates questionable. Recent heats of solution data[11] of the esters in water (and in water–dimethylformamide mixtures) were interpreted in terms of the cage-formation concept,[15] as being due essentially to the formation of hydrophobic hydration clusters surrounding the trialkylphosphate molecules in water. The size of the hydration cage is very nearly the same regardless of the size of the alkyl groups. It was estimated[11] that about 30 water molecules participate in the formation of the cage. Though the stability of the hydration cage increases with the number of carbon atoms, the number of water molecules remains constant.

Experimental Section

Trimethylphosphate (BDH), triethylphosphate (BDH), and tri-*n*-propylphosphate (Fluka) were dried under vacuum and kept over Perlform molecular sieve. GLC analysis indicated purities of better than 97.5, 99.5, and 96%, respectively. Densities of the esters at 25 °C were 1.2086, 1.066, and 1.005, as compared to Beilstein data at 20 °C of 1.2144, 1.0695, and 1.0121, respectively. The tri-*n*-butylphosphate was from the batch previously employed.[16] The water content of all liquids was determined by Karl Fischer titration, and found to be less than 0.01 mol %.

The calorimeter (Tronac Model 1000 A continuous automatic titration equipment) used for direct determination of heats of mixing and solution and the procedure employed were as before.[16] No vapor pressure corrections were applied, though some inaccuracy might be expected for evaporation or condensation. Previous calibration data[17] on heat of mixing of *n*-hexane–cyclohexane system under identical experimental conditions indicated that a systematic deviation due to these effects cannot exceed 2 J mol^{-1}.

TABLE I: Excess Enthalpies of Mixing of Trialkylphosphates (x_1) with Water at 298.15 K

$(MeO)_3PO$		$(EtO)_3PO$		$(PrO)_3PO$	
x_1	H^E, J mol^{-1}	x_1	H^E, J mol^{-1}	x_1	H^E, J mol^{-1}
0.0060	−67.10	0.0075	−150.6	0.7126	−223.6
0.0121	−126.7	0.0276	−414.7	0.8041	−156.1
0.0482	−408.9	0.0558	−647.3	0.8139	−148.5
0.0959	−631.3	0.0882	−791.8	0.8611	−111.0
0.1530	−845.2	0.1242	−902.8	0.8974	−82.06
0.2222	−1110	0.1660	−990.0	0.9254	−59.83
0.4520	−1648	0.2102	−1061	0.9450	−44.18
0.5502	−1710	0.2600	−1105	$(BuO)_3PO$	
0.6401	−1650	0.3132	−1110	0.6910	106.8
0.7200	−1484	0.3671	−1088	0.7703	112.8
0.8172	−1084	0.6150	−805.1	0.8242	87.92
0.8768	−723.6	0.7648	−544.0	0.8703	66.84
0.9470	−312.1	0.8020	−471.3	0.9036	50.33
		0.8920	−284.2	0.9468	29.04

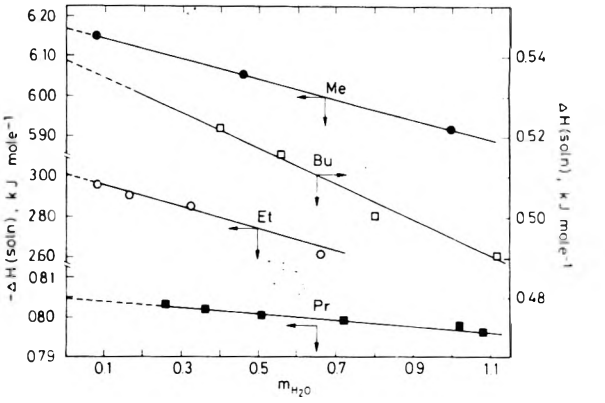

Figure 1. Enthalpies of solution of water in trialkylphosphates, 298.15 K.

Results

The experimental values of excess heats of mixing at 298.15 K are listed in Table I. For the two systems which are miscible in all proportions, the results, fitted by least-squares, gave the following smoothing equations and standard deviations, where x_1 is the mole fraction of the trialkylphosphate: Trimethylphosphate + water, 298.15 K, J mol^{-1}

$$H^E = x_1x_2[-6615 - 2865(x_1 - x_2) - 1133(x_1 - x_2)^2 + 5878(x_1 - x_2)^3] \quad (1)$$

$\sigma = 4.1$ J mol^{-1}

Triethylphosphate + water, 298.15 K, J mol^{-1}

$$H^E = x_1x_2[-3673 + 2046(x_1 - x_2) - 3873(x_1 - x_2)^2 + 3074(x_1 - x_2)^3 + 463(x_1 - x_2)^4] \quad (2)$$

$\sigma = 9.0$ J mol^{-1}

The experimentally determined enthalpies of solution of water in all four trialkylphosphates and of trimethyl- and triethylphosphate in water at 298.15 K are plotted in Figures 1 and 2, respectively. Values for the enthalpies of solution at infinite dilution $\Delta H°$(soln) were obtained both by the linear extrapolation of the experimental heat data on a large scale plot, and by least-squares analysis. The numerical data are listed in Table II, where the uncertainties are the maximum deviations derived from

TABLE II: Standard Enthalpies of Solution and Solvation in Trialkylphosphate-Water Systems at 298.15 K (kJ mol^{-1})

Ester	ΔH°(soln)		ΔH(vap)	ΔH°(solv)	
	Ester in water	Water in ester		Ester in water	Water in ester
$(MeO)_3PO$	−21.2 ± 0.2	−6.17 ± 0.02	13.1[a]	−34.3	−50.06
$(EtO)_3PO$	−25.9 ± 0.2	−3.01 ± 0.02	13.7[b]	−39.6	−47.00
$(PrO)_3PO$		−0.805 ± 0.005			−44.80
$(BuO)_3PO$		0.535 ± 0.005			−43.45

[a] Reference 20. [b] Reference 19.

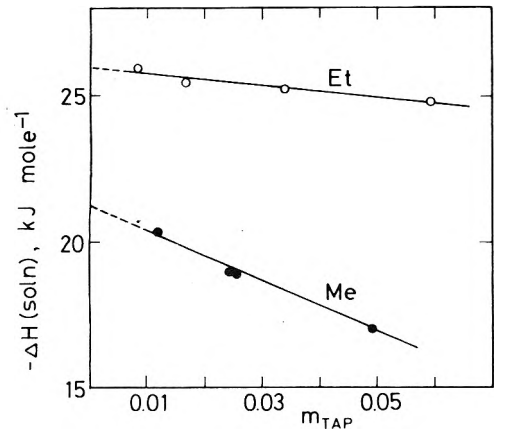

Figure 2. Enthalpies of solution of trimethyl- and triethylphosphate in water, 298.15 K.

the slope of the straight line extrapolation and the constant of the least-squares equations.

Table II gives also the corresponding enthalpies of solvation defined as

$$\Delta H^\circ(\text{solv}) = \Delta H^\circ(\text{soln}) - \Delta H^\circ(\text{vap}) \quad (3)$$

The enthalpy of vaporization of water at 298.15 K has been taken[18] as 43.99 kJ mol^{-1}, and those for the two alkylphosphates are given in Table II.

Heat of mixing data for $(PrO)_3PO$ and $(BuO)_3PO$ reported in Table I do not extend to the whole range of their water miscibility. Repeated experiments have shown that as the ester approaches saturation the dissolution of water in a mixture containing more than half of that needed for complete saturation becomes increasingly slow, thus the measured heat effects less reproducible. Similarly, because of large uncertainty arising from the prolonged dissolution time of tripropyl ester in water at 25 °C, heat of solution data are considered unreliable, thus not reported. This is also true for the integral heat of solution measurements of tributylphosphate in water, where, in addition, the very limited solubility results in low heat effects under the experimental conditions of the present calorimetric measurements.

Discussion

It is rather obvious that no simple interaction model can describe the thermodynamic properties of the ester–water mixtures in the systems under consideration, which involve polar and self-associated liquids, some of them exhibiting a limited miscibility only. A reasonable approximation of an idealized system should consider three exchange enthalpies contributing to the mixture properties. Two are the enthalpies associated with the breaking of bonds, hydrogen bonds for water and dipole–dipole bonds for the esters, and the third contribution is associated with the enthalpy of formation of hydrogen bonds between the components. Any scheme involving this last chemical interaction between the phosphoryl oxygen and water must predict some variation of the hydrogen-bond strength with the relative donicity of the ester. The latter depends on the electronegativity of the alkyl groups attached to the phosphorus atom. Though the trialkylphosphates are unlikely to be strong bases, electronegativity considerations predict that basicity decreases with increasing length of the hydrocarbon chains. It has indeed been argued[21] that the hydrogen bond in the tributylphosphate hydrate(s) is weaker than that in pure water, so that the newly formed H bonds between the components offer little competition to the water–water structural effects. In the terms of the three energy contributions, the excess enthalpies of mixing must approach zero as the exothermic heat of formation of new bonds compensates for the endothermic effects of breaking the bonds of both associated components. Indeed, the experimentally determined H^E values show that the enthalpies of mixing are decreasingly negative with increasing molecular weight of the ester, becoming slightly positive in the tributylphosphate–water system.

An interpretation of standard heats of solution data is usually more straightforward than that of heats of mixing, since the accuracy of the ΔH°(soln) results is unlikely to be seriously hampered by the fact that not all of the contributing factors could be evaluated satisfactorily. In the systems under consideration, an extrapolation of enthalpy of solution data to infinite dilution implies that the heat effect of cleavage of self-associated bonds are included.

Ester-Rich Region. The standard heat of solution of water in the esters, Table II and Figure 1, is decreasingly negative with an increase in the molecular weight of the ester, and becomes slightly positive in tributylphosphate. The fact that the ΔH°(soln) values are not a linear function of the number of carbon atoms can be taken as an indication that the nonspecific contribution to nonideality must be only a minor factor. Namely, the size of the ester molecule is the property which governs that contribution. Assuming thus that the ester–hydrate formation for all four esters involves no change in the stoichiometry of the adduct and in the number of hydrogen bonds per interacting molecules, the observed trend implies different strength of the newly formed ester–water bonds. It increases with decreasing number of carbon atoms in the ester.

As expected, the same trend is reflected in the excess enthalpies of mixing throughout the whole, though limited, experimental range for the propyl and butyl derivatives, and up to a water mole fraction of about 0.3 for the two lower homologues. For them an inversion of the trend becomes apparent at higher water contents. Thus, the molar volume of the ester, reflecting the effect of the chain length, works in the same direction as the basicity of the phosphoryl oxygen, and no clear distinction between the two effects can be made from the present data. Additionally, part of what is assumed to be due to the basicity of the functional group and/or to the chain length might be simple steric hindrance to the ease with which water molecules can approach the phosphoryl oxygen. In these terms, any hydrate formation in the tributylphosphate–water system is more than offset by the steric difficulty of forming the bond.

TABLE III: Numerical Values of Constants in Eq 9 at 298.15 K[a]

Ester	s_i	α_1^u	α_1^v	A_{12}
$(MeO)_3PO$	3.350	0.8135	0.1865	−2630 ± 120
$(EtO)_3PO$	5.500	0.8863	0.1136	−1030 ± 50
$(PrO)_3PO$	7.750	0.9193	0.0807	−330 ± 20
$(BuO)_3PO$	10.000	0.9375	0.0625	215 ± 5

[a] Group sections: $s^{CH_3} = 0.875$, $s^{CH_2} = 0.750$, $s^H = 0.875$, $s^O = 0.750$, $s^{PO_4} = 0.625$; molecular cross section of water, $s_{H_2O} = s_2 = 2.500$.

The statistical thermodynamic model employed previously to several binary liquid mixtures,[22] among them to those containing tributylphosphate,[23] based on a combination of the group interaction model and the zeroth approximation form of the lattice theory of mixtures for molecules of different sizes[24] has been tested and found to explain in quantitative terms the arguments outlined above. Briefly, applying the model to the ester-rich region, $x_{H_2O} < 0.3$, the only domain in which the four esters can be compared, we take that the surface of the ester molecules is composed of aliphatic (CH_3 and CH_2) and phosphatic (PO_4) elements, and that of the water molecules of one element. Thus, in terms of the theory,[22] the three interacting surfaces are the aliphatic (u), phosphatic (v), and water (t). Each segment on the surface of the various molecules has a characteristic capability of interaction proportional to the group cross sections s^u, s^v, and s^t of u, v, and t type surfaces of molecule i. The molecular group sections are the sum of the appropriate group cross sections and defined as

$$s_i = \Sigma m_i^u s^u \tag{4}$$

where m_i represents the segments of molecule i. The corresponding molecular coverages are defined as the ratio

$$\alpha_{is} = m_i^u s^u / s_i \tag{5}$$

The numerical values of the group and molecular cross sections and of the corresponding molecular coverages are compiled in Table III.

The experimentally determined excess enthalpy of mixing per mole of mixture is defined[25] as

$$H^E = s_1 s_2 \frac{x_1 x_2}{s_1 x_1 + s_2 x_2} A_{12} \tag{6}$$

where x is the mole fraction of components (subscript 1, ester; 2, water), s is the corresponding molecular cross section, and A_{12} is the so-called molecular interaction parameter, defined for the type of systems under consideration as

$$A_{12} = -[k^{uv}(\alpha_1^u - \alpha_2^u)(\alpha_1^v - \alpha_2^v) + k^{ut}(\alpha_1^u - \alpha_2^u)(\alpha_1^t - \alpha_2^t) + k^{vt}(\alpha_1^v - \alpha_2^v)(\alpha_1^t - \alpha_2^t)] \tag{7}$$

where k^{uv} (aliphatic–phosphatic), k^{ut} (aliphatic–water), and k^{vt} (phosphatic–water) are the molar interchange enthalpies accounting for the thermal effect of interactions of the various groups in solution. The sum of all molar coverages for any given molecule is equal to unity

$$\alpha_1^u + \alpha_1^v + \alpha_1^t = \alpha_2^u + \alpha_2^v + \alpha_2^t = 1 \tag{8}$$

k^{uv} has been determined previously[23] from heat of mixing data of tributylphosphate with n-alkanes and found to have the value of $k^{uv} = 130\,600 \pm 6400$ J mol^{-1} at 30 °C, or $k^{uv} = 142\,000 \pm 7000$ J mol^{-1} at 25 °C estimated from the temperature coefficient of mixing in these systems. The additional two molar interchange enthalpies, calculated from the experimentally determined H^E data of the four systems using eq 7 which simplifies to

$$A_{12} = -k^{uv}(\alpha_1^u)(\alpha_1^v) + k^{ut}(\alpha_1^u) + k^{vt}(\alpha_1^v) \tag{9}$$

when $\alpha_2^t = 1$ and $\alpha_1^t = \alpha_2^u = \alpha_2^v = 0$, have the values $k^{ut} = 3500 \pm 200$ J mol^{-1} and $k^{vt} = 86\,800 \pm 4000$ J mol^{-1} at 298.15 K. The fit of the calculated H^E values is shown in Figure 3, along with the experimentally determined points. The agreement should be considered satisfactory.

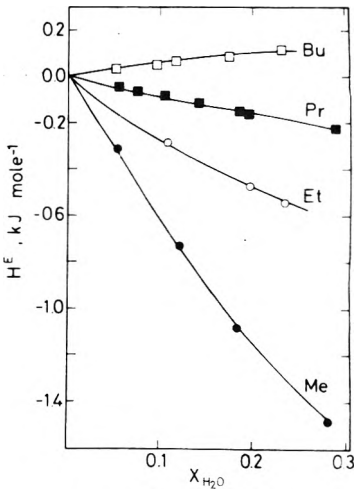

Figure 3. Comparison of experimental (points) and calculated (lines) excess enthalpies of mixing of trialkylphosphates with water, 298.15 K.

Water-Rich Region. It is one of the interesting features of the present data that an opposite trend holds true in dilute aqueous solutions. Heats of mixing and solution for triethylphosphate are more negative than for trimethylphosphate. Unreported data for tripropylphosphate show that the enthalpies in this system are more negative than those for triethylphosphate, in qualitative agreement with recent data.[11] In all three systems, enthalpies of solution are very strongly concentration dependent, decreasingly negative with increasing concentration. In dilute aqueous solutions at a given mole fraction of the ester, the trend that enthalpies become more negative with increasing chain length implies that the positive contribution due to cleavage of water–water bonds decreases in that order. This correlation assumes that the differences due to the extent of self-association of the esters are negligible in view of the small and similar values of their dimerization constants (vide supra). It is thus rather obvious that the enhancement of the water structure increases with the length of the alkyl chains of the solute due to hydrophobic stabilization. With increasing ester concentration the fraction of water which persists in clusters whose structure resembles that of bulk water decreases, and an increased number of water–water bonds are broken, manifested in less negative ΔH(soln) values.

Comparison with Literature Data. The only previous data which are, to some extent, comparable with the present sets of enthalpy data are those of Lindenbaum et al.[11] on the heats of solution of the esters in water. They have measured calorimetrically at 25 °C enthalpies of solution of trimethyl-, triethyl-, and tri-n-propylphosphate in water when the final concentration of the esters was stated to be about 0.03 mol kg^{-1}. They reported values for the standard heats of solution $\Delta H°$(soln) of −12.424, −21.139, and −22.561 kJ mol^{-1}, respectively, on the assumption that their datum at the single ester concentration required no correction to infinite dilution. The present data shown in Figure 2 provide evidence to the contrary, showing that their assumption is not justified. Additionally, the slope of the ΔH lines in Figure 2 for trimethyl-

and triethylphosphate indicate that the solute concentration at their single point was considerably higher than the final concentration claimed.

No data appear to have been reported on the heat of solution of water in the esters except those for tributylphosphate. Most of that information is rather fragmentary, and obtained under experimental conditions not directly comparable with the present results. Part of the reported enthalpies have been derived from the temperature dependence of water solubility (extraction) in the ester. Such are the values of −1210 J mol^{-1} of water[21] at 25 °C, −1460 J mol^{-1} of water at an unspecified temperature,[26] and −4200 J mol^{-1} of water at 25 °C.[12] The last, extremely negative value has been invoked as an argument in favor of the stability of the hydrated ester. In order to prove the opposite, Rozen[7,9] quotes an unspecified source and notes the value of −420 J mol^{-1} of water at an undisclosed temperature and without presenting experimental evidence. These data refer to experimental conditions in which the concentration of water in tributylphosphate is about 3.5 mol kg^{-1}, and the molar ratio of the components in the mixture is around unity. These estimates must be considered unreliable on the ground of grave errors inherent in applying the van't Hoff equation to solubilities rather than the appropriate equilibrium constants. It is thus not surprising that these data are in significant disagreement with the present results, and previous calorimetrically determined heats of solution.[27,28] At 25 °C and at a water concentration of about 0.03 mol kg^{-1}, Katzin et al.[27] have found that ΔH(soln) = 590 J mol^{-1} of water. Afanasev and Nikolaev,[28] noting that the enthalpies of solution of water in tributylphosphate are concentration dependent, and claiming an accuracy not better than 20–30%, report a ΔH(soln) range between 200 and 500 J mol^{-1} of water at an undisclosed temperature.

Calorimetrically measured heats of mixing data reported in the literature are strikingly different, and much in disagreement with those reported here. With no exception, they refer to experimental conditions of either complete saturation of tributylphosphate with water, or an excess of water in a two-liquid phase system. Kettrup and Specker[29] found that the heat of mixing at an equimolar ratio of the components at 20 °C is −400 J mol^{-1}, but is −670 J mol^{-1} in the presence of undissolved excess water. Apparently under comparable equimolar conditions, Belousov et al.[26] found the value of −1500 J mol^{-1}, in good agreement with the value derived from the temperature variation of water solubility in the ester. Marcus and Kolarik[30] found that the heat of mixing (termed heat of hydration by the authors) of water with the ester at 25 °C under conditions of a large molar excess of water, molar ratio of 200, is −520 ± 50 J mol^{-1} of tributylphosphate.

It is rather difficult, and perhaps premature, to assess critically the numerical data of the water–tributylphosphate system which have been attained under widely varying conditions. Nevertheless, it seems reasonable to distinguish between two extreme experimental conditions: those at low water content, and the other at complete saturation of the ester or above it. Because of the scarcity of the disclosed experimental details in the majority of the sources quoted, little close comparison with the present data is possible. Those of Katzin et al.[27] and Afanasev et al.[28] appear to be in more than just qualitative agreement with our results, all indicating that the process of water dissolution in tributylphosphate is an endothermic process, as long as the amount of water in the ester is kept well below that needed for its complete saturation. Perhaps somewhat surprisingly, most literature data appear to be in agreement as far as the exothermicity of the process is concerned when the ester is approaching saturation, roughly at a unit mole ratio of the components. However, it should be emphasized that our experience has shown that the process of dissolution of water in the ester under conditions of saturation is apparently a slow process. This in turn implies that perhaps some of the data refering to these conditions might have been measured under nonequilibrium conditions. Recent kinetic studies[31] indeed suggest that the diffusion of water into tributylphosphate depends on the total water content in the ester. A maximum in the diffusion coefficient appears at an ester–water mole ratio of about 2 (half-way to saturation), up to which water diffuses by a jump mechanism by which a water molecule passes from one ester molecule to another by making and breaking of hydrogen bonds. At higher water content the fraction of unhydrated tributylphosphate molecules available for the jump process obviously decreases, leading to a decrease in the diffusion coefficient. At or near saturation, the jump mechanism is gradually replaced by the diffusion of hydrated ester molecular units, until this process becomes the only effective mode of diffusion.

In an attempt to correlate the above interpretation[31] of diffusion data with the thermodynamic ones presented here, it seems reasonable to assume that the jump mechanism of making and breaking hydrogen bonds in ester solution of low water content is associated with an endothermic enthalpy change, namely, the strength of the bond formed between the molecules of the components is weaker than that in pure water.

References and Notes

(1) D. M. Petkovic, B. A. Kezele, and D. R. Rajic, *J. Phys. Chem.*, **77**, 922 (1973); P. Mauret and J. P. Fayet, *J. Chim. Phys.*, **65**, 549 (1968); J. Michalczyk, *Nukleonika*, **8**, 237 (1963).
(2) V. Gutmann, "Coordination Chemistry in Nonaqueous Solutions", Springer-Verlag, Wien, 1968, p 19.
(3) Dj. M. Petkovic, *J. Inorg. Nucl. Chem.*, **30**, 603 (1968); Dj. M. Petkovic and Z. B. Maksimovic, *ibid.*, in press.
(4) J. H. Rytting, A. Goldkamp, and S. Lindenbaum, *J. Solution Chem.*, **4**, 1005 (1975).
(5) A. V. Nikolaev, Yu. A. Dyadin, I. I. Yakovlev, V. B. Durasov, N. I. Yakovleva, and I. D. Khol'kina, *Russ. J. Phys. Chem.*, **41**, 972 (1967).
(6) K. Alcock, S. S. Grimley, T. V. Healy, J. Kennedy, and H. A. C. McKay, *Trans. Faraday Soc.*, **52**, 39 (1956); C. E. Higgins, W. H. Baldwin, and B. A. Soldano, *J. Phys. Chem.*, **63**, 113 (1959).
(7) A. M. Rozen, *Radiokhimiya*, **10**, 273 (1968).
(8) Y. Marcus and A. S. Kertes, "Ion Exchange and Solvent Extraction of Metal Complexes", Wiley-Interscience, London, 1969, p 661; J. W. Roddy and J. Mrocheck, *J. Inorg. Nucl. Chem.*, **28**, 3019 (1966); A. V. Nikolaev, Yu. A. Dyadin, I. I. Yakovlev, V. B. Durasov, and Z. B. Mironova, *Izv. Sib. Otd. Akad. Nauk SSSR*, (1) 27, (2) 28 (1965); *Chem. Abstr.*, **63**, 14140 (1965); **64**, 4325 (1966).
(9) A. M. Rozen, L. P. Khorkhorina, G. D. Agashkina, E. G. Teterin, A. N. Malytzeva, and E. V. Voronetzkaya, *Radiokhimiya*, **12**, 345 (1970).
(10) D. G. Tuck, *J. Chem. Soc.*, 2283 (1958).
(11) S. Lindenbaum, D. Stevenson, and J. H. Rytting, *J. Solution Chem.*, **4**, 893 (1975).
(12) R. C. Axtmann, *Nucl. Sci. Eng.*, **16**, 240 (1963).
(13) L. Tsimering, Ph.D. Thesis, The Hebrew University, Jerusalem, 1976.
(14) A. V. Karyakin and G. A. Muradova, *Russ. J. Phys. Chem.*, **45**, 591 (1971).
(15) H. S. Frank and W. Y. Wen, *Discuss. Faraday Soc.*, **24**, 133 (1957); D. N. Glew, H. D. Mank, and N. S. Rath, *Chem. Commun.*, 264 (1968); C. J. Clement, *J. Chem. Soc. A*, 455 (1969).
(16) L. Tsimering and A. S. Kertes, *J. Chem. Thermodyn.*, 6, 411 (1974).
(17) L. Tsimering and A. S. Kertes, *J. Chem. Eng. Data*, in press.
(18) J. Polak and G. C. Benson, *J. Chem. Thermodyn.*, **3**, 235 (1971).
(19) J. D. Cox and G. Pilcher, "Thermochemistry of Organic and Organometallic Compounds", Academic Press, London, 1970, p 483.
(20) Calculated by Wadso's equation, ref 19, p 119.
(21) C. J. Hardy, D. Fairhurst, H. A. C. McKay, and A. M. Wilson, *Trans. Faraday Soc.*, **60**, 1626 (1964).
(22) A. S. Kertes and F. Grauer, *J. Phys. Chem.*, **77**, 3107 (1973); H. V. Kehiaian, *J. Chim. Phys.*, **68**, 935 (1971).
(23) L. Tsimering and A. S. Kertes, *Thermochim. Acta*, **12**, 206 (1975).
(24) H. Tompa, *Trans. Faraday Soc.*, **45**, 101 (1949); O. Redlich, E. L. Derr, and G. J. Pierotti, *J. Am. Chem. Soc.*, **81**, 2283 (1958); R. W. Kershaw and G. N. Malcolm, *Trans. Faraday Soc.*, **64**, 323 (1968).

(25) M. Tamres, S. Searles, E. M. Leighly, and D. W. Mohrman, *J. Am. Chem. Soc.*, **76**, 3983 (1954).
(26) E. A. Belousov, A. A. Alovyainikov, V. V. Bocharov, and V. E. Mironov, *Russ. J. Phys. Chem.*, **47**, 598 (1973).
(27) L. I. Katzin, D. M. Simon, and J. R. Ferraro, *J. Am. Chem. Soc.*, **74**, 1191 (1952).
(28) Yu. Afanasev and A. V. Nikolaev, *Izv. Sibirsk. Otd. Akad. Nauk SSSR*, (3) 118, (1963); *Chem. Abstr.*, **60**, 12710 (1964).
(29) A. Kettrup and H. Specker, *Z. Anal. Chem.*, **230**, 241 (1967).
(30) Y. Marcus and Z. Kolarik, *J. Chem. Eng. Data*, **18**, 155 (1973).
(31) J. C. Hipfner and D. G. Tuck, *J. Chem. Soc., Faraday Trans. 1*, **70**, 528 (1974), and references therein.

Thermodynamic Studies of Protein–Salt Interaction. Phycocyanin–Tetrabutylammonium Bromide and –Tetraethylammonium Bromide

Chang-Hwei Chen* and Donald S. Berns

Physical Chemistry Laboratories, Division of Laboratories and Research, New York State Department of Health, Albany, New York 12201 *(Received March 4, 1976; Revised Manuscript Received August 26, 1976)*

Publication costs assisted by the Division of Laboratories and Research, New York State Department of Health, Albany, New York

The heats of interaction of tetrabutylammonium bromide (Bu_4NBr)–phycocyanin and tetraethylammonium bromide (Et_4NBr)–phycocyanin systems were studied by microcalorimetry. Due to its specific interaction with the protein, Bu_4NBr dissociates the hexamer of phycocyanin into a trimer. In the concentration ranges studied, Et_4NBr has little effect on phycocyanin aggregation, and the heat of interaction is very small. For the Bu_4NBr–phycocyanin binding reaction at pH 6.0, the thermodynamic parameters at 25 °C are 49 kcal mol^{-1} for ΔH_B, −1.8 kcal mol^{-1} for ΔG_B, and 170 eu for ΔS_B. The molar binding ratio is 1, which characterizes the specific binding between Bu_4NBr and phycocyanin. A mechanism involving the interaction between the hydrophobic area of the protein and the bulky alkyl groups of tetraalkylammonium salts is suggested.

Introduction

When phycocyanin is extracted from blue-green and red algae, where it is widely distributed, the extract contains several aggregates. The association and dissociation of this biliprotein by certain small molecules have been qualitatively characterized, and some possible mechanisms have been proposed.[1,2] Hydrophobic interaction is believed to play an important role in its aggregation from trimer (6S) to hexamer (11S).

In model membrane studies, phycocyanins have been shown to modify the intensity and direction of electron flow across bileaflet membranes,[3] but the thermodynamic aspects of biliprotein aggregation and interaction with small molecules have seldom been investigated. We report here the results of a study in which calorimetry was used to provide basic thermodynamic information.

The application of calorimetry to biochemical systems has been reviewed recently.[4,5] It measures accurately the enthalpy of reactions of binding of small molecules to biopolymers such as hexokinase-catalyzed reactions,[6] the equilibrium of organic phosphates with horse oxyhemoglobin,[7] and magnesium binding to yeast phenylalanine tRNA.[8] The combination of the measured enthalpy with the known Gibbs free energy leads to the entropy of the system.

The present study is an extension of our qualitative determination of the effect of some tetraalkylammonium salts (R_4NX) on the dissociation of phycocyanin.[1] Calorimetry was employed to investigate the quantitative energetic aspects in the phycocyanin–tetrabutylammonium bromide (Bu_4NBr) and phycocyanin–tetraethylammonium bromide (Et_4NBr) systems. These two salts were chosen for contrast: Bu_4NBr has strong solvent structure-making properties and strong interaction with protein, while Et_4NBr is a borderline salt (between solvent structure-maker and structure-breaker) with much less interaction with protein. The heats of interaction between protein and salts were measured, and the enthalpy, free energy, and entropy of binding between Bu_4NBr and phycocyanin are reported. The Et_4NBr and Bu_4NBr–phycocyanin systems are analyzed and compared with each other. Elucidation of the factors possibly responsible for thermodynamic stability involving the binding between phycocyanin and Bu_4NBr is discussed.

Experimental Section

Calorimeter. A twin-reaction cell batch microcalorimeter equipped with a known resistor for electric calibration was used in these studies. It was designed and built by Dr. Rex Lovrien, Department of Biochemistry, University of Minnesota.[7] The cells were made of 18K gold, and each was divided into two compartments with capacities of about 1.6 and 1.2 ml. The output of the thermoelectric units was magnified by an amplifier with maximum gain of 0.33×10^5 and reversible polarities. It was recorded on a Leeds & Northrup Model 620 Speedomax XL flatbed recorder equipped with a disk integrator and having a baseline deflection of 0.7 μV. Areas under the voltage–time traces were measured by the disk integrator and also weighed on a Mettler balance. The experiments were carried out at 25 °C.

The resistor for electrical calibration was determined as 52.9 Ω by a Wayne-Kerr 8221 universal bridge. The input voltage was measured on a Keithley 616 digital electrometer and the duration of the current pulse on a Precision Scientific timer.

The calorimeter cells were washed several times with distilled water by using a syringe and were dried by applying a vacuum line. A 0.5-ml gas-tight Hamilton syringe connected to a Hamilton PB 600-1 calibrated repeating dispenser was used to fill the cells accurately with appropriate volumes of solution.

Chemical calibration was obtained employing the heat of dilution of HCl. In the mixing reaction, 0.2016 ml of

TABLE I: Electrical and Chemical Calibration Constants

Method	mJ/g of area under peak[a]	mJ/count of disk integrator[b]
Electrical[c]	133.4 ± 1.9	1.588 ± 0.031
Chemical[d]	135.6 ± 3.7	1.561 ± 0.027

[a] Full scale of recorder = 15.0 μV. [b] Full scale of recorder = 30.0 μV. [c] Average of 36 experiments covering the range 1-167 mJ. [d] Average of four experiments.

a standardized HCl solution (0.920 M) and an equal volume of H_2O were used. The heat of the mixing reaction, computed[9] from enthalpy of formation of $HCl \cdot H_2O$, was 21.3 mcal. The density of HCl used in the calculation was taken from the International Critical Tables.

The scheme of the salt–protein mixing experiments was as follows: The two compartments of the reaction cell contained 0.2964 ml of a phycocyanin solution (41 mg ml^{-1} in sodium phosphate buffer, pH 6.0, I 0.1), and an equal volume of the appropriate concentration of R_4NBr in the pH 6.0 phosphate buffer. The compartments of the reference cell each contained 0.2964 ml of pH 6.0 phosphate buffer. An equal volume of the appropriate R_4NBr concentration in phosphate buffer could have been used in one compartment of the reference cell to cancel the heat of dilution of R_4NBr in the mixing process, but a direct measurement of the heat of dilution of R_4NBr in phosphate buffer was desired as information on the hydrophobic interaction of Bu_4NBr in the buffer solution. The present scheme did not employ a dilution blank. After the cells were filled, the calorimeter was allowed to sit for temperature equilibrium for at least 2 h prior to thermochemical measurement.

Sedimentation Velocity Measurements. Sedimentation velocity experiments[1] were performed in a Spinco Model E ultracentrifuge with schlieren optics. Kodak spectroscopic type 1N photographic plates, a Corning No. 5031 filter, and a phase angle of 60° were used. The solutions were placed in a single sector 2° centerpiece and centrifuged at 56 000 rpm at 25 °C in an AN-D rotor. Immediately after the calorimetry measurement, the mixed protein–salt solution was removed from the calorimeter and prepared for the sedimentation run. The relative areas under the schlieren peaks were evaluated by tracing enlargements of the negative plate from a Nikon Model 6 microcomparator.

Chemicals. Phycocyanin (PC) from *Phormidium luridum*, purified as described previously,[1] was stored in 50% saturated ammonium sulfate solution at 4 °C until used. The solution was then spun down, and the precipitate was dissolved and dialyzed in sodium phosphate buffer, pH 6.0, I 0.1. The protein solution at this pH contained a mixture of 6S (trimer), 11S (hexamer), and 19S (dodecamer) aggregates.[1] To eliminate the 19S the solution was dialyzed overnight in a pH 8.7 solution (prepared from pH 8.1 sodium phosphate–NaOH buffer adjusted with additional NaOH) and it was followed by dialysis back to pH 6.0. The concentration of PC in the solution was calculated on the basis that a 1-mg ml^{-1} solution at pH 6.0 in a 1-cm cuvette has an extinction coefficient of 6.0 at 620 nm.[1] The R_4NX used (Eastman Kodak Co.) were at least 98% pure by titration and were not purified further. All the R_4NBr solutions were prepared in sodium phosphate buffer, pH 6.0, I 0.1.

Results

The electrical and chemical calibration constants for the calorimeter (Table I) agreed quite well. In the measurements of heat of mixing involving dilution of HCl, X (Bu_4NBr or Et_4NBr), or PC, or mixing of PC and X, the experimental reproducibility was good and the mean deviation was less than 3%. The chemical calibration constant, 135.6 mJ/g of area under the peak, was used in the treatment of the data.

The heat of dilution measurements with Bu_4NBr and Et_4NBr (X) in pH 6.0 sodium phosphate buffer is presented in Table II (see paragraph at end of text regarding supplementary material). The process used for the evaluation is

$$X(M_x, V_x) + \text{pH 6.0 buffer}(V_x) \xrightarrow{\Delta Q_{dil(x)}} X(\tfrac{1}{2}M_x, 2V_x) \quad \text{(A)}$$

where the concentration M_x ranges from 0.020 to 0.160 M and volume V_x = 0.2964 ml. To demonstrate the hydrophobic interaction of R_4NBr in the buffer solution, its results are compared with the known heats of dilution of X with respect to infinitely dilute aqueous solution.[10] For such a comparison the present data must be extrapolated to infinitely dilute buffer solution by the following scheme: First, the experimental dilution data are nonlinearly fitted (using a program from Oak Ridge National Laboratory) to a least-squares equation of the type

$$Q = aM + bM^2 + cM^3 \quad (1)$$

where M and Q denote M_x and $\Delta Q_{dil(x)}$ as shown in process A. Then, according to eq 1, the successive dilution processes can be described in the following scheme:

Dilution process	$\Delta Q_{dil(x)}$
$M \rightarrow {}^1/_2 M$	$Q_1 = aM + bM^2 + cM^3$
${}^1/_2 M \rightarrow {}^1/_4 M$	$Q_2 = a({}^1/_2 M) + b({}^1/_2 M)^2 + c({}^1/_2 M)^3$
${}^1/_4 M \rightarrow {}^1/_8 M$	$Q_3 = a({}^1/_4 M) + b({}^1/_4 M)^2 + c({}^1/_4 M)^3$

(B)

For $M \rightarrow$ infinite dilution

$$\Delta Q_M^{\infty} = \sum_{i=1}^{\infty} Q_i$$

$$= aM(1 + {}^1/_2 + {}^1/_4 + \ldots) + bM^2(1 + ({}^1/_2)^2 + ({}^1/_4)^2 + \ldots) + cM^3(1 + ({}^1/_2)^3 + ({}^1/_4)^3 + \ldots)$$

$$= 2aM + {}^4/_3 bM^2 + {}^8/_7 cM^3 \quad (2)$$

where $\Sigma_{l=0}^{\infty}(1/2)^l = 2$, $\Sigma_{l=0}^{\infty}(1/2)^{2l} = 4/3$, $\Sigma_{l=0}^{\infty}(1/2)^{3l} = 8/7$, and ΔQ_M^{∞} is the heat of dilution of a salt with M_x and V_x in pH 6.0 being brought to infinitely dilute buffer solution. The least-squares coefficients of eq 2 are listed in Table III, when M_x = 0.144 M, ΔQ_M^{∞} = 126 and −137

TABLE III: Comparison of ΔQ_M^{∞} in pH 6.0 Buffer and in Aqueous Solution

Salt	a, 10^1	b, 10^2	c, 10^3	Solvent	M, M	ΔQ_M^{∞}, cal mol^{-1}
Et_4NBr	−1.647 50	12.9725	−2.434 12	pH 6.0	0.144	126
				Water	0.144	130[a,b]
Bu_4NBr	2.094 75	−5.6628	−4.296 38	pH 6.0	0.144	−137
				Water	0.144	−202[a]

[a] Reference 10. [b] Extrapolated value.

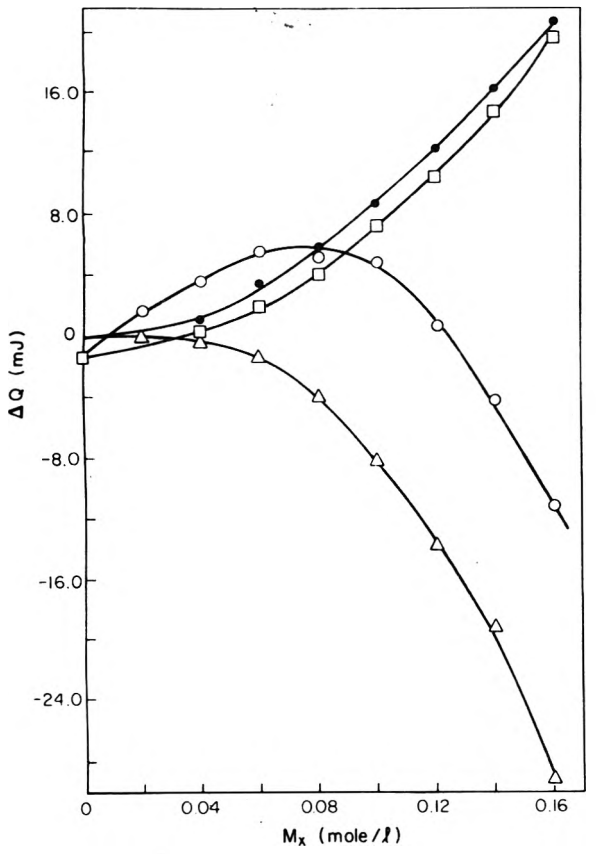

Figure 1. Plot of ΔQ vs. concentration of R_4NBr in the reaction cell before mixing (M_x): (Δ) ΔQ of dilution of Bu_4NBr in buffer; (O) ΔQ of mixing between Bu_4NBr and phycocyanin solution in buffer; (●) ΔQ of dilution of Et_4NBr in buffer; (□) ΔQ of mixing between Et_4NBr and phycocyanin solution in buffer. In all cases the buffer was at pH 6.0.

cal mol^{-1} for Et_4NBr and Bu_4NBr, respectively.

In the present studies, the protein–salt mixing reactions at pH 6.0 are described by the following scheme:

$$PC(M_{pc}, V_{pc}) + X(M_x, V_x) \xrightarrow{\Delta Q_{mix}} PC(^1/_2 M_{pc}, V_{pc} + V_x), X(^1/_2 M_x, V_{pc} + V_x) \quad (C)$$

where $V_{pc} + V_x = 2V_{pc} = 2V_x$. PC, X, and ΔQ_{mix} denote phycocyanin, salt (Bu_4NBr or Et_4NBr), and heat of mixing, respectively. M_{pc}, V_{pc}, V_x, and M_x represent values before mixing of the concentration (mg ml^{-1}) of PC, the volumes (0.2964 ml) of PC and X, and the concentrations (M) of X, respectively. Process C indicates that the concentration of PC or X is diluted to one-half during a mixing reaction. The results of the calorimetry measurements in process C are listed in Table II. The observed ΔQ_{mix} can be represented by the expression

$$\Delta Q_{mix} = \Delta Q_{int} + \Delta Q_{dil(pc)} + \Delta Q_{dil(x)} \quad (3)$$

where $\Delta Q_{dil(pc)}$ and $\Delta Q_{dil(x)}$ represent the heats of dilution for the following process and process A, respectively:

$$PC(M_{pc}, V_{pc}) + \text{pH 6.0 buffer}(V_{pc}) \xrightarrow{\Delta Q_{dil(pc)}} PC(^1/_2 M_{pc}, 2V_{pc}) \quad (D)$$

and ΔQ_{int} is the heat of interaction between PC and X during the mixing reaction. The observed $\Delta Q_{dil(pc)}$ and heat of interaction (ΔQ_{int}) calculated from eq 3 are also listed in Table II. Plots of ΔQ_{mix} and $\Delta Q_{dil(x)}$ against M_x are presented in Figure 1.

We propose that the interaction between PC and X involves a two-step mechanism,[1] the first being the dissociation of S_6 into S_3, as represented in eq 4, where S_6 and S_3 denote hexamer and trimer of PC, respectively:

$$S_6 \xrightarrow{\Delta H_d} 2S_3 \quad (4)$$

where ΔH_d, the enthalpy of dissociation, has a value of −17 kcal mol^{-1} (recalculated from ref 11 where a value of −21 kcal mol^{-1} was originally reported). Assuming that dissociation and association were negligible during sedimentation and that the areas under the peaks reflected the initial equilibrium compositions, ref 11 estimated the relative compositions of S_6 and S_3 from the areas under the schlieren patterns. This assumption is adopted in the treatment of the present sedimentation data.

The second step is the interaction of X and trimer that leads to the binding of X to S_3 (X dissociates S_6 into S_3):

$$S_3 + mX \xrightarrow{\Delta H_B} S_3\text{-}X_m \quad (5)$$

where ΔH_B is the enthalpy of binding (kcal mol^{-1}) and m is the molar binding ratio of X to S_3. A combination of eq 4 and 5 gives the enthalpy of interaction (ΔH_{int}) between PC and X:

$$\Delta H_{int} = \Delta H_d + 2\Delta H_B \quad (6)$$

or

$$\Delta Q_{int} = \delta n_6 \Delta H_d + 2n_{3x}\Delta H_B \quad (7)$$

where n_{3x} is the number of moles of S_3 binding with X, $\delta n_6 = n_6$(in the absence of X) − n_6(in the presence of X), and n_6 is the number of moles of S_6 in the solution. Therefore

$$\Delta H_B = \frac{\Delta Q_{int} - \delta n_6 \Delta H_d}{2n_{3x}} \quad (8)$$

The calculated values of δn_6, $\delta n_6 \Delta H_d$, n_{3x}, and ΔH_B are presented in Table IV (supplementary material). The average ΔH_B (see footnote 19) is found to be 49 ± 7 kcal mol^{-1} of S_3. The percentages of S_3 and S_6 needed to compute δn_6 and the percentages of binding used to calculate n_{3x} for eq 8 are included in the results of sedimentation velocity measurements on the effects of X on PC, as shown in Table V (supplementary material). The error of these percentage estimations (and the corresponding concentrations) is believed to be about ±5%.

The macromolecular dissociation constant (K_d) for the reaction in eq 4 can be represented as

$$K_d = (C_3)^2/(C_6) = 7.4 \times 10^{-5}\ \text{M} \quad (9)$$

where C_3 and C_6, as given in Table V, are 7.5×10^{-5} and 7.6×10^{-5} M at $C_x = 0$, respectively. The free energy change (ΔG_d) for eq 4 is

$$\Delta G_d = -RT \ln K_d = 5.6\ \text{kcal mol}^{-1} \quad (10)$$

From eq 10 and ΔH_d (eq 4), the entropy change (ΔS_d) is

$$\Delta S_d = \frac{(\Delta H_d - \Delta G_d)}{T} = -76\ \text{cal mol}^{-1}\ \text{deg}^{-1} \quad (11)$$

where T is 298 K. The thermodynamic parameters of polymerization of S_6 of PC from S_3 and those of three other protein systems are listed in Table VI.

The dissociation constant (K) for the binding of X with S_3 can be expressed as

$$S_3X_m \rightarrow S_3 + mX \quad (12)$$

$$K = \frac{(C_3)_u (C_x)^m}{(C_3)_b} \quad (13)$$

where C_x is the concentration (M) of X in the solution after mixing and $(C_3)_u$ and $(C_3)_b$ are the concentrations of

TABLE VI: Thermodynamic Functions of Binding and Polymerization of Some Proteins

A. Binding of Salt to Protein at 25 °C

Salt	Protein	pH	ΔH_B, kcal mol^{-1}	ΔG_B, kcal mol^{-1}	ΔS_B, eu
Bu_4NBr	Phycocyanin	6	49	−1.8	170
$MgCl^a$	Folded phenylalanine tRNA	7	0	−8.2	28
$NaSCN^b$	Polyacrylamide		−3.3	1.5	−16

B. Polymerization

Protein	pH	t, °C	Polymn process	ΔH, kcal mol^{-1}	ΔG, kcal mol^{-1}	ΔS, eu
Phycocyanin	6	25	$2S_3 \rightarrow S_6$	17	−5.6	76
Tryptophanase[c]	8	5	$2S_2 \rightarrow S_4$	50	−5.2	198
β-Lactoglobulin[c]	5	5	$4S_2 \rightarrow S_8$	−56	−15	−151
Hemoglobin[c]	7	20	$2S \rightarrow S_2$	−7	−6.5	−1.5

[a] Reference 15. [b] Reference 16. [c] Reference 17.

unbound and bound trimers, respectively, in the solution. From eq 13, one has

$$1 + K^{-1}(C_x)^m = (C_3)/(C_3)_u \tag{14}$$

where

$$(C_3) = (C_3)_b + (C_3)_u \tag{14a}$$

The apparent macromolecule dissociation constant (K_{app}) in the presence of X can be defined as

$$K_{app} = \frac{(C_3)^2}{(C_6)} = \frac{(C_3)_u^2}{(C_6)}\left[\frac{(C_3)}{(C_3)_u}\right]^2 \tag{15}$$

where C_3 and C_6 are given in Table V.

Combination of eq 14 and 15 gives

$$K_{app} = \frac{(C_3)_u^2}{(C_6)}[1 + K^{-1}(C_x)^m]^2 \tag{16}$$

Since $K_{app} = K_d$ when $C_x = 0$, therefore

$$K_{app} = K_d[1 + K^{-1}(C_x)^m]^2 \tag{17}$$

Comparing eq 14 and 17, one has

$$\frac{(C_3)_b}{(C_3)} = 1 - \left(\frac{K_d}{K_{app}}\right)^{1/2} \tag{18}$$

Rearranging the terms in eq 17 and taking logarithm, one has

$$\ln\left[\left(\frac{K_{app}}{K_d}\right)^{1/2} - 1\right] = m \ln C_x - \ln K \tag{19}$$

Values of K_{app}, $\ln [(K_{app}/K_d)^{1/2} - 1]$, and $\ln C_x$ are also listed in Table V. From the slope and intercept of a good straight line obtained by plotting $\ln [(K_{app}/K_d)^{1/2} - 1)]$ vs. $\ln C_x$, one has

$$m = 1.10 \tag{20}$$

$$-\ln K = 3.01$$

$$K^{-1} = K_B = 20\ M^{-1} \tag{21}$$

where K_B is the association constant for binding. The free energy change (ΔG_B) in the binding reaction is then given by

$$\Delta G_B = -RT \ln K_B = -1.8\ \text{kcal/mol} \tag{22}$$

The entropy of binding between S_3 and X can be calculated from the expression:

$$\Delta S_B = \frac{(\Delta H_B - \Delta G_B)}{T} = 170\ \text{cal mol}^{-1}\ \text{deg}^{-1} \tag{23}$$

where T is 298 K. The thermodynamic functions characteristic of the binding between S_3 and Bu_4NBr and those of two other salt–protein systems are presented in Table VI.

Discussion

The least-squares fit of $\Delta Q_{dil(x)}$ to eq 1 has a standard deviation of 1% for Et_4NBr and 4% for Bu_4NBr in the range of M_x = 0.160–0.08 M. Table III shows that the heat absorbed in the dilution of Et_4NBr at 0.144 M, pH 6.0, to infinitely dilute pH 6.0 solution (ΔQ_M^∞ = 126 cal mol^{-1}), performed in the microcalorimeter, is in excellent agreement with the result (130 cal mol^{-1}) in a solution containing no buffer and carried out in a conventional calorimeter. This finding suggests that the interaction between Et_4NBr, 0.144 M, and pH 6.0 buffer salts (containing, per liter, 0.01 mol of Na_2HPO_4 and 0.07 mol of NaH_2PO_4) are not significant compared with the interactions between Et_4NBr–solvent and Et_4NBr–Et_4NBr. In the case of Bu_4NBr, ΔQ_M^∞ is −202 cal mol^{-1} in an aqueous solution containing no buffer and −137 cal mol^{-1} in pH 6.0 buffer solution. A high negative heat of dilution for this salt is expected because of the strong hydrophobic interaction of Bu_4NBr.[12,13] The loss of some negative ΔQ_M^∞ (65 cal mol^{-1}) in the buffer system is due to the weakening of the hydrophobic interaction between Bu_4NBr and solvent through the interference of Na_2HPO_4 and NaH_2PO_4.

Values of ΔQ_{mix} and $\Delta Q_{dil(x)}$ (Table II) indicate that the hydrophobic interaction of Bu_4NBr becomes strong at M_x > 0.06 M. The heat of interaction (ΔQ_{int}) between Bu_4NBr and PC is positive. It is also independent of salt concentration within the limits of experimental error (see Table II for $\Delta Q_{int}/M_x$), indicating that in the salt concentration range under study, a large excess of Bu_4NBr exists in the solution. The excess of salt thus makes no significant contribution and does not interfere significantly with the specific interaction between Bu_4NBr and PC. The apparent enthalpy of binding may be a combination of the true binding enthalpy change and the conformation enthalpy change. The observation of a negligible heat of interaction of Et_4NBr with PC can be interpreted as evidence of a weak binding of Et_4NBr with PC. It is not possible with the present experiments to comment on the magnitude of the ΔH_B for Et_4NBr–PC system. A significant contribution from a conformation enthalpy change is expected in the Bu_4NBr–PC system on the basis of the observed ΔH_B. The significant difference in ΔQ_{int} between the Bu_4NBr–PC and Et_4NBr–PC systems obviously reflects a specific interaction of Bu_4NBr with PC.

The hexamer aggregate of PC appears to be stabilized by hydrophobic forces relative to the trimer aggregate.[1,2] The previous studies[1] demonstrated that at C_x = 0.16 M, all the four tetraalkylammonium salts, Me_4NBr (tetramethylammonium bromide), Et_4NBr, Pr_4NBr (tetrapropylammonium bromide), and Bu_4NBr, interact with PC and have effect on the dissociation of hexamer into trimer. The order of effect on disaggregation of the protein is $Bu_4NBr > Pr_4NBr > Et_4NBr > Me_4NBr$. It was proposed that the water structure change caused by R_4NBr in this concentration range is not important in PC aggregation and that specific interaction (binding) of the cations to the protein is likely.

Two mechanisms are possible in the binding between the bulky tetraalkylammonium cation (R_4N^+) and S_3 of protein: (1) The hydrophobic interaction between the

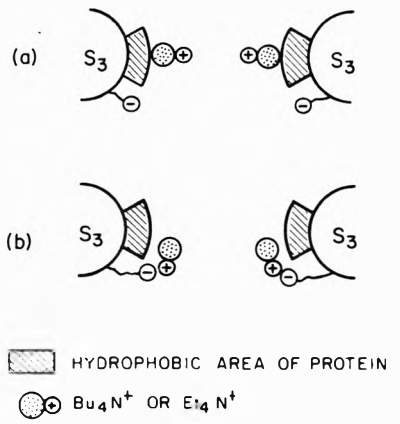

Figure 2. Possible mechanisms involving separation of two S_3 units of phycocyanin. (a) Hydrophobic interaction between hydrophobic area of protein and bulky alkyl groups of R_4N^+. (b) Ionic interaction between bulky R_4N^+ and an anionic group of protein. Mechanism b appears to be ruled out by very small value of ΔQ_{int} for Et_4NBr and much larger value for Bu_4NBr; see Discussion.

hydrophobic area of the protein and the bulky alkyl group of R_4N^+, as shown in Figure 2a, is able to inhibit the assembly of S_3 to S_6 due mainly to some possible steric interference at the hydrophobic area and possibly the ionic repulsion of the two R_4N^+. (2) The ionic interaction between R_4N^+ and an anionic group of the protein, in addition to some hydrophobic interaction between bulky alkyl groups of R_4N^+ and the hydrophobic area of protein, as shown in Figure 2b, is also able to inhibit the assembly of two S_3 due only to the steric effect of bulky alkyl groups of R_4N^+.

The second mechanism can be ruled out as follows: If the ionic interaction indicated in this mechanism were important, ΔQ_{int} of Et_4NBr would have a stronger ionic interaction with an anionic group of the protein than Bu_4NBr, since Et_4NBr has a higher charge:volume ratio. However, ΔQ_{int} for Et_4NBr is much less than that for Bu_4NBr. The fact that the butyl group has a stronger interaction (binding) with protein than the ethyl group has been demonstrated by measurements of the solubility[13] and transition temperature of ribonuclease.[14]

The thermodynamic parameters of association of S_3 to S_6 and those of three other proteins are presented in Table VI. In the polymerization process, the overlap of hydration regions of two individual units to form an aggregation unit, with a release of solvent due to the hydrophobic effect, will give a positive contribution to the entropy, while the formation of a more ordered (less random) conformation of protein unit will result in a loss in entropy. The gain of 76 eu during the association of S_6 suggests the importance of the hydrophobic interaction in PC aggregation. Similarly, the formation of S_3–X from strong hydrophobic Bu_4NBr and S_3 will give a positive contribution to entropy due to the release of solvent. The interaction of X and S_3 leading to a more random structure of S_3 in S_3–X than unbound S_3 will also contribute a positive entropy. These positive entropy contributions due to release of solvent and loosening of the S_3 structure are consistent with the gain of 170 eu in entropy as X binds to S_3 (Table VI).

The molar binding ratio (m) between S_3 and X, evaluated from eq 19 and 20, is 1, which means that binding a single molecule of X to S_3 can effectively inhibit the aggregation of two S_3 units. A low value of m can be interpreted as consistent with the well-characterized ability of a single amino acid residue substitution to dramatically affect the aggregation properties and physiological function of hemoglobin.[18] In addition, this calorimetric study suggests that a small molecule similar to R_4NX could bind strongly to a protein such as S-hemoglobin in a possible 1:1 binding ratio and severely inhibit its aggregation properties.

Supplementary Material Available: Tables II, IV, and V, containing heat of interaction data for PC in Bu_4NBr and Et_4NBr, calculations of the enthalpy of binding of S_3–Bu_4NBr, and sedimentation velocity measurements on the effects of R_4NBr on PC and the percentages of binding, respectively (3 pages). Ordering information is available on any current masthead page.

References and Notes

(1) C-H. Chen, R. MacColl, and D. S. Berns, *Arch. Biochem. Biophys.* **165**, 554 (1974).
(2) R. MacColl, D. S. Berns, and N. L. Koven, *Arch. Biochem. Biophys.* **146**, 477 (1971).
(3) C-H. Chen and D. S. Berns, *Proc. Natl. Acad. Sci. U.S.A.*, **72**, 3407 (1975).
(4) J. M. Sturtevant, *Annu. Rev. Biophys. Bioeng.*, **3**, 35 (1974).
(5) I. Wadso, *Pure Appl. Chem.*, **38**, 529 (1974).
(6) R. N. Goldberg, *Biophys. Chem.*, **3**, 192 (1975).
(7) B. Hedlund, C. Danielson, and R. Lovrien, *Biochemistry*, **11**, 4660 (1972).
(8) D. Bode, U. Schernau, and T. Ackermann, *Biophys. Chem.*, **1**, 214 (1974).
(9) Selected values of chemical thermodynamic properties, *Natl. Bur Stand., Techn. Note* **No. 270** (1968).
(10) S. Lindenbaum, *J. Phys. Chem.*, **70**, 814 (1966).
(11) E. Scott and D. S. Berns, *Biochemistry*, **4**, 2597 (1965).
(12) W. Y. Wen in "Water and Aqueous Solution—Thermodynamics and Transport Process of Tetraalkylammonium Salts", R. A. Horne, Ed., Wiley-Interscience, New York, N.Y., 1971.
(13) A. Wishnia and T. W. Pinder, Jr., *Biochemistry*, 5, 1534 (1966).
(14) P. H. von Hippel and K-Y. Wong, *Science*, **145**, 577 (1964).
(15) G. Rialdi, J. Levy, and R. Biltonen, *Biochemistry*, **11**, 2472 (1972).
(16) P. H. von Hippel, V. Peticolas, L. Schack, and L. Karlson, *Biochemistry*, **12**, 1256 (1973).
(17) I. M. Klotz, D. W. Darnell, and N. R. Langerman in "The Proteins", Vol. 1, H. Neurath and R. L. Hill, Ed., Academic Press, New York, N.Y., 1975, Chapter 5.
(18) M. Murayama, *CRC Crit. Rev. Biochem.*, **1**, 461 (1973).
(19) The average ΔH_B (49 ± 7 kcal/mol) is an average value of ΔH_E for C_x = 0.08 to 0.02 M (Table IV) and those for C_x = 0.12, 0.16, and 0.20 M (ΔH_B = 49, 37, and 39 kcal/mol, respectively). In the additional mixing reaction measurements in which M_{pc} = 35 mg/l M_x = 0.240, 0.320, and 0.400 M and V_{pc} = V_x = 0.3010 ml were used, it was found that $\Delta Q_{dil(pc)}$ = −1.30 mJ; ΔQ_{mix} = −65.9, −155.3 and −244.4 mJ; $\Delta Q_{dil(x)}$ = −82.9, −175.4, and −269.6 mJ; ΔQ_{int} = 18.3, 21.4, and 26.5 mJ; % of S_3 = 66, 83, and 100; % of S_6 = 34, 17 and 0; and $2n_{3x}\Delta H_B$ = 19.67, 23.48, and 29.29 mJ for C_x = 0.12, 0.16, and 0.20 M, respectively. The percentages of S_3 binding are 61 and 78 for C_x = 0.120 and 0.160 M, respectively, and that calculated from eq 14 is 78% for C_x = 0.200 M. Therefore, values of n_{3x} are 4.75, 7.57, and 9.10 × 10^{-8} mol and those of ΔH_B are 49, 37, and 39 kcal/mol for C_x = 0.120, 0.160, and 0.200 M respectively. The observation that the measured ΔH_B (39 kcal/mol at C_x = 0.200 M, where only S_3 exists, is comparable with the average ΔH_B (49 ± 7 kcal/mol), suggests that the proposal involving the binding of X to S_3 in the second step of the interaction between PC and X is reasonable.

Charged Micelle Shape and Size

J. E. Leibner and John Jacobus*

Department of Chemistry, Clemson University, Clemson, South Carolina 29631 *(Received August 12, 1976)*

Publication costs assisted by NIGMS, U.S. Public Health Service

The shape of micelles incapable of attaining spherical geometry has previously been discussed in terms of an oblate ellipsoidal model. Calculations are presented which indicate that this model is most probably incorrect, the correct model being a hemisphere capped cylinder. This latter model is discussed relative to available experimental data.

Introduction

Although numerous studies of micellization have appeared in the literature[1] and although the gross characteristics of micellar catalysis of various chemical processes have been described,[2] relatively fewer studies have been conducted in which the major emphasis centered on the size and shape of micelles. Prior to 1955, the major models considered were spherical and lamellar.[3-7] In 1955 Tartar described[8] an ellipsoidal model for aggregated surfactants which, due to constraints introduced by the length of their hydrocarbon chains ("tails"), were thought incapable of aggregation to spheres. This same model was subsequently adopted[9] and refined[10] by others.

In 1959 Tartar concluded[11] that numerous systems previously described[8] by the oblate ellipsoidal model were, in fact, spherical. A similar conclusion has been more recently reiterated[12] by others. Within the confines of the models chosen it is abundantly clear that a spherical model cannot accommodate micelles of large aggregation number,[8,10] i.e., shape alteration must occur. Micelles incapable of adopting spherical shape have been modeled[8-10] as oblate ellipsoids.

A second model for nonspherical micelles, a cylinder possessing a diameter twice the length of the tail of the constitutent monomers, originally proposed[13] by Debye and Anacker, has been employed by others, e.g., Stigter,[14] but, to our knowledge, no comprehensive comparison of this latter model to the ellipsoidal models has appeared. In view of extensive experimental evidence[13,15,16] that the cylinder is the most probable shape of a number of micellar aggregates, we have performed such an analysis. The results are reported herein.

Models

Upon micellization in water the hydrocarbon chains of surfactant ions are removed from the surrounding solvent and, concurrently, the charged head groups become proximate. A priori, a number of assumptions concerning the micelle are required to construct a model, viz., (1) the interior of the micelle (core) should resemble bulk hydrocarbon; (2) the charged head groups should be as widely separated as possible to minimize electrostatic interactions; (3) voids should not exist in the core; and (4) little, if any, solvent should exist in the core.[17] These assumptions, previously employed by others,[8,10,12] allow comparisons of shape and size to be made for various micelle models.

If the *minimum* extension for any model is chosen as l (Figure 1), the core volumes of the models (V) are readily calculated. The *maximum* number of monomers (N_{max}) capable of occupying these volumes are

$$N_{max} = V/v \qquad (1)$$

where v is the volume of the tail of an individual monomer. Both Tartar[8] and Tanford[10] have previously presented expressions for the length (l) and volume (v) of surfactant monomers in terms of n_c, the number of carbon atoms in the surfactant tail. Although the expressions presented[8] by Tartar are essentially equivalent to those of Tanford,[10] we shall employ those of Tanford which consider half of the head group–α carbon bond in the chain:

$$l = 1.5 + 1.265n_c \text{ Å} \qquad (2)$$

and

$$v = 27.4 + 26.9n_c \text{ Å}^3 \qquad (3)$$

For the spherical model, employing l as the radius, N_{max} as a function of n_c is presented graphically in Figure 2. At the core surface (radius = l) the surface area per monomer is essentially invariant (Figure 3). In general, however, interest lies in the surface area per monomer (SA/N_{max}) at some distance $l + d$, where d is the distance increment from the core to the polar head groups. For the sake of comparison we have chosen d = 2.0 Å. The surface area per monomer (head group 2.0 Å removed from the hydrocarbon core) is also presented in Figure 3. A marked decrease in SA/N_{max} is noted as n_c increases. The net effect expected upon increasing n_c is to increase head group repulsions. In order to counteract this increased repulsion it should be expected that if surfactants micellize to spherical shapes the number of monomers required to form a "stable" micelle should increase as n_c increases (provided that the electrostatic repulsive interactions dominate the desolvation energy of the hydrophobic tails) and/or that the fraction of charge (the fraction of "free" counterions) should decrease as n_c increases. We shall return to these points subsequently.

Granted that certain micelles are incapable of assuming spherical geometry and that a change in shape is therefore required, those shapes should be preferred which afford the greatest possible surface area per monomer at the polar head groups. Tartar[8] and Tanford[10] have suggested an oblate ellipsoid (the solid of revolution generated by revolution of an ellipse about its minor axis) as a possible model and have demonstrated that N_{max} can be markedly increased by minor changes in the axial ratio ($nl/l = n$ in Figure 1). It should be noted, however, that any increase in the axial ratio ($n >$ unity (n = unity for the sphere)) must perforce increase the core volume and consequently increase N_{max}. The question that remains is whether or not the oblate ellipsoid, within the constraints of our original assumptions, affords greater surface area per monomer than any other *reasonable* model.

Although a cylindrical model (rod) was considered by Tanford,[10] the model chosen was unreasonable in the sense

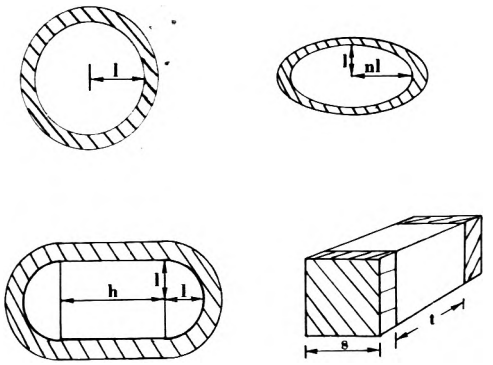

Figure 1. Micelle model dimensions for sphere, oblate spheroid, hemisphere capped cylinder, and bilayer. Cross hatched = head group volume.

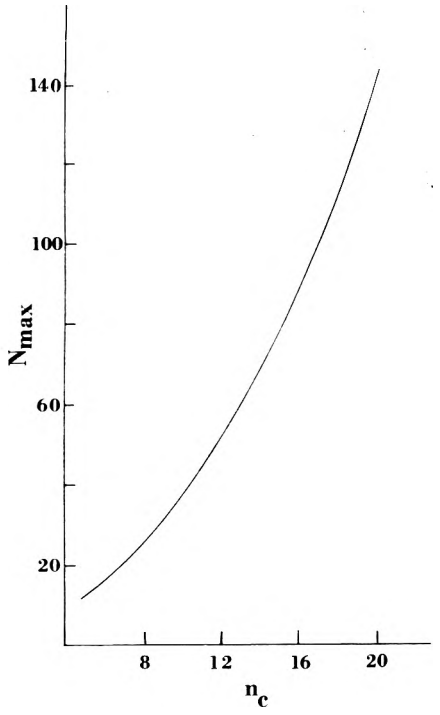

Figure 2. N_{max} as a function of n_c for spherical micelles.

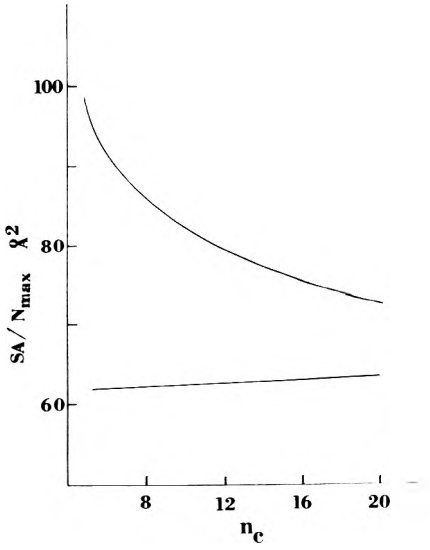

Figure 3. Surface area/N_{max} at l (lower) and at l + 2.0 Å (upper).

that the ends of the cylinder were uncapped, i.e., the hydrocarbon tails on the cylinder ends were exposed to solvent. If the cylindrical model is slightly modified to include hemispherical end caps, a reasonable model emerges; this model is readily generated from the sphere ("Hartley micelle")[3] by growth of a cylindrical body of radius l ("Debye–Anacker model")[13] within which the monomer packing resembles that of the monomers found about any great circle of the original sphere.

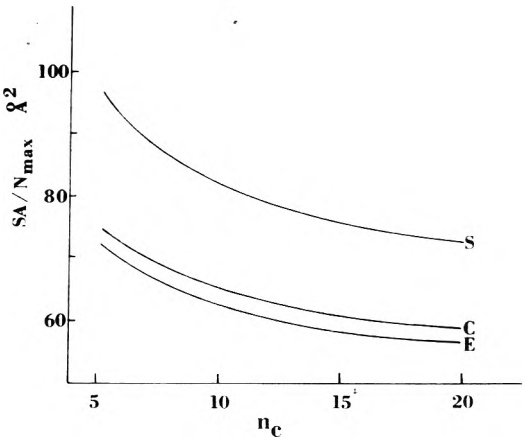

Figure 4. Surface area/N_{max} for sphere (S), ellipsoid (E), and cylinder (C) at l + 2.0 Å.

For any axial ratio n of an oblate ellipsoid (major semiaxis = nl; minor semiaxis = l), it is readily shown that *at constant volume* the length h of the corresponding hemisphere capped cylinder (Figure 1) is

$$h = \frac{4}{3}l(n^2 - 1) \tag{4}$$

Quantitatively, it can be shown that at the core surface at constant volume the difference in surface area between a hemisphere capped cylinder and an oblate spheroid is

$$\Delta SA = \pi l^2\left(\frac{2}{3}n^2 + \frac{4}{3} - \frac{1}{\epsilon}\ln\frac{1+\epsilon}{1-\epsilon}\right) \tag{5}$$

where n and ϵ are the axial ratio and eccentricity, respectively, of the ellipsoid. The surface area of an oblate ellipsoid will exceed that of a hemisphere capped cylinder of equal volume (semiminor axis = cylindrical radius = hemisphere cap radius = l) if and only if

$$\frac{1}{\epsilon}\ln\left(\frac{1+\epsilon}{1-\epsilon}\right) + \frac{2}{3}(\epsilon^2 - 1)^{-1} > \frac{4}{3} \tag{6}$$

a condition which cannot be met for any value of ϵ. Similar, but more complex expressions have been derived at a distance d from the core surface ($l + d$); the hemisphere capped cylinder exhibits greater surface area than the oblate ellipsoid of equal volume for all values of d. The constant volume constraint was chosen such that N_{max}(cylinder) = N_{max}(ellipsoid) and it is therefore obvious (inequality 6) that the surface area per monomer of the cylinder exceeds that of the ellipsoid.

For the sake of comparison we have chosen core volumes of ellipsoids and cylinders twice those of the sphere of equal n_c. The generated models possess at least one dimension in common with the corresponding sphere (radius of sphere = semiminor axis of ellipsoid = radius of cylinder and radius of hemisphere cap). Thus, the surface area per monomer for the sphere of volume V is compared with the ellipsoid and cylinder of volume $2V$ (containing $2N_{max}$ monomers) in Figure 4. The ellipsoids have semimajor axis equal to $\sqrt{2}l$ (eccentricity = 0.707) at the core surface and varying eccentricity at a distance increment d of 2.0 Å. At d = 2.0 Å the hemisphere capped cylinder possesses greater surface area per head group than the corresponding

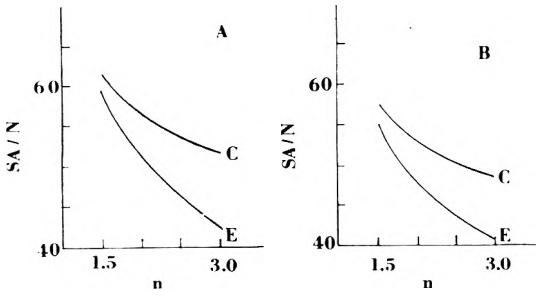

Figure 5. Surface area/monomer at $l + 2.0$ Å for the cylindrical (C) and ellipsoidal (E) model: (A) $n_c = 10$; (B) $n_c = 20$.

TABLE I: Surface Area Per Monomer for Bilayer

		(Surface area/monomer), Å^2	
n_c	t(Å) = 2l	Single chain	Double chain
8	23.24	20.87	41.74
10	28.30	20.95	41.90
12	33.36	21.00	42.00
14	38.42	21.03	42.06
16	43.48	21.06	42.12
18	48.54	21.08	42.16
20	53.60	21.10	42.20

oblate spheroid of equal core volume (equal N_{max}). The ratio $\Delta SA_{C-E}/N_{max}$ is ca. 1.9 Å^2 per head group.

Similarly, comparison of cylinders with oblate ellipsoids of equal core volume as a function of axial ratio (eccentricity) leads to the conclusion that as the axial ratio becomes large (approaches 3.0; eccentricity approaching unity) the ratio $\Delta SA_{C-E}/N_{max}$ becomes larger. These results are depicted in Figure 5 for $n_c = 10$ and 20; at $n = 3$ and $d = 2.0$ Å the values of $\Delta SA_{C-E}/N_{max}$ are 8.99 and 7.76 Å^2 per head group, respectively. Similar calculations reveal that the prolate ellipsoid is inferior to the oblate ellipsoid, i.e., at constant core volume the surface area per head group is less for the prolate model than for the oblate model. Although the surface area per head group differences between the hemisphere capped cylinder and the oblate ellipsoid model are small at small eccentricities (Figure 5), we believe that the cylindrical model is superior to an oblate or prolate ellipsoidal model when the main consideration is surface area per head group.

The bilayer model chosen is similar to that of Tanford.[10] For the model depicted in Figure 1

$$V = ts^2 \tag{7}$$

where $t = 2l$. For any aggregation number (N_{agg}) of monomers

$$V = N_{agg}(27.4 + 26.9n_c) \tag{8}$$

If the monomer possesses two hydrophobic tails, the volume must be multiplied by a factor of 2. The results are presented in Table I for monomers possessing one and two hydrophobic tails. Single chain surfactants possess only half the surface area per monomer available to the corresponding double chain surfactant. The exceedingly low values of surface area per monomer for single chain surfactants, approaching those of hydrocarbons in the crystalline state, would appear to preclude transitions from "normal" micelles (cylinders) to bilayer (or vesicle) geometries.

Granted that the cylindrical model is applicable to normal micelles, we have graphically depicted the surface area per monomer for a 16 carbon amphiphile as a function of the aggregation number (Figure 6). After an initial rapid decrease of surface area per monomer (to N_{agg} ca. 500), further large increases in N_{agg} result in small decreases in surface area per monomer. Up to N_{agg} of ca. 10^4, the surface area per head group has not reached values required (predicted on the basis of the model) for bilayer formation (Table I).

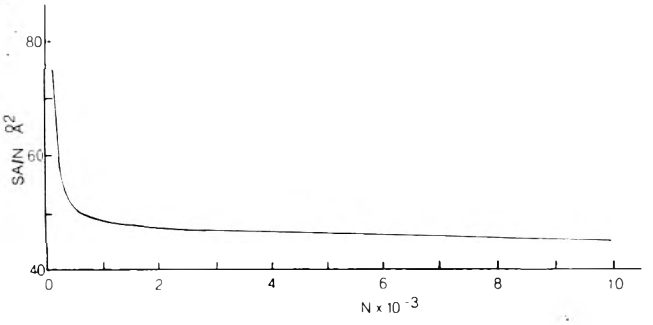

Figure 6. Surface area/monomer at $l + 2.0$ Å for a C_{16} micelle as a function of N_{agg}.

Tanford, by ignoring the effects of the ends of cylinders, concluded[10] that micelles undergo spherical to oblate ellipsoidal to cylindrical shape alteration. Our analysis indicates that the ellipsoidal model is inferior to the hemisphere capped cylinder (Debye and Anacker model)[13] in terms of available surface area per polar head group. We are aware of the fact that the increased surface area per head group is a consequence of the cylinder end caps. We will show that this model is reasonable and consistent with a large body of experimental evidence.

The Question of Chain Length

So far in our discussion we have not addressed the question of the number of chain atoms considered to be contained in the core of the micelle. Tanford has suggested[10] that n_c should not represent the entire hydrocarbon tail but, rather, due to decreased hydrophobicity of the carbons proximate to the head group, that the two carbons adjacent to the head group be excluded in the calculation of the dimension l. Stigter has more recently suggested[17] that the whole hydrocarbon chain be considered in the core of micelles, i.e., that the hydrophobicity of all carbons is essentially equal and that solvent interpenetration of such micellar cores is minimal.

The actual determination of chain length for inclusion in a micellar core has been a point of contention; Schott reached the conclusion[9] that most micelles in aqueous solution at the critical micelle concentration (cmc) could not be spherical. This claim was subsequently refuted[12] by Zografi and Yalkowsky on the grounds that Schott employed unreasonably short chain lengths. Tartar, in contrast to his earlier conclusions,[8] subsequently concluded[11] that numerous micelles were spherical at the cmc in the absence of supporting electrolytes.

Recent experimental evidence, e.g., laser Raman spectroscopy[18] and ^{13}C spin–lattice relaxation times,[19-21] indicates that near the polar head group the hydrocarbon chains of micelles exhibit a fair degree of rigidity. If this rigidity is interpreted as evidence for a preferred anti conformation of the chain near the head group, then regardless of the length of chain chosen to exist in the core, the locus of the head groups must be $l + d$, where l is the maximum chain extension. In this regard the arguments advanced[10] by Tanford to reduce aggregation numbers of micelles by reduction of the number of chain atoms contained in the core are open to question.

If a reduced core is described by $n_c - 2$ carbon atoms and if the excluded two-carbon "fragments" are radially extended away from the reduced core surface so as to afford maximum separation of head groups, a void volume

TABLE II: Aggregation Numbers of Micelles at Cmc in Water

Surfactant		Aggregation no.	Ref
	A. Alkyl sulfates ($RSO_4^-M^+$)		
R = n-C_8	M = Na	20	24
n-C_9	Na	31	25
n-C_{10}	Na	36;42;50	25;11;26
n-C_{12}	Na	40;41;57;62;70;80	27;11;28;29;26;30
n-C_{12}	Li	63	29
	B. Alkyl sulfonates ($RSO_3^-M^+$)		
R = n-C_8	M = Na	24	26
n-C_{10}	Na	41	26
n-C_{12}	Na	45;54	11;26
n-C_{14}	Na	70;80	11;26
	C. Alkyl trimethylammonium bromides ($RNMe_3Br$)		
R = n-C_8		23	31
n-C_9		30	31
n-C_{10}		36;44	23;31
n-C_{12}		40;50;50;62	11;23;26;31
n-C_{14}		75;92	23;31
n-C_{16}		80;95	11;32
	D. N-Alkylpyridinium bromides (R-Pyr$^+$Br$^-$)		
R = n-C_8		24	31
n-C_{11}		42	31
n-C_{12}		58	33
n-C_{14}		79	31
n-C_{16}		87	11

(solvent interpenetration volume) can be described as a function of the number of monomers capable of existing in the reduced core by

$$\Delta V = V_{n_c} - V_{n_c-2} \quad (9)$$

$$v_2 = 53.8(N_{n_c-2}) \quad (10)$$

and

$$\frac{\text{void}}{\text{monomer}} = \frac{\Delta V - v_2}{N_{n_c-2}} \quad (11)$$

where ΔV is the volume difference between a sphere n_c atoms in radius and a sphere $n_c - 2$ atoms in radius, v_2 is the total volume of two-carbon "fragments" beyond the core, and N_{n_c-2} is the aggregation number of the sphere of reduced core. For $n_c - 2$, the void volume decreases by 20% from $n_c = 7$ to $n_c = 16$, indicating that the two carbons most proximate to the head group of the hexadecyl system are 20% less solvated than the corresponding two atoms in the heptyl system. On the other hand, if the total chain length is employed to calculate N_{max}, the surface area per monomer at the core–solvent interface is, for all practical purposes, invariant (Figure 3). If minimization of the hydrocarbon–solvent interface is a major driving force for micellization, all n_c atoms should occupy the core and solvent should be maximally excluded, a conclusion previously reached by Stigter.[17]

Calculation of N_{max} based on truncated chain lengths may actually underestimate the aggregation numbers of micelles. If it is assumed that l (calculated from n_c) is an *average* value and that the micellar surface is irregular[22] (rough) then some volume is still allowed for solvent penetration and N_{max} (based on n_c) becomes a reasonable *estimate* for the aggregation number. We have therefore chosen to roughly *estimate* core volumes (and aggregation numbers) on the basis of the maximum extended chain length of a monomer.

Discussion

The most widely employed method for determining the size (aggregation number (N_{agg})) and shape of micelles is the scattering technique developed by Debye.[7,13,23] This technique has been applied to a number of micellar systems and some of the pertinent results are collected in Table II for systems at (or near) the cmc in pure water, i.e., in the absence of supporting electrolyte. The errors associated with the determination of N_{agg} have been discussed[11] and the higher values of N_{agg} reported for a particular surfactant can generally be disregarded.[11] The aggregation numbers from Table II are presented in Figure 7 relative to the curve of N_{max} calculated for spherical models employing n_c for the calculation of l (eq 2). Most of these experimentally determined aggregation numbers are less, within experimental error,[11] than N_{max} for a particular n_c. Granted that these micelles possess spherical geometry, as has been suggested by others,[8,11,12] the chain truncation procedure employed by Tanford[10] suggests premature changes from spherical to nonspherical geometry.

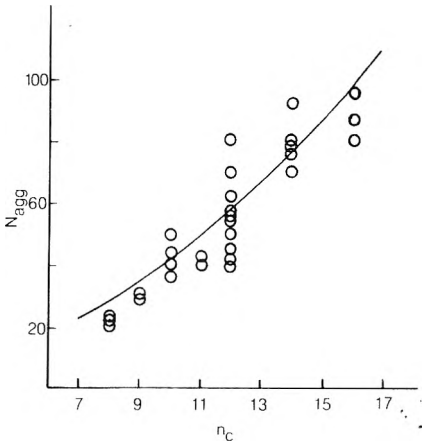

Figure 7. Aggregation numbers (Table II) as a function of n_c; solid line is N_{agg} calculated as described in text.

TABLE III: Calculated Surface Area per Monomer

n_c	N_{agg}[a]	Core surface	Head group[b]
8	23	66.16	78.72
9	30	64.94	75.79
10	36	65.11	74.99
11	42	63.44	74.69
12	40	70.25	79.96
14	75	62.67	69.32
16	80	66.67	73.30

[a] Lowest N_{agg} for a particular n_c for series C and D from Table II. [b] Assumed 1.0 Å beyond core surface.

Aggregates containing less than N_{max} monomers are acceptable entities. A priori, it should not be expected that aggregation numbers should necessarily equal N_{max} due to the extremely wide range of surface area per head group at reasonable distance increments from the core surface. Calculation of the surface area per monomer for the lower aggregation numbers presented in Table II shows that the average surface area per monomer (assuming spherical geometry) at the core surface for all C_8 to C_{16} surfactants (in Table II) is 65.6 ± 4.6 Å^2 (Table III), within experimental error of that calculated above (Figure 3) for spherical micelles. Assuming a core free of solvent, the radius required for the requisite volume of hydrocarbon can be calculated. If the head groups are assumed[17] to lie 1.0 Å beyond the core surface for the trimethylammonium and pyridinium compounds in Table II, the surface area per head group is found to be 75.3 ± 5.9 Å.^{2} This narrow range is indicative of similar, if not identical, head group interactions as might be expected within a homologous series. If the surface area per monomer at the head group

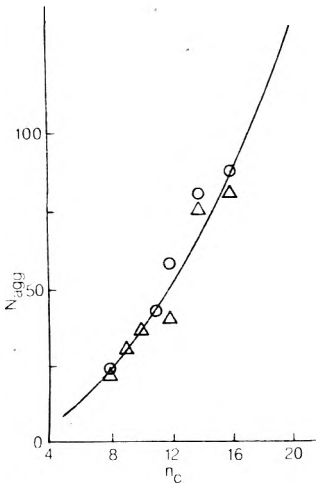

Figure 8. Aggregation numbers (Table II) as a function of n_c; solid line is N_{agg} as a function of n_c for $l - 0.6$ Å.

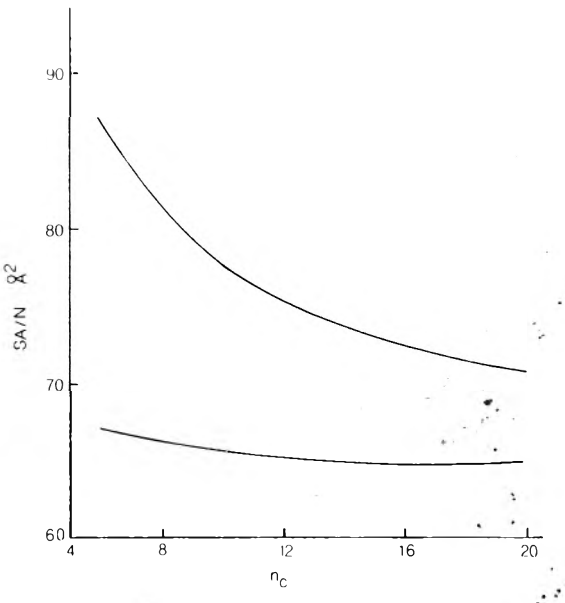

Figure 9. Surface area/monomer at $l - 0.6$ and at $l + 0.6$ Å.

were constant, it would be expected that the fraction of charge should, within a homologous series, be invariant.

The calculation of radii of spherical cores from aggregation numbers less than N_{max} (ammonium and pyridinium compounds in Table II) reveals that these radii are, in general, ca. 0.6 Å less than l calculated from n_c (eq 2). Radii of length less than l are reasonable if conformational mobility is considered for the hydrocarbon tails. Spectroscopic results[18-21] indicate chain mobility remote from the polar head groups. In order to occupy the total volume of the reduced core extensive chain "crimping" must occur, i.e., the chains cannot be arranged in a radial fashion away from the center of the core nor can they exist exclusively in the anti conformation. Whether or not this dimensional reduction is real, or an artifact of these calculations, is unclear. The dimension in question could actually be greater than that calculated above; such would be the case if extensive solvent penetration occurs to occupy the unfilled volume so produced.

Calculation of maximum aggregation numbers for spheres of radius 0.6 Å less than l calculated from eq 2 yields resulting values (Figure 8) remarkably close to those experimentally determined for the alkyltrimethylammonium and alkylpyridinium bromides listed in Table II. The surface area per monomer at the core surface (radius = $l - 0.6$ Å) and at the polar head groups (radius = $l + 0.6$ Å; the C–N bond is ca. 1.5 Å) are graphically depicted in Figure 9. For n_c in the range 8–16, the average surface area per monomer at the core is 65.41 ± 0.62 Å^2, while at the head groups it is 76.15 ± 5.05 Å^2. Thus, with all carbon atoms considered in the core, the water–hydrocarbon surface area per monomer is invariant, but head group solvation (void volume) is greater for short chain amphiphiles than for long chain amphiphiles. The wider separation of head groups for small n_c implies that the fraction of charge should decrease with increasing chain length of monomer. Unfortunately, data of sufficient degree of accuracy are unavailable to test this prediction for the compounds discussed above. However, we believe that the aggregation numbers presented in Figure 8 should be regarded as predictions for studies involving the determination of aggregation numbers at the cmc in pure water of alkyltrimethylammonium bromides and alkylpyridinium bromides. These calculations are not meant to imply that all spherical micelles will assume core volumes consistent with surface areas per monomer (at the core surface) of ca. 66 Å^2. For the systems listed in Table II this is apparently the case, but the actual surface area per monomer at the core surface may, depending on the electrostatic demands of a particular head group, vary from this value.

As surfactant concentrations are increased beyond the cmc, numerous micellar systems display increased aggregation numbers, e.g., hexadecyltrimethylammonium bromide (CTAB) exhibits a large increase in micelle molecular weight.[32,34,35] A similar increase in aggregation number is observed for many systems upon addition of common gegenion, e.g., CTAB, spherical at the cmc, displays a markedly increased aggregation number upon addition of KBr (N_{agg} ca. 2000 and 5000 in the presence of 0.178 and 0.233 M KBr, respectively; $c_0 = 2.72 \times 10^{-3}$ M).[13] Sodium dodecyl sulfate (SDS), a particularly well-characterized system,[36] displays increased aggregation number in the presence of NaCl.[27,29,36]

Counterion binding studies[37] employing ^{81}Br nuclear magnetic resonance spectroscopy indicates that as CTAB concentrations are increased (no supporting electrolyte) enhanced bromide binding (to a rod shaped micelle)[32,34,35] is observed. Such enhanced binding would be predicted for any model which displays decreasing surface area as a function of aggregation number. It is readily shown that at constant volume the coalescence of n spheres (or n cylinders) to a (larger) cylinder results in a loss of surface area of

$$\Delta SA = (1 - n)\frac{4}{3}\pi l^2 \qquad (12)$$

where l = micelle chain length. This loss of surface area must be compensated for by increased gegenion binding (to minimize electrostatic interactions). It is interesting to note that at high concentrations potassium salts of n-alkanoic acids (in the cylindrical (M_1)[38] phase) possess surface areas per polar head group of 47–57 Å^2, values closely approximated by consideration of the change in surface area as N_{agg} becomes large (Figure 6).[39]

Determinations of micelle shapes above the cmc and/or in the presence of added common gegenion have indicated the presence of rod-shaped micelles.[13,15,32,34,35,40] To our knowledge, charged micelles have never been unequivocally demonstrated to exist as oblate ellipsoidal aggregates. Debye and Anacker[13] and Reiss-Husson and Luzzati[15] have, to the contrary, ruled out the existence of oblate ellipsoidal aggregates for a number of the more common charged micelles. Transition from a spherical micelle with

greater surface area per monomer at the head group to a cylindrical micelle with reduced surface area per monomer at the head group requires either increased monomer concentration or addition of common gegenion, both circumstances are manifest as higher ionic strength, to balance the expected increase in repulsive electrostatic interactions. We believe that the calculations presented herein indicate that the most likely transition observed during increasing aggregation is from sphere to hemisphere capped cylinder, without the intermediacy of ellipsoidal (oblate or prolate) geometries.[41]

If increased aggregation (beyond N_{max}) with retention of spherical geometry were to occur, successively more of the constituent monomer hydrocarbon chains would be forced to be exposed to solvent, i.e., the hydrocarbon–water interface would increase. Since such an increase is energetically prohibitive, it should not be expected to occur. Rather, due to increasing ionic strength, a reduction of surface area per head group should be favored and a smooth transition from spherical to cylindrical geometry should result.

Although cylindrically shaped micelles are preferred above the cmc of most amphiphiles,[15,28] the production of bilayers is possible if the surface area per monomer is sufficiently reduced. For single chain amphiphiles the calculated surface area reduction is drastic (to ca. 21 Å^2 per head group). Experimentally, bilayers (lamellar (G)[38] phases) have been observed in concentrated solutions of the potassium (and other) salts of *n*-alkanoic acids which exhibit surface area per head group of ca. 32–38 Å^2,[39] close to the range calculated for amphiphiles possessing two chains (Table I). This large discrepancy between calculated and experimental surface areas demonstrates the inadequacy of any model which ignores specific head group interactions.

Conclusions

The models presented here have been concerned with the geometry of micelles. The sizes discussed for spherical micelles represent most probable aggregation numbers, but a limited range of sizes is not ruled out. The actual size of a micelle, either spherical or cylindrical, will intimately depend on a variety of conditions, e.g., concentration, supporting electrolyte, polar head group, gegenion, temperature, etc. Further, the models are based on the simplifying assumption that a major contributing factor to micelle shape (and size) is the surface area per head group (as a qualitative substitute for the electrical free energy) and have ignored the possibility that the configurational chain entropy might be a dominant factor in the determination of micelle shape and size. Thus, the models presented are of limited utility in a predictive sense; the ab initio calculation of aggregation numbers and critical micelle concentrations must await further improvement of our understanding of the various factors affecting micellization. Attempts in this direction have recently been undertaken.[42]

We should like to emphasize that our remarks pertain exclusively to charged micelles. A priori, there is no reason to believe that the models discussed here are applicable to uncharged (or zwitterionic) surfactants, the micellization of which are assuredly controlled by hydrophobic interactions, but whose head group interactions are not strictly comparable to charged systems.

Acknowledgment. This work was supported by Grant No. 1-R01-GM22788-01 from the NIGMS, U.S. Public Health Service. We thank Professor Janos Fendler, Professor Gary Powell, and Dr. Dirk Stigter for their cogent comments on this work.

References and Notes

(1) See, for example, the critical review of micellization by P. Mukerjee and K. J. Mysels, *Natl. Stand. Ref. Data Ser., Natl. Bur. Stand.*, **No. 36** (1971).
(2) This work has recently been reviewed (J. H. Fendler and E. J. Fendler, "Catalysis in Micellar and Macromolecular Systems", Academic Press, New York, N.Y., 1975).
(3) G. S. Hartley, "Aqueous Solutions of Paraffin-Chain Salts", Hermann et Cie, Paris, 1936.
(4) J. W. McBain, "Colloid Chemistry", Vol. 5, Reinhold, New York, N.Y., 1944.
(5) W. D. Harkins, *J. Chem. Phys.*, **16**, 156 (1948).
(6) M. L. Corrin, *J. Chem. Phys.*, **16**, 844 (1948).
(7) P. Debye, *Ann. N.Y. Acad. Sci.*, **51**, 575 (1949).
(8) A. D. Abbot and H. V. Tartar, *J. Phys. Chem.*, **59**, 1195 (1955).
(9) H. Schott, *J. Pharm. Sci.*, **60**, 1594 (1971).
(10) (a) C. Tanford, *J. Phys. Chem.*, **76**, 3020 (1972); (b) C. Tanford, "The Hydrophobic Effect: Formation of Micelles and Biological Membranes", Wiley, New York, N.Y., 1973.
(11) H. V. Tartar, *J. Colloid Sci.*, **14**, 115 (1959).
(12) G. Zografi and S. H. Yalkowsky, *J. Pharm. Sci.*, **61**, 651 (1972).
(13) P. Debye and E. W. Anacker, *J. Phys. Colloid Chem.*, **55**, 644 (1951).
(14) D. Stigter, *J. Colloid Interface Sci.*, **47**, 473 (1974).
(15) F. Reiss-Husson and V. Luzzati, *J. Phys. Chem.*, **68**, 3504 (1964).
(16) D. Stigter, *J. Phys. Chem.*, **70**, 1323 (1966).
(17) D. Stigter, *J. Phys. Chem.*, **78**, 2480 (1974).
(18) K. Kalyanasundaram and J. K. Thomas, *J. Phys. Chem.*, **80**, 1462 (1976).
(19) E. Williams, B. Sears, A. Allerhand, and E. H. Cordes, *J. Am. Chem. Soc.*, **95**, 4871 (1973).
(20) R. T. Roberts and C. Chachaty, *Chem. Phys. Lett.*, **22**, 348 (1973).
(21) K. Kalyanasundaram, M. Gratzel, and J. K. Thomas, *J. Am. Chem. Soc.*, **97**, 3915 (1975).
(22) D. Stigter and K. J. Mysels, *J. Phys. Chem.*, **59**, 45 (1955).
(23) P. Debye, *J. Phys. Colloid Chem.*, **53**, 1 (1947).
(24) E. Hutchinson and J. C. Melrose, *Z. Phys. Chem. (Frankfurt am Main)*, **2**, 363 (1954).
(25) W. Prins and J. J. Hermans, *K. Ned. Akad. Weterschap., Ser. B*, **59**, 298 (1955).
(26) H. V. Tartar and A. L. M. Lelong, *J. Phys. Chem.*, **59**, 1185 (1955).
(27) L. M. Kushner and W. D. Hubbard, *J. Colloid Sci.*, **10**, 428 (1955).
(28) F. Reiss-Husson and V. Luzzati, *J. Colloid Interface Sci.*, **21**, 534 (1966).
(29) K. J. Mysels and L. Princen, *J. Phys. Chem.*, **63**, 1696 (1959).
(30) J. N. Phillips and K. J. Mysels, *J. Phys. Chem.*, **59**, 325 (1955).
(31) H. J. L. Trap and J. J. Hermans, *K. Ned. Akad. Wetenschap., Ser. B*, **58**, 97 (1955).
(32) P. Ekwall, L. Mandell, and P. Solyom, *J. Colloid Interface Sci.*, **35**, 519 (1971).
(33) W. P. J. Ford, R. H. Ottewill, and H. C. Parreira, *J. Colloid Interface Sci.*, **21**, 522 (1966).
(34) K. G. Gotz and K. Heckmann, *J. Colloid Sci.*, **13**, 266 (1958).
(35) E. Graber, J. Lang, and R. Zana, *Kolloid-Z. Z. Polym.*, **238**, 470 (1970).
(36) E. W. Anacker, R. M. Rush, and J. S. Johnson, *J. Phys. Chem.*, **68**, 81 (1964).
(37) G. Lindblom, B. Lindman, and L. Mandell, *J. Colloid Interface Sci.*, **42**, 400 (1973).
(38) P. A. Windsor, *Chem. Rev.*, **68**, 1 (1968).
(39) B. Gallot and A. Skoulios, *Kolloid-Z. Z. Polym.*, **208**, 37 (1966).
(40) N. A. Mazer, G. B. Benedek, and M. C. Carey, *J. Phys. Chem.*, **80**, 1075 (1976).
(41) C. A. J. Hoeve and G. C. Benson, *J. Phys. Chem.*, **61**, 1149 (1957).
(42) E. Ruckenstein and R. Nagarajav, *J. Phys. Chem.*, **79**, 2622 (1975); *J. Colloid Interface Sci.*, **57**, 388 (1976).

Theory of Electrified Interfaces

Lesser Blum

Physics Department, College of Natural Sciences, University of Puerto Rico, Rio Piedras, Puerto Rico 00931 *(Received July 21, 1976)*

A new theory for the electrified interfaces, using the mean spherical and exponential approximations as the starting point, is proposed. This theory is based on a general result of Blum and Stell. It treats the exclusion volume effects exactly and consistently, but the long-range electrostatic forces are treated in an approximation; for the mean spherical case it is equivalent to the linearized Debye–Hückel theory. General expressions for the differential capacitance are given; in the limiting cases of zero potential, equal size, and low concentration they agree with the classic result of the linear Guoy–Chapman theory. The exponential approximation result with no image forces has a parabolic dependence in the applied potential for low potentials, but, unlike the classical result, it remains finite as the applied potential grows.

1. Introduction

The theory of the thermodynamics and structure of simple fluids and solutions has seen a dramatic change in the last 15 years; very precise yet simple equations have been derived that account quantitatively for the observed properties of fluids in equilibrium. Most of the successful equations (Percus–Yevick, hypernetted chain, mean spherical approximation, optimized cluster expansions, etc.) derive from what Percus[1] calls linear response theory, since they can be derived from a functional Taylor expansion, keeping only linear terms in the disturbance. This progress entrained a substantial improvement in the theory of electrolytic solutions. Ever since Arrenhius proposed his theory of electrolysis, physical chemists have been fascinated by the peculiar thermodynamic and electric properties of ionic solutions. This interest is quite justified by the widespread applications of ionic systems in chemical technology and biochemistry.

Historically, the first milestone on the way toward a quantitative understanding of electrolytes was, no doubt, the Debye–Hückel (DH) theory.[2] However one must not forget that the basic concept of the DH theory, the ionic cloud, was also present in some form in the Guoy–Chapman (GC)[3] theory for flat electrodes (interfaces), and that preceded the DH theory by some 15 years. Strangely enough, while the bulk of electrolytic solutions have been extensively studied, the theory of electrodic interfaces has seen little change in the basic approach since Guoy, Chapman, and Stern.[4]

The DH theory is a limiting theory for very dilute solutions. It is in good agreement with experiment only for very dilute solutions ("slightly contaminated water", as is often quoted). Therefore, a great deal of theoretical effort has been dedicated to the task of getting workable and sound theories for more concentrated ionic solutions. Basically there are two kinds of approaches that have been considered: the first, older and perhaps more popular, is to try and improve on the DH theory itself. This approach has a serious fallacy in that the DH theory is basically inconsistent in its treatment of the hard exclusion core. However one does obtain easy equations with good accuracy, if perhaps the meaning of the adjustable parameters is not always clear. The more fundamental approach was pioneered by the work of Mayer,[5] Friedman, and Stell and Lebowitz,[6] who showed the precise relation between the cluster expansions and the DH theory, and how the theory could be improved. It was the hypernetted chain equation (HNC) of Allnatt[7] that the very extensive work of Friedman and collaborators[8] showed to be such a successful equation for both the so-called primitive model of charged hard spheres and also the more realistic models that included soft core interaction and also the very important solvation effects.

As was mentioned above, one of the assumptions of the DH theory is that the ionic cloud that surrounds a given charge is effectively formed by point charges with no repulsion core, although the central charge is of finite size. This is the origin of the inconsistencies that are also responsible for the poor performance of this theory. However it also predicts that net charge density surrounding a given ion decays exponentially as a function of the distance to the ion. For concentrated solutions this is in violation of the so-called second moment condition of Stillinger and Lovett[9] which predicts charge oscillations in the ionic cloud. In addition there is also another theory, the mean spherical approximation (MSA) of Lebowitz and Percus,[10] that gives exactly the second moment, as was first shown by Groeneveld.[11] Furthermore, the MSA that is essentially a version of the DH theory with the exclusion core treated exactly and *consistently* was solved analytically for quite a few models of interest and relevance. The first analytic solution for the restricted primitive model (a neutral mixture of hard charged spheres of equal size and opposite charge) is due to Waisman and Lebowitz,[12] who showed that this theory was in excellent agreement with computer simulations and hypernetted chain equation results that are numerical and quite hard to obtain. This initial success promoted the search for analytic solutions of the MSA for a number of models with central and noncentral forces. Recently we found a solution for the primitive model of ionic solutions for the general mixture of unequal charge and size ions,[13] which is in reasonably good agreement with the HNC results,[14] and also turns out to be a convenient way to represent the data of real solutions of simple electrolytes.[15] Another relevant case that has a known solution is the mixture of hard spheres with charges and point dipoles.[16] This case should be interesting in view of the role that is assigned to the solvent by some current theories of the inner Helmholtz layer. Last, but not least, the MSA can be corrected systematically using a sequence of approximations that should converge to the exact answer; these approximations will be discussed below.

Quite recently, the distribution of hard spheres in the neighborhood of a hard wall was found in the Percus–Yevick approximation (Henderson, Abraham, and Barker,[17] Percus[18]), and was found to be in excellent agreement with machine computations (Liu[19]) except perhaps for small deviations in the vicinity of the wall. The small remaining discrepancy was later eliminated using the

generalized MSA[20] by Waisman, Henderson, and Lebowitz.[21]

One of the obvious shortcomings of the GC theory is the neglect of hard core exclusion effects. In a rigorous statistical mechanical theory a system without repulsions would just collapse[22] because of the infinite attraction of the image charges right at the wall. The occurrence of this catastrophe is prevented by assuming the existence of a distance of closest approach (Stern[4]) that is equal to the repulsion core of the ion (Grahame[23]) and that can be accounted for by an equivalent parallel plate capacitor.[24] This takes us to the dual model of the electric interface, in which the double layer is subdivided into two regions: the compact, inner Helmholtz layer, in which the ions are at fixed positions near the electrode wall, and the diffuse region where the GC theory is valid. To explain the observations of the dependence of the capacitance on the applied voltage and ionic concentration, it has been frequently assumed that the structure of the inner layer plays the dominant role and also that the orientation of the solvent (water) molecules in this inner layer causes some of the anomalous shapes seen in some cases. This last assertion seems very doubtful in view of the relatively low hydration energies of many ions[25] but, apart from that, the general scheme of the dual theory seems not to be very consistent since it does introduce a phase separation in a rather ad hoc manner. Recently, Cooper and Harrison[26] showed that this division into inner and outer regions will lead to gross inconsistencies, such as the necessity of assuming negative capacitances for the inner region. These authors have also criticized the role assigned to the solvent adsorption.

Furthermore, all the theories up to this point have treated the ionic clouds using the DH approach. This even applies to the more satisfying and statistically sound approach of Buff and Stillinger.[27] It will be amusing to notice that the numerical solution of the Buff–Stillinger equations that we performed about 10 years ago[28] showed them to produce even higher accumulation of ions near the electrode than the GC theory. While this is not unexpected, it just underlines the necessity of including the correct form of the excluded volume effects in a workable theory. Let us mention also in this connection that none of these theories satisfies the second moment condition,[9] and would therefore fail to exhibit the charge oscillations that these moment conditions predict. One is therefore naturally led into the necessity of formulating a theory of electrified interfaces that incorporates the modern theory of electrolytic solutions (in our present work, the MSA[10,12,13,16]) to the recent spectacular progress in the theory of hard interfaces,[17,18,21] since both theories are in good general agreement with the computer experiments done on the same Hamiltonian systems. Such a theory is implicit in the recent general solution of the Ornstein–Zernike equation for hard interfaces found by Blum and Stell.[29] In this work, which is summarized at the beginning of next section, a very general formula for the density profile is given as a function of the direct correlation function outside the hard wall (the closure) and the Wiener–Hopf factor correlation function for the bulk phase. In the MSA of the primitive model of electrolytes the factor correlation functions are explicitly known[13,16] and the closure is just given by the total interaction potential of the ions with the electrode. This interaction is divided into two contributions: (a) the image charge contribution, which is a complex, many body force, and which depends on the ionic concentration around the ion and on the nature of the solid surface (dielectric or metallic); and (b) the surface charge force which is derived from simple electrostatics.

Since the MSA does not yield the correct low density limiting form of the binary correlation function the results are then used to calculate the density profile in the exp approximation, which is the next order correction in the optimized cluster expansion of Andersen and Chandler[30] (the MSA is the lowest order approximation in this hierarchy).

We have also considered the functional Taylor series expansion of Stell[29,31] which is also formally exact. However in the present work we will not include this approach which will be left for future publications. We should remark, however, that the mean spherical approximation used in this article is by no means a natural limitation of the theory, but rather a result that is at hand which treats the exclusion effects exactly and gives a fair representation of the properties of bulk electrolytes. It is not excluded that, in the future, numerical methods will be at hand to compute the Wiener–Hopf factor functions for more elaborate representations and more elaborate approximations, such as, for example, the HNC equations with hydration shell corrections (see, for example, ref 25 and references cited therein).

In section 2 we give the basic equations for the MSA and exp approximations of the density profile of the individual ions. In section 3 some general formulas for the relevant properties, charge and potential profiles, capacitance, and excess energy, are given. Section 4 is devoted to the discussion of several limiting cases for the restricted primitive model of electrolytes.

2. Mean Spherical and Exp Approximations

To introduce the notation, let us restate the main results of Blum and Stell[29] for the case of primitive model electrolytes. The system under consideration is therefore a neutral mixture of n ionic species, which are charged hard spheres of number density ρ_i, diameter σ_i, and charge z_i (in electron units) ($1 \leq i \leq n$). The correlation function for the wall particle pair is $g_{0i}(x)$, where x is the distance from the particle to the wall. Clearly $\rho_i g_{0i}(x)$ is the probability of finding an ion of species i at a distance x from the wall. The indirect correlation function

$$h_{0i}(x) = g_{0i}(x) - 1 \tag{2.1}$$

together with the wall–particle Ornstein–Zernike equation defines the corresponding direct correlation function $c_{0i}(x)$[17,18]

$$h_{0i}(x) = c_{0i}(x) + 2\pi\Sigma_j \rho_j \int_0^\infty dt \int_{x-t}^{x+t} ds \times t\, c_{ij}(t)\, h_{0j}(s) \tag{2.2}$$

the quantity $c_{ij}(t)$ in this equation is the bulk direct correlation function of the ionic pair i,j.[32] When the bulk properties of the fluid phase are studied, and we have to solve the OZ equation for the pair correlation function $h_{ij}(t)$, we need to know the value of the function $c_{ij}(t)$ *inside* the hard repulsion core of the pair. Finding $c_{ij}(t)$ in this region is always the difficult part of the problem, to the point that only a very few approximations, in which the direct correlation function is either zero or a combination of exponentials, can be solved explicitly. In the flat wall case, however, the problem is of the classic Wiener–Hopf type that is extensively discussed in many textbooks. It turns out that the wall–particle direct correlation function $c_{0i}(x)$ inside the hard wall just drops out of the solution, which is a most welcomed feature since it allows for a solution of the very general case in which the direct correlation function is any arbitrary function of the dis-

tance x.[29] A simpler way of putting it is to say since only $h_{0i}(x)$ for $x > \sigma_i/2$ is required, then to solve (2.2) we need to know

$$c_{0j}(x) = \phi_j(x) \tag{2.3}$$

for $x > \sigma_j/2$ only. Our major approximation is then the assumed form of $\phi_j(x)$ which, as was said above, is simply the interaction potential for the MSA. The central result of ref 29 was the reduction of the OZ equation (eq 2.2) to the ordinary integral equation

$$g_{0j}(x) - \sum_l \rho_l \int_{\lambda_{jl}}^{x-\sigma_l/2} dr\, g_{0l}(x - r)\, Q_{lj}(r) = \sum \tilde{Q}_{lj}(0) - F_j(x) \tag{2.4}$$

$$= \frac{1}{2\pi} Q_j'' - F_j(x) \tag{2.5}$$

Here, (2.4) is completely general, while (2.5) is valid for the MSA and GMSA.[20] A summary of the main results and properties of the Baxter factor correlation function $Q_{lj}(r)$ are given in Appendix A. We did use also the definitions

$$\lambda_{lj} = \frac{1}{2}(\sigma_l - \sigma_j) \tag{2.6}$$

$$F_j(x) = \frac{1}{2\pi} \int_{-\infty}^{\infty} d\kappa \sum_l \tilde{\phi}_l(\kappa) [\tilde{Q}^T(-\kappa)]_{lj}^{-1} e^{-i\kappa x} \tag{2.7}$$

and

$$\tilde{\phi}_l(\kappa) = \int_{\sigma_l/2}^{\infty} dx\, e^{i\kappa x} \phi_l(x) \tag{2.8}$$

Alternatively, using Parseval's formula, we obtain $F_j(x)$ as a real space integral

$$F_j(x) = \sum_l \int_{\lambda_{lj}}^{\infty} dr\, \phi_l(x + r)\, P_{lj}(r) \tag{2.9}$$

where $P_{lj}(r)$ is the factor correlation function for the bulk pair correlation function $h_{ij}(t)$, and is defined by (see also appendix A)

$$P_{lj}(r) = \frac{1}{2\pi} \int_{-\infty}^{\infty} d\kappa\, e^{i\kappa r} [\tilde{Q}^T(-\kappa)]_{lj}^{-1} \tag{2.10}$$

It is apparent that an explicit solution for $g_{0j}(x)$ can be obtained by Laplace transformation, since (2.4) and (2.5) are convolutions. If we write

$$g_{0i}(x) = g_{0i}^{0}(x) + \Delta g_i(x) \tag{2.11}$$

then

$$g_{0i}^{0}(s) = \int_{\sigma_{i/2}}^{\infty} dx\, e^{-sx}\, g_{0i}^{0}(x) = \sum_j \frac{e^{-s\sigma_{j/2}}}{2\pi s} Q_j''[\tilde{Q}(is)]_{ji}^{-1} \tag{2.12}$$

which is the Precus–Yevick hard core contribution to the wall particle pair correlation function.[1,17,18] Equation 2.12 is the generalization to mixtures of the results of Henderson et al.[17] and Percus.[18]

The external or soft core contribution in (2.11) is given by

$$\Delta\tilde{g}_i(s) = \int_{\sigma_{i/2}}^{\infty} dx\, e^{-sx}\, \Delta g_i(x) = -\sum_j \tilde{F}_j(s) \{\tilde{Q}(is)\}_{ij}^{-1} \tag{2.13}$$

where

$$F_j(s) = \int_{\sigma_{j/2}}^{\infty} dx\, e^{-sx}\, F_j(x) \tag{2.14}$$

Using the convolution property of the Laplace transforms we can obtain the useful form of $\Delta g_i(x)$ in terms of the factor correlation function $P_{lj}(r)$

$$\Delta g_i(r) = -\sum_{lj} \int_{\sigma_{i/2}}^{r} dx \int_{\lambda_{lj}}^{\infty} dy\, \phi_l(x + y) \times P_{lj}(y)\, P_{ji}^{T}(r - x) \tag{2.15}$$

Equations 2.13 and 2.15 are the basic results of our previous work (although in a somewhat different form).[29] It can also be verified that for the single component case, in the exponential closure $\phi(x) = Ae^{-\mu x}$, our result agrees with that of Waisman et al.[21] which was obtained by a different method.

Consider now the MSA for the interface. Then

$$\phi_j(x) = +\beta\, u_{0j}(x) \tag{2.16}$$

where $u_{0j}(x)$ is the wall ion potential interaction. Perhaps we should mention at this point that although the MSA does not go to the right limits at low dilution concentration, it should however be a reasonably good theory for the more dense systems, and especially for the difference correlation function[33,34]

$$\sum_{i=1}^{n} \rho_i z_i g_{ij}(x)$$

Stell and collaborators have shown that the results for the bulk are quite good. It is perhaps not justified to extrapolate these conclusions to the flat wall case, but we should notice that the quantities studied in the next section are functions of precisely this correlation function difference. Therefore it is only reasonable to expect fair agreement in the more concentrated solutions.

Let us now analyze the potential that goes into (2.16) for our model system. It will be the sum of two contributions, the first one due to the excess charge at the surface of the wall and the second due to the image charges

$$\phi_j(x) = \phi_j^{PT}(x) + \phi_j^{IM}(x) \tag{2.17}$$

The first term is simply the potential energy of a charge in an uniform field[35]

$$\phi_j^{PT}(x) = (z_j/\epsilon_0)\beta e E_0 x \tag{2.18}$$

where E_0 is the bare uniform field caused by the excess surface charge at the electrode, $\beta = 1/k_\beta T$ is the Boltzmann thermal factor, ϵ_0 the dielectric constant, and e the elementary charge.

The contribution to the potential of the image charges is much more complex. If the wall is flat and homogeneous with dielectric constant $\epsilon \neq \epsilon_0$, then every charge in the bulk, z_i, will have an image of charge

$$z_i' = z_i \frac{\epsilon_0 - \epsilon}{\epsilon_0 + \epsilon} \tag{2.19}$$

located at the point

$$\mathbf{r}_i' = (-x_i, y_i, z_i)$$

If the electrode is metallic, then the dielectric constant is $|\epsilon| \to \infty$ so that $z_i' = -z_i$ and the interaction is attractive. If the wall is a biological membrane, then $\epsilon < \epsilon_0$ and the image force is repulsive. Notice that the very general nature of (2.13) and (2.15) makes it possible to study more realistic interfaces in which the dielectric constant does depend on the distance to the wall x. This will be the case even for a realistic representation of a metallic interface, because the electron density is not uniform at the surface because of the surface states. It will be the case also for the technologically interesting layered electrodes, or

semiconducting electrodes, and in biological membranes. In all of these cases (2.19) is replaced by a sum over infinitely many images. A very elegant method to deal with this problem has been proposed by Buff and Stillinger.[27] Again here we will have to restrict our treatment to the case of a single image, leaving the other cases for some future work.

Now in our system, every ion interacts not only with its own image, but also with the images of all the remaining ions in the system

$$\phi_i^{IM}(x_i) = z_i \frac{\beta e^2}{\epsilon_0} \sum_j{}' z_j' \left\{ \frac{\delta_{ij}}{2x_i} + \int d\vec{r}_j \, \rho_j(\vec{r}_j|\vec{r}_i) \frac{1}{|\vec{r}_j' - \vec{r}_i|} \right\} \tag{2.20}$$

In this equation, the first term represents the interaction of the charge i with the images of the remaining ions in the system. $\rho_j(\vec{r}_j|\vec{r}_i)$ gives the conditional probability of finding ion j at $\vec{r}_j$, knowing that ion i is at $\vec{r}_i$. For simplicity we will take

$$\vec{r}_i = (x_i, 0, 0)$$

The second term in (2.20) is just the interaction of i with its own image.

Consider now the conditional probability $\rho_j(\vec{r}_j|\vec{r}_i)$. When the particles i and j are far from each other, then it should be true that for a fluid interface

$$\lim_{r_{ij} \to \infty} \rho_j(\vec{r}_j|\vec{r}_i) \to \rho_j(x_j) \tag{2.21}$$

where

$$\vec{r}_{ij} = \vec{r}_i - \vec{r}_j$$

It will be convenient at this point to define the position dependent binary correlation function

$$g_{ij}(\vec{r}_i, \vec{r}_j) = \rho_j(\vec{r}_j|\vec{r}_i)/\rho_j(x_j) \tag{2.22}$$

From (2.21), the asymptotic behavior of this function is

$$\lim_{|r_{ij}| \to \infty} g_{ij}(\vec{r}_i, \vec{r}_j) = 1 \tag{2.23}$$

Clearly also if the pair of molecules is far from the wall, then the correlation function must be that of the bulk. Then

$$\lim_{x_i, x_j \to \infty} g_{ij}(\vec{r}_i, \vec{r}_j) = g_{ij}(r_{ij}) \tag{2.24}$$

We remember also that

$$\rho_j(x) = \rho_j \, g_{0j}(x)$$

is the unknown quantity of our problem. It is then only natural to rewrite the integral of the first term in (2.20) as

$$\int d\vec{r}_j \, \rho_j(\vec{r}_j|\vec{r}_i) \frac{1}{|\vec{r}_j - \vec{r}_j'|} = \int_0^\infty dx_j \, \rho_i(x_j) \, G_{ij}(x_j|x_i) \tag{2.25}$$

with

$$G_{ij}(x_j \, x_i) = 2\pi \int_0^\infty dR \, R \times g_{ij}(\vec{r}_i, \vec{r}_j)/[R^2 + (x_i + x_j)^2]^{1/2} \tag{2.26}$$

where

$$R^2 = y_j^2 + z_j^2$$

However from (2.23) the integrand in (2.26) clearly tends to unity and therefore $G_{ij}(x|x')$ does not seem to exist because the integral of the right-hand side of (2.26) is divergent. This difficulty is resolved when we consider the potential of a charged sheet of constant surface density $\rho(x) \, \delta(x - x_1)$

$$\begin{aligned} \phi(x) &= \int dy_1 \, dz_1 \, \rho(x_1) \frac{1}{|\vec{r} - \vec{r}_1|} \\ &= 2\pi\rho(x_1) \int_0^\infty \frac{dR \, R}{[R^2 + (x - x_1)^2]^{1/2}} \\ &= \lim_{L \to \infty} 2\pi\rho(x_1) \int_0^L dR \frac{R}{[R^2 + (x - x_1)^2]^{1/2}} \\ &= \lim_{L \to \infty} 2\pi\rho(x_1)[[L^2 + (x - x_1)^2]^{1/2} - |x - x_1|] \end{aligned} \tag{2.27}$$

Clearly, the first term diverges like L. However it does not contribute to the field because it is constant, and merely amounts to a shift in the potential. Therefore it can be supressed with no further consequence. Then

$$\phi(x) = -2\pi\rho(x_1)|x - x_1| \tag{2.28}$$

Just as a check let us differentiate (2.28) twice. We obtain the correct result

$$\frac{\partial^2 \phi(x)}{\partial x^2} = -4\pi\rho(x_1) \, \delta(x - x_1)$$

where $\delta(x)$ is the Dirac delta function. It is now clear that the same kind of constant infinity should appear in (2.25). We can therefore proceed to remove it using the above procedure. First, we replace

$$g_{ij}(\vec{r}_i, \vec{r}_j) = h_{ij}(\vec{r}_i, \vec{r}_j) + 1 \tag{2.29}$$

in (2.26). Hence

$$G_{ij}(x_j|x_i) = 2\pi \int_0^\infty dR \frac{R \, h_{ij}(\vec{r}_i, \vec{r}_j)}{[r_{ij}^2 + 4x_i x_j]^{1/2}} + 2\pi \int_0^\infty dR \frac{R}{[R^2 + (x_i + x_j)^2]^{1/2}} \tag{2.30}$$

Eliminating the constant infinity, we obtain

$$G_{ij}(x_j|x_i) = 2\pi \left[\int_0^\infty dR \frac{R \, h_{ij}(\vec{r}_i, \vec{r}_j)}{[r_{ij}^2 + 4x_i x_j]^{1/2}} - |x_i + x_j| \right] \tag{2.31}$$

which is now perfectly well behaved. Replacing this equation into (2.26) and then into (2.20), we obtain the image potential contribution

$$\phi_i^{IM}(x_i) = \frac{\beta e^2}{\epsilon_0} z_i \sum_j z_j' \left[\frac{\delta_{ij}}{2x_i} + \int_0^\infty dx_j \, G_{ij}(x_j|x_i) \, \rho_j(x_j) \right] \tag{2.32}$$

In the most general case $\phi_i^{IM}(x)$ is a nonlinear functional of $\rho_j(x)$ because h_{ij} is also dependent on the density distribution $\rho_j(x)$. This is essentially a three-body correlation function (the two particles and the wall). Reasonable

approximations of this function have been discussed in the literature (Buff and Stillinger,[27] Pressing and Mayer,[36] Tøxvaerd[37]), all of which are simple but nonlinear functionals of $\rho_j(x)$. Again here we will leave the discussion of this point and its consequences for the future. We can, nevertheless, give a qualitative idea of its behavior. In the strict limit $\rho \to 0$ the integral term in (2.32), which represents the shielding of the image of i by the other charges, goes to zero and we are left with the bare charge–image interaction

$$\frac{\beta e^2}{\epsilon_0}\frac{z_i z_i'}{2x_i}$$

which is not density dependent. Clearly also, this term will give the dominant contribution in this case. However it is clear also that if the charge i is touching the wall, then the shielding will be minimal also, and the same term will give most of the image potential contribution. Therefore we do expect that the changes in the image shielding brought about by the density dependence of $h_{ij}(\vec{r}_i, \vec{r}_j)$ should be small, if not totally negligible. If we then take $h_{ij}(\vec{r}_i, \vec{r}_j)$ as the bulk correlation function, we can replace the explicit form[38] (see Appendix C) into (2.31). Even with these simplifications the integrations are complex and we have not been able, as yet, to obtain a closed form expression in terms of known functions. One would expect, however, that in a sufficiently dilute solution the image potential will take the form assumed in the classic papers by Loeb[39] and Levine and Bell[40]

$$\phi_i^{IM}(x_i) \approx \frac{e^{-\Gamma x_i}}{2x_i} \tag{2.33}$$

For more concentrated solutions there should be charge oscillations, so that the shape of the image potential will be considerably more complicated.

Let us now turn to the functions $F_j(x)$ defined by eq 2.9. From (2.17) we see that they can also be split into the sum of two contributions, the image term and the potential term

$$F_j(x) = F_j^{PT}(x) + F_j^{IM}(x) \tag{2.34}$$

with

$$F_j^{PT}(x) = \sum_l \int_{\lambda_{lj}}^{\infty} dr\, \phi_j^{PT}(r + x)\, P_{lj}(r) \tag{2.35}$$

and

$$F_j^{IM}(x) = \sum_l \int_{\lambda_{lj}}^{\infty} dr\, \phi_j^{IM}(r + x)\, P_{lj}(r) \tag{2.36}$$

From (2.18) we see that

$$F_j^{PT}(x) = \frac{\beta e E_0}{\epsilon_0} \sum_l z_l \int_{\lambda_{lj}}^{\infty} dy\, (x + y)\, P_{lj}(y) \tag{2.37}$$

or

$$F_j^{PT}(x) = \lim_{s \to 0} \frac{\beta e E_0}{\epsilon_0} \sum_l z_l \left(x - \frac{\partial}{\partial s}\right) \tilde{P}_{lj}(s) \tag{2.38}$$

where

$$\tilde{P}_{lj}(s) = \int_{\lambda_{lj}}^{\infty} dy\, e^{-sy}\, P_{lj}(y) \tag{2.39}$$

However (see Appendix B), in the MSA

$$\lim_{s \to 0} \sum_l z_l \tilde{P}_{lj}(s) = 0 \tag{2.40}$$

$$\lim_{s \to 0} -\frac{\partial}{\partial s} \sum_l z_l \tilde{P}_{lj}(s) = -M_j \tag{2.41}$$

from where we obtain the very simple potential contribution to $F_j^{PT}(x)$

$$F_j^{PT}(x) = -\frac{\beta e E_0}{\epsilon_0} M_j \tag{2.42}$$

For the case of equal size ions, the constant M_j has been evaluated in Appendix B. We should remark that this result is in agreement with the one obtained directly from the MSA of different diameter and charge mixture,[13] in which one of the components dwindles in concentration and grows in charge and size. (However, there is no way of including the image charges in this treatment.)

The image contribution is from (2.19), (2.36), and (2.32) after exchanging the order in the integrations

$$F_j^{IM}(x) = -\sum_k z_k \int_0^{\infty} dx_k\, K_{kj}(x_k|x)\, \rho_k(x_k) - L_j(x) \tag{2.43}$$

where we defined

$$K_{kj}(x_k|x) = \frac{\epsilon - \epsilon_0}{\epsilon + \epsilon_0}\frac{\beta e^2}{\epsilon_0} \times \sum_l z_l \int_{\lambda_{lj}}^{\infty} dr_1\, P_{lj}(r_1)\, G_{kl}(x_k|x + r_1) \tag{2.44}$$

$$L_j(x) = \frac{\epsilon - \epsilon_0}{\epsilon + \epsilon_0}\frac{\beta e^2}{2\epsilon_0} \times \sum_l z_l^2 \int_{\lambda_{lj}}^{\infty} dr_1\, P_{lj}(r_1)/(x + r_1) \tag{2.45}$$

A very interesting quantity in electrochemistry is the direct contact adsorption on the electrode wall. The relevant statistical quantity, the contact correlation function, can be obtained very easily from (2.5)

$$g_{0j}(\sigma_j/2) = \frac{1}{2\pi} Q_j'' - F_j(\sigma_j/2) \tag{2.46}$$

Therefore, from (2.34), (2.42), and (2.43) we obtain the MSA contact distribution function

$$g_{0j}(\sigma_j/2) = \frac{1}{2\pi} Q_j'' + \frac{\beta e E_0}{\epsilon_0} M_j + L_j(\sigma_j/2) + \sum_k z_k \int_0^{\infty} dx_k\, \rho_k(x_k)\, K_{kj}(x_k|\sigma_j/2) \tag{2.47}$$

The contact values of the MSA are not expected to be in very good agreement with experiment,[33,34] so that one should use the more reliable exp approximation[30]

$$g_{0j}(\sigma_j/2) = \frac{1}{2\pi} Q_j'' \exp\left\{\frac{\beta e E_0}{\epsilon_0} M_j + L_j(\sigma_j/2) + \sum_k z_k \int_0^{\infty} dx_k\, \rho_k(x_k)\, K_{kj}(x_k|\sigma_j/2)\right\} \tag{2.48}$$

The adsorption probability that is given by $\rho_j\, g_{0j}(\sigma_j/2)$ also plays an important role in electrokinetic phenomena.

Finally, we shall calculate the density distribution profile

$$\rho_j(x) = \rho_j\, g_{0j}(x) \tag{2.49}$$

From (2.11), (2.13), and (2.34) we write

$$\Delta g_i(x) = \Delta g_i^{PT}(x) + \Delta g_i^{IM}(x) \tag{2.50}$$

where Δg_i^{PT} is the potential contribution to the excess density while Δg_i^{IM} is the contribution due to the image forces. From (2.13), (2.14), and (2.42), we obtain at once

$$\Delta \tilde{g}_i^{PT}(s) = \frac{\beta e E_0}{\epsilon_0} \sum_j M_j \frac{e^{-s\sigma_j/2}}{s} [\tilde{Q}(is)]_{ji}^{-1} \tag{2.51}$$

For the equal size case the explicit inversion of this formula

is discussed in Appendix C. For the more general case of different size ions, the algebra is considerably more complicated, but we hope to obtain simple enough formulas of sufficient accuracy. This work is already in progress.

The image contribution is best obtained from (2.15) in conjunction with (2.32) (since the integrations cannot be performed analytically)

$$\Delta g_i^{IM}(x) = -\sum_{l,j} \int_{\sigma_{j/2}}^{x} dr \int_{\lambda_{lj}}^{\infty} dy\ P_{lj}(y)\ P_{ji}^{T}(x - r) \frac{\beta e^2}{\epsilon_0} z_l \sum_k z_k \left[\frac{\delta_{lk}}{2x_l} + \int_0^{\infty} dx_k \times G_{lk}(x_k | r + y)\ \rho_k(x_k) \right] \quad (2.52)$$

Using the definitions (2.43), (2.44), and (2.45), eq 2.52 can be rearranged into

$$\Delta g_i^{IM}(x) = \sum_j \int_{\sigma_{j/2}}^{x} dr\ P_{ji}^{T}(x - r) \times \left\{ \sum_k z_k \int_0^{\infty} dx_k\ K_{kj}(x_k | r)\ \rho_k(x_k) - L_j(r) \right\} \quad (2.53)$$

and

$$\Delta g_i^{IM}(x) = \sum_k z_k \int_0^{\infty} dx_k\ \gamma_{ki}(x_k | x)\ \rho_k(x_k) - \Lambda_i(x) \quad (2.54)$$

with

$$\gamma_{ki}(x_k | x) = \sum_j \int_{\sigma_{j/2}}^{x} dr\ P_{ji}^{T}(x - r)\ K_{kj}(x_k | r) \quad (2.55)$$

and

$$\Lambda_i(x) = \sum_j \int_{\sigma_{j/2}}^{x} dr\ P_{ji}^{T}(x - r)\ L_j(r) \quad (2.56)$$

Equation 2.54, together with the Laplace inverse of (2.51)

$$\Delta g_i^{PT}(x) = \frac{\beta e E_0}{\epsilon_0} N_i(x) \quad (2.57)$$

where

$$N_i(x) = \sum_j M_j \int_{\sigma_{j/2}}^{x} dr\ P_{ji}^{T}(x - r) \quad (2.58)$$

constitute, when replaced into (2.50), the MSA solution to the stated problem of finding the density profile. The exp approximation[30] is obtained from the MSA by simply exponentiating the above result. Then, from (2.11) and (2.50)

$$\rho_i(x) = \rho_i\ g_{0i}^{0}(x) \exp[\Delta g_i^{PT}(x) + \Delta g_i^{IM}(x)] \quad (2.59)$$

where g_{0i}^{0} is given by (2.12), Δg_i^{PT} by (2.57), and Δg_i^{IM} by (2.54). The result in this case, eq 2.59, is a nonlinear integral equation for $\rho_i(x)$. However for the reasons already stated above, we do expect that the density dependence of the image potential should be weak and, therefore, a simple iterative solution should be quite rapidly convergent.

We should also mention that there is another kind of nonlinear behavior which has to do with the accumulation of ions near the electrode and its effect on the shielding of the ions.[27,40] This effect is included in the correction terms of the functional expansion (eq 4.3.b of ref 29), but will not be discussed here.

3. Properties of the Interface

In the last section we discussed two approximate equations for the excess density of the individual ions near the electrode wall. Of the two, the exp approximation is certainly the better one, but also more difficult to handle since most of the calculations have to be made numerically. For the MSA, however, we can obtain explicit formulas for some of the physically interesting quantities. Therefore, in spite of the weakness of the MSA at low concentrations, we will include the MSA in this section because they are simple and illustrative.

Let us first recall a few basic equations for interfaces in equilibrium.[24] The Lippmann equation

$$(\partial \Delta\gamma / \partial \Delta\psi)_\rho = -q_s \quad (3.1)$$

relates the change in surface tension $\Delta\gamma$ to the change in the potential drop $\Delta\psi$ across the interface, at constant composition, to the excess surface charge on the electrode, q_s, at constant composition $\rho \equiv (\rho_1 \ldots \rho_n)$. From here we can derive the differential capacitance

$$(\partial q_s / \partial \Delta\psi)_\rho = C_D \quad (3.2)$$

which can also be measured directly. Other measured properties, such as integral capacitances or excess entropies, are not commonly discussed in the experimental literature, and therefore we will not consider them here.

The statistical mechanics of the interface can be then derived starting with either the surface tension (3.1) or the excess surface charge (3.2). The first approach is more complicated than the second because the equations for the surface tension usually involve the position dependent correlation functions[36,37] that are difficult to calculate. In an exact theory both approaches, that is, this one and the one starting with (3.2), should give the same result. However this is not necessarily true if an approximate theory is being used and, in fact, the agreement of the two approaches should be a measure of the quality of the theory. In this initial work, however, we will only consider the simpler approach, namely, the second one. Let us start by defining the charge density per unit volume at a distance x from the interface:

$$q(x) = e \sum_i z_i\ \rho_i(x) \quad (3.3)$$

where $\rho_i(x)$ is calculated from the results of the last section. Because of the electroneutrality, the total charge per unit area near the electrode must equal the surface charge density q_s in absolute value. In other words

$$q_s = -\int_0^{\infty} dx\ q(x) \quad (3.4)$$

Furthermore, the electrostatic potential due to a charge distribution is[35]

$$\psi(\vec{r}) = \int d\vec{r}_1\ q(\vec{r}_1)/\epsilon_0 |\vec{r} - \vec{r}_1| \quad (3.5)$$

to integrate this expression, we have to substract the constant infinity term (see eq 2.27 and ensuing discussion). Furthermore, we will set the potential of the bulk electrolyte to zero. Then

$$\psi(x) = -\frac{4\pi}{\epsilon_0} \int_x^{\infty} dx_1\ (x_1 - x)\ q(x_1) \quad (3.6)$$

from where the potential drop across the electrode is

$$\Delta\psi = -\frac{4\pi}{\epsilon_0} \int_0^{\infty} dx_1\ x_1\ q(x_1) \quad (3.7)$$

Now, from the results of section 2 we know that both q_s and $\Delta\psi$ are functions of the "bare" field E_0 (2.18), so that by the well-known formula of parameter differentiation

$$c_D = \frac{(\partial q_s/\partial E_0)}{(\partial \Delta\psi/\partial E_0)} \tag{3.8}$$

In the exp approximation (2.59)

$$q(x) = e\sum_i z_i \rho_i g_{0i}^{e}(x) \exp\left[\Lambda_i(x) + \frac{\beta e E_0}{\epsilon_0} N_i(x) + \sum_k z_k \int_0^\infty dx_k\ \gamma_{ki}(x_k|x)\ \rho_k(x_k)\right] \tag{3.9}$$

To obtain the differential capacitance, we have to combine (3.4), (3.7), and (3.8)

$$C_D = \frac{\epsilon_0}{4\pi} \frac{\int_0^\infty dx\ (\partial q(x)/\partial E_0)}{\int_0^\infty dx\ x(\partial q(x)/\partial E_0)} \tag{3.10}$$

and then replace the charge density given by (3.9) and (2.59). As was mentioned earlier we are in the process of developing approximate expressions for the Laplace inverses of the distribution functions, and therefore we will leave the study of the quantitative consequences of (3.10) for a future publication. Otherwise the integrations will have to be done numerically.

Notice that if we use the Laplace transform of the charge density

$$\tilde{q}(s) = \int_0^\infty dx\ e^{-sx} q(x) \tag{3.11}$$

$$-\tilde{q}'(s) = \int_0^\infty dx\ x e^{-sx} q(x) \tag{3.12}$$

we can rewrite C_D as

$$C_D = -\frac{\epsilon_0}{4\pi} \frac{\partial \tilde{q}(0)}{\partial \tilde{q}'(0)} \tag{3.13}$$

In the MSA we obtain explicit expressions from (2.50), (2.54), and (2.57), together with (2.49) and (3.3)

$$C_D = -\frac{\epsilon_0}{4\pi} \left\{ \frac{\beta e^2}{\epsilon_0} \sum_i \rho_i z_i \tilde{N}_i(0) + e\int_0^\infty \sum_k z_k \frac{\partial}{\partial E_0} \left[\sum_i \rho_i z_i \tilde{\gamma}_{ki}(x_k|0)\ \rho_k(x_k)\ dx_k \right\} \Big/ \left\{ \frac{\beta e^2}{\epsilon_0} \sum_i \rho_i z_i \tilde{N}_i'(0) + e\int_0^\infty \sum_k z_k \frac{\partial}{\partial E_0} \left[\sum_i \rho_i z_i \tilde{\gamma}_{ki}'(x_k|0)\ \rho_k(x_k) \right] dx_k \right\} \tag{3.14}$$

for very low fields we can neglect the second term in both the numerator and the denominator so that we obtain the very simple formula[41]

$$C_D = -\frac{\epsilon_0}{4\pi} \frac{\sum \rho_i z_i \tilde{N}_i(0)}{\sum \rho_i z_i \tilde{N}_i'(0)} \tag{3.15}$$

which is explicitly evaluated in the next section for the equal size case. There are other quatities of interest. The surface tension can be calculated using the extensions of the van der Waals formula[42] but the published equation has to be adapted to the case of the electrified interface. Other properties such as the surface excess internal energy are simply

$$\Delta E = \int_0^\infty dx\ q(x)\ \psi(x) = \frac{2\pi}{\epsilon_0} \int dx\ dx_1\ q(x)\ q(x_1)|x - x_1| \tag{3.16}$$

Finally, the excess free energy and entropy can be obtained from the thermodynamic relations

$$\beta\Delta A = \int_0^\beta d\beta_1\ \Delta E(\beta_1) \tag{3.17}$$

$$\Delta S = k_B [\beta\Delta E - \int_0^\beta d\beta_1\ \Delta E(\beta_1)] \tag{3.18}$$

4. Limiting Cases of the Restricted Primitive Model

We discuss now some limiting cases of the restricted primitive model of ionic solutions, that is, a system of equal size, opposite charge hard spheres. There is no such electrolyte in nature, but, apart from the comparison to the previous work on this model, we hope that in a near future, computer simulations will be available. These simulations will then provide the basis of a meaningful test of the theory.

As shown in Appendix C, for the restricted primitive model the factor correlation function $\tilde{P}_{ij}(s)$ (2.10) decouples into the hard core and electrostatic parts

$$\tilde{P}_{ij}(s) = [I - \rho\hat{Q}(s)]_{ij}^{-1} = \delta_{ij} + (\rho_j/\rho)\,\tilde{P}^0(s) + \rho_j \frac{z_i z_j}{\eta_0} \tilde{P}^{\pm}(s) \tag{4.1}$$

The inverse Laplace transforms of these functions for dilute and concentrated solutions are also given in Appendix C ((C.21), (C.26), and (C.29)). When these results are plugged into the equations derived in section 2, we obtain in the MSA

$$\Delta g_i(x) = \Delta g_i^{IM}(x) + \beta e z_i \zeta_0\ \Delta g^{\pm}(x) \tag{4.2}$$

here, we have introduced the bare, or unscreened potential (see Appendix C)

$$\zeta_0 = E_0/(\epsilon_0 \mathcal{H}_0)$$

which now is the free parameter, instead of the bare field E_0. The reason for this change is that for infinite dilution, if we keep E_0 constant, (4.2) diverges, as a consequence of the fact that the potential of an infinite plane plate condenser with a finite charge density has an infinite potential if the plate separation is also infinite. In our case, infinite dilution just amounts to separating the charges to infinity, but in a real experimental situation the potential difference is maintained finite. Then, from (2.52) and (2.58)

$$\Delta g^{\pm}(x) = \int_{\sigma/2}^x dr\ [\delta(r) + P^{\pm}(r)] \tag{4.3}$$

$$\Delta g^{IM}(x) = -\sum_{l,j} \int_{\sigma/2}^x dr \int_0^\infty dy\ \times \phi_l^{IM}(r + y)\, P_{lj}(y)\, P_{ji}^{T}(x - r) = -\int_{\sigma/2}^x dr \int_0^\infty dy\ \phi^{IM}(r + y)\{[\delta(y) + P^0(y)][\delta(x - r) + P^0(x - r)]\} \tag{4.4}$$

so that

$$\Delta g^{IM}(x) = \phi^{IM}(x) + \int_{\sigma/2}^\infty dr\ \phi^{IM}(r)\, P^0(|r - x|) + \int_{\sigma/2}^x dr \int_0^\infty dy\ \phi^{IM}(r + y)\, P^0(y)\, P^0(x - r) \tag{4.5}$$

Let us remark first that the image contribution is quite strongly biased toward preferential adsorption of small ions. However, in this example the image force is the same for both ions, and no preferential adsorption will be present in this model. A second remark is that while the MSA is certainly correct in the zero potential limit, the correct low density limit is given by the exp approximation.[30] Now we will show that the exp approximation also gives the correct parabolic dependence for low potentials. We have (2.59)

$$g_i(x) = g_0^0(x) \exp[\Delta g(x)] = g_0^0(x) \exp[\Delta g^{IM}(x) + z_i \zeta_0 \beta e \Delta g^{\pm}(x)] \quad (4.6)$$

and from (3.3) we get the charge density

$$q(x) = 2e g_0^0(x) \exp[\Delta g^{IM}(x)] \times \sinh[e\beta\zeta_0 \Delta g^{\pm}(x)] \quad (4.7)$$

so that the electrode surface charge and total potential drop ((3.4 and (3.7)) are

$$q_s = -2e \int_{\sigma/2}^{\infty} dx\, g_0^0(x) \exp[\Delta g^{IM}(x)] \times \sinh[e\beta\zeta_0 \Delta g^{\pm}(x)] \quad (4.8)$$

$$\Delta\psi = -\frac{8\pi}{\epsilon_0} e \int_{\sigma/2}^{\infty} dx\, x\, g_0^0(x) \exp[\Delta g^{IM}(x)] \times \sinh[e\beta\zeta_0 \Delta g^{\pm}(x)] \quad (4.8a)$$

If we also ignore the dependence of the image shielding on the applied bare field ζ_0, then the differential capacitance is

$$C_D = \frac{\epsilon_0}{4\pi} \left\{ \int_{\sigma/2}^{\infty} dx\, g_0^0(x) \Delta g^{\pm}(x) \times \exp[\Delta g^{IM}(x)] \cosh[e\beta\zeta_0 \Delta g^{\pm}(x)] \Big/ \int_{\sigma/2}^{\infty} dx\, x\, g_0^0(x) \Delta g^{\pm}(x) \exp[\Delta g^{IM}(x)] \times \cosh[e\beta\zeta_0 \Delta g^{\pm}(x)] \right\} \quad (4.9)$$

This expression has to be evaluated by numerical methods. However, for low fields we can show that the above expression has the right qualitative form. Consider first the image term

$$\Delta g^{IM}(x) = \phi^{IM}(x) + \int_{\sigma/2}^{\infty} dr\, \phi^{IM}(r)\, P^0(|r - x|) + \int_{\sigma/2}^{x} dr \int_0^{\infty} dy\, \phi^{IM}(r + y)\, P^0(y) \times P^0(x - r) \quad (4.10)$$

From (2.32)

$$\phi_i^{IM}(x) = \frac{\beta e^2}{\epsilon_0} \left\{ \frac{1}{2x} + z_j \Sigma z_j \int_0^{\infty} dy\, \rho(y) \times G_{ij}(y|x) \right\} \quad (4.11)$$

where $G_{ij}(y|x)$ is given by (2.31). There are already some noticeable differences between these equations and the one in the classic papers by Loeb,[37] Levine and Bell,[38] and Buff and Stillinger,[27] the biggest one being that the hard core interactions or, better correlations, modulate the image contributions. This will prevent the system from collapsing against the walls, in the extreme case, and also will tend to prevent the abnormally high ionic concentrations that one gets from the above-mentioned treatments.[28] Also, the hard core correlations have an oscillatory character, and we would expect that this should also modulate the shape of the differential capacitance. For highly diluted systems the dominant term in the image contributions is simply

$$\Delta g^{IM}(x) \approx \frac{\beta e^2}{2\epsilon_0 x} \quad (4.12)$$

Suppose also that the size of the ions is very small, so that we can safely assume

$$\Delta g^{IM}(\sigma/2) >> \Delta g^{\pm}(x) \quad (4.13)$$

then we obtain the asymptotic formula for σ going to zero

$$C_D = \epsilon_0/2\pi\sigma \qquad \sigma << 1 \quad (4.14)$$

We see then that the image force contribution in this extreme case amounts to producing a constant term in the differential capacitance similar to the one that one obtains from the Helmholtz–Perrin, but without an ad-hoc assumption.

Consider now the case in which there is no image term present. This is so only for the unlikely situation in which the wall material and the bulk solvent have the same dielectric constant. However is also present in the old GC theory. Then

$$g_0^0(x) \approx 1$$

$$C_D = \frac{\epsilon_0}{4\pi} \times \frac{\int_{\sigma/2}^{\infty} dx\, \Delta g^{\pm}(x) \cosh[e\beta\zeta_0 \Delta g^{\pm}(x)]}{\int_{\sigma/2}^{\infty} dx\, x\, \Delta g^{\pm}(x) \cosh[e\beta\zeta_0 \Delta g^{\pm}(x)]} \quad (4.15)$$

This equation should be compared to the GC result

$$C_D = \frac{\epsilon_0}{4\pi} \mathcal{K}_0 \cosh[e\beta\Delta\psi] \quad (4.16)$$

where

$$\mathcal{K}_0 = \alpha \sqrt{\eta_0} = \left[\frac{8\pi e^2 \beta \rho}{\epsilon_0} \right]^{1/2} \quad (4.17)$$

and $\Delta\psi$ is the potential drop across the interface.[3,24] For low applied potentials, both expressions have the same parabolic dependence on the applied potential. However, the GC formula has a divergence (an essential one), while our new formula (4.15) is clearly bounded in this limit. This is a most welcomed feature of (4.15).

Since the applied potential $\Delta\psi$ is a monotonous function of the bare potential ζ_0, for $\Delta\psi \sim \zeta_0 << 1$ we obtain

$$C_D \simeq C_D^0 + {}^1/_2 A \zeta_0^2 = C_D^0 + {}^1/_2 A' (\Delta\psi)^2 \quad (4.18)$$

where

$$A' = \frac{1}{2[\Delta g^{\pm}(0)]^4} \left[\frac{\epsilon_0}{8\pi e} \right]^2 \int_{\sigma/2}^{\infty} dx\, dy\, y \times [\Delta g^{\pm}(x)]^3 \Delta g^{\pm}(y) [1 - (\Delta g^{\pm}(y))^2] \quad (4.19)$$

Combining (3.15) with (2.51) and the results of Appendix C, we obtain the zero potential coefficient

$$C_D^0 = -\frac{\epsilon_0}{4\pi} \frac{\sum_i \rho_i z_i^2 \frac{E_0}{4\pi e} \frac{1}{\eta_0}}{-\sum \rho_i z_i^2 \frac{E_0}{4\pi e} \frac{1}{\eta_0} \left[\frac{\sigma}{2} + \frac{1 - \Gamma\sigma}{2\Gamma} \right]} = \frac{\epsilon_0}{4\pi}(2\Gamma) \quad (4.20)$$

This nontrivial limit agrees in the limit of low concentration with the one of the linearized GC theory[24] since $2\Gamma \to \mathcal{K}_0$. We should remark also that this limit is also obtained from the appropriate limiting case of the unequal diameter MSA.[13] It will be constructive to compare this result to the treatment of Grahame,[43] who assumed that the core repulsion just produces a shift in the coordinates of the exponential damping of the surface charge.[24] In our case the shift should just equal the sphere radius $\sigma/2$, and one would obtain

$$C_D^0 = \frac{\epsilon_0}{4\pi} \frac{\mathcal{K}_0}{1 + \mathcal{K}_0(\sigma/2)} \quad (4.21)$$

while the correct limiting formula is clearly (4.20). This is not surprising, but just a consequence of the inconsistencies of the DH theory in its treatment of the repulsion core. However, eq 4.21 is more satisfying than (4.20) due to the additional capacitance $\epsilon_0/2\pi\sigma$, that again takes the place of the Helmholtz–Perrin inner layer contribution in a non ad-hoc manner. In a more realistic treatment of the metal–solution interface,[41] one should take into account the structure of the surface. The electron density near the interface is certainly lower than in the bulk so that one would expect that the metal edge should be somewhat removed and in the interior of the hard wall edge. If we call this distance $\Delta\sigma$ then the limiting expression for zero field of (4.20) yields

$$C_D^0 = \frac{\epsilon_0}{4\pi}\frac{2\Gamma}{1 + 2\Gamma\Delta\sigma} \tag{4.22}$$

which is formally identical with Grahame, but with a different physical interpretation.

5. Conclusion

The short discussion of the preceding section served to give the feeling for the correctness of the theory presented in sections 2 and 3 because this theory gives the right asymptotic limits and has the right qualitative behavior. However we do expect this theory to work reasonably well for intermediate and weak fields, at relatively high ionic strengths, because the hard core exclusion effects are included everywhere. The best judgement as to how accurate this approach really is can come only from the comparison to computer experiments on appropriate systems, similar to those of Liu.[19] A weaker test, that of the consistency of different ways of getting the same properties, is left for a future publication.

Acknowledgment. The author is indebted to Professors P. F. Williams, I. Cooper, S. Levine, J. L. Lebowitz, and very especially, G. Stell, for very instructive discussions and correspondence.

Appendix A. Summary of MSA Results and Notation

In this appendix we give the results of ref 13 that are used in this work, together with some new ones (Høye and Blum[45]) for the correlation function. We recall that in ref 13 we solved the MSA for the primitive model using Baxter's method,[44] so that the notation will also be quite similar to his. In this formalism, the thermodynamic properties and the correlation functions are given in terms of the factor correlation function, which in our case is

$$Q_{ij}(r) = (r - \sigma_{ij})\,Q_{ij}' + \frac{1}{2}(r - \sigma_{ij})^2\,Q_{ij}'' - z_i a_j \qquad \lambda_{ji} \leq r \leq \sigma_{ji} \tag{A.1}$$

$$= -z_i a_j \qquad r > \sigma_{ij} \tag{A.2}$$

with

$$\sigma_{ij} = \frac{1}{2}(\sigma_i + \sigma_j) \tag{A.3}$$

$$Q_{ij}' = \frac{2\pi}{\Delta}\left[\sigma_{ij} + \sigma_i\sigma_j\zeta_2\frac{\pi}{4\Delta}\right] - \frac{2\Gamma^2}{\alpha^2}a_i a_j \tag{A.4}$$

$$Q_{ij}'' = \frac{2\pi}{\Delta}\left[1 + \zeta_2\sigma_j\frac{\pi}{2\Delta}\right] + \frac{\pi}{\Delta}a_j P_n \tag{A.5}$$

and

$$\zeta_\alpha = \sum_i \rho_i\sigma_i^\alpha \tag{A.6}$$

$$\Delta = 1 - \frac{\pi}{6}\zeta_3 \tag{A.7}$$

$$a_i = \frac{\alpha^2}{2\Gamma}\frac{z_i}{1 + \Gamma\sigma_i}\left(1 - P_n\frac{\pi\sigma_i^2}{2\Delta z_i}\right) \tag{A.8}$$

$$P_n = \sum\frac{\rho_i\sigma_i z_i}{1 + r\sigma_i}\Big/\left[1 + \frac{\pi}{2\Delta}\sum\frac{\rho_k\sigma_k^3}{1 + \Gamma\sigma_k}\right] \tag{A.9}$$

$$\alpha^2 = 4\pi\beta e^2/\epsilon_0 \tag{A.10}$$

where $\beta = 1/k_B T$ is the Boltzmann thermal factor, e the electron charge, and ϵ_0 the dielectric constant. Apart from the sizes, charges, and concentrations, the key parameter is the scaling inverse length Γ, which is found by solving an algebraic equation.[14,15] As has been shown, Γ is the analogous quantity to the inverse Debye screening length and, in fact, for equal size it becomes[12]

$$\Gamma = \frac{1}{2\sigma}\left[-1 + \sqrt{1 + 2\mathcal{K}_0\sigma}\right] \tag{A.11}$$

$$\mathcal{K}_0^2 = \alpha^2\sum\rho_i z_i^2 \tag{A.12}$$

where $\mathcal{K}_0$ is the Debye screening constant. For very dilute solutions, a Taylor expansion shows that

$$2\Gamma = \mathcal{K}_0 \tag{A.13}$$

For the equal size case P_n is identically zero. However even for different sizes, if the concentration is 1 N or less, this will be a very small quantity, and can be ignored. Then the algebraic equations become much simpler. The equation for Γ becomes

$$\frac{\alpha^2}{4}\sum_{i=1}^{n}\rho_i\left[\frac{z_i}{1 + \Gamma\sigma_i}\right]^2 = \Gamma^2 \tag{A.14}$$

which can be easily solved with a desk calculator. To compute the pair correlation functions we will need the Laplace transform of the factor correlation function $Q_{ij}(r)$ (A.1), which is

$$\hat{Q}_{ij}(s) = \int_0^\infty dr\, e^{-sr}\,Q_{ij}(r) = e^{\lambda_{ij}s}[Q_{ij}'\,\sigma_i^2 \times \varphi_1(s\sigma_i) + Q_{ij}''\,\sigma_i^3\,\varphi_2(s\sigma_i) - z_i a_{j/s}] \tag{A.15}$$

where we have used the incomplete gamma functions

$$\varphi_1(z) = (1/z^2)[1 - z - e^{-z}] \tag{A.16}$$

$$\varphi_2(z) = (1/z^3)[1 - z + z^2/2 - e^{-z}] \tag{A.17}$$

The Fourier transform is then

$$\tilde{Q}_{ij}(k) = \delta_{ij} - \rho_i\hat{Q}_{ij}(-ik) \tag{A.18}$$

and the Laplace transform of the binary correlation function (Høye and Blum[45])

$$g_{ij}(s) = \int_0^\infty dr\, e^{-sr}\,r\,g_{ij}(r) = \frac{1}{2\pi s^2}\sum(sQ_{ik}' + Q_{ik}'')e^{-s\sigma_{ik}}[\tilde{Q}(is)]_{kj}^{-1} \tag{A.19}$$

For the general case of different diameter particles, the derivation and explicit form of (A.19) will be given in a separate publication.

Let us now summarize some of the main properties of the factor correlation function $P_{ij}(r)$ (2.10). From its definition and the fact that $\tilde{Q}^T(-\kappa)$ is nonsingular in the

lower complex x plane, we can show by closing a contour around it that

$$P_{lj}(r) = 0 \qquad r < \lambda_{lj} \tag{A.20}$$

and therefore

$$\tilde{P}_{lj}(\kappa) = \{\tilde{Q}^{T}(-\kappa)\}_{lj}^{-1} = \int_{\lambda_{lj}}^{\infty} dr\, e^{-i\kappa r} P_{lj}(r) \tag{A.21}$$

Also, using the matrix, κ space, Ornstein–Zernike equation, we have the suggestive form

$$[\mathbf{I} + \rho \tilde{\mathbf{H}}(\kappa)] = \tilde{\mathbf{P}}^{T}(\kappa)\, \tilde{\mathbf{P}}(-\kappa) \tag{A.22}$$

which is the analogous to the Wiener–Hopf factorization of the direct correlation function[44]

$$[\mathbf{I} - \rho \tilde{\mathbf{C}}(\kappa)] = \tilde{\mathbf{Q}}^{T}(\kappa)\, \tilde{\mathbf{Q}}(-\kappa) \tag{A.23}$$

Appendix B

For the general case of the unequal diameter primitive model in the MSA we show explicitly that

$$\lim_{s\to 0} \Sigma\, z_j\, \tilde{P}_{lj}(s) = 0 \tag{B.1}$$

Using the result of the preceding Appendix A (A.15), and taking the limit $s \to 0$ we write

$$[\mathbf{I} - \rho \hat{Q}(s)]_{kj} = e^{-s\lambda_{jk}} [\delta_{kj} - \alpha_k \beta_j - \gamma_k \zeta_j - \epsilon_k \phi_j] \tag{B.2}$$

where, to leading order in s

$$\alpha_k = -\frac{\pi}{6\Delta}\sigma_k^{3} \qquad \beta_k = \rho_k \tag{B.3}$$

$$\gamma_k = -\frac{\pi}{2\Delta}\sigma_k^{2}\left(1 + \frac{\pi}{6\Delta}\zeta_2\sigma_k\right) \qquad \delta_k = \rho_k \sigma_k \tag{B.4}$$

$$\epsilon_k = -z_k/s \qquad \phi_k = \rho_k a_k \tag{B.5}$$

Then, (B.2) has a simple inverse. Using the shorthand notation

$$(\alpha\cdot\beta) = \Sigma\, \alpha_k \beta_k \tag{B.6}$$

and since by electroneutrality

$$(\epsilon\cdot\beta) = 0 \tag{B.7}$$

then

$$\begin{aligned}\lim_{s\to 0} e^{-s\lambda_{jk}}\, \tilde{P}_{kj}(s) = \delta_{kj} + \frac{1}{D}\Big\{&\alpha_k\beta_j[-(\epsilon\cdot\phi)(1 - \gamma\cdot\delta) - (\gamma\cdot\phi)(\epsilon\cdot\delta)] - \alpha_k\delta_j(\gamma\cdot\beta)(\epsilon\cdot\phi)\\ &+ \alpha_k\phi_j(\beta\cdot\gamma)(\delta\cdot\epsilon) - \gamma_k\delta_j(\epsilon\cdot\phi)(1 - \alpha\cdot\beta)\\ &+ \gamma_k\beta_j[(\epsilon\cdot\delta)(\alpha\cdot\phi) - (\alpha\cdot\delta)(\epsilon\cdot\phi)] + \gamma_k\phi_j(\epsilon\cdot\delta)(1\\ &- \alpha\cdot\beta) + \epsilon_k\phi_j[(1 - \alpha\cdot\beta)(1 - \gamma\cdot\delta) - (\alpha\cdot\delta)(\beta\cdot\gamma)]\\ &+ \epsilon_k\beta_j[(\alpha\cdot\phi)(1 - \gamma\cdot\delta) + (\alpha\cdot\delta)(\gamma\cdot\phi)]\\ &+ \epsilon_k\delta_j[(\gamma\cdot\phi)(1 - \alpha\cdot\beta) + (\alpha\cdot\phi)(\beta\cdot\gamma)]\Big\}\end{aligned} \tag{B.8}$$

with

$$\begin{aligned}\lim_{s\to 0} D = &-(\epsilon\cdot\phi)[(1 - \alpha\cdot\beta)(1 - \gamma\cdot\delta) - (\alpha\cdot\delta)(\beta\cdot\gamma)]\\ &+ (\epsilon\cdot\delta)[-(\gamma\cdot\psi)(1 - \alpha\cdot\beta) - (\alpha\cdot\phi)(\beta\cdot\gamma)]\end{aligned} \tag{B.9}$$

After some lengthy algebra, we finally obtain

$$\begin{aligned}\lim_{s\to 0} \Sigma z_j P_{kj}(0) = \frac{1}{D}\Big\{&\alpha_k[-(\epsilon\cdot\delta)(\gamma\cdot\beta)(\epsilon\cdot\phi)\\ &+ (\epsilon\cdot\phi)(\beta\cdot\gamma)(\epsilon\cdot\delta)] + \gamma_k[-(\epsilon\cdot\delta)(\epsilon\cdot\phi)(1 - \alpha\cdot\beta)\\ &+ (\epsilon\cdot\delta)(\epsilon\cdot\phi)(1 - \alpha\cdot\beta)]\Big\} = 0\end{aligned} \tag{B.10}$$

The proof of the second relation

$$\lim_{s\to 0} -\Sigma_j z_j \frac{\partial}{\partial s}\tilde{P}_{kj}(s) = M_j \tag{B.11}$$

is much more complicated for the general case. However for the equal size case, some very drastic simplifications take place. We obtain in this case

$$\Sigma_k z_k\, \tilde{P}_{jk}(s) = z_j \frac{s^2}{s^2 + 2\Gamma s + 2\Gamma^2(1 - e^{-s\sigma})} \tag{B.12}$$

Quite clearly

$$\lim_{s\to 0} \Sigma_k z_k\, \tilde{P}_{jk}(s) = 0 \tag{B.13}$$

and

$$\lim_{s\to 0} -\Sigma_k z_k \frac{\partial}{\partial s}\tilde{P}_{jk}(s) = \frac{z_j}{2\Gamma(1 + \Gamma\sigma)} = \frac{-z_j}{\mathcal{H}_0} \tag{B.14}$$

Appendix C. Correlations for the Equal Size Case

It can be shown that, for the equal size case, the factor correlation functions are the sum of a hard core and a charge parts

$$\tilde{P}_{kj}(s) = \delta_{kj} + (\rho_j/\rho_T)\, \tilde{P}^{0}(s) + (\rho_j z_k z_j/\eta_0)\, P^{\pm}(s) \tag{C.1}$$

where

$$\rho_T = \Sigma\rho_i \qquad \eta_0 = \Sigma\rho_i z_i^{2} \tag{C.2}$$

$\tilde{P}^{0}(s)$ is the hard core part and is given by

$$\tilde{P}^{0}(s) = \rho_T\, \tilde{Q}_0(s)/(1 - \rho_T\, \tilde{Q}_0(s)) \tag{C.3}$$

and the charge part is, explicitly

$$\tilde{P}^{\pm}(s) = \frac{-2\Gamma(s + \Gamma - \Gamma e^{-s\sigma})}{[s^2 + 2\Gamma s + 2\Gamma^2(1 - e^{-s\sigma})]} \tag{C.4}$$

The Laplace inverse of the hard core part is[45] obtained from

$$1 + \tilde{P}^{0}(s) = \frac{s^3}{M(s) + N(s)e^{-s\sigma}} \tag{C.5}$$

where

$$M(s) = s^3 + m_2 s_2 + m_1 s + m_0 \tag{C.6}$$

$$N(s) = sn_1 + n_0 \tag{C.7}$$

and

$$m_2 = \rho\pi\sigma^2/\Delta \tag{C.8}$$

$$m_1 = {}^1/_2(m_2)^2 \tag{C.9}$$

$$m_0 = -\frac{2\pi\rho}{\Delta^2}\left(1 + \frac{\pi\rho\sigma^3}{3\Delta}\right) \tag{C.10}$$

$$n_1 = \frac{2\pi\rho\sigma}{\Delta}\left(1 + \frac{\pi\rho\sigma^3}{4\Delta}\right) \tag{C.11}$$

$$n_0 = \frac{2\pi\rho\sigma}{\Delta}\left(1 + \frac{\pi\rho\sigma^3}{2\Delta}\right) \tag{C.12}$$

There are basically two different ways of doing the Laplace inversion of (C.5). The first one is just to look for all the zeros of the denominator. These can be calculated numerically from the knowledge that in the strip $-2k\pi <$ Im

$s < 2k\pi$ there will be $4k + 1$ zeros,[46] with negative real parts. A more explicit inverse can be found from the observation that for Re $s > 0$

$$|N(s)e^{-s\sigma}/M(s)| < 1 \tag{C.13}$$

Then, we have[45]

$$1 + \tilde{P}^{(l)}(s) = s^{l}\left\{\frac{1}{M(s)}\sum_{b=0}\left[-\frac{N(s)e^{-s\sigma}}{M(s)}\right]^{l}\right\} \tag{C.14}$$

For the Laplace inverse of this series we need only the three roots of

$$M(s) = 0 \tag{C.15}$$

which are

$$\mu_1 = \mu^+ - {}^1/_3 m_2 \tag{C.16}$$

$$\mu_2 = \mu^+ e^{2\pi i/3} + \mu^- e^{-2\pi i/3} - ({}^1/_3)m_2 \tag{C.17}$$

$$\mu_3 = \mu^+ e^{-2\pi i/3} + \mu^- e^{2\pi i/3} - ({}^1/_3)m_2 \tag{C.18}$$

with

$$\mu^{\pm} = \left[\xi \pm \left(\frac{m_2^3}{5832} + \xi^2\right)^{1/2}\right]^{1/3} \tag{C.19}$$

$$\xi = \frac{\pi\rho}{\Delta^3}\left(1 + \frac{\pi\rho\sigma^3}{6} - \frac{\rho^2\pi^2 v^6}{108}\right) \tag{C.20}$$

from where the stepwise inverse is

$$\rho_T\, P^{(l)}(r) = \sum_{i=1}^{3}\sum_{l=0}^{\infty}\frac{1}{l!}\left(-\frac{\partial}{\partial\mu_i}\right)^{l}\left\{\frac{e^{\mu_i(r-l\sigma)}[N(\mu_i)]^l}{[M'(\mu_i)]^{l+1}} \times [\theta(r - l\sigma)\mu_i^3 - e^{-\mu_i\sigma}N(\mu_i)\theta(r - \sigma l - \sigma)]\right\} \tag{C.21}$$

Here $\theta(x)$ is the Heaviside function. For the hard core part this expansion is very useful, since it gives the exact result in the neighborhood of the wall.

Consider now the electrostatic part (C.4). Since

$$1 + \tilde{P}^{\pm}(s) = \frac{s^2}{s^2 + 2\Gamma s + 2\Gamma^2(1 - e^{-s\sigma})} \tag{C.22}$$

then for Re $s > 0$

$$\frac{2\Gamma^2 e^{-s\sigma}}{s^2 + 2\Gamma s + 2\Gamma^2} < 1 \tag{C.23}$$

$$1 + \tilde{P}^{\pm}(s) = s^2\sum_{l=0}^{\infty}\frac{(2\Gamma^2 e^{-s\sigma})^l}{(s^2 + 2\Gamma s + 2\Gamma^2)^{l+1}} \tag{C.24}$$

The denominator of this series has two roots

$$\Gamma^{\pm} = -\Gamma(1 \pm i) \tag{C.25}$$

from where the explicit, stepwise Laplace inverse is[38]

$$P^{\pm}(r) = \sum_{l=0}^{\infty}\frac{2^{3/2}}{l!}\left(\frac{-\Gamma^2}{\sqrt{2}}\right)^{l+1}\left\{\theta(r - l\sigma - \sigma) \times \left(\frac{\partial}{\partial\Gamma}\right)^{l} e^{-\Gamma\sigma}\sin\left[\Gamma(r - \sigma l) - \frac{3l\pi}{4} - \sigma\right] - \frac{\theta(r - l\sigma)}{\Gamma^2}\left(\frac{\partial}{\partial\Gamma}\right)^{l}\Gamma^2\cos\left[\Gamma(r - l\sigma) + \frac{3l\pi}{4}\right]\right\} e^{-\Gamma(r - l\sigma)}/\Gamma^{l+1} \tag{C.26}$$

This expression is, however, not a very convenient one for dilute solutions, because then the decay rate is slow, and one must take many terms of the series (C.26). A more convenient expansion is obtained from the observation that if

$$\Gamma\sigma < 1$$

then

$$\frac{2\Gamma^2}{s(s + 2\Gamma)}(1 - e^{-s\sigma}) < 1 \tag{C.27}$$

and then (C.4) has a very simple inverse. The leading terms are

$$L^{-1}\left[\frac{1}{s}(1 + \tilde{P}^{\pm}(s))\right] = e^{-2\Gamma r} - \frac{1}{2}\left\{\theta(\sigma - r) - e^{-2\Gamma r}\left[1 + \frac{\Gamma r}{2} - \theta(r - \sigma)e^{2\Gamma\sigma}(1 + \left(\frac{r - \sigma}{2}\right)\Gamma)\right]\right\} \tag{C.28}$$

and from (A.11), we have in the limit of infinite dilution

$$2\Gamma \approx \mathcal{K}_0$$

from where we obtain the classic result (linear GC theory[24])

$$e^{-\mathcal{K}r}$$

References and Notes

(1) J. K. Percus, Lecture notes "Enseignement du 3 eme Cycle de Physique en Suisse Romande", Laussanne Switzerland, 1975.
(2) P. Debye and E. Huckel, *Z. Phys.*, **24**, 133, 305 (1923).
(3) C. Guoy, *J. Phys.*, **9**, 457 (1910); D. L. Chapman, *Phil. Mag.*, **25**, 475 (1913).
(4) O. Stern, *Z. Elektrochem.*, **30**, 508 (1924).
(5) J. E. Mayer, *J. Chem. Phys.*, **18**, 1426 (1950).
(6) H. L. Friedman, "Ionic Solution Theory", Interscience, New York, N.Y., 1962; G. Stell and J. L. Lebowitz, *J. Chem. Phys.*, **49**, 3706 (1968).
(7) A. R. Allnatt, *Mol. Phys.*, **8**, 409 (1970).
(8) J. C. Rasaiah and H. L. Friedman, *J. Chem. Phys.*, **48**, 2742 (1968); **50**, 3965 (1969); H. L. Friedman and P. S. Ramanathan, *J. Phys. Chem.*, **74**, 3756 (1970).
(9) F. H. Stillinger and R. Lovett, *J. Chem. Phys.*, **48**, 3858 (1968).
(10) J. L. Lebowitz and J. K. Percus, *Phys. Rev.*, **144**, 251 (1966).
(11) J. Groeneveld, unpublished results, as quoted by E. Waisman, Thesis, Yeshiva University, New York, N.Y., 1970.
(12) E. Waisman and J. L. Lebowitz, *J. Chem. Phys.*, **56**, 3086, 3093 (1972).
(13) L. Blum, *Mol. Phys.*, **30**, 1529 (1975).
(14) J. R. Grigera and L. Blum, *Chem. Phys. Lett.*, **38**, 486 (1976).
(15) R. Triolo, J. R. Grigera, and L. Blum, *J. Phys. Chem.*, **80**, 1858 (1976); R. Triolo and L. Blum, unpublished calculations.
(16) L. Blum, to be published. The equal size case was solved in L. Blum, *J. Chem. Phys.*, **61**, 2129 (1974).
(17) D. Henderson, F. F. Abraham, and J. A. Barker, *Mol. Phys.*, **31**, 1291 (1976).
(18) J. K. Percus, *J. Statistical Phys.*, in press.
(19) K. S. Liu, unpublished results; *J. Chem. Phys.*, **60**, 4226 (1974).
(20) J. S. Hoye, J. L. Lebowitz, and G. Stell, *J. Chem. Phys.*, **61**, 3253 (1974).
(21) E. Waisman, D. Henderson, and J. L. Lebowitz, *Mol. Phys.*, in press.
(22) E. H. Lieb and J. L. Lebowitz, "Lectures in Theoretical Physics", Vol. 14, University of Colorado Press, Boulder, Colo., 1972.
(23) D. C. Grahame, *Chem. Rev.*, **41**, 441 (1947); *J. Am. Chem. Soc.*, **76**, 4819 (1954); **79**, 2093 (1957).
(24) J. O'M. Bockris and A. K. Reddy, "Modern Electrochemistry", Plenum Press, New York, N.Y., 1970.
(25) H. L. Friedman and C. V. Krishnan, *Water, Compr. Treatise*, **3**, 1 (1973).
(26) I. L. Cooper and J. A. Harrison, *J. Electroanal. Chem.*, **66**, 85 (1975); in press.
(27) F. P. Buff and F. H. Stillinger, *J. Chem. Phys.*, **39**, 1911 (1963).
(28) L. Blum and C. A. D'Alkaine, unpublished work.
(29) L. Blum and G. Stell, *J. Statistical Phys.*, in press.
(30) H. C. Andersen and D. Chandler, *J. Chem. Phys.*, **57**, 1918 (1972).
(31) G. Stell, *Physica*, **29**, 517 (1963).
(32) H. L. Frisch and J. L. Lebowitz, "Classical Fluids", W. A. Benjamin, New York, N.Y., 1964.
(33) G. Stell and K. C. Wu, *J. Chem. Phys.*, **63**, 491 (1975).

(34) G. Stell and S. F. Sun, *J. Chem. Phys.*, in press.
(35) J. D. Jackson, "Classical Electrodynamics", Wiley, New York, N.Y., 1962.
(36) J. Pressing and J. E. Mayer, *J. Chem. Phys.*, **59**, 2711 (1973).
(37) S. Tøxvaerd, *J. Chem. Phys.*, in press.
(38) F. Hirata and K. Arakawa, *Bull. Chem. Soc. Jpn.*, **48**, 2139 (1975).
(39) A. L. Loeb, *J. Colloid Sci.*, **6**, 75 (1951).
(40) S. Levine and G. M. Bell, *J. Phys. Chem.*, **64**, 1188 (1960).
(41) A. Many, Y. Goldstein, and N. B. Grover, "Semiconductor Surfaces", North-Holland Publishing Co., Amsterdam, 1965.
(42) D. G. Triezenberg and R. Zwanzig, *Phys. Rev. Lett.*, **28**, 1183 (1972); R. Lovett, P. W. deHaven, J. J. Vieceli, and F. P. Buff, *J. Chem. Phys.*, **58**, 1880 (1973).
(43) D. C. Grahame, *J. Am. Chem. Soc.*, **79**, 2093 (1957).
(44) R. J. Baxter, *J. Chem. Phys.*, **52**, 4559 (1970).
(45) M. S. Wertheim, *J. Math. Phys.*, **5**, 643 (1964); W. R. Smith and D. Henderson, *Mol. Phys.*, **21**, 187 (1971); J. S. Høye and L. Blum, *Ark. Fys. Semin. Trondheim*, **No. 4** (1976).
(46) R. Bellmann and K. L. Cooke, "Differential-Difference Equations", Academic Press, New York, N.Y., 1963.

Solvent and Substitution Effects on the Phosphorescence Properties of Several Purine Molecules

G. Moller and A. M. Nishimura*

Department of Chemistry, Wichita State University, Wichita, Kansas 67208 *(Received May 7, 1976; Revised Manuscript Received November 11, 1976)*

Publication costs assisted by the Petroleum Research Fund and the National Institutes of Health

The effects of solvent and substitution on the phosphorescence properties of several purine related molecules are reported. The properties include phosphorescence decay rate constants from the lowest triplet state and zero field splitting (zfs) parameters arising from the anisotropic spin–spin interaction of the triplet electrons. The method of phosphorescence microwave double resonance is used to extract the zfs parameters.

Studies on the excited electronic states of nucleic acid molecules have been numerous.[1-6] In particular the study of hydrogen bonding in these molecules has been of considerable interest to researchers.[7-9] In this paper we report the results of a study involving the closer examination of the phosphorescence properties of a series of purine molecules in several host types, specifically polar solvents, such as ethanol, chlorinated benzenes and in some nonpolar hydrocarbons. Study of the nonpolar solvents was limited by the solubility of the purine molecules in the solvent system. A preliminary investigation was initiated to study methylated purines and its effect on the phosphorescence properties because of the interest concerning the effects of methylation in the hydrogen bonding properties of these bases. Pairwise combinations of purine and pyrimidine bases of the Watson–Crick type were studied, including heterocyclic bases, nucleotides, and polymeric nucleic acids.

Experimental Section

For the molecules under study, dimethylnaphthalene (DMN), quinoline, hydroxyquinolines (HQ), indene, indole, azaindole, benzimidazole, and azabenzimidazole were purchased commercially and purified either by multiple vacuum distillation or by recrystallization and sublimation at reduced pressures. The geometries of these molecules are shown in Figure 1, along with the numbering system used in the text. The purine and pyrimidine bases were recrystallized from water while the polynucleic acids were used without further purification.

Ethanol (U.S. Industrial Chemical Co., Red Label) was found to be free of impurity emission. The crystalline hosts included *p*-dichlorobenzene (DCB), *p*-xylene, and phenol. DCB was obtained from Fisher Scientific Co., and was extensively zone refined under an inert atmosphere for an equivalent of over 200 passes. *p*-Xylene was purchased from J. T. Baker Chemical Co. and purified by shaking with concentrated sulfuric acid, washed, dried, and chromatographed. Finally, the solvent was subjected to multiple vacuum distillation. The phenol host, purchased from Mallinckrodt Chemical Works, was recrystallized from methanol and sublimed under vacuum. The solution for each guest–host combination investigated was sealed under vacuum in a thin walled pyrex ampoule which was fitted into a slow wave helical structure attached to a semirigid 50-Ω stainless steel coaxial cable suspended in a liquid helium cryostat equipped with a quartz optical tip. Single crystals of DCB and *p*-xylene containing appropriate guest molecules were grown in a standard Bridgman furnace at room temperature for DCB or in a cold room for *p*-xylene host. Single crystals were cut from the resulting ingots and mounted inside the slow wave helix and immersed in liquid helium.

The zero field transitions of the triplet sublevels were detected by microwave induced delayed phosphorescence (MIDP) technique.[10,11] The method requires an appreciable difference in the populations of the two sublevels when the transition is adiabatically swept with the microwave power. In some cases, the transitions were found using a method described by Winscom and Maki[12] in which the microwave power was frequency modulated at approximately 100 kHz through the zero field resonance energy while continuously pumping the triplet state via CW excitation.[13]

The microwave field was generated in the slow wave helix by a Hewlett-Packard sweep generator amplified by a 1-W TWT amplifier and terminated with a semirigid 50-Ω coaxial assembly. An Alfred microwave sweeper with appropriate plug-in was used in several cases (vide infra) where simultaneous pumping of two zero field transitions was necessary. The microwave sweep was calibrated utilizing a Hewlett-Packard Model 540B transfer oscillator in conjunction with a Phillips 6630 frequency counter.

In several cases two of the transitions could be observed in the manner just described, but the detection of the third transition required the continuous pumping of a different transition with another microwave generator, the monitoring of a weak phosphorescence band of an asymmetric

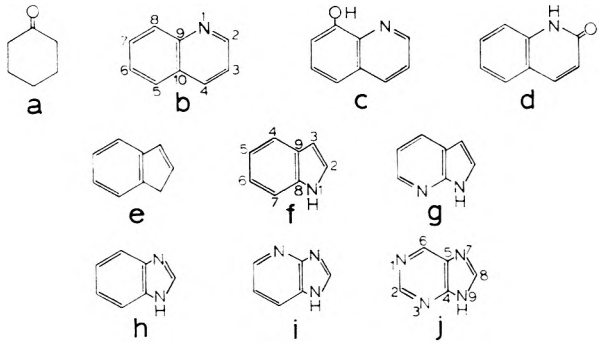

Figure 1. Geometries and numbering system used: (a) cyclohexanone, (b) quinoline, (c) 8-hydroxyquinoline, (d) 2-hydroxyquinoline (lactam form), (e) indene, (f) indole, (g) 7-azaindole, (h) benzimidazole, (i) 4-azabenzimidazole, and (j) purine.

vibration, or a combination of the two methods.

For experiments requiring a continuous excitation (CW) source, a 100-W xenon–mercury high-pressure arc lamp was used with adequate filtering by a solution containing $NiSO_4$ and $CoSO_4$ and additional filtering through a Corning 7-54 filter. The lamp was placed in a 45° configuration to a 0.75-m Czerny-Turner spectrometer with ≤100-cm^{-1} slits. A cooled EMI 6256B photomultiplier tube was used for detection of the phosphorescence. To obtain temperatures below 4.2 K, the vapor above the liquid helium was pumped and temperatures as low as 1.4 K were routinely obtained as determined by vapor pressure measurements of the liquid helium.

For phosphorescence decay measurements, a vibronic band of the phosphorescence (usually the 0,0 band) was isolated with the spectrometer and the excitation source was extinguished in about 2 ms by an electronically controlled mechanical shutter, or alternatively, the decay was measured following a xenon flash lamp excitation of 10-μs duration. The signals were repetitively accumulated in a Tracor-Northern NS-570 signal averager. The resulting data composed of 2048 points were computer fitted to an equation describing the time-dependent decay of the phosphorescence intensity. The program used the Newton-Raphson nonintegral method of curve fitting with approximated gradients.[14]

Results and Discussion

The excited electronic states are sensitive to external interactions with solvent types. Since the phosphorescence decay rates are a measure of the facility with which relaxation proceeds, the rate constants can be used as an indicator of the degree and type of external solvent perturbation. Such solvents can be selected so that the type of interaction is analogous to hydrogen bonded base pairs of the Watson and Crick model. In addition, the method of phosphorescence microwave double resonance extends the study into the nature of the phosphorescence triplet state via zfs data which is a function of spin–spin and spin–orbit interactions of the two triplet electrons.

In an attempt to find simple model systems for the hydrogen-bonded pair formation in purine and pyrimidine bases, we chose to study initially the effects of hydrogen bonding in nitrogen heteroaromatic molecules and in a carbonyl containing hydrocarbon. In the former cases quinoline and the hydroxyquinolines (HQ) were studied while, in the latter case, cyclohexanone, in several different hosts was observed. The results are shown in Table I. It should be emphasized that the axis system used in the table is arbitrary and no correlation between the spin axes of the various molecules is implied.

TABLE I: Solvent Effects on the Phosphorescence Rate Constants (in cm^{-1}) of Quinoline, Hydroxyquinoline, and Cyclohexanone at 1.4 K (±20%)[a,b]

Guest/Host		*p*-Xylene	*p*-Dichlorobenzene	Ethanol
Quinoline	k_3	3.1[c]	3.5[d]	
	k_2	0.37	1.4	1.1
	k_1	0.20	0.58	0.5
2-Hydroxyquinoline	k_3	71		*16*
	k_2	10	3.1	1.5
	k_1	2.9	2.3	0.86
5-Hydroxyquinoline	k_3	150	81	
	k_2	17	16	3200
	k_1	1.1	1.1	1400
8-Hydroxyquinoline	k_3	>2000	120	
	k_2	700	36	2600
	k_1	90	11	1900
2,3-Dihydroxyquinoxaline	k_3	220	76	
	k_2	43	9.4	4000
	k_1	0.15	1.9	650
Cyclohexanone	k_3	~600	180	
	k_2	~600	45	2300
	k_1	77	1.7	760

[a] Arbitrarily, $k_3 > k_2 > k_1$ assumed. No correlation of the spin axes is implied. Cf. text. [b] Dashed lines indicate that the intensity was too low to be observed. [c] From ref 10 in durene. [d] In tetrachlorobenzene.

That the lowest triplet state of quinoline and many substituted quinolines is $^3\pi,\pi^*$ is firmly established from examination of Table I and by previous work.[10,15] In molecules where intramolecular hydrogen bonding is possible, such bonding exhibits a larger increase in the phosphorescence decay rate than intermolecular hydrogen bonding with the solvent. This trend is apparent when comparing the rate constants of 2-HQ in *p*-xylene and ethanol solvents. A parallel trend is observed for 8-HQ in the same solvents. The data generally show a decrease in decay rate constants in the chlorinated host, *p*-DCB. Since the total rate constant is a sum of the radiative and radiationless rate constants, this decrease can be attributed to an increase in the radiative rate due to external spin–orbit interaction with a concomitant larger decrease in the nonradiative rate. Similar results and conclusions were observed in a study of chloroquinoline doped tetrachlorobenzene host crystals, the results of which will be reported elsewhere.[16]

The data reported in Table I are in contrast to the study on 5-HQ and 8-HQ reported by Goldman and Wehry in which phosphorescence was not observed.[17] 5-HQ exhibited fairly weak phosphorescence, whereas 8-HQ showed strong emission which decayed extremely rapidly. The strong intramolecular hydrogen bonding which is possible in a hydrocarbon solvent such as *p*-xylene might explain the rapid decay. Such strong interaction can cause the nonradiative relaxation to become vary facile, leading to the rapid phosphorescence decay. Another possible explanation which has been postulated by Bailey and Hercules is that the phosphorescent state is $^3n,\pi^*$ in 8-HQ, which would then account for the characteristic large rate constant.[18] 2-HQ, for which tautomeric forms can be postulated, appears to have the rate constants only slightly larger than that of quinoline, whereas 8-HQ, for which such lactam–lactim tautomerism is not energetically favorable, exhibits rate constants very different from that of quinoline.

The zero field splittings for some representative molecules are shown in Table II. The results are complimentary to the phosphorescence decay rate constants of Table I and provide further evidence that the nature of

TABLE II: Zero Field Transitions Observed in Quinolines, Hydroxyquinolines, and Purines in *p*-Dichlorobenzene and Other Substituted Benzenes at 1.4 K

Guest	Zero field transition, MHz	
Quinoline	3585[a]	3615[b]
	1000.5	1040
2-Hydroxyquinoline	4170[c]	
	2495	
	1675	
5-Hydroxyquinoline	4730	
	2410	
	1120	
Cyclohexanone	5010	5021.9[d]
	3370	3397.3
	1660	1624.6
Indene	4610	
	2805	
	1795	
Indole	4340	
	2970	
	1370	
4-Azabenzimidazole	4710	
	3125	
	1585	
Purine	4750	
	3425	
	1325	
Adenine	4850	
	3495	
	1355	

[a] In durene from ref 10. [b] In phenol. [c] In *p*-xylene. [d] For cyclopentanone in *n*-hexane from ref 19.

TABLE III: Phosphorescence Decay Rate Constants for Purine and Pyrimidine Bases in Ethanol at 1.4 K (±20%)

Solute molecules	Rate constant, s^{-1}		
Indene[a]		0.48	0.22
Indole		0.15	0.07
7-Azaindole	0.47	0.18	
Benzimidazole	0.45	0.22	0.10
4-Azabenzimidazole	1.6	0.80	0.29
Purine	1.7	0.60	0.32
Adenine	4.2	0.70	0.32
Guanine	113	21	7.4
Xanthine	410	16	1.5
Hypoxanthine	104	34	
Cytosine	57	6.5	1.8
Thymine	18	2.0	0.39
Cytosine-guanine	37	8.0	1.9
Adenine-thymine	110	2.8	0.66
Uracil-adenine	74	2.8	0.43

[a] In DCB.

the triplet state of these molecules is $^3\pi,\pi^*$. The zero field energies of π,π^* states are not expected to undergo dramatic shifts in different solvents. The differences in the resonance energies are due primarily to contribution from second-order spin–orbit interaction with the solvent molecules.

The triplet state of the ketone cyclopentanone in *n*-hexane was investigated by Sharnoff et al.[13,19] Compared to their results, our data on the triplet state of cyclohexanone in DCB shown in Table II reveal little difference in the zfs for the ketone in *n*-hexane and in DCB, but a significant decrease in the rate constants for the phosphorescence decay process for the ketone in DCB as compared to the ketone in *p*-xylene. It would seem reasonable to conclude that the nature of the triplet remains unaltered since the zfs remained nearly the same in the two hosts. However the decrease in the rate constants for the ketone in DCB seems to indicate the magnitude of the decrease in the nonradiative processes to be larger than any increase in the radiative rate constants caused by the solvent heavy atom interaction. This is analogous to the previous discussion for HQ in chlorinated hosts.

TABLE IV: Phosphorescence Rate Constants for Polynucleic Acids in Ethanol at 1.4 K (±20%)

Solute	Rate constant, s^{-1}		
Polyadenylic acid	25	2.7	0.51
Polyguanylic acid	100	17	1.1
Polycytidylic acid	180	22	3.9
Polyuridylic acid	210	19	1.2
Polycytidylic acid–polyguanylic acid	180	15	2.5
Polyuridylic acid–polyadenylic acid	280	21	3.1

The kinetic data for the monomer and dimer complexes of the base components of the nucleotides are shown in Table III. The solvent used was ethanol which formed clear glasses at liquid helium temperatures. It has been shown that the heteromolecular complex is energetically preferred over the tendency to form homomolecular complex.[20] The change in phosphorescence decay rate constant of the complexes reflect the preferential formation of the Watson–Crick model base pairs. Such a change has been observed in other hydrogen bonded systems where similar interaction increased radiationless processes which in turn tend to increase the rate constants for the depopulation process.[21] In the series of complexes shown in Table III, the energy is transferred from the left to right species owing to the lower triplet energies of the base on the right.[2,22] The decay rate constants for indole agree well with the study by Zuclich et al.[23] Shown in Table IV are the phosphorescence rate constants for the polynucleic acids. The solution containing the complementary polynucleic acids are not assumed to form helices, but are presumably stacked in some globular conformation.

The effect of methylation upon the electronic spectra of aromatic molecules has been investigated both experimentally and theoretically.[24] As a general rule, the red shift of the 0,0 band of benzene upon methylation has been calculated to be about 620 cm^{-1} per methyl group and observed to be ca. 600–650 cm^{-1}.[24] It seems likely that the smaller shift observed in DMN of 631 cm^{-1} in total for the two methyl groups can be attributed to the larger second-order conjugative and charge-transfer perturbation according to the treatment by Petruska.[24] (Cf. Table V.) Assuming that the signs of the zfs do not change in DMN relative to naphthalene, the large change in the value of D (ca. 8%) seems to indicate a significant degree of either (1) delocalization by hyperconjugation and therefore a decrease in the spin–spin interaction or (2) spin–orbit interaction due to the methyl substituents. In the first case, it seems reasonable to conclude that in light of the evidence that methylation of the purine bases causes a weakening of the pairing by hydrogen bond,[25] that the hyperconjugation observed in DMN can also be effective in the methylated bases as seen in Table V. Since this will lower the strength of hydrogen bonding, methylation would be one possibility as to the cause of the disruption of the base pairing. This conclusion is very tentative and more evidence is required. In the second case, Kothandaraman et al.[26] and others[27] have shown that the spin–orbit contributions to the zfs in $^3\pi,\pi^*$ state occur in halogen substituted naphthalenes and benzenes. The argument rests upon the spin–orbit coupling of the lowest $^3\pi,\pi^*$ state with states of the same spin multiplicity, viz. of the $^3\sigma,\pi^*$ type. If we consider the effects of such spin–orbit contributions to the zfs in DMN, then according to the arguments analogous to that given by Kothandaraman, Yue,

TABLE V: Decay Rate Constants for Methylated Naphthalene and Purines in Ethanol at 1.4 K

Guest	Rate constant, s^{-1}		
1,4-Dimethylnaphthalene[a]	0.92	0.70	0.15
2-Methyladenine	5.7	0.94	0.33
6-Dimethylaminopurine	5.8	0.86	0.41
2-Dimethylamino-6-hydroxypurine	85	5.0	0.69

[a] In durene, (0,0) at 4851 Å, zfs: 3240, 2350, and 820 MHz. For comparison, naphthalene in durene (0,0) 4707 Å, zfs: 3420, 2598, 822 MHz, and rate constants 0.65, 0.40, 0.15 s^{-1}, ref 10 and 26.

and Pratt,[26] ΔE_z should be negative as should ΔE_x. ΔE_i is the change in zero field energy along the i axis relative to the parent compound naphthalene. The axis system is chosen such that x and y are along the in-plane long and short axes, respectively. Since the two methyl groups are aligned along the y molecular axis, ΔE_y should be relatively small. Since the two methyl groups are coincident to the y direction, the spin–orbit interaction favors the angular momentum operator along the y direction. Thus, τ_x and τ_z are most affected, and are energetically more depressed than τ_y. The net effect is a smaller $2E$ with a concomitant decrease in D. The increase in spin–orbit interaction along the y direction is consistent with the data shown in Table V.

In conclusion the study reported here shows the feasibility of applying models composed of simple host–guest systems in the application to hydrogen bonded Watson–Crick type base pairing in nucleic acids. The sensitivity of the rate constants to dipolar perturbations via external heavy atom interactions allows these rate constants to serve as a qualitative measure of spatial conformations.

Acknowledgment. Acknowledgment is made to the donors of the Petroleum Research Fund, administered by the American Chemical Society, for partial support of this work. We also thank the National Institutes of Health for supporting this research.

References and Notes

(1) A. D. McLaren and D. Shugar, "Photochemistry of Proteins and Nucleic Acids", Macmillan, New York, N.Y., 1964.
(2) M. Gueron, J. Eisinger, and A. A. Lamola, "Excited States of Nucleic Acids", in "Basic Principles in Nucleic Acid Chemistry", Vol. I, P. Ts'o, Ed., Academic Press, New York, N.Y., 1974.
(3) "The Purines", Proceedings of Jerusalem International Symposium on Quantum Chemistry and Biochemistry, Vol. IV, E. D. Bergmann and B. Pullman, Ed., Jerusaleum Academic Press, Jerusalem, Israel, 1972, and references therein.
(4) J. W. Longworth, R. O. Rohn, and R. G. Shulman, *J. Chem. Phys.*, **45**, 2930, 2955 (1966).
(5) R. G. Shulman and R. O. Rohn, *J. Chem. Phys.*, **45**, 2940 (1966).
(6) R. O. Rohn, T. Yamane, J. Eisinger, J. W. Longworth, and R. G. Schulman, *J. Chem. Phys.*, **45**, 2947 (1966).
(7) S. Lunell and G. Sperber, *J. Chem. Phys.*, **46**, 2119 (1967); A. A. Lamola, M. Gueron, T. Yamane, J. Eisinger, and R. G. Shulman, *ibid.*, **47**, 2210 (1967).
(8) J. Drobnik and L. Augenstein, *Photochem. Photobiol.*, **5**, 13, 83 (1966).
(9) V. Kleinwachter, J. Drobnik, and L. Augenstein, *Photochem. Photobiol.*, **6**, 133, 147 (1967).
(10) J. Schmidt, W. S. Veeman, and J. H. van cer Waals, *Chem. Phys. Lett.*, **4**, 341 (1969).
(11) D. A. Antheunis, J. Schmidt, and J. H. van der Waals, *Chem. Phys. Lett.*, **6**, 255 (1970).
(12) C. J. Winscom and A. H. Maki, *Chem. Phys. Lett.*, **12**, 264 (1971).
(13) A. L. Shain and M. Sharnoff, *Chem. Phys. Lett.*, **16**, 503 (1972).
(14) M. J. D. Powell, *Comp. J.*, **8**, 303 (1965).
(15) J. S. Vincent and A. H. Maki, *J. Chem. Phys.*, **42**, 865 (1965).
(16) A. M. Nishimura, to be published. See also: T. Azumi, *Chem. Phys. Lett.*, **19**, 580 (1973); T. H. Cheng, N. Hirota, and S. W. Mao, *ibid.*, **15**, 274 (1972).
(17) M. Goldman and E. L. Wehry, *Anal. Chem.*, **42**, 1173 (1970).
(18) D. N. Balley and D. M. Hercules, *Anal. Chem.*, **39**, 877 (1967).
(19) A. L. Shain, W. T. Chiang, and M. Sharnoff, *Chem. Phys. Lett.*, **16**, 206 (1972).
(20) Y. Kyogoku, B. S. Yu, R. C. Lord, and A. Rich, "IR Studies on the Selective Hydrogen Bonding of the Nucleic Acid Purine and Pyrimidine Derivatives and Some Other Compounds", "The Purines", Vol. IV, E. D. Bergmann and B. Pullman, Ed., Jerusalem Academic Press, Jerusalem, Israel, 1972, p 223.
(21) G. R. Brunk, K. A. Martin, and A. M. Nishimura, to be published.
(22) C. Helene, P. Douzou, and A. M. Nichelson, *Biochim. Biophys. Acta*, **109**, 201 (1965).
(23) J. Zuclich, J. V. von Schutz, and A. H. Maki, *Mol. Phys.*, **28**, 33 (1974).
(24) T. Petruska, *J. Chem. Phys.*, **34**, 1111, 1120 (1961).
(25) J. Ramstein, D. Genest, and M. Leng, "A Study of Chemically Methylated DNA-Proflavine Complexes", "The Purines", Vol. IV, E. D. Bergmann and B. Pullman, Jerusalem Academic Press, Jerusalem, Israel, 1972, p 593.
(26) G. Kothandaraman, H. J. Yue, and D. W. Pratt, *J. Chem. Phys.*, **61**, 2102 (1974).
(27) G. Kothandaraman and D. S. Tinti, *Chem. Phys. Lett.*, **19**, 225 (1973).
(28) A. H. Francis and C. B. Harris, *J. Chem. Phys.*, **57**, 1050 (1972); A. H. Francis, C. B. Harris, and A. M. Nishimura, *Chem. Phys. Lett.*, **14**, 425 (1972).
(29) C. A. Hutchison, Jr., and B. W. Mangum, *J. Chem. Phys.*, **34**, 908 (1961).

Linear and Circular Dichroism of Polymeric Pseudoisocyanine

Bengt Norden

Department of Inorganic Chemistry 1, Chemical Center, University of Lund, S-220 07 Lund, Sweden *(Received June 28, 1976)*

The dye 1,1′-diethyl-2,2′-cyanine iodide (pseudoisocyanine = PIC) was studied by circular dichroism (CD) and linear dichroism (LD). PIC forms optically active aggregates in aqueous (+)tartrate solution and as complexes with DNA. They are characterized by J bands at 572 (tartrate) and 553 nm (DNA), with negative and positive CD, respectively, which may be explained by helical band arrays of dye molecules (left- and right-handed helices, respectively). At higher degrees of aggregation in (+)tartrate a positive J band may be due to helical stacking of PIC polymers such as in a cholesteric liquid crystal. Intense LD indicates that the solution is not random but contains large domains with local order. It is shown that earlier conclusions about helicity reversals and mechanical induction of optical activity in aggregated PIC when formed in optically inactive media may have been due to instrumental sensitivity to linear dichroism from possibly nonhelical PIC fibers. The PIC aggregation was also studied by LD at different linear flow gradients in aqueous NaCl solution. From LD relaxation lengths of 4000–100 000 Å were estimated for the orientable aggregates. The ratio of LD to random absorption at different degree of aggregation suggests that also unalignable $(PIC)_N$ oligomers may exhibit J bands. By exciton theory N was tentatively estimated to be more than 10. An earlier "card-pack" model, with angle α close to 90°, between the monomer long axis and the polymer axis, is discarded. The suggested structure of PIC_∞ is a coiled band with α = 30–40°. Influence of flow on aggregation was observed: At low gradients the formation of aggregates with low rotational diffusion is favored (by applying a constant gradient apparently very elongated aggregates may be synthesized in this way). Above a certain value (ca. 1000 s^{-1}) the effect of the gradient was the opposite, leading to the destruction of aggregates. PIC was also studied in oriented polyvinyl alcohol film in which it was monomeric, and in polystyrene film where a J band was observed at 585 nm. In the Appendix factors determining the instrumental LD response are analyzed.

Introduction

Since the beginning of this century considerable attention has been devoted to the aggregation of dyes, phenomena which are of crucial importance in biological and artificial photosensitive systems. Perhaps the most popular dye in this connection,[1] 1,1′-diethyl-2,2′-cyanine$^+$ (also known as pseudoisocyanine, PIC), is monomeric in

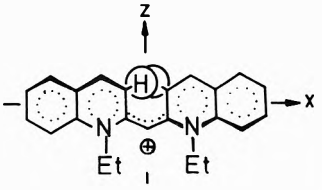

ethanol but in water at concentrations above 10^{-3} M forms a fluorescent polymer (discovered by Jelley and Scheibe, often referred to as the "Scheibe polymer"[2,3]) well known for its characteristic very sharp absorption band (the "J band") at a longer wavelength (572 nm) than the monomer 0–0 band (525 nm).[4] The polymer has been suggested to contain at least seven[5] monomer units. The interest in PIC was intensified after reports by Stryer and Blout and by Mason on the optical activity of the Scheibe polymer induced in the presence of poly-α,L-glutamic acid[6] and of (+)tartrate,[7] respectively. Mason suggested that PIC tends to form helical aggregates and that the chiral environment partially selects the sense of aggregation. Scheibe, Haimerl, and Hoppe[8] have, on the other hand, pointed out the fact that PIC by steric hindrance is twisted out of planarity and that an alternative explanation of the optical activity is a planar packing involving only one sense of PIC molecules. This structure was found in crystallites;[8] a dihedral angle of 54° was obtained between the planes of the two quinolinium moieties. However other crystal studies imply centrosymmetry by pairing of the enantiomers.[9,10] The structural question of the Scheibe polymer was further discussed by Maurus and Bird as the background of their discovery of transient circular dichroism effects when precipitating PIC with tartrate.[11] They conclude that the helical aggregate yields the more economical hypothesis. Recently Honda and Hada showed that a circularly dichroic Scheibe polymer can be produced by "regular stirring"[12] without any chiral additives and correlation was claimed between the optical sign and the sense of stirring.

In a Fourier transform ^1H NMR study Graves and Rose[13] find shifts to higher field for all resonances as the PIC concentration is increased from 10^{-5} to 10^{-2} M and they conclude an aggregate structure in which the dye molecules stack face to face with considerable overlap between the quinolinium systems. The shift change with higher concentration is interpreted in terms of a polymer composed of units similar to the dimer. No evidence for any unique J aggregate was however obtained.

Upon testing the experiments reported in the optical studies above we found it difficult to reproduce the results obtained with circular dichroism. For instance the correlation claimed by Honda and Hada was impossible to verify. In several cases we could establish causality between the observed circular dichroism and an accidental orientation in the optical cell even at large cell lengths. We have used linear dichroism (LD) to study such orientation effects and have by subjecting the sample in a Couette rotation cell to a defined flow gradient also been able to characterize the Scheibe polymer hydrodynamically in a more reproducible way.

During the course of the investigation we observed that PIC forms Scheibe-like polymers in polystyrene and as a complex with DNA which have J bands strongly shifted to longer and shorter wavelengths, respectively.

Experimental Section

PIC was obtained as the iodide from Koch-Light Laboratory Ltd. After recrystallization from ethanol the UV spectrum (200–620 nm) was well reproduced (ϵ_{520} =

Chart I

Mixture	PIC, 10^{-4} M	Polystyrene, %
I	7.3	0
II	1.0	1.8
III	5.2	3.7
IV	0.5	0.9
V	0.5	0.5
VI	2.1	9.3
VII	1.0	11.1

6.0×10^4 M^{-1} cm^{-1} at about 10^{-4} M concentration in water) and no further purification was considered necessary.

Polystyrene (unspecified molecular weight, commercial hard-plastic quality, Polystyrenfabriken, Kavlinge) was applied as a thin (2–10 μm) film on both sides of quartz plates by dipping in $CHCl_3$ solutions. A 10% aqueous solution of PIC in polyvinyl alcohol (UV transparent Elvanol, DuPont Nemoirs) was evaporated to dryness on a glass plate to give a film which was then stretched at 80 °C.

Linear dichroism spectra were obtained by the lock-in technique on a modified Legrand-Grosjean circular dichroism spectrometer (Jasco J-40).[14] Circular dichroism could be recorded on the same instrument. Absorption spectra were recorded on a Cary 118-C spectrophotometer. Both instruments were wavelength calibrated by the low pressure mercury line spectrum.

Linear dichroism, $LD = A_{\parallel} - A_{\perp}$, is given in absorbance units and the reference axis ($\parallel$) is, in the discussions of perturbed circular dichroism, the direction of vibration of the electric vector in the light path before the Pockels' cell (in Jasco J-40 horizontal polarization). When referring to the Couette cell $\parallel$ is perpendicular to the rotation axis. LD was corrected for optical factors[14] only in numerical estimates of LD/A, where A represents the absorption of the random solution.

The flow experiments were performed in a Couette cell described elsewhere (light path perpendicular to rotation axis, gap 0.05 cm, gradient range 0–5000 s^{-1}).[15] It was checked before and after each run so that no visible PIC threads were contaminating the sample. The total optical path length (as well as in absorption measurements) was 0.100 cm. The flow apparatus' tachometer was connected to a xy recorder so that a LD vs. gradient (G) curve could be obtained with a scan time of less than 10 s.

Mixtures 1–5. Aqueous salt solutions were prepared by adding 5.0 ml, 50 °C, of 5.0×10^{-4} M aqueous PIC solution to 5.0 ml of a x M NaCl solution. These solutions are referred to as mixture 6 when $x = 1$, 5 when $x = {}^1/_2$, ..., and 1 when $x = {}^1/_{32}$.

Mixtures I–VII. Chloroform solutions containing PIC and polystyrene were evaporated to thin films on quartz plates (the evaporation was performed in a $CHCl_3$ atmosphere and completed in 30 s); the compositions are given in Chart I.

Experimental Result

Circular Dichroism Measurements. When produced at low concentration in saturated (+)tartrate solution a time-stable optically active Scheibe polymer with a negative J band is obtained (Figure 1). The dissymmetry factor was low, $(CD/A)_{572} = -0.003$. The solution exhibits no linear dichroism, but the aggregates can be oriented by flow; $(LD/A)_{572} = +0.016$ was observed at $G = 1080$ s^{-1}.

At higher PIC or salt concentrations the polymer behaves differently and a permanent linear dichroism suggests that domains are present with high local order (Figures 1 and 2). Thus the apparent circular dichroism is seriously affected and negative as well as positive deflections can be observed. The fact that the oscillations with time, probably due to turbulence by filling the cell and thereafter to Brownian motion, are not blurred by increasing the aperture indicates that the domains are very large, at least in two dimensions. The frequency of large apparent circular dichroism deflections is higher for PIC samples in (+)tartrate than when aggregation is induced by optically inactive salts (NaCl, Na_2SO_4) and the sign of the J band (here appearing at 574 nm in circular dichroism but at 572.5 nm in absorption) is then generally positive. It seems near at hand to suspect that the solution has a spiral structure related to that of cholesteric mesophases, by a stack of skewed nematic layers.

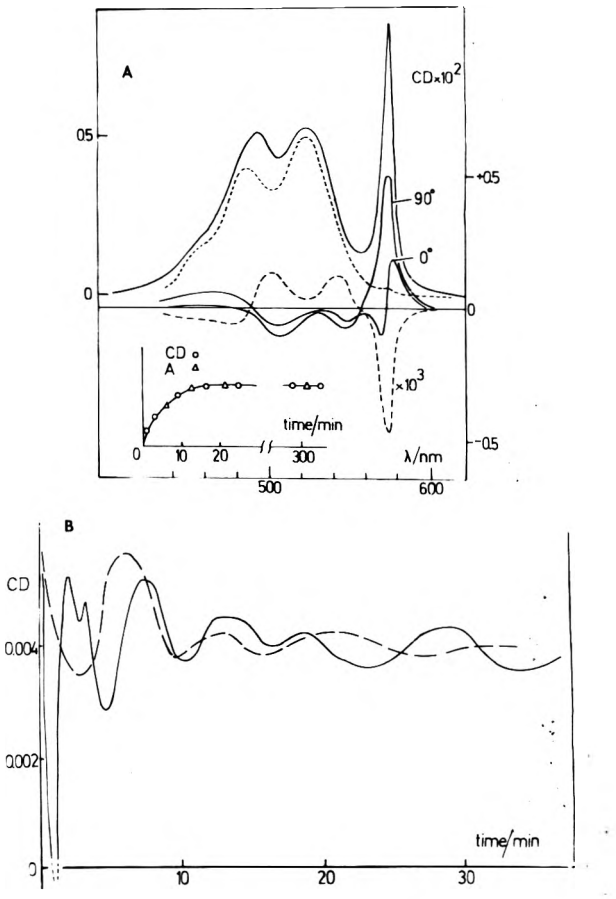

Figure 1. Absorbance (top —) and circular dichroism (bottom —) spectra (0.3 ml of 1.0×10^{-4} M PIC + 2 ml of 2.0 M disodium (+)tartrate) of intrinsically optically active Scheibe polymer. Absorbance (Δ) and circular dichroism (O) growths with time, 572 nm. Absorbance (top —) and circular dichroism (bottom — at two mutually perpendicular cell orientations; 0.2 ml of 2.5×10^{-4} M PIC + 2 ml of 2.0 M disodium (+)tartrate) of liquid crystalloid Scheibe polymer. Time dependence of circular dichroism at 574 nm (B) after filling the optical cell (1 cm) with (- - - 3 × 1 mm) and without (— 12 × 5 mm) aperture diminishing lens. Accidental linear dichroism: −0.018, fluctuation 30%.

With a further higher degree of aggregation, e.g., produced as mixture 5 in an optically inactive salt, very large circular dichroism deflections are observed of any sign and the spectra have shapes similar to the linear dichroism spectrum of the oriented polymer. A spectral change resembling that reported by Maurus and Bird (an effect which was claimed to prove the coexistence of helices of both senses)[11] could be produced by turning the cell carefully in the plane perpendicular to the light beam. No connection was found between the resulting circular dichroism and the sense of stirring the solution[12] and we find it plausible that several reported observations may have been due to the sensitivity in the Legrand-Grosjean circular dichroism detection system[16] to linear dichroism and not

TABLE I: $(PIC)_N$ in Different Environments

Medium	Concn, M	N	Linear dichroism bands: Other bands λ, nm	Other bands LD/A	J band λ, nm	J band LD/A
Aqueous solutions	$<10^{-4}$	1	500			
Aqueous salt solutions:						
Mixture 3	2.5×10^{-4}	$10-10^4$			572.5	0.02
Mixture 4	2.5×10^{-4}	$10-10^3$	521	−0.3	572.5	+2 ± 0.5
			483	−0.7	(fresh: 0.05)	
Mixture 5	2.5×10^{-4}	$10-10^3$			574	+1.5 ± 0.5
Mixture 5 (fresh)	2.5×10^{-4}				(560-580 neg)	
Polyvinyl alcohol (40 μm)	6×10^{-3}	1	526 (0-0)	+0.036		
			491	+0.036		
			460	+0.035		
Polystyrene (2 × 1.0 μm, mixture VII)	0.08		540-550	−0.005	582-585	+0.05
			500-510	−0.01		
DNA (C_L/C_N = 0.005)	3.2×10^{-5}	1	530	−0.20		
			500	−0.15		
			460	−0.13		
DNA (C_L/C_N = 0.09)	4.5×10^{-5}	1-2	530	−0.13		
			500	−0.10		
			460	−0.08		
DNA (C_L/C_N = 0.55)	1.4×10^{-4}	$10-10^4$	525	−0.032	553	+1.3 ± 0.5

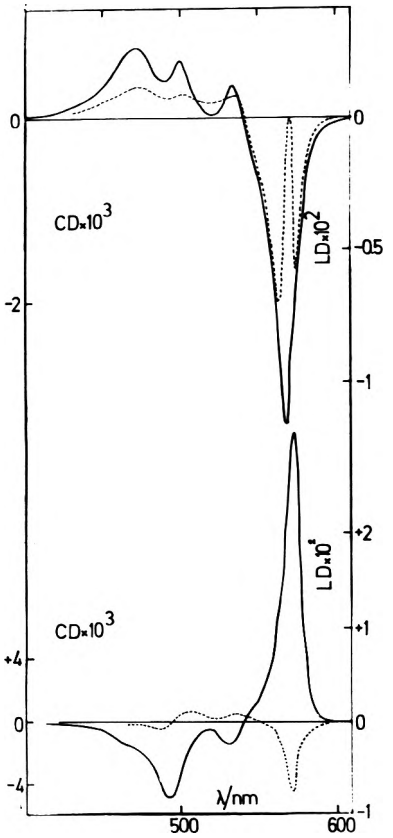

Figure 2. Circular dichroism of polymer PIC (top ...) due to accidental orientation (linear dichroism, top —) in 0.1-cm cell of aggregates of the Honda–Hada type (1 ml of 5×10^{-4} M PIC + 2 ml of 2 M disodium tartrate). Below: Corresponding accidental circular dichroism (..., 1 cm cell at rest) and linear dichroism observed at flow (—, G = 500 s^{-1}) for mixture 4 10 min after preparation.

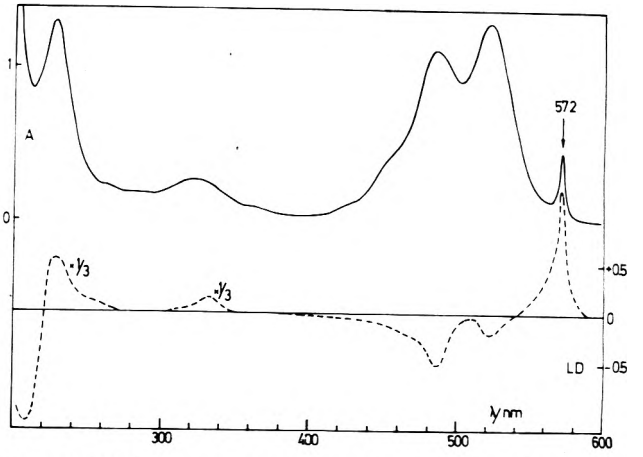

Figure 3. PIC in aqueous salt solution (mixture 4), LD at G = 100 s^{-1} (- - -) and A at G = 0 (—).

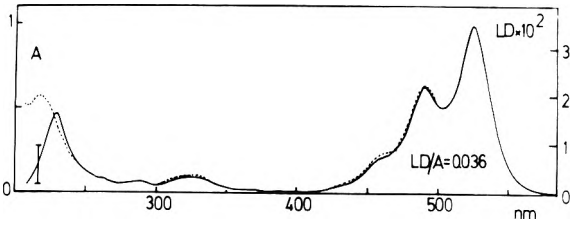

Figure 4. PIC in stretched polyvinyl alcohol (stretch ratio 1.02), LD (—) and A(...).

to molecular circular dichroism (outlined in the Appendix).

Attempts to induce circular dichroism by circularly polarized photolysis (before, during, or after precipitating the Scheibe polymer in aqueous as well as in polystyrene solutions) failed. In polystyrene the degree of photolytical destruction was easy to follow, and, for instance, if PIC had been present as helices of different senses an easily detectable circular dichroism (high dissymmetry factor[11]) should have resulted after 10% destruction by irradiation in the J band.

Medium or Complexation Effects. In Figures 3–6 and Table I spectra and LD/A values are summarized for PIC in different environments. In polyvinyl alcohol PIC appears to exist as a monomer and from the fact that LD/A is approximately constant over the visible region the x polarization is confirmed also for the higher vibronic levels (vide infra). A decrease in LD/A by 4% in the 460–480-nm region might be explained by the presence of the dimer, which can be expected to orient less effectively and to have a pronounced absorption in this region.[18,19] When obtained as a pure thin film (1 μm) on quartz, PIC shows no J band which is interesting in view of suggested parallels between the structures in the Scheibe polymer and in the crystal state.[8] New positions of the J band of polymeric PIC in a complex with DNA (to be studied elsewhere[20]) and in

TABLE II: D_1 Rationalized for Two Hypothetical Fractions from LD Decays

Curve no.	Sample: mixture 4	Fast fraction %	Fast fraction $10^4 D/s^{-1}$	Slow fraction %	Slow fraction $10^4 D/s^{-1}$
1	Fresh	93	20	7	0.8
2	After $G = 40\ s^{-1}$ (5 min)	50	4.6	50	0.36
3	After $G = 20\ s^{-1}$ (5 min)	42	3.6	58	0.33
4	After 10 min at rest	61	7	39	0.33
5	After 20 min at rest	84	15	39	0.69
6	After $G = 1600\ s^{-1}$ (1 min)	90	19	10	0.69
7	After $G = 3000\ s^{-1}$ (1 min)	100	3000	0	
8	After 2 min at rest	83	12	17	0.80
9	Mixture 4 aged for 2 days, diluted to 50% with 0.25 M NaCl. Decay reproduced six times	95	19	5	0.8

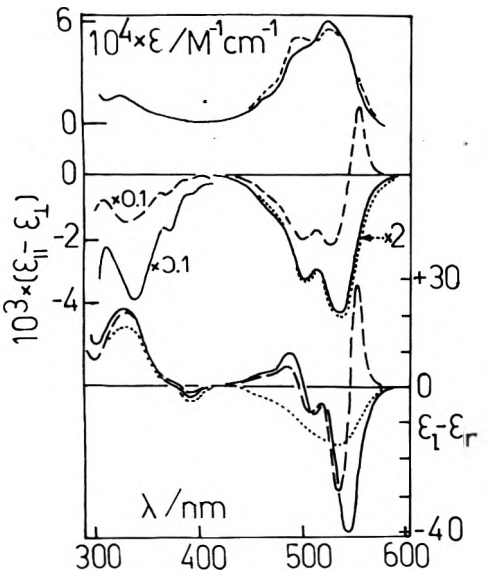

Figure 5. PIC as complexes with DNA at different PIC to nucleotide residue concentration ratios C_L/C_N. Intercalated monomer (C_L/C_N = 0.005, ...), presumably dimer (C_L/C_N = 0.09, —), oligomer PIC (C_L/C_N = 0.55, —). Absorbance (top), linear dichroism at 3000 s^{-1} (middle) and circular dichroism (bottom) normalized to unit length and unit total PIC concentration (M^{-1} cm^{-1}). Ionic strength 0.02 M NaCl.

polystyrene are observed. In polystyrene the flow, when drying the dipped quartz plate in the vertical position, was sufficient to give the Scheibe polymer considerable orientation. The fact that the polystyrene chains did not gain any detectable orientation (the aryl L_b band at 260 nm should have yielded positive LD) may be grasped as indicative of the relative lengths and flexibilities of the polymer chains.

Structural Linear Dichroism Studies. Even though it seems obvious that the LD in the present samples is due to contributions from a wide range of polymer dimensions, and perhaps also from various coexisting structures, the signs and magnitudes of LD/A can give useful qualitative information about the structures. According to a relation employed elsewhere,[15] between LD/A (where A represents the absorbance of the random solution) and the angle, θ, between the apparent effective transition dipole moment responsible for the absorption and the long axis of a stiff rodlike molecule

$$\mathrm{LD}/A = \frac{3}{2}(3\langle\cos^2\theta\rangle - 1)F \qquad (1)$$

F is the Peterlin–Stuart orientation factor which depends upon the flow gradient, G, the axial ratio, and the rotation diffusion constant, D_1, of the particle. For long rods (axial ratio ≥25) with very low D_1, F approaches unity already at modest G values. In Figure 7 different suggested[8,17] structural alternatives, A–D, of polymeric PIC are sketched. It is generally agreed that the J band can be derived by exciton theory within the dipole approximation

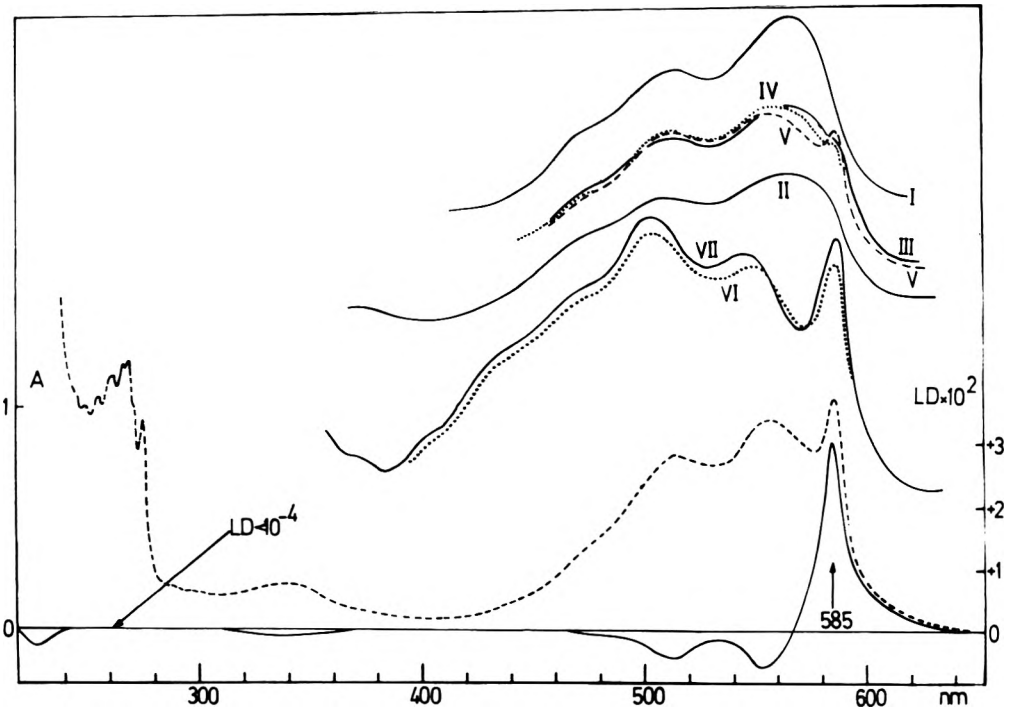

Figure 6. PIC in polystyrene films. Top: mixtures I–VII, A (curves vertically displaced). Bottom: mixture VII (evaporation time 15 s), LD (—, vertical) and A (---).

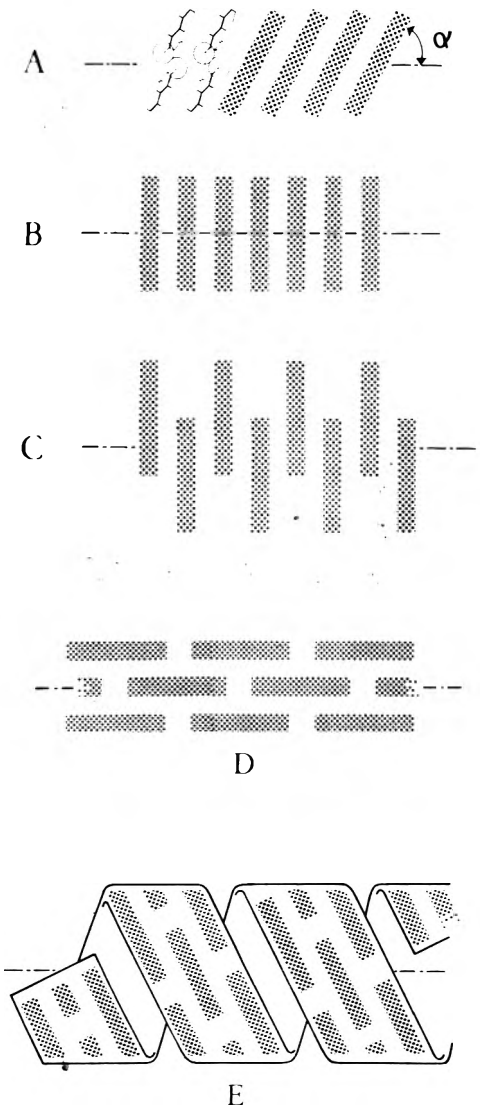

Figure 7. Different possible arrangements of polymeric PIC.

from coupling between transitions with x polarization (0–0 band at 525 nm, 0–1 at 500 nm)[18,21] in the monomeric PIC molecules. The resonance effect breaks down the degeneracy of the original singly excited states of the oligomer, PIC_N, producing a group of $K = 1,2,...,N$ quantum states which may be expressed as a linear combination of the original states. From the dipole strength, derived by Bradley, Tinoco, and Woody,[22] associated with excitation of a helical oligomer (with P monomeric residues per turn) to the Kth level, it is easy to obtain an expression for the ratio $A_\parallel/A_\perp = \langle\cot^2\theta\rangle$ for the rod at perfect order:

$$\langle\cot^2\theta\rangle = \left(\cos\frac{\pi K}{N+1} - \cos\frac{2\pi}{P}\right)^2 \sin^2\frac{\pi K}{2} \times \cot^2\alpha \Big/ \left(\cos\frac{\pi K}{N+1} - 1\right)^2 \sin^2\left(\frac{\pi K}{2} - \frac{(N+1)\pi}{P}\right) = R(P, K, N)\cot^2\alpha \qquad (2)$$

Here α denotes the angle between the monomeric transition moment (x axis in PIC) and the rod axis. The total dipole strength is always distributed among more than one K level regardless of the chain length, but has maxima at $K = 1$ (the parallel band) and $K \to 2(N+1)/P$ (the perpendicular band). With this formalism we are also allowed to consider the simple case of a straight stack ($P = 1$). By means of eq 1 and 2 the following is concluded.

Complexes with DNA. At 257 nm (the intrinsic DNA chromophore) $LD/A = -0.12$ was observed before as well as after complexing with PIC, indicating that the DNA conformation is essentially unperturbed by the complexation. The value is smaller than expected from the ideal Watson–Crick model, in which the planes of the purine and pyrimidine bases are almost perpendicular to the helix axis. F estimated to be between 0.43 (from $LD/A = +1.3$ for the parallel band of PIC_N–DNA) and 0.5 (from the Peterlin–Stuart model with $G = 3000\ s^{-1}$ and $D_1 = 50\ s^{-1}$)[15] then implies that the bases are tilted by 30° from the perpendicular orientation ($\theta = 59 \pm 1°$). A similar analysis for the monomeric PIC–DNA indicates that the PIC x axis is parallel to the base planes ($LD/A = -0.20 \pm 0.07$) an orientation supporting the idea (based upon a large stability of the complex)[20] that the dye molecules slip into slots between adjacent base pairs ("intercalate").

The J band of the PIC_N–DNA complex at 553 nm has a large positive LD/A corresponding to a fairly large positive CD ($CD/A = +0.02 \pm 0.01$). The circular dichroism indicates that the structure may be a right-handed helix which is consistent with models showing that a helix with six PIC per turn fits the DNA strands. α should then be around 50°. This is not contradicting the large LD/A (+1.3) which by $F = 0.5$ yields $\theta = 17°$, since we then according to eq 2 have $\cot^2\theta = 10.2 = R(P, K, N)\cot^2\alpha = Rx(0.84 \pm 0.3)$. With $K = 1$ (the J band) and $P = 6$, $R = 12.1 \pm 5$ a value which may already be obtained with a single-turn helix [$R = 2$ for $N = 3$, 7.5 ($N = 5$), 72 ($N = 10$), 10^6 ($N = 100$)]. Thus irrespective of α (as long as it deviates from 90°) a sufficiently long helix can always explain the pure parallel polarization of the J band.

Scheibe PIC_N. The large positive LD at the J band immediately rules out the extreme structure alternatives B and C in which $\alpha = 90°$. If the structure is a straight stack, type A, eq 1 and 2 yield α by inserting $R = 1$. E.g., for mixture 4 at $G = 1000\ s^{-1}$ F appears close to unity so $LD/A = +2$ here should mean $\alpha = 28°$. Taking into consideration uncertainties in chain length and in alignment (both tending to reduce LD/A) we may as well have $\alpha = 0$, i.e., band structure D. On the other hand, as above, with a regularly coiled structure the parallel polarization is automatically selected by an infinite R at large N (see Discussion).

Hydrodynamical Linear Dichroism Studies. From the very rapid growth of LD with gradient (in mixture 4 LD is half way to maximum before $G = 1\ s^{-1}$, in mixture 2 about the same value is obtained) we conclude that the aggregates are extremely elongated and stiff. Further as is visualized in Figures 8 and 9, above a certain gradient the flow acts in a destructive way degrading the aggregates and the LD vs. G spectrum is generally not reproduced in the reversed scan. However, at lower gradients a synthesis of more orientable aggregates is favored to an even more pronounced extent than in the absence of flow. Such a constructive action of a flow field may be interpreted as a basic criterion of viscoelasticity[23] and we tentatively propose the PIC solution (mixture 4) should be characterized as elastic below $G = 1000\ s^{-1}$. In Figures 4–7 representative LD vs. G curves are shown, on destructive and constructive responses to constant gradients and on orientational decays from different starting gradients. We have chosen mixture 4 since it proved easier to reproduce than mixtures 3 and 5 and remained stable for several days. Mixtures 1 and 2 gave only small amounts of Scheibe polymer (after standing over night). No hydrodynamic evidence was obtained indicating that the polymer formed in mixture 1 should be of a smaller dimension than the one

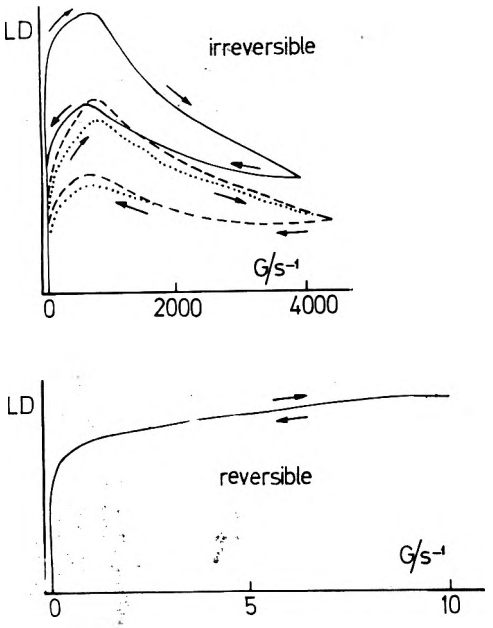

Figure 8. Linear dichroism of mixture 4 at 572 nm (arbitrary units on vertical axes) vs. Couette flow gradient or time. On one sample repeated cyclic scannings (top: 1–; 2,—; 3,...) G = 0–4000–0 s^{-1} and (bottom) G = 0–10–0 s^{-1}.

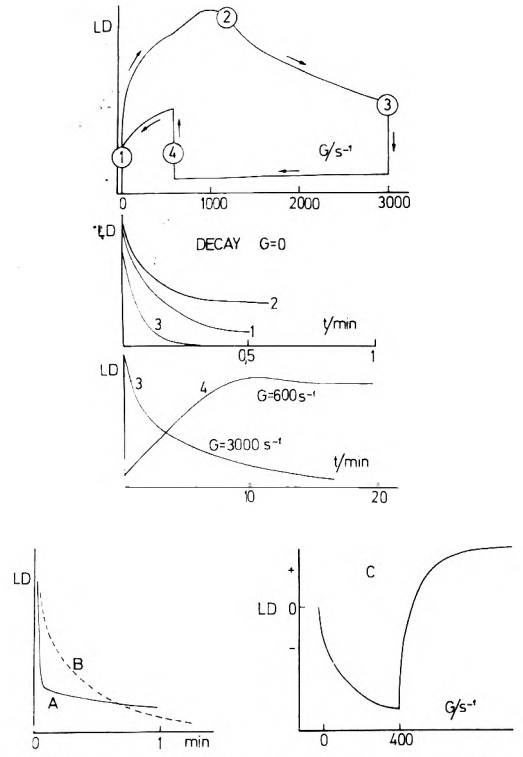

Figure 9. Orientational time dependence of the linear dichroism of mixture 4 at constant gradient and examples on decay. (1) Decay from low gradient of mixture 4 that has been at rest for several hours. (2) Decay from gradient at LD-G maximum. (3) Destructive effect of constant gradient below LD-G maximum. Bottom: Aged mixture 5, decay from low gradient before (A) and after (B) rotation at 2700 s^{-1} for 5 min. Fresh mixture 5 (C), linear dichroism (575 nm) vs. G.

formed in mixture 4. However, LD/A at 572 nm is of a larger magnitude in mixtures 4 and 5 than in mixtures 1 and 2 (+0.03) or in freshly prepared mixture 4, which indicates a more effective orientation in the former solutions.

In mixture 5 immediately after preparation the J band was still very weak (A = 0.02) but broader than usual and shoulders at 560 and 576 nm could be distinguished. This was accompanied by a strange LD vs. G dependence (Figure 9): Below 400 s^{-1} the J band showed negative LD which increased with gradient in a way which could fit a rigid particle with an axial ratio[15] of less than 10[2]; above 400 s^{-1}, however, this "particle" is apparently destroyed yielding the usual Scheibe polymer with positive LD. This sign reversal occurred at a distinct gradient irrespective of whether upfield or downfield scanning was used. The high reproducibility even at high scan rate suggests that we are not dealing with a disrupture into pieces of a large particle but rather with some structural transformation of a single species. The sensitivity to flow, and a preliminarily obtained lower rotational diffusion constant below rather than above 400 s^{-1}, suggest that the structures have different hydrodynamical shapes, as if for instance the change was defined by the uncoiling of a helix, e.g., structure E in Figure 3.

Mixture 5 aged fairly quickly and a precipitation of distinguishable crystals appeared when viewed under a microscope. It is characteristic for the micellar PIC solutions that aging implies deteriorated orientation and lower viscosity. Figure 9 shows the considerably more rapid relaxation of the aged mixture 5, but also how the "micellar" state may be restored by subjecting the solution to flow. The dispersion into smaller and more elongated aggregates was confirmed from the absorption spectrum, where the apparent intensity in the J band as well as in the 0–0 region was increased (some 20% by decreased absorption statistics,[24] and the scattering (baseline) simultaneously reduced.

Relaxation Studies. When the flow field is switched off the linear dichroism decays as the distribution function $F(\theta, \phi, \psi, t)$ (θ, ϕ, ψ = Eulerian angles defining the orientation of the particle, t = time) is randomized. According to Perrin F has to satisfy

$$\frac{\partial F(\theta, \phi, \psi, t)}{\partial t} = D_1\left(\frac{\partial^2 F}{\partial \theta^2} + \cot\theta \frac{\partial F}{\partial \theta} + \frac{1}{\sin\theta}\frac{\partial^2 F}{\partial \phi^2} + \cot^2\theta \frac{\partial^2 F}{\partial \phi^2} - 2\frac{\cot\theta}{\sin\theta}\frac{\partial^2 F}{\partial \phi\, \partial \psi}\right) + D_3\frac{\partial^2 F}{\partial \psi^2} \quad (3)$$

where D_i is the rotational diffusion constant around axis i (D_3 = symmetry axis of the assumed ellipsoid of revolution).[25] The simplifications introduced by Benoit[26] and Tinoco[27] for electric birefringence relaxation may be employed here if uniaxial symmetry of the orienting field is assumed. This is a priori not the case in Couette flow[28] but the assumption is justified when starting from high orientations. The treatment of Benoit was recently called to question by Wright and Keefe who reported that the decay should be represented by a complex sum of exponentials.[29] Their claim seems, however, to have been in error[30] and the LD decay should be expected to yield D_1 according to a single exponential:

$$\mathrm{LD}(t) = \mathrm{LD}(t = 0)\exp(-6D_1 t) \quad (4)$$

In a solution of particles which are polydisperse with respect to rotational diffusion LD(t) is a sum of exponentials $\Sigma_i \mathrm{LD}_i(t = 0)\exp(-6D_{1i}t)$ so it should be possible to conclude from the decay of dichroism whether a population is monodisperse or polydisperse.

From Figure 10 it is clear that the observed relaxations do not fit a single exponential, and that the hydrodynamics cannot be explained by a single species. Both from the experience with the growth of orientation with gradient and from the general appearance of the decay curves, we find it reasonable in a first approach to assume that the aggregate dimensions are localized to two points of gravity, one representing a fairly fast decay ($t_{1/2}$ = 50 s) and one

with a slower decay ($t_{1/2}$ = 500 s). Rotational diffusion constants referring to fractions resolved according to this pattern are found in Table I, for some experiments with mixture 4. The conclusion is essentially the same as is obtained by inspection of LD vs. G diagrams: Very low gradients favor the formation of easily oriented slowly rotating species while higher gradients degrade them. Curve 9, run as a check, reproduced several times showing that the result in this mixture is not extremely sensitive to dilution or aging and that the composition is not perturbed by the transient gradient (1000 s^{-1} for 1 s) employed to start the relaxation.

Discussion

Assuming a minimum fiber thickness (b = 100 Å, not a crucial choice) the length (a) corresponding to the range of the observed rotational constants is 4000–100 000 Å as obtained by the Perrin equation.[31] The lower value is only a consequence of the experimental decay time resolution (the flow has to stop) and a limited orientational potentiality. Hence the coexistence of shorter aggregates must be suspected. We may use the energy dependence on chain length as formulated by the exciton theory[22] to make a tentative estimate of the dimension of the shortest PIC oligomer which is manifested by J-band absorption. Equation 5 gives the shift expected between the monomer

$$\nu_N - \nu_1 = 2V_{12} \cos \frac{\pi}{N+1} \quad (5)$$

0–0 band and the parallel J band of a helical oligomer with N residues. V_{12} is the interaction energy within the nearest neighbor approximation. Assuming a constant V_{12}, it should be possible to estimate N according to eq 6 for

$$N + 1 \approx \pi\sqrt{(\nu_1 - \nu_\infty)/2(\nu_N - \nu_\infty)} \qquad N \geq 3 \quad (6)$$

PIC_N. The "uncertainty" (2 nm) observed for the J-band peak in aqueous solution at various concentrations and possibly various degrees of polymerization, in this way gives us a lower limit $N \geq 10 \pm 1$. We come further lower if the same V_{12} also applies for the PIC_N–DNA complex (N = 3). However, the latter assumption seems unjustified if the PIC structure is adapted to fit DNA. Thus the PIC_N array is likely to be a "super-helix" (with the pitch of the DNA helix) attached to the negatively charged phosphate strand. A different structure implies a certain change in ν via the geometrical factor in V_{12}.

The observation of a J band in polystyrene is interesting in view of the generally accepted understanding[32] of dye aggregation as a phenomenon of hydrophobic interaction, the energy being provided by an expulsion of water molecules from the first hydration shell. Thus no J band is observed in nonpolar solvents even at the point of precipitation. A possible explanation is the following: 1. From symmetry selection rules the J band is expected in asymmetric aggregates—such may be favored in irregular glassy polystyrene. 2. The slow diffusion in the congealing solvent prevents formation of crystallites but favors the oligomeric species. The different J-band position as compared to that in an aqueous solution probably results from a changed V_{12} and not a significantly changed length. It may be noted that a number of exciton levels are visible on the high energy side (mixture VII) as far as at 400 nm.

The idea of coexistance of Scheibe oligomers with small N is supported by the observation of strongly decreased LD/A at decreased degree of aggregation. This could be explained by a low average orientation (F = 0.01) due to short chains, e.g., with a < 200 Å, b < 10 Å (that is with N < 100 by model D, Figure 3). However, studies of LD vs. G suggest instead a small fraction (1%) of well oriented longer aggregates ($N \geq 10^4$) and a randomly oriented remainder.

The increase in circular dichroism magnitude[33] when passing from monomer to oligomer PIC associated to DNA is in agreement with the concept of rotational strength due to coupling between electric dipole transitions of symmetric chromophore units. In the complex with the monomer a weak rotational strength can be explained by a preferred screw sterically induced by the pitch of the strands at intercalation. This screw sense which is (in the case of right-handed DNA) the one depicted in the structure in Introduction, implies a charge displacement along a left-handed screw, in agreement with the observed negative CD over the whole region of x polarization. The CD in the monomer is interesting in view of the fact that it has been inferred that PIC only can gain optical activity through aggregation.[32] The rotational strength of the monomer (discussed elsewhere)[20] is of the same magnitude as was recently predicted theoretically by Nolte for a dihedral angle of 25°.[34]

The CD pattern with a positive band at 553 nm and a negative band at 540 nm in Figure 9 resembles the spectrum reported by Scheibe et al. on PIC–heparin mixtures (564 and 546 nm)[32] but in our case it was found from the titration that the two bands belong to different PIC–DNA species.

The tentative assignment of the intermediate PIC–DNA spectrum to the dimer was based on the positive CD band at 490 nm where the "D band" has been estimated to be positioned theoretically (presuming a parallel "sandwich" dimer)[32,35] and experimentally.[19,36] If this conclusion is correct, the corresponding negative LD can be imagined with two PIC intercalated in adjacent base pair slots as well as with a structure with only one of the dye molecules intercalated. It may be noted that ethidium bromide, which intercalates,[37] appears unable to occupy adjacent slots.[15]

The effect of linear dichroism on the detection of circular dichroism requires some comment. As is shown (Appendix) nonideal electronic filter and optical birefringence are two practically inevitable instrumental errors which lead to recorder deflection for linearly dichroic samples. In general the apparent circular dichroism will be the linear dichroism times a positive or negative factor (depending on the direction of alignment). However due to dispersion in the birefrigence (if that is the main error) this factor can vary (and even change sign) over the spectrum. In the present case its maximum value was 0.1. Thus in Figure 1 the apparent circular dichroism spectrum contains a large amount of "true" circular dichroism while in Figure 2 it may be entirely due to linear dichroism. This fact throws doubt on earlier interpretations (in terms of optical activity) of transient phenomena and mechanically induced circular dichroism. However, this does not mean that we can eliminate PIC_N (e.g., produced in optically inactive salt solution) as a helix or the possibility of observable optical activity due to a stochastic excess of one helicity sense.

For infinite helical chains eq 2 cannot be used to determine α since $R \to \infty$, so another way of estimating the polarization of the monomer transition is desirable. According to Moffitt[38] such a possibility is provided by the integrated absorption intensities of the perpendicular and parallel exciton bands: $I_\perp/I_\parallel = tg^2\alpha$. This is equivalent to studying the areas under the corresponding LD bands.[39]

$$tg^2\alpha = -\int \mathrm{LD}(\lambda_\perp)\, d\lambda_\perp / \int \mathrm{LD}(\lambda_\parallel)\, d\lambda_\parallel \quad (7)$$

Depending on how much of the intensity around 480 nm

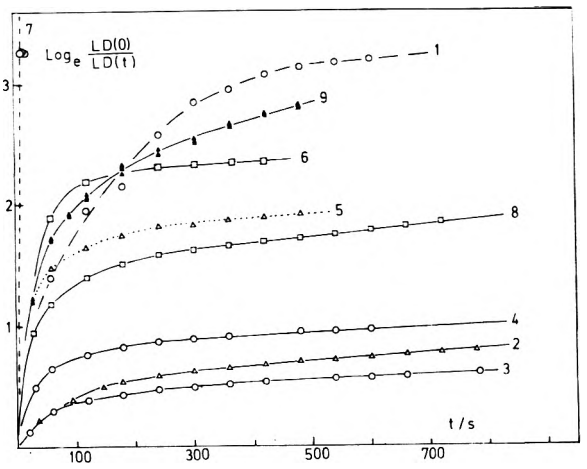

Figure 10. Decay of linear dichroism of mixture 4 at different gradients and treatments (see Table I).

one assigns to the perpendicular band one obtains α values between 30 and 40°.

Acknowledgment. The support of the Swedish Natural Science Research Council (Contract No. K 3216-006) is gratefully acknowledged. I wish to thank the Knut and Alice Wallenberg Foundation for the cost defrayal of the J-40 circular dichroism spectrometer.

Appendix

Effect of Linear Dichroism on Apparent Circular Dichroism. Modern circular dichroism spectrometers employ sinusoidal optical phase modulation, for which the following analysis holds. Let a sample have a macroscopic[40] linear dichroism $-\gamma b_3$, a circular dichroism $-\gamma b_2$, and a total absorption γC (following the nomenclature used in a recent discussion on the operation of a dichrometer and on its conversion to linear dichoism detection).[14,16] Light before impinging on the sample passes an electrobirefringent modulator and the emerging polarization is determined by a time-dependent phase retardation $\delta_0 \sin \omega t$, δ_0 is around $\pi/2$. The photomultiplier current is then found to be

$$I \propto I_0 \exp(-\gamma C)\{1 + [(\gamma b_2)^2 + (\gamma b_3)^2]/2 - \gamma b_2 \times \sin(\delta_0 \sin \omega t) + \gamma b_3 \cos(\delta_0 \sin \omega t)\} \quad (8)$$

The recorder deflection in any commercial CD spectrometer is proportional to the ratio between the ac and dc photocurrent levels. Expanding the cosine and sine expressions in Fourier series one obtains

$$I \propto I_0 \exp(-\gamma C)\{1 + [(\gamma b_2)^2 + (\gamma b_3)^2]/2 + \gamma b_3 J_0(\delta_0) - 2\gamma b_2 J_1(\delta_0) \sin \omega t + 2\gamma b_3 J_2(\delta_0) \cos 2\omega t - 2\gamma b_2 J_3(\delta_0) \times \sin 3\omega t + \ldots\} \quad (9)$$

where J_k is the Bessel function of order k. δ_0 is generally set at 105° to maximize J_1. Different sources of perturbation by γb_3 may now be distinguished.

A. *The dc Term in an Ideal Instrument.* Even with ideal optics and ideal filter function (retaining only ground frequency ωt terms) the deflection will depend on γb_3.

$$\langle I_{AC}\rangle/I_{DC} \propto -2\gamma b_2 J_1(\delta_0)/\{1 + [(\gamma b_2)^2 + (\gamma b_3)^2]/2 + \gamma b_3 J_0(\delta_0)\} \quad (10)$$

When the sample is rotated so that γb_3 changes sign the recorder spectrum will only be distorted and a "CD" sign change is in practice never observed.

B. *Nonideal Electronics.* If a certain intensity, say of fraction q, is picked up from signals at 2ω, LD will deliver a contribution also to the numerator of eq 10.

$$\langle I_{AC}\rangle/I_{DC} \propto (-2\gamma b_2 J_1(\delta_0) + q2\gamma b_3 \times J_2(\delta_0))/\{1 + [(\gamma b_2)^2 + (\gamma b_3)^2]/2 + \gamma b_3 J_0(\delta_0)\} \quad (11)$$

C. *Nonideal Optics.* A static birefringence ($\mathcal{H}$ at an angle β_0, see ref 16) in the modulator crystal yields an effect similar to that in B. When LD >> CD the instrumental recording is obtained from eq 8 in ref 14:

$$CD_{recorded} = tgh\left(\frac{1}{2} LD \ln 10\right)[2J_1(\delta_0)/J_1(\delta_0{}^0) \times \cos \mathcal{H}^0 \ln 10] \sin \mathcal{H} \cos 2\beta_0/[1 - tgh\left(\frac{1}{2} LD \ln 10\right)(1 + \cos \delta_0)(\sin^2 2\beta_0 + \cos^2 2\beta_0 \cos \mathcal{H})/2] \quad (12)$$

Here $\delta_0{}^0$ and $\mathcal{H}^0$ refer to the wavelength at which the instrument has been calibrated, and due to the dispersion of the refractive index of the modulator and to nonideal wavelength program for its excitation voltage, δ_0 as well as $\mathcal{H}$ will be wavelength dependent. Recently these parameters were analyzed in connection with absolute CD determinations:[16] δ_0 typically varied between 80 and 100° and $\mathcal{H}$ between 2 and 5° for λ between 200 and 800 nm. From transmitted intensities at different frequencies $q = I(370 \text{ Hz})/I(740 \text{ Hz}) = 0.01$ was estimated.

The demonstrated instrumental limitation seems important regarding the growing interest in studying optically active liquid crystals and other systems with potential macroscopic anisotropy together with the fact that modern modulators by necessity have sinusoidal character (oscillating stress modulators).

References and Notes

(1) See, for instance, advertisement by Kodak Co. in *Sci Am.*, **234**, No. 5, 49 (1976).
(2) E. E. Jelley, *Nature (London)*, **138**, 1009 (1936).
(3) G. Scheibe, *Z. Angew. Chem.*, **49**, 563 (1936).
(4) G. Scheibe, E. Daltrozzo, O. Worz, and J. Heiss, *Z. Phys. Chem.*, **64**, 97 (1969).
(5) E. Daltrozzo, G. Scheibe, R. Geschwind, and F. Haimerl, *Photogr. Sci. Eng.*, **18**, 441 (1974).
(6) L. Stryer and E. R. Blout, *J. Am. Chem. Soc.*, **83**, 1411 (1961).
(7) S. F. Mason, *Proc. Chem. Soc. London*, 119 (1964).
(8) G. Scheibe, F. Haimerl, and W. Hoppe, *Tetrahedron Lett.*, **35**, 3067 (1970).
(9) H. Dammeier and W. Hoppe, *Acta Crystallogr., Sect. B*, **27**, 2364 (1971).
(10) H. Yoshiokoa and K. Nakatsu, *Chem. Phys. Lett.*, **11**, 255 (1971).
(11) J. K. Maurus and G. R. Bird, *J. Phys. Chem.*, **76**, 2982 (1972).
(12) C. Honda and H. Hada, *Tetrahedron Lett.*, **3**, 177 (1976).
(13) R. E. Graves and P. I. Rose, *J. Phys. Chem.*, **79**, 746 (1975).
(14) Å. Davidsson and B. Norden, *Chem. Scr.*, **9**, 49 (1976).
(15) B. Norden and F. Tjerneld, *Biophys. Chem.*, **4**, 191 (1976).
(16) Å. Davidsson and B. Norden, *Spectrochim. Acta*, **32**, 717 (1976).
(17) V. Czikkely, H. D. Forsterling, and H. Kuhn, *Chem. Phys. Lett.*, **6**, 11 (1970).
(18) W. Cooper, *Chem. Phys. Lett.*, **7**, 73 (1970).
(19) W. West and S. Pearce, *J. Phys. Chem.*, **69**, 1894 (1965).
(20) B. Norden and F. Tjerneld, *Biophys. Chem.*, to be submitted for publication.
(21) G. S. Levinson, W. T. Simpson, and W. Curtis, *J. Am. Chem. Soc.*, **79**, 4314 (1957).
(22) D. F. Bradley, I. Tinoco, and R. W. Woody, *Biopolymers*, **1**, 239 (1963).
(23) B. Norden, to be submitted for publication.
(24) L. N. Duysens, *Biochem. Biophys. Acta*, **19**, 1 (1956).
(25) F. Perrin, *J. Phys. Rad.*, **7**, 1 (1936).
(26) H. Benoit, *Ann. Phys.*, **6**, 561 (1951).
(27) I. Tinoco, *J. Am. Chem. Soc.*, **77**, 4486 (1955).
(28) A. Peterlin and H. A. Stuart, *Z. Phys.*, **112**, 119 (1939).
(29) A. K. Wright and W. E. Keefe, *Biopolymers*, 9, 1503 (1970).
(30) J. Greve, Thesis, Amsterdam, 1970.
(31) The diffusion constant was assumed to be governed by[25]

$$D = (3kT/16\pi\eta a^3)[2 \ln(2a/b) - 1]$$

where the viscosity η was put equal to 1 g cm^{-1} s^{-1} (water) and b (length of short axis) was assumed to be 10^{-6} cm (that $a/b > 50$ is evident from the LD vs. G behavior).[15]

(32) G. Scheibe, O. Worz, F. Haimerl, W. Seiffert, and J. Winkler, *J. Chim. Phys.*, **65**, 146 (1968).
(33) The stability constants have been estimated to be ca. 9×10^5 M^{-1} for the complex PIC-DNA and 2×10^4 M^{-1} for PIC$_N$-DNA. This means that the $\epsilon_i - \epsilon_r$ (and also $\epsilon_\parallel - \epsilon_\perp$) for the polymer should be multiplied by a factor 1.5 to correspond to unit complexed PIC concentration.
(34) H. J. Nolte, *Chem. Phys. Lett.*, **31**, 134 (1975).
(35) J. S. Briggs, *Z. Phys. Chem.*, **75**, 214 (1971).
(36) V. I. Permogorov, *Izv. Akad. Nauk. SSSR*, **34**, 1185 (1970).
(37) W. Bauer and J. Vinograd, *J. Mol. Biol.*, **33**, 141 (1968).
(38) W. Moffitt, *J. Chem. Phys.*, **25**, 467 (1956).
(39) For a rod-shaped molecule the orientation tensor is diagonal with the trace $f_\parallel + 2f_\perp = 0$. See, e.g., R. A. Levenson, H. B. Gray, and G. P. Ceasar, *J. Am. Chem. Soc.*, **92**, 3653 (1970). Then

$$-\int \mathrm{LD}(\lambda_\perp)\mathrm{d}\lambda / \int \mathrm{LD}(\lambda_\parallel)\,\mathrm{d}\lambda = -\int [f_\parallel \epsilon_\parallel(\lambda_\perp) + 2f_\perp \epsilon_\perp(\lambda_\perp)]\,\mathrm{d}\lambda_\perp / \int [f_\parallel \epsilon_\parallel(\lambda_\parallel) + 2f_\perp \epsilon_\perp(\lambda_\parallel)]\,\mathrm{d}\lambda_\parallel = -\int f_\parallel \epsilon_\perp(\lambda_\perp)\,\mathrm{d}\lambda_\perp / \int f_\parallel \epsilon_\parallel(\lambda_\parallel)\,\mathrm{d}\lambda_\parallel = \int \epsilon_\perp(\lambda_\perp)\,\mathrm{d}\lambda_\perp / \int \epsilon_\parallel(\lambda_\parallel)\,\mathrm{d}\lambda_\parallel = I_\perp / I_\parallel$$

(40) The interaction between the microscopic phenomena has also to be considered. See N. Go, *Phys. Soc. Jpn.*, **23**, 88 (1967).

Solvated Electron Spectra. Study of the Absorption Curves by a Method of Moments

Marc G. Debacker,*

Laboratoire des Métaux alcalins dans NH_3 liquide,[1] 59046 Lille Cedex, France

J. N. Decarpigny, and M. Lannoo

Laboratoire de Physique des Solides[1] I.S.E.N., 59046 Lille Cedex, France *(Received March 22, 1976)*

The optical spectrum of the solvated electron in liquid ammonia is analyzed by a method of moments. A general formalism to compute the theoretical moments is presented. These moments are function of only the ground state wave function. The moments of the experimental curves are obtained by using a fit to a skewed Gaussian. A comparison of theory and experiment is presented using a spherical well model. The parameters of the well thus obtained are $V_w = 1.85$ eV and $a = 4.1$ Å and only one bound state is allowed.

I. Introduction

The optical absorption spectrum of solvated electrons in liquid ammonia consists of a broad asymmetric band centered in the near-infrared and tailing in the visible.[2] The nature of this absorption band has been extensively studied and various approaches such as the cavity model,[3] the semicontinuum model,[4,6] or ab initio calculations[7,8] have been used. In most of these works, one starts from a given theoretical model and directly calculates the quantities of interest, namely, the position of the absorption peak, which are then compared to the experimental results. Nevertheless, some workers have attempted to reproduce the shape of the spectrum. Delahay[9] has decomposed the spectrum into several bands arising from bound–bound and bound–continuum transitions, but this does not fit the solvated electron absorption band in ammonia. More recently, Mazzacurati et al.[10] have used an exact expression of the absorbance for the case of a particle in a spherical box. Their results are in good agreement with experiment but the method cannot be extended to more realistic model potentials.

In this paper, a general method to derive, from the experimental spectrum, the characteristic parameters of a given model potential featuring the solvated electron potential is presented. From this, it is then possible to discuss the nature of the allowed optical transitions and, for instance, the number of bound states in the case of a spherical box. For this purpose a method of moments is used. The theoretical expressions for the moments of the absorption curve can be determined from the ground state wave function in terms of the parameters of the model potential. By equating these expressions to the experimental values of the lowest order moments, a set of equations allowing the determination of the parameters is then obtained. Moreover, when the number of calculated moments is greater than the number of parameters, a critical test of the validity of the model potential can be done.

In section II, a formalism is developed showing that one only requires the knowledge of the ground state wave function, without any assumptions concerning the transitions. In section III, the computation of the experimental moments is described and in section IV a simple application to the case of an electron in a spherical box is given. Then, in section V, numerical results are discussed and possible improvements are described.

II. General Formalism

The contribution of a solvated electron to the imaginary part of the dielectric constant is given by[11]

$$\epsilon_2(E) = 4\pi^2 \Sigma \langle g|\zeta|e\rangle\langle e|\zeta|g\rangle \delta\,[E - (E_e - E_g)] \qquad (1)$$

where atomic units are used. $|e\rangle$ represents the wavefunction of one of the excited states, and E_e the energy associated to this state; $|g\rangle$ the wave function of the ground state, and E_g the ground state energy; ζ is the component of the electron position along a given direction. In this expression, it is implied that the ground state is nondegenerate. The summation is extended over all the excited states.

The nth order moment of $\epsilon_2(E)$ is defined by

$$M_n = \frac{2}{\pi} \int \epsilon_2(E) E^n \,\mathrm{d}E \qquad (2)$$

Using the closure relation, Lannoo and Decarpigny[12] have shown that these moments can be expressed in the form

$$M_n = 8\pi [\langle g|\zeta[n]|g\rangle - \langle g|\zeta|g\rangle\langle g|[n]|g\rangle] \qquad (3)$$

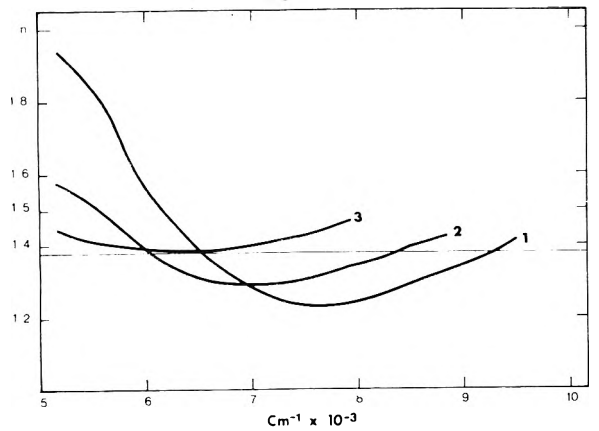

Figure 1. Variation of the refractive index with energy calculated from ref 12: curve 1, 1 MPM; curve 2, 0.5 MPM; curve 3, 0.1 MPM. The horizontal line indicates the refractive index of the pure solvent.[13]

where $[n]$ is the commutator of order n:

$$[n] = [H, [H, \ldots [H,\zeta] \ldots] \tag{4}$$

and H is the electron Hamiltonian.

This expression shows that it is possible to evaluate the moments knowing only the Hamiltonian and the exact wave function of the ground state. Equation 3 takes into account all the transitions to all excited states: bound–bound transitions as well as bound–continuum transitions.

In the following sections, the moments needed for computation are normalized to unit M_0. They are referred to as m_n where

$$m_n = M_n/M_0 \tag{5}$$

III. Experimental Moments

The absorptivity α of the solution is related to the imaginary part of the dielectric constant by

$$\alpha(E) = \frac{2\pi E \epsilon_2(E)}{hcn(E)} \tag{6}$$

where $n(E)$ is the refractive index and c the velocity of light. In order to obtain $\epsilon_2(E)$ from the absorption curve, one has to know the values of $n(E)$ for each wavelength.

The work of Koehler[14] on the reflectance spectra of metal–ammonia solutions gives some values of the real and imaginary parts of the dielectric constant as a function of the energy. From these data, the variation of the refractive index with energy can can be calculated. These values are plotted in Figure 1 for the three concentrations used by Koehler: 1, 0.5, and 0.1 MPM at about −50 °C. The variation of $n(E)$ as a function of energy becomes smaller as the concentration is decreased.

Since the concentrations used in studies of the spectrum of solvated electrons are factor of 100 smaller than 0.1 MPM, we can consider that the refractive index is a constant equal to the refractive index of pure ammonia.[15] Thus, it follows from (6) that the moment of order n of $\epsilon_2(E)$ is related to the $(n-1)$th order moment of the absorption curve.

To calculate the moments, the optical spectrum was fitted with a skewed-Gaussian equation[16]

$$\alpha(E) = \alpha_{max} \exp\left[-\ln 2\left[\ln\left(1 + \frac{2b(E - E_{max})}{\Delta E}\right)\frac{1}{b}\right]^2\right] \tag{7}$$

TABLE I: Experimental Results for $NaNH_3$ Solutions at −65 °C

No.	Concn, M	E_{max}, cm^{-1}	ΔE, cm^{-1}	b
1[a]	1.26×10^{-3}	6830 ± 50	3241 ± 80	0.465 ± 0.050
2[a]	1.63×10^{-3}	6815 ± 20	3105 ± 30	0.493 ± 0.020
3[a]	3.89×10^{-3}	6705 ± 30	3180 ± 45	0.532 ± 0.028
4[b]	0	6920 ± 40	3319 ± 55	0.506 ± 0.024
5[c]	1.39×10^{-4}	6950 ± 35	3365 ± 50	0.465 ± 0.022

[a] Taken from ref 16 curves 10, 25, and 28 for nos. 1, 2, and 3, respectively. [b] Reference 17. Data extrapolated to infinite dilution. [c] Reference 17 curve 4.

TABLE II: Experimental Moments (in atomic units)

No.	$\bar{\mu}_0$	$\bar{\mu}_1$	$\bar{\mu}_2$
1	3.368×10^{-2}	1.190×10^{-3}	4.431×10^{-5}
2	3.378×10^{-2}	1.195×10^{-3}	4.449×10^{-5}
3	3.364×10^{-2}	1.191×10^{-3}	4.479×10^{-5}
4	3.450×10^{-2}	1.253×10^{-3}	4.819×10^{-5}
5	3.427×10^{-2}	1.234×10^{-3}	4.694×10^{-5}

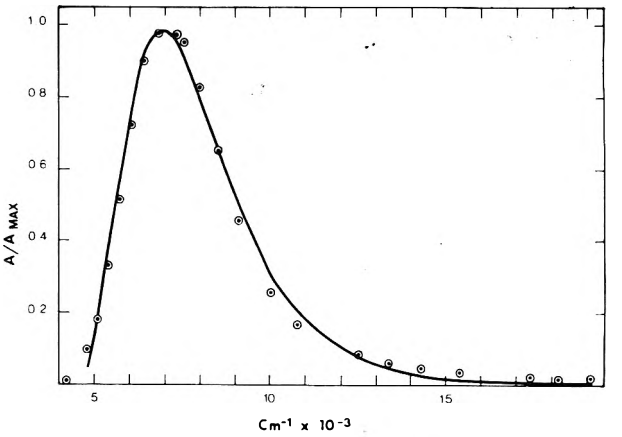

Figure 2. Nonlinear least-squares fit of $NaNH_3$ spectrum at infinite dilution and −65 °C.[17]

where α_{max} is the value of the absorptivity at the maximum E_{max}, b is an asymmetry parameter, and ΔE is related to the half-width w by the relation

$$w = \Delta E \frac{\sinh b}{b} \tag{8}$$

The moments of this curve are defined and can be evaluated in an analytical form.[17] The experimental moments are designed μ_n. It follows from (6) that μ_n corresponds to M_{n+1}. Therefore the experimental moments are normalized in the following way:

$$\bar{\mu}_n = \mu_n/\mu_{-1} \tag{9}$$

so that $\bar{\mu}_n$ corresponds to m_{n+1}.

The experimental data were taken from the literature. The values used were those of Dye and Douthit[18] and of Rubenstein[19] for $NaNH_3$ solutions. For the later,[19] both the experimental data and data extrapolated to infinite dilution were used.

The spectra were fitted to eq 7 by using a nonlinear weighted least-squares program.[20] The parameter used for the fit were α_{max}, E_{max}, ΔE, and b. The weights were calculated using the standard deviation given in Rubenstein's thesis.

The values of the parameters with their standard error are given in Table I. A typical fit is shown in Figure 2.

The moments were calculated by numerical integration of eq 7. The normalized values are given in Table II.

TABLE III: Final Results

No.	m_3	V_0, eV	a, Å	E, eV
1	5.448×10^{-5}	1.83	4.11	−0.70
2	5.470×10^{-5}	1.84	4.14	−0.72
3	5.489×10^{-5}	1.82	4.05	−0.67
4	5.913×10^{-5}	1.87	4.01	−0.69
5	5.769×10^{-5}	1.86	4.05	−0.70

IV. Application of the Theory to a Simple Potential Well

The evaluation of the theoretical moments necessitates the choice of a model Hamiltonian for which the ground state wave function must be determined.

The cavity model has been widely used, and we have chosen to apply our method to one of the simplest cases: the particle in a spherical box of radius a and of depth V_w. For this model the 1s wave function of the ground state is known. The number of excited states is given by the size of the potential well.

The values of the moments are (in atomic units)

$$m_1 = \frac{3K^2}{2T}\left(Ka - \frac{\sin 2Ka}{2} + \frac{K}{\chi}\sin^2 Ka\right) \quad (10a)$$

$$m_2 = K^5 a/T \quad (10b)$$

$$m_3 = \frac{2K^3\chi}{T} V_0\left(1 + \frac{1}{\chi a}\right)\sin^2 Ka \quad (10c)$$

where

$$T = \frac{(Ka)^3}{3} - \frac{\sin 2Ka}{2}\left[(Ka)^2 - \frac{1}{2}\right] - \frac{Ka\cos 2Ka}{2} + \frac{K^3}{\chi^3}\sin^2 Ka\left[(\chi a)^2 + \chi a + \frac{1}{2}\right] \quad (11)$$

with

$$K = \sqrt{2(E + V_w)};\ \chi = \sqrt{-2E};\ -\chi = K\ \mathrm{cotg}\ Ka \quad (11b)$$

and E is the energy of the ground state.

The two unknowns are V_w and a. They can be obtained by solving the two equations

$$\bar{\mu}_0 = m_1$$

$$\bar{\mu}_1 = m_2$$

The values of V_w and a are obtained with a program solving simultaneous nonlinear equations.[20] These values were used to recalculate m_3. The results are shown on Table III.

V. Discussion

The values obtained for V_w and a, satisfying the Landau condition,[21] indicate that, in the framework of the spherical box model, there is only one bound state in the well. Therefore the optical band is due to transitions to the continuum. This confirms the results obtained by Mazzacurati et al.[10] who have fitted the optical spectrum with the complete expression for the absorbancy first derived in this case by Breit and Condon.[22]

The values of m_3 recalculated from V_w and a are of the right order of magnitude, being systematically 20% higher than the experimental values. Since m_3 is very sensitive to the magnitude of the ground state wave function at the edge of the well, this discrepancy can be considered as an indication of a slight inadequacy of the model.

The calculated energy $|E|$ can be compared with the threshold on the low energy side. The values we have obtained, though reasonable, are too high. This point can be related to the discrepancy mentioned above with regard to m_3, since, when the well's edge is rounded off, the bound level moves upward.[23]

The energy E cannot be directly compared with the experimental data of photoemission by solvated electron solutions,[24,25] since these values include transitions to the vacuum and not to the delocalized states in the bulk of the solution.

This difference is well pointed out in the model of Copeland, Kestner, and Jortner[3b] in which a constant term V_0 represents the difference between the energy of the quasi-free electron in the medium and that of the electron under vacuum. This difference was described by Magat.[26]

Our calculations based only on the shape of the optical spectrum cannot give the value of V_0. It could be obtained by the difference between the values of the photoemission threshold and that of the threshold to the delocalized states in the bulk of the solutions.

These results obtained in a simple case show that the application of the method of moments to the analysis of the solvated electron spectra can give important informations about the potential well, the electronic ground state, and the type of transitions involved. Its main interest resides in the fact that the calculations are relatively easy and thus can be extended to more realistic potentials where the calculation of the complete absorption spectrum is no longer possible. It is also to be remembered that no particular assumptions concerning the transitions are necessary.

In a further work, we intend to compute the moments using a more realistic potential model, as well as to correlate the characteristic parameters of these potentials for solvated electrons in various media.

References and Notes

(1) Laboratoire associé au CNRS No. 253.
(2) For a general review on this subject see the Proceedings of Colloque Weyl IV, *J. Phys. Chem.*, **79**, (26), 2789–3079 (1975).
(3) (a) R. A. Ogg, *Phys. Rev.*, **69**, 668 (1946); (b) D. A. Copeland, N. R. Kestner, and J. Jortner, *J. Chem. Phys.*, **53**, 1189 (1970).
(4) D. E. O'Reilly, *J. Chem. Phys.*, **41**, 3736 (1964).
(5) T. Kajlwara, K. Funabashi, and C. Naleway, *Phys. Rev. A*, **6**, 808 (1972).
(6) K. Iguchi, *J. Chem. Phys.*, **48**, 1735 (1968).
(7) B. J. Mc Aloon and B. C. Webster, *Theor. Chim. Acta*, **15**, 385 (1969).
(8) B. C. Webster and G. Howat, *Radiat. Res. Rev.*, **4**, 259 (1972).
(9) R. Lugo and P. Delahay, *J. Chem. Phys.*, **57**, 2122 (1972).
(10) V. Mazzacurati and G. Signorelli, *Lett. Nuovo Cimento*, **12**, 347 (1975).
(11) J. M. Ziman, "Principles of the Theory of Solids", Cambridge University Press, New York, N.Y., 1969, p 226.
(12) M. Lannoo and J. N. Decarpigny, *J. Phys. (Paris)*, **35**, C3-97 (1974); *Phys. Rev. B*, **14**, 538 (1976).
(13) "The Optical Properties of Solids", J. Tauc, Ed., Academic Press, New York, N.Y., p 37.
(14) W. H. Koehler and J. J. Lagowski, *J. Phys. Chem.*, **73**, 2329 (1969).
(15) A. W. Francis, *J. Chem. Eng. Data*, **5**, 534 (1960).
(16) R. D. B. Fraser and E. Suzuki, *Anal. Chem.*, **41**, 37 (1969).
(17) P. F. Rusch and J. P. Lelieur, *Anal. Chem.*, **45**, 1541 (1973).
(18) R. C. Douthit and J. L. Dye, *J. Am. Chem. Soc.*, **82**, 4472 (1960).
(19) G. Rubenstein, Ph.D. Thesis, Brandeis University, 1972.
(20) J. L. Dye and V. A. Nicely, *J. Chem. Ed.*, **48**, 443 (1971).
(21) L. D. Landau and E. M. Lifsnitz, "Quantum Mechanics", Pergamon Press, New York, N.Y., 1965, p 109.
(22) G. Breit and E. V. Condon, *Phys. Rev.*, **49**, 904 (1936).
(23) "Problems in Quantum Mechanics", D. Ter Haar, Ed., Infosearch Ltd., London, p 31.
(24) J. Hasing, *Ann. Phys.*, **37**, 509 (1940).
(25) H. Aulich, B. Baron, P. Delahay, and R. Lugo, *J. Chem. Phys.*, **58**, 4439 (1973).
(26) M. Magat, *Ber. Bunsenges. Phys. Chem.*, **75**, 666 (1971).

Electron Paramagnetic Resonance Study of Radicals from Aliphatic Formate Esters[1]

Peter Smith, Richard A. Kaba,[2] Luis M. Dominguez, and Stephen M. Denning

Paul M. Gross Chemical Laboratory, Department of Chemistry, Duke University, Durham, North Carolina 27706 *(Received August 19, 1976)*

The $TiCl_3$–H_2O_2 radical-generating method has been used within an aqueous continuous-flow system to study by EPR at ca. 25 °C the following substrates: allyl, ethyl, isopropyl, isobutyl, and *tert*-butyl formates. Attention was directed to the characterization of radicals having the following structures: ·C–O–OC–H and ·C–C–O–OC–H. Few radicals of these two structural types have been characterized before in aqueous solution. In general, each type of radical showed a formyl-proton coupling, but the size of this coupling in radicals of the same type depended on radical structure, e.g., for $\cdot CH_2CH_2OOCH$ and $\cdot CH_2CH(CH_3)OOCH$, respectively, $a_{\delta\text{-H}}^{OOCH}$ was 2.2 and 0.8 G. A possible explanation of the experimental data for these γ- and δ-CH formyl-proton couplings has been obtained with the use of INDO molecular-orbital calculations.

Introduction

There seem to have been few electron paramagnetic resonance, EPR, studies of aliphatic formates as substrates by means of the $TiCl_3$–H_2O_2 continuous-flow, radical-generating method.[3-7] In an earlier investigation[4] of a series of aliphatic carboxylic acids and their esters as substrates with use of the $TiCl_3$–H_2O_2 system, methyl and ethyl formate were found to give only the π radicals $\cdot CH_2OOCH$, **1**, and $CH_3\dot{C}HOOCH$, **2**, respectively; the spectrum for each radical showed a small (2.5 G) γ-CH formyl-proton coupling. These two substrates have since been reinvestigated by others[5] using this same radical-generating system. These workers[5] confirmed the earlier results[4] but, in addition, observed for each ester a broad singlet which was assigned to the σ radical formed by formyl-hydrogen-atom abstraction. Vinyl formate and allyl formate have also been examined in dilute solution as substrates within the $TiCl_3$–H_2O_2 system at ca. 25 °C. The former gave[6] only $HOCH_2\dot{C}HOOCH$, **3**, its spectrum showing a small γ-CH formyl-proton coupling similar in size to those in both **1** and **2**.[4,5] The latter yielded[7] only $HOCH_2\dot{C}HCH_2OOCH$, **4**, and $\cdot CH_2CH(OH)CH_2OOCH$, **5**. The spectrum of **4** had a small (2.8 G) δ-CH formyl-proton coupling which, to our knowledge, is of a long-range type not previously reported.

In this present work, the earlier studies of aliphatic formates[4,5,7] as substrates within the $TiCl_3$–H_2O_2 radical-generating system have been extended with special emphasis on long-range formyl-proton couplings. The substrates examined were allyl, ethyl, isopropyl, isobutyl, and *tert*-butyl formates. For the case of allyl formate, the results obtained were in general agreement with those from the previous study[7] and particular attention was given to investigating the temperature dependence of the coupling constants of **4**. In studying the other substrates, it proved possible to characterize all radicals bearing either an α- or β-(–OOCH) group which could conceivably be formed by hydrogen-atom abstraction from the alkoxy group. A possible explanation of the γ- and δ-CH formyl-proton couplings observed in this present study and the earlier investigations[4,5,7] has been obtained by means of INDO molecular-orbital calculations.

Experimental Section

Except when the *tert*-butyl compounds were examined, the experimental arrangement and procedures were as given elsewhere[7] except that a Varian F-80A X-Y recorder was used for the temperature-dependence study of **4**. For the *tert*-butyl compounds, the only difference was that the EPR system was the Varian E-9 spectrometer and accessories described previously.[8] Spectra were recorded as the first derivative and g values taken as before against aqueous potassium peroxylaminedisulfonate, which also served as the field standard.[7] The field-modulation amplitude was normally ca. 0.1–0.4 G, but was raised to as high as ca. 2 G when an effort to detect a σ radical was made.

One of the two streams was an aqueous solution of $TiCl_3$ containing added H_2SO_4 and the other, aqueous H_2O_2. Normally, to minimize hydrolysis of the esters,[4] the substrate was included only in the H_2O_2 stream and this was kept free of added H_2SO_4. However, occasionally H_2SO_4 was added to this stream to favor hydrolysis and thus facilitate study of the possible contribution of alcohol-derived radicals to the spectrum observed in the absence of added H_2SO_4. This procedural variation was useful since, in general, a given alcohol tended to be more reactive than its formate, as expected.[9] Unless specified otherwise, the results reported refer to the use of the normal procedure.

The following esters were examined without further purification: allyl formate (Eastman, reagent grade), ethyl formate (Eastman, practical grade), and isopropyl formate (City Chemical and K & K). Isobutyl formate (Eastman, reagent grade) was found by GLC analysis to contain ca. 1 mol % isobutyl alcohol. Triple distillation of this substrate from P_2O_5 reduced the alcohol impurity below detection level.[5,10] However, control EPR spectra showed the unpurified and purified substrate to give about the same proportion of radicals derived from isobutyl alcohol. *tert*-Butyl formate was prepared by the method of Stevens and van Es[11] and used without further purification, since no sign of impurity was detected by analysis of its 60-MHz NMR spectrum (that this substrate was adequately free of *tert*-butyl alcohol was shown by EPR measurements, see later).

The reaction conditions were as follows: total flow rate, 2–4 ml s^{-1} equally divided between the two streams, the results obtained being not noticeably dependent on flow rate over this range; the reaction temperature, 25 ± 2 °C, unless stated otherwise; the reducing stream, 0.004 and 0.2 M in $TiCl_3$ and H_2SO_4, respectively; and the oxidizing stream, 0.1 M in H_2O_2 and, normally, with no added H_2SO_4. As mentioned before, substrates were included only in the oxidizing stream, with concentrations as follows: allyl formate, 0.03 M; isopropyl formate and isobutyl formate, 0.1 M; *tert*-butyl formate and ethyl formate, 0.2 M.

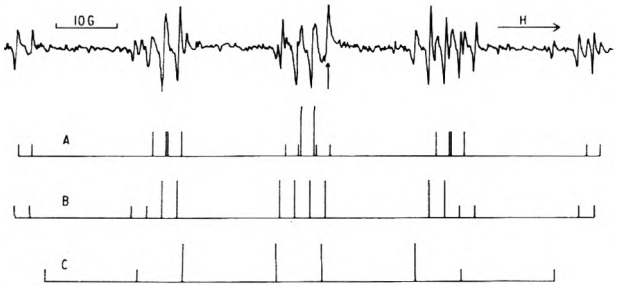

Figure 1. EPR spectrum for the substrate ethyl formate: temperature 25 °C; $[TiCl_3]$ = 0.004 M and $[H_2SO_4]$ = 0.2 M, in the reducing stream; $[H_2O_2]$ = 0.1 M and $[CH_3CH_2OOCH]$ = 0.2 M, in the oxidizing stream; total flow rate 3 ml s^{-1}, equally divided between the two streams. The arrow indicates the position of the single line from the $CH_3CH_2OOC\cdot$, **9**, see text. (A) Stick plot for $\cdot CH_2CH_2OOCH$, **7**, a triplet (1:2:1) of triplets (1:2:1) of doublets (1:1). (B) Stick plot for $CH_3CHOOCH$, **2**, a quartet (1:3:3:1) of doublets (1:1) of doublets (1:1). (C) Stick plot for CH_3CHOH, **8**, from ethyl alcohol present as impurity, a quartet (1:3:3:1) of doublets (1:1).

Allyl formate was also studied with the use of the $TiCl_3$–NH_2OH radical-generating system.[12] For those investigations, the reaction conditions were as for the $TiCl_3$–H_2O_2 work except that the oxidizing stream was water made 1 M in hydroxylamine hydrochloride (Eastman, reagent grade) and the allyl formate and $TiCl_3$ concentrations raised to 0.12 and 0.008 M, respectively.

Results

Allyl Formate, CH_2:$CHCH_2OOCH$. This substrate was studied with both the $TiCl_3$–H_2O_2 and $TiCl_3$–NH_2OH systems. As before,[7] only **4** and **5** were observed[13] with the former system and, in the case of **4**, a small (2.8 G) doublet (1:1) splitting was found which was assigned to the formyl proton. The spectrum from **4** was carefully investigated while raising the temperature from 7 to 44 °C, the only coupling constant showing temperature dependence being $a_{\beta\text{-H}}^{CH_2OH}$ which had a positive temperature coefficient of ca. 8 mG deg^{-1}. With the $TiCl_3$–NH_2OH system, only $H_2NCH_2\dot{C}HCH_2OOCH$, **6**, was observed. Although rather poorly resolved, the spectrum[7] of **6** was successfully analyzed as a quartet (1:3:3:1) of triplets (1:2:1) of triplets (1:1:1) of small (2.8 G) doublets (1:1). The quartet was attributed to the chance equivalence of the α-CH proton and two β-CH_2 protons, these being reasonably assigned to the $-CH_2OOCH$ group.[7] As in the case of **4**, the small doublet splitting was attributed to the formyl proton. The spectrum of **6** was simplified not only by $a_{\beta\text{-H}}^{CH_2OOCH}$ and $a_{\alpha\text{-H}}^{CH}$ being equal, within experimental error, but because $(a_{\beta\text{-H}}^{CH_2OOCH} - a_{\beta\text{-H}}^{CH_2NH_2}) \sim a_{\delta\text{-H}}^{OOCH} \sim a_N/2$.

Ethyl Formate, CH_3CH_2OOCH. Under normal field-modulation-amplitude conditions, the spectrum obtained was completely interpretable in terms of **2** and $\cdot CH_2CH_2OOCH$, **7**, from the ester and $CH_3\dot{C}HOH$, **8**, from ethyl alcohol[14] present as impurity.[15] As expected,[4,5] **2** gave a quartet (1:3:3:1) of doublets (1:1) of small (2.5 G) doublets (1:1), the last coupling from the formyl proton.[4,5] Radical **7**, not observed in the earlier studies[4,5] of ethyl formate, gave a triplet (1:2:1) of triplets (1:2:1) of small (2.2 G) doublets (1:1). The two triplets were assigned by comparison with those in related radicals studied in this present work and elsewhere.[16] The small doublet was attributed to the formyl proton. Figure 1 illustrates the spectrum from ethyl formate: the spectra from **2** and **7** are both intense and overlapped.

In their previous study of ethyl formate, Metcalfe and Waters[5] found not only **2** but also a broad singlet of g value 2.0005 ± 0.0003 assignable to the σ radical $CH_3CH_2OOC\cdot$, **9**. Such a signal was not found under the normal field-modulation-amplitude conditions used here or in the earlier study reported from this laboratory.[4] However, upon raising the field-modulation amplitude, one of the lines increased in intensity at the expense of all others, see Figure 1. This line was assigned to **9**, with a g value of 2.0008.

Isopropyl Formate, $(CH_3)_2CHOOCH$. This substrate gave an organic-radical absorption of rather low intensity and the signal from the titanium–radical complex[17] was never completely suppressed. This situation could not be avoided since the oxidizing stream was saturated with respect to the ester. However, by time-averaging techniques, this absorption was completely analyzable in terms of $\cdot CH_2CH(CH_3)OOCH$, **10**, $(CH_3)_2\dot{C}OOCH$, **11**, and $(CH_3)_2CHOOC\cdot$, **12**, with no evidence for radicals from isopropyl alcohol.[14] Radical **10** gave a quartet (1:3:3:1) of small (1.8 G) quartets (1:3:3:1) of small (0.8 G) doublets (1:1). The larger quartet was attributed to the chance equivalence of the α-CH_2 and β-CH proton couplings and the small quartet, to the γ-CH_3 protons. Although end lines were not observed, the spectrum of **11** appeared to be a septet (1:6:15:20:15:6:1) of small (1.3 G) doublets (1:1). The small doublets in both **10** and **11** were assigned to the formyl proton. A broad (ca. 1 G peak-to-peak) absorption observed at a g value of 2.0008 was assigned to σ radical **12**.

Isobutyl Formate, $(CH_3)_2CHCH_2OOCH$. The spectrum observed was fully accountable in terms of $\cdot CH_2CH(CH_3)CH_2OOCH$, **13**, $(CH_3)_2\dot{C}CH_2OOCH$, **14**, and $(CH_3)_2CH\dot{C}HOOCH$, **15**, from the formate and $\cdot CH_2CH(CH_3)CH_2OH$, **16**, and $(CH_3)_2\dot{C}CH_2OH$, **17**, from isobutyl alcohol[14] present as impurity. All attempts to observe the σ radical from this substrate by procedures similar to those employed for **9** failed. Also, no evidence for the presence of $(CH_3)_2CH\dot{C}HOH$, **18**, was found. However, when H_2SO_4 was included in the oxidizing stream so that the substrate reacting was largely isobutyl alcohol, the predominant radical observed was **18**, as expected.[9,14] Since this seemingly different selectivity of hydrogen-atom abstraction from the alcohol in the presence of the formate was irrelevant to the present study, it was not investigated further.

It should be noted that **13** and **16**[14] would be expected to yield similar, overlapping patterns of lines, each a triplet (1:2:1) of doublets (1:1). Only one such triplets-of-doublets pattern was observed, this finding being in line with the presence of either one or both of **13** and **16**. Based on the amount of alcohol in the reaction mixture, as crudely inferred from the signal intensity of **17**, which was small in comparison with that from **14** or **15**, it appears unlikely that this pattern could have arisen solely from **16**. Thus, both **13** and **16** were suspected to be present. However, since this point was unimportant to the chief thrust of the present work, and because of the previously noted question of the seeming change in the selectivity of hydrogen-atom abstraction from the alcohol in the presence of the formate, no attempt was made to pursue it further. The spectrum of **14** was a septet (1:6:15:20:15:6:1) of triplets (1:2:1) of small (3.2 G) doublets (1:1); that of **15** was a doublet (1:1) of doublets (1:1) of small (2.4 G) doublets (1:1). For **14** and **15**, the small doublets were assigned to the formyl proton. The two larger doublet splittings for **15** were assigned by comparison with the couplings in the analogous radical **2** since these are known unambiguously.

tert-Butyl Formate, $(CH_3)_3COOCH$. Even though the oxidizing stream was saturated with respect to the substrate, the organic-radical absorption produced was of somewhat low intensity and there was a residual signal

TABLE I: Spectroscopic Data for Formate-Derived Radicals[a]

Radical	Coupling constants, G			g value
	α-CH	β-CH	Other	
2, $CH_3\dot{C}HOOCH$[b]	19.42	24.28	2.49[c]	2.00275
4, $HO\dot{C}H_2CHCH_2OOCH$[d]	21.82	17.87,[e] 23.42[f]	2.80[g,h]	
	21.75	17.96,[e] 23.40[f]	2.80[g]	2.0024[i]
	21.74	18.13,[e] 23.40[f]	2.78[g,j]	
5, $\cdot CH_2CH(OH)CH_2OOCH$[k]	22.25	24.52		2.0024
6, $H_2N\dot{C}H_2CHCH_2OOCH$[k]	22.39	19.64,[l] 22.39[f]	2.78,[g] 5.56[m]	2.0024
7, $\cdot CH_2CH_2OOCH$	22.14	24.59	2.18[g]	2.0024
9, $CH_3\dot{C}H_2OOC\cdot$				2.0008[n,o]
10, $\cdot CH_2\dot{C}H(CH_3)OOCH$	22.18	22.18	0.83,[g] 1.82[p]	2.0024
11, $(CH_3)_2\dot{C}OOCH$		22.29	1.27[c]	2.00265
12, $(CH_3)_2\dot{C}HOOC\cdot$				2.0008[n]
13, $\cdot CH_2\dot{C}H(CH_3)CH_2OOCH$[q]	21.87	27.50		2.0025
14, $(CH_3)_2\dot{C}CH_2OOCH$		23.22,[r] 12.98[f]	3.22[g]	2.00255
15, $(CH_3)_2\dot{C}HCHOOCH$	18.70	23.24	2.40[c]	2.0025
19, $\cdot CH_2\dot{C}(CH_3)_2OOCH$[s]	22.13		0[g,t], 1.38[p]	2.0026

[a] All data are mean values based on several full field scans. Unless specified otherwise, at 25 ± 2 °C and with the maximum uncertainties for a and g values being 0.10 G and ca. 0.0001, respectively. [b] These a values are in reasonable agreement with the literature,[4,5] considering that the previous workers did not allow for the presence of overlapping lines from **7**, see Figure 1. [c] $a_{\gamma\text{-H}}^{OOCH}$. [d] The assignment of the β-CH_2 proton couplings in **4** is justified elsewhere.[7] [e] $a_{\beta\text{-H}}^{CH_2OH}$. [f] $a_{\beta\text{-H}}^{CH_2OOCH}$. [g] $a_{\delta\text{-H}}^{OOCH}$. [h] All data taken at 9 ± 1 °C, the standard deviation of the mean being 0.04, 0.03, 0.05, and 0.01 G, respectively, left to right. [i] All data taken at 23 ± 1 °C, the standard deviation of the mean for the a values being 0.03, 0.02, 0.02, and 0.01 G, respectively, left to right. [j] All data taken at 44 ± 1 °C, the standard deviation of the mean being 0.04, 0.03, 0.05, and 0.01 G, respectively, left to right. [k] All data taken from ref 7. [l] $a_{\beta\text{-H}}^{CH_2NH_2}$. [m] a_N. [n] In agreement with the literature.[5,22] [o] Maximum uncertainty 0.0002. [p] $a_{\gamma\text{-H}}^{CH_3}$. [q] The data attributed here to **13** refer to a mixture of **13** and **16**, see the text. [r] $a_{\beta\text{-H}}^{CH_3}$. [s] In order to make the most reliable comparison, the results for **19** and **20** (see ref 20) were taken in close succession under the same recording conditions. [t] Not resolved; <0.4 G, the peak-to-peak line width approximately equal to the field-modulation amplitude (owing to the low intensity of the signal, smaller field-modulation amplitudes were not possible).

from the titanium–radical complex.[17] Nevertheless, the organic-radical absorption was readily assignable to $\cdot CH_2C(CH_3)_2OOCH$, **19**, and an isomer, **14**, their relative steady-state molar proportions being roughly 3:1. As with isopropyl formate, all attempts to observe the σ radical failed. The production of **14** presumably arose via **19**, similar isomerizations having been observed in the case of analogously structured radicals.[18,19] The spectrum of **19** consisted of a triplet (1:2:1) of small septets (1:6:15:20:15:6:1), with no evidence of a coupling with the formyl proton. The spectroscopic properties of **19** are sufficiently different from those for the analogous radical $\cdot CH_2C(CH_3)_2OH$, **20**, from *tert*-butyl alcohol[14,20] to leave little doubt as to the source of the EPR signal attributed to **19**. This assignment is strengthened by the following evidence: first, NMR analysis indicated the substrate to be free of impurities and to undergo negligible hydrolysis in aqueous solution over time periods comparable to those employed in the EPR investigations; secondly, the apparent reactivity of the substrate within the $TiCl_3$–H_2O_2 system was appreciably less than that of *tert*-butyl alcohol when run under the same reaction and recording conditions; thirdly, the spectra obtained were independent of flow rate.

The coupling constants and g values for the formate-derived radicals are summarized in Table I.

Discussion

Each saturated formate ester underwent hydrogen-atom abstraction at every carbon position in the alkoxyl group; the reactivity characteristics of the alkoxyl group toward hydrogen-atom abstraction, as judged by the relative steady-state molar concentrations[4] of radicals observed, agreed with the general pattern of results of the previous analogous study[4] of saturated aliphatic carboxylic esters. However, for ethyl formate, **7** was clearly observed in the present work, unlike previously.[4,5] This discrepancy probably stems from differences in reaction and recording conditions.[21] Only with ethyl and isopropyl formate was the spectrum of the σ radical found. In each case, this was a rather broad singlet which, for ethyl formate, was overlapped by lines from other radicals. In view of the observation of a σ radical with ethyl and isopropyl formate and based on past experience with carboxylic acid esters as substrates in this laboratory[4] and elsewhere,[5,22] it is not clear why an analogous σ radical was not detected from either isobutyl or *tert*-butyl formate.

The radicals in Table I fall into four categories, viz. σ radicals and π radicals with a single –OOCH substituent, this being in either the α, β, or γ position. The σ radicals, **9** and **12**, have the same characteristically low g value, 2.0008, and, as might be expected in view of the breadth of the lines observed, show no hyperfine splittings.[5,22] The α-(–OOCH) radicals, **2**, **11**, and **15**, have g, $a_{\alpha\text{-H}}^{CH}$, and $a_{\gamma\text{-H}}^{OOCH}$ values of 2.0025–2.0028, 18.7–19.4 G, and 1.3–2.5 G, respectively, which are in line[4,5] with their common important structural feature, the α-(–OOCH) group. The β- and γ-(–OOCH) radicals **4–7**, **10**, **13**, **14**, and **19**, have g and $a_{\alpha\text{-H}}^{CH}$ values of 2.0024–2.0026 and 21.8–22.4 G, typical of hydrocarbon-like radicals.[23] Also, for the β-(–OOCH) radicals, $a_{\delta\text{-H}}^{OOCH}$ is 0.8–3.2 G, except for **19** where it is too small to be resolved, <0.4 G.

The relationship

$$a_{\beta\text{-H}}^{CH_3} = Q_H^{CCH_3}\rho_{\alpha\text{-C}}^{\pi} \quad (1)$$

with $Q_H^{CCH_3}$ equal to 29.3 G[24] gives $\rho_{\alpha\text{-C}}^{\pi}$ as 0.829, 0.761, and 0.792, respectively, for **2**, **11**, and **14**. Furthermore, if Δ(–CH_3) is set equal to 0.081,[24] these $\rho_{\alpha\text{-C}}^{\pi}$ values indicate that Δ(–OOCH) in **2** and **11** are 0.098 and 0.099, respectively, and, as expected,[4,23-25] Δ(–CH_2OOCH) in **14** is somewhat lower, 0.062. These Δ(–OOCH) values agree reasonably with those calculated from the data of Smith et al.[4] and Metcalfe and Waters,[5] viz. 0.091 and 0.090, respectively. However, from another study of ethyl formate with the use of the $TiCl_3$–H_2O_2 system, a substantially different result for Δ(–OOCH), 0.136, has been reported.[24] This value seems likely to refer to Δ(–OH)[24]

TABLE II: Formyl-Proton Coupling Constants in ·C(X$_1$)(X$_2$)OOCH Type Radicals[a]

Radical	X_1-	X_2-	$a_{\gamma\text{-H}}^{OOCH}$, G
1	H-	H-	2.51[b]
2	CH_3-	H-	2.49
15	$(CH_3)_2CH$-	H-	2.40
11	CH_3-	CH_3-	1.27

[a] Unless specified otherwise, from Table I. [b] Reference 4, 25 ± 1 °C; in reasonable agreement with the literature.[5,22]

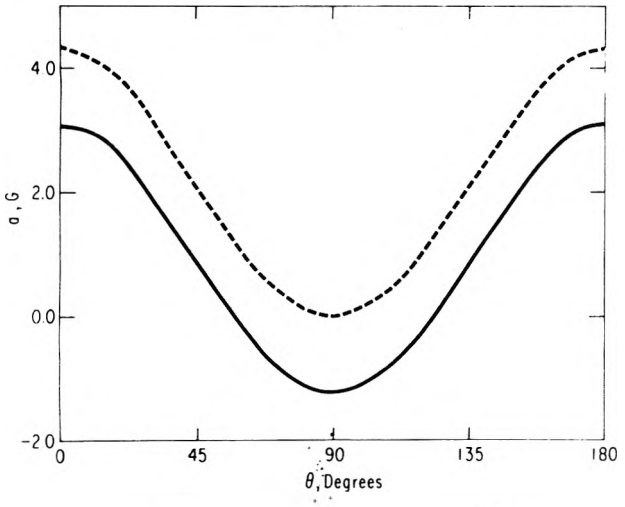

Figure 2. Dependence of the INDO-based values of $a_{\gamma\text{-H}}^{OOCH}$ [·CH_2OOCH, **1**] (solid line) and $a_{\delta\text{-H}}^{OOCH}$ [·CH_2CH_2OOCH, **7**] (broken line) on the angle of twist, θ, as defined in the text for each radical.

rather than Δ(–OOCH), i.e., significant hydrolysis of the ester may have occurred.[4,5]

As pointed out already, the α-(–OOCH) radicals (i.e., of structure ·C(X$_1$)(X$_2$)OOCH, **22**) possessed a long-range γ-CH formyl–proton coupling, as expected,[4,5] see Table II. There is considerable evidence[26] to indicate that, for simple aliphatic carboxylic esters, R_1OOCR_2 where R_1 and R_2 are small, in the liquid phase at about room temperature, the s-trans is preferred over the s-cis conformation and, for

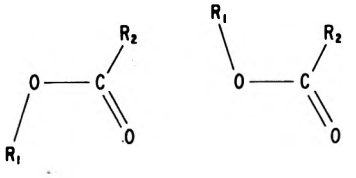

methyl and ethyl formate, the s-trans is highly favored over the s-cis conformation.[26c,d,g,j-l,p,q,t-z] If **22**-type radicals exist preferentially in the s-trans conformation, then their conformational properties may be discussed in terms of the two conformations I and II which differ only by a 90°

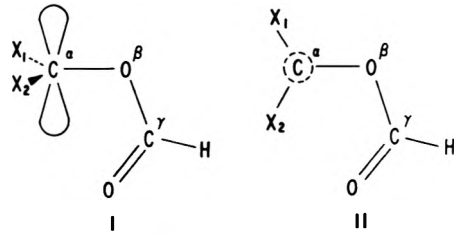

rotation about the C_α–O_β bond.

Preliminary molecular orbital calculations using the INDO approximation[27,28] and following this conformational approach were carried out on **1**, the simplest radical[29] of structure **22**. Figure 2 illustrates the results obtained by

TABLE III: Proton Coupling Constants in ·C(X$_1$)(X$_2$)C(X$_3$)(X$_4$)OOCH Type Radicals[a]

Radical	X_1-	X_2-	X_3-	X_4-	$a_{\beta\text{-H}}$, G[b]	$a_{\delta\text{-H}}$, G[b]
14	CH_3-	CH_3-	H-	H-	12.98	3.22
4	H-	$HOCH_2$-	H-	H-	23.40	2.80
6	H-	H_2NCH_2-	H-	H-	22.39	2.78
7	H-	H-	H-	H-	24.59	2.18
10	H-	H-	CH_3-	H-	22.18	0.83
19	H-	H-	CH_3-	CH_3-		<0.4

[a] From Table I. [b] In the -C(X$_3$)(X$_4$)OOCH group.

plotting the INDO-calculated value of $a_{\gamma\text{-H}}^{OOCH}$ [**1**] as a function of θ, the angle of twist of the plane of the –OOCH group about the C_α–O_β bond with respect to the C_α $2p_z$ orbital. Figure 2 shows the calculated value of $a_{\gamma\text{-H}}^{OOCH}$ [**1**] to range from a maximum of 3.1 G for I, θ = 0°, to a minimum of –1.2 G for II, θ = 90°. However, since the sign of the experimental value of $a_{\gamma\text{-H}}^{OOCH}$ [**1**] is not known, it is impossible to determine the preferred conformation of **1** on the basis of the INDO-calculated numerical results for $a_{\gamma\text{-H}}^{OOCH}$ [**1**], assuming these results are approximately correct.[30]

However, the data in Table II may be explained partially, assuming that the INDO results for $a_{\gamma\text{-H}}^{OOCH}$ [**1**] generally apply to **22**, as follows: for the radicals of type **22** where X_1 is H, CH_3, or $(CH_3)_2CH$ and X_2 is H, viz. **1**, **2**, and **15**, respectively, the preferred conformation (or manifold of conformations centered about that conformation) should be similar. Thus for these **22** radicals, any variation in $a_{\gamma\text{-H}}^{OOCH}$ should be small being the result of variation in $\rho_{\alpha\text{-}C}^{\pi}$, which should also be small.[24] The results in Table II for **1**, **2**, and **15** support this view. However, when both X_1 and X_2 in **22** are CH_3, there is a distinct change in $|a_{\gamma\text{-H}}^{OOCH}|$. If $a_{\gamma\text{-H}}^{OOCH}$ [**1**] is negative and $a_{\gamma\text{-H}}^{OOCH}$ [**11**] is positive or negative, simple steric arguments show that this change may come from a variation in preferred conformation (i.e., **1**, **2**, and **15** being closer than **11** to conformation II). On the other hand, if $a_{\gamma\text{-H}}^{OOCH}$ [**1**] is positive and $a_{\gamma\text{-H}}^{OOCH}$ [**11**] either positive or negative, then this change appears to demand an increased likelihood of the –OOCH group being nonplanar in **11** compared with **1**, **2**, and **15**. Such an effect also would be of steric origin. Evidence for this increased likelihood from studies of the parent formate esters is fragmentary and seemingly conflicting.[31] However, INDO calculations on **1** entailing simultaneous rotation about C_α–O_β and O_β–C_γ show that (O_β–C_γ)-bond rotation should, in general, tend to cause $|a_{\gamma\text{-H}}^{OOCH}|$ to fall.[32] Also, these INDO calculations show that (O_β–O_γ)-bond rotation could be a contributing source of the observed change in $|a_{\gamma\text{-H}}^{OOCH}|$ if the formyl–proton couplings in **1** and **11** are negative and positive, respectively, or both negative. Fuller discussion of the formyl–proton couplings in **22**-type radicals, as well as assignment of specific conformations, must await the experimental determination of the signs of these couplings.

It was noted earlier that all the β-(–OOCH) radicals (i.e., of structure ·C(X$_1$)(X$_2$)C(X$_3$)(X$_4$)OOCH, **23**) except **19** showed a δ-CH formyl–proton coupling, see Table III; also, in ethyl formate, the s-trans is highly favored over the s-cis conformation. Hence, if **23**-type radicals exist preferentially in the s-trans conformation, their conformational properties may be discussed[33] in terms of conformations III and IV which differ only by a 90° rotation about the C_α–C_β bond, i.e., the conformation of the $-CH_2OOCH$ group remains unchanged.

The results of INDO calculations[34] on the simplest radical of this type, **7**, are illustrated in Figure 2 by way of a plot of the INDO-calculated value $a_{\delta\text{-H}}^{OOCH}$ [**7**] as a

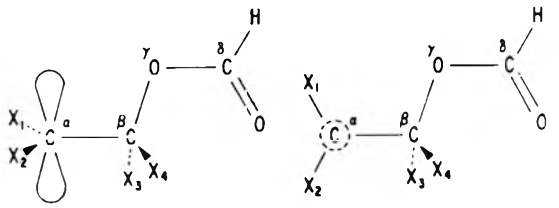

III IV

function of θ, the angle of twist of the plane of the $-C_\beta OOCH$ group about the C_α–C_β bond with respect to the C_α $2p_z$ orbital. Figure 2 shows $a_{\delta\text{-H}}^{OOCH}$ [7] to be a maximum of 4.3 G in III, $\theta = 0°$, and to fall to a minimum of essentially zero in IV, $\theta = 90°$. If the INDO-calculated a value results are accepted as being approximately correct, the experimentally observed $a_{\delta\text{-H}}^{OOCH}$ [7] value, 2.2 G, supports no strong preference for either conformation III or IV,[35] and tends to suggest that essentially free rotation occurs about the C_α–C_β bond (other evidence for the presence of such free rotation is given later).

From the INDO calculations, it appears that, if the β-(-COOCH) group remains planar, $a_{\delta\text{-H}}^{OOCH}$ [7] would take the form

$$a_{\delta\text{-H}}^{OOCH}\ [7] \propto \langle \cos^2 \theta \rangle \qquad (2)$$

where $\langle\rangle$ denote the time-averaged value. However, it seems reasonable to expect that, as the H atoms at X_3 and X_4 in **7** are replaced by CH_2 groups, rotation about the C_β–O_γ and O_γ–C_δ bonds is more likely to occur.[36] Further INDO calculations on **7** with simultaneous rotation about the C_α–C_β, C_β–O_γ, and O_γ–C_δ bonds show that these extra bond rotations should, in general, tend to reduce the experimentally observed value of $a_{\delta\text{-H}}^{OOCH}$ and cause it even to approach zero.[32b,37] However, this same replacement of the H atoms at X_3 and X_4 in **7** by CH_3 groups would tend to favor conformation III over IV on steric grounds,[38] leading to an increase in the average value of $a_{\delta\text{-H}}^{OOCH}$. The significance of this latter contribution relative to that arising from the (C_β–O_γ) and (O_γ–C_δ) bond rotations is apparently small, since the experimentally observed $a_{\delta\text{-H}}^{OOCH}$ values for the radical series **7**, **10**, and **19** show a marked drop as each H atom at C_β is replaced by a CH_3 group.

That there is essentially free rotation about the C_α–C_β bond in **4**, **6**, **7**, and **10** may be inferred from the values of the coupling constants of the C_β proton or protons in these radicals.[24] When an H atom on C_α in **7** is replaced by either $-CH_2OH$ or $-CH_2NH_2$, the rotation about the C_α–C_β bond should become slightly more hindered[39] relative to **7**, with III becoming somewhat favored over IV and $a_{\delta\text{-H}}^{OOCH}$ tending to increase. Such an increase is observed, see Table III. Replacing both C_α hydrogens in **7** by CH_3 groups to form **14** should further restrict rotation about the C_α–C_β bond. The low value for $a_{\beta\text{-H}}^{CH}$ [14] shows that there is restricted rotation about this bond and that the preferred conformation is III.[40] Thus, $a_{\delta\text{-H}}^{OOCH}$ [14] should be appreciably larger than $a_{\delta\text{-H}}^{OOCH}$ in **23** radicals with essentially free rotation about the C_α–C_β bond; and, in fact $a_{\delta\text{-H}}^{OOCH}$ [14] is the largest δ coupling observed in this radical series. As discussed for **1**, this same replacement of an α-H atom in **7** by other groups may also favor (C_β–O_γ) and (O_γ–C_δ) bond rotations, leading to a fall in $a_{\delta\text{-H}}^{OOCH}$. Apparently, however, this effect is small relative to that stemming from the restriction to rotation of the C_α–C_β bond.[41]

In the foregoing, discussion of possibly significant spin-transmission mechanisms operating in radicals **22** and **23** has been omitted. This omission was thought appropriate because of the absence of experimental evidence about the signs of the coupling constants and the radical conformations.[42]

Acknowledgment. The hydrogen peroxide was a gift from FMC Corp., Inorganic Chemicals Division. The Varian F-80A X-Y recorder and the INDO program[43] were kindly provided by Dr. D. B. Chesnut.

References and Notes

(1) Supported by National Science Foundation Grants No. GP-7534, GP-17579, and GP-32292 and the North Carolina Board of Science and Technology.
(2) National Defense Education Act Predoctoral Fellow.
(3) E.g., R. O. C. Norman, *Chem. Soc., Spec. Publ.*, **No. 24**, 177 (1970).
(4) P. Smith, J. T. Pearson, P. B. Wood, and T. C. Smith, *J. Chem. Phys.*, **43**, 1535 (1965).
(5) A. R. Metcalfe and W. A. Waters, *J. Chem Soc. B*, 340 (1967).
(6) R. A. Kaba and P. Smith, unpublished results.
(7) P. Smith, R. A. Kaba, and P. B. Wood, *J. Phys. Chem.*, **78**, 117 (1974).
(8) P. Smith, R. A. Kaba, and J. T. Pearson, *J. Magn. Reson.*, **17**, 20 (1975).
(9) E.g., ref 4; W. T. Dixon, R. O. C. Norman, and A. L. Buley, *J. Chem. Soc.*, 3625 (1964).
(10) A. Weissberger and E. Proskauer, "Organic Solvents", Oxford University Press, Oxford, 1935, p 150.
(11) W. Stevens and A. van Es, *Recl. Trav. Chim. Pays-Bas*, **83**, 1287 (1964).
(12) E.g., P. Smith and W. M. Fox, *Can. J. Chem.*, **47**, 2227 (1969).
(13) The spectroscopic characteristics of **4** and **5** under conditions similar to those of this present work are detailed elsewhere.[7]
(14) Apart from ref 4, some of the many EPR studies of radicals formed from simple aliphatic alcohols are: (a) W. T. Dixon and R. O. C. Norman, *J. Chem. Soc.*, 3119 (1963); (b) T. Shiga, *J. Phys. Chem.*, **69**, 3805 (1965); (c) R. Livingston and H. Zeldes, *J. Chem. Phys.*, **44**, 1245 (1966); (d) R. Livingston and H. Zeldes, *J. Am. Chem. Soc.*, **88**, 4333 (1966); (e) P. Smith and P. B. Wood, 151st National Meeting of the American Chemical Society, Pittsburgh, Pa., 1966, Abstract N 90; (f) J. R. Steven and J. C. Ward, *Aust. J. Chem.*, **20**, 2005 (1967).
(15) For a given ester, removal of the alcohol impurity was undertaken only when the presence of the derived alcohol radicals hindered either the analysis of the spectrum or measurement of the coupling constants. Usually, the spectroscopic parameters for alcohol-derived radicals were not determined.
(16) E.g., ref 4, 7, 14c; R. W. Fessenden and R. H. Schuler, *J. Chem. Phys.*, **39**, 2147 (1963).
(17) E.g., H. Fischer, *Ber. Bunsenges. Phys. Chem.*, **71**, 685 (1967); G. Czapski, A. Samuni, and D. Meisel, *J. Phys. Chem.*, **75**, 3271 (1971).
(18) E. J. Hamilton, Jr., and H. Fischer, *Helv. Chim. Acta*, **56**, 795 (1973).
(19) A. L. J. Beckwith and P. K. Tindal, *Aust. J. Chem.*, **24**, 2099 (1971); M. J. Perkins and B. P. Roberts, *J. Chem. Soc., Perkin Trans. 2*, 77 (1975).
(20) To help settle this point, *tert*-butyl alcohol was run separately as substrate, with the following results for **20**: $a_{\alpha\text{-H}}^{CH_2}$ = 21.94 G, $a_{\gamma\text{-H}}^{CH_2}$ = 1.38 G, g value 2.0025, in moderate agreement with the most comparable literature data available for this radical.[14a,b,d,19] No radical other than **20** was detected.
(21) E.g., ref 7, 14e; P. Smith and P. B. Wood, *Can. J. Chem.*, **45**, 649 (1967).
(22) H. Hefter and H. Fischer, *Ber. Bunsenges. Phys. Chem.*, **74**, 493 (1970); D. Griller and B. P. Roberts, *J. Chem. Soc., Perkin Trans. 2*, 747 (1972).
(23) E.g., ref 14c, 14d; R. O. C. Norman and R. J. Pritchett, *Chem. Ind. (London)*, 2040 (1965).
(24) H. Fisher, *Z. Naturforsch. A*, **20**, 428 (1965).
(25) P. Smith, R. A. Kaba, T. C. Smith, J. T. Pearson, and P. B. Wood, *J. Magn. Reson.*, **18**, 254 (1975).
(26) (a) A. J. Bowles, W. O. George, and D. B. Cunliffe-Jones, *Chem. Commun.*, 103 (1970); (b) W. O. George, D. V. Hassid, and W. F. Maddams, *J. Chem. Soc., Perkin Trans. 2*, 400 (1972); (c) *ibid.*, 1029 (1972); (d) *ibid.*, 1798 (1972); (e) *ibid.*, 952 (1973); (f) J. S. Byrne, P. F. Jackson, K. J. Morgan, and N. Unwin, *ibid.*, 845 (1973); (g) M. Oki and H. Nakanishi, *Bull. Chem. Soc. Jpn.*, **43**, 2558 (1970); (h) *ibid.*, **44**, 3144 (1971); (i) *ibid.*, **44**, 3197 (1971); (j) T. Miyazawa, *ibid.*, **34**, 691 (1961); (k) R. J. B. Marsden and L. E. Sutton, *J. Chem. Soc.*, 1383 (1936); (l) B. Krishna, S. C. Srivastava, and S. V. Mahadane, *Tetrahedron*, **23**, 4801 (1967); (m) J. M. Riveros and E. B. Wilson, Jr., *J. Chem. Phys.*, **46**, 4605 (1967); (n) T. Drakenberg and S. Forsen, *J. Phys. Chem.*, **76**, 3582 (1972); (o) A. Bjørseth and O. Gropen, *Acta Chem. Scand.*, **25**, 3184 (1971); (p) H. Wennerstrom, S. Forsen, and B. Roos, *J. Phys. Chem.*, **76**, 2430 (1972); (q) E. Bock and E. Tomchuk, *Ber. Bunsenges. Phys. Chem.*, **77**, 425 (1973); (r) N. S. True and R. K. Bohn, *J. Am. Chem. Soc.*, **98**, 1188 (1976); (s) J. Karpovich, *J. Chem. Phys.*, **22**, 1767 (1954); (t) D. Tabuchi, *ibid.*, **28**, 1014 (1958); (u) D. N. Hall and J. Lamb, *Trans. Faraday Soc.*, **55**, 784 (1959); (v) S. V. Subrahmanyam and J. E. Piercy, *J. Acoust. Soc. Am.*, **37**, 340 (1965); (w) J. E. Piercy and S. V. Subrahmanyam, *J. Chem. Phys.*, **42**, 1475 (1965); (x) K. M. Bu-

rundukov and V. F. Yakovlev, *Russ. J. Phys. Chem.*, **42**, 1141 (1968); (y) J. Bailey and A. M. North, *Trans. Faraday Soc.*, **64**, 1499 (1968); (z) J. Bailey, S. Walker, and A. M. North, *J. Mol. Struct.*, 6, 53 (1970).
(27) J. A. Pople and M. Gordon, *J. Am. Chem. Soc.*, **89**, 4253 (1967).
(28) J. A. Pople, D. L. Beveridge, and P. A. Dobosh, *J. Am. Chem. Soc.*, **90**, 4201 (1968).
(29) For the calculations, it was assumed[27,28] that the C–H, C_α–O_β, O_β–C_γ, and C_γ=O bond lengths were 1.08, 1.43, 1.36, and 1.22 Å, respectively; and the bond angles about C_α and C_γ were 120°, whereas angle C_α–O_β–C_γ was 109.47°. Only the angle of twist of the (–OOCH)-group plane about the C_α–O_β bond with respect to the $2p_z$ orbital, θ, was varied. Since $a_{\beta\text{-H}}^{CH_2}/a_{\alpha\text{-H}}^{CHOOCH}$ for **2** is 1.25, see Table I, the deviation from planarity at C_α in **2** would appear to be small at most. Consequently, such a deviation in **1** would be expected to be even less [A. J. Dobbs, B. C. Gilbert, and R. O. C. Norman, *J. Chem. Soc., Perkin Trans. 2*, 786 (1972); R. O. C. Norman, P. M. Storey, and P. R. West, *J. Chem. Soc.*, 1087 (1970)].
(30) However, **1** is preferred over II based on the dependence of the INDO calculated total energy, *E*, of **1** on θ: $|E(\text{II}) - E(\text{I})| = 0.95$ kcal mol^{-1} with *E*(II) and *E*(I), respectively, being the maximum and minimum values of the *E* vs. θ plot.
(31) E.g., cf. ref 26g,k,n and 26t–z.
(32) (a) Starting with conformation II, the C_α–O_β bond was rotated in 10° increments and for each increment the O_β–C_γ bond was rotated in 20° increments. (b) It is hoped to discuss the details of these calculations in a later paper.
(33) Radicals analogous to **23** have been studied by EPR at ca. –100 °C in hydrocarbon solvents [D. J. Edge and J. K. Kochi, *J. Am. Chem. Soc.*, **94**, 7695 (1972); **95**, 2635 (1973)]. The results of these studies appear compatible with the assumption of restricted rotation about the C_β–O_γ bond made in this present report.
(34) For these calculations, it was assumed[27,28] that the C–H, C_α–C_β, C_β–O_γ, O_γ–C_δ, and C_δ=O bond lengths were 1.08, 1.52, 1.43, 1.36, and 1.22 Å, respectively; and the bond angles about both C_α and C_γ were 120°, whereas those about C_β were 109.47°. The only variable was θ, the angle of twist of the –CH_2OOCH group about the C_α–C_β bond with respect to the C_α $2p_z$ orbital with C_β remaining in the plane of the –OOCH group.
(35) The dependence of the INDO calculated total energy, *E*, of **7** on θ gives $[E(\text{III}) - E(\text{IV})] = 2.96$ kcal mol^{-1} with *E*(III) and *E*(IV), respectively, being the maximum and minimum values of the *E* vs. θ plot. These data, if reliable [J. A. Pople and G. A. Segal, *J. Chem. Phys.*, **44**, 3289 (1966); J. A. Pople, D. L. Beveridge, and P. A. Dobosh, *ibid.*, **47**, 2026 (1967); J. A. Pople and D. L. Beveridge, "Approximate Molecular Orbital Theory", McGraw-Hill, New York, N.Y., 1970, Chapter 4], suggest that IV ought to be favored over III; this conclusion agrees with expectation based on simple steric arguements.
(36) This follows from steric considerations analogous to those discussed in ref 31, e.g., see ref 26g,j,x. The evidence for this tendency in the case of both bonds is scanty and for the O_γ–C_δ bond is seemingly contradictory.[26e–g,k–m,o,r,t–z]
(37) Starting with conformation IV, the C_α–C_β bond was rotated in 10° increments; for each increment, the C_β–O_γ bond was rotated in 10° increments and, for each of these increments, the O_γ–C_δ bond was rotated in 30° increments.
(38) That $a_{\beta\text{-H}}^{CH_2}$ [10] is somewhat less than $a_{\beta\text{-H}}^{CH_2}$ [7] tends to support this idea.
(39) This conclusion is in line with the observed $a_{\beta\text{-H}}^{CH_2OOCH}$ values in these radicals if we assume plausible values for $\Delta(\text{–}CH_2OH)$ and $\Delta(\text{–}CH_2NH_2)$, viz. 0.059 and 0.043, respectively.[7]
(40) For **14**, use of eq 1 modified to include the commonly assumed dependence[24] of $a_{\beta\text{-H}}^{CH}$ on the angle of twist about the C_α–C_β bond between the C_α $2p_z$ orbital and the plane of the C_α–C_β–H group, θ', gives $\langle\cos^2\theta'\rangle = 12.98/[2(23.22)]$ or $\theta' = 58°$, i.e., $\theta \sim 0°$.
(41) That the steric effect of a bulky substituent may vary, depending whether it is on the α- or the β-C, seems reasonable.
(42) F. W. King, *Chem. Rev.*, **76**, 157 (1976). It is hoped to include discussion of these mechanisms and related topics in a later paper. However, it is worth mentioning here that the INDO calculated formyl–proton couplings of this present paper agree substantially with expectation based on the W-plan reviewed by King.
(43) P. E. S. Wormer and D. B. Chesnut, *Theor. Chim. Acta*, **20**, 250 (1971).

Excited Electronic States of Alternant π Electron Systems from Projected Unrestricted Hartree–Fock Theory

John C. Schug* and Dana A. Brewer

Department of Chemistry, Virginia Polytechnic Institute and State University, Blacksburg, Virginia 24061 *(Received July 16, 1976)*

Excited states of naphthalene, anthracene, naphthacene, and pentacene have been calculated using unrestricted Hartree–Fock theory in the PPP approximation. Energies of the projected states of pure multiplicity were determined using the density matrix expressions of Harriman and co-workers. Results are in good agreement with experiment and with configuration-interaction calculations. Unique problems arose in the UHF calculations due to accidental degeneracies in the starting Hückel calculation and due to degenerate natural orbitals associated with the Coulson–Rushbrooke pairing properties. The sources of the degeneracies and their resolution are discussed in detail.

I. Introduction

Unrestricted Hartree–Fock (UHF) theory[1] is the simplest available method for allowing the orbital rearrangement that is necessary in calculating excitation and ionization energies.[2] It is therefore a useful alternative to configuration-interaction (CI) treatments for predicting molecular electronic spectra. The task of setting up and diagonalizing a CI matrix is eliminated. However, the single-determinant functions provided for open shells by UHF theory are not pure spin states, and it is necessary to apply Lowdin's spin projection operators[3] to eliminate this defect. Harriman and co-workers[4] have provided the basic means of calculating the reduced one- and two-particle density matrices for the spin-projected states, and the amount of computation time involved is comparable to that for singly excited CI calculations.

We have recently reported[5] some projected UHF calculations of the electronic spectra of several small molecules at the INDO level of approximation. The results were somewhat better than those obtained with singly excited CI. In view of the large amount of past effort that has gone into spectral calculations on π-electron systems, we felt it would be of interest to make some similar comparisons employing the Pariser–Parr–Pople (PPP) π-electron approximations.[6] We therefore wish to report some calculated spectra for naphthalene, anthracene, naphthacene, and pentacene.

In comparison with CI calculations, the projected UHF results for these molecules are somewhat mixed. For about half the excited states the projected UHF calculation

TABLE I: Charge Density Natural Orbitals and Occupation Numbers[a]

	Indices	Occupation no. (γ)	Relation to corresponding orbitals[b]
ϕ_p	$p = 1, 2, \ldots, D$	2	$a_p = b_p = \phi_p$
ϕ_i	$i = D + 1, D - 2, \ldots, \nu$	$1 + d_i$	$a_i = t_i\phi_i + u_i\phi_{i'}$
$\phi_{i'}$	$i' = N + 1 - i$	$1 - d_i$	$b_i = t_i\phi_i - u_i\phi_{i'}$
$\phi_{\nu+j}$	$j = 1, 2, \ldots, 2m$	1	$a_{\nu+J} = \phi_{\nu+J}$
ϕ_{N+r}	$r = 1, 2, \ldots, B - N$	0	

[a] μ = no. of α electrons; ν = no. of β electrons; $N = \mu + \nu$; $2m = \mu - \nu \geq 0$; B = no. of basis functions. The empty natural orbitals, ϕ_{N+r}, occur only if $B > N$. [b] $t_i = [(1 + d_i)/2]^{1/2} \geq 0$; $u_i = [(1 - d_i)/2]^{1/2} \geq 0$.

provides a lower energy than does the CI; for the other half the situation is reversed. As far as comparisons with experiment are concerned, there is little to choose between the two methods. Possibly of greater interest than the particular numbers are some peculiarities that arose during the UHF calculations. In particular, degeneracies appeared at several places in the computations, and it was necessary to understand and resolve them before consistent results could be obtained. These problems are discussed in section II of this paper, before the calculated results are given in section III.

II. Some Facets of Projected UHF Theory

The expressions provided by Harriman et al.[4] for the reduced one- and two-particle density matrices of the spin-projected states require the use of the charge-density natural orbitals $\{\phi\}$, which are eigenfunctions of the charge-density matrix, and the corresponding orbitals, $\{a\}$ and $\{b\}$, that were introduced by Amos and Hall.[7] The α corresponding orbitals $\{a\}$ are defined by a unitary transformation of the occupied α-SCF orbitals; the β corresponding orbitals $\{b\}$ are defined by a unitary transformation of the occupied β-SCF orbitals. The unitary transformations are chosen so as to diagonalize the matrix of overlap integrals between the two sets of orbitals:

$$\langle a_i | b_j \rangle = d_i \delta_{ij} \tag{1}$$

There are simple relationships between the corresponding orbitals and the charge density natural orbitals, and the overlap integrals, d_i, are related to the natural orbital occupation numbers.[4] These relationships are listed in Table I. It is important to note that the expressions for the two-particle density matrix given by Harriman et al. are valid only for the case $t_i, u_i \geq 0$.[8]

The calculation of excitation energies proceeds as follows: The closed-shell ground state is obtained by the standard restricted Hartree–Fock procedure[9]

$$\Psi_0 = A[\psi_1(1)\alpha(1)\psi_1(2)\beta(2)\ldots\psi_{N/2}(N - 1)\alpha(N - 1)\psi_{N/2}(N)\beta(N)] \tag{2}$$

The desired open-shell excited state is formed by replacing one of the occupied ψ_i by a virtual orbital ψ_k

$$\Psi_{i\to k} = A[\psi_1(1)\alpha(1)\psi_1(2)\beta(2)\ldots\psi_i(2i - 1)\alpha(2i - 1)\psi_k(2i)\beta(2i)\ldots] \tag{3}$$

which is iterated to self-consistency using the UHF equations of Brickstock and Pople.[1] The molecules studied belong to point group D_{2h} which has no degenerate irreducible representations. If $\tau(i)$ and $\tau(k)$ represent the irreducible representations to which orbitals ψ_i and ψ_k belong, the unrestricted wave function (3) transforms according to the representation which is the direct product $\tau_{ik} = \tau(i) \times \tau(k)$. When $\tau(i) \neq \tau(k)$, τ_{ik} will not be the totally symmetric representation. Pure spin states are obtained by application of Löwdin's spin projectors,[3] θ^s

$$\Psi^s_{i\to k} = \theta^s \Psi_{i\to k} \tag{4}$$

and the energy associated with $\Psi^s_{i\to k}$ is calculated from

$$E^s_{i\to k} = \sum_{i=1}^{B} \gamma^s_i \langle \phi_i | h | \phi_i \rangle + \sum_{i,j,k,l}^{B} \Gamma^s_{ijkl} \langle \phi_k \phi_l | g | \phi_i \phi_j \rangle \tag{5}$$

where h is the core Hamiltonian and $g = e^2/r_{12}$. The natural orbitals occurring in eq 5 are the same as those in the unprojected state (3), but the occupation numbers, γ^s_i and the coefficients, Γ^s_{ijkl}, do change as a result of projection.

At several stages of the calculation, degeneracies occurred; these had to be resolved before consistent results could be obtained.

In the first place, determination of the wave functions (2) and (3) begins with a Hückel calculation. For some symmetric molecules, the Hückel solutions possess accidental degeneracies. In the linear polyacenes treated here, this occurs when the molecule contains an odd number of fused rings. Diagonalization of the Hückel Hamiltonian matrix of course produces arbitrary combinations of the degenerate orbitals rather than the desired symmetry orbitals. If either or both of the orbitals i and k involved in the excitation $\Psi_{i\to k}$ is not a symmetry orbital, the spatial symmetry will be lost when the excitation is carried out. In order for the density matrices to reflect the full spatial symmetry of the molecule, it is necessary to carry out spatial projection of the degenerate orbitals before creating the excited state. This is straightforward because usually examination of the Hückel orbitals quickly reveals which irreducible representations are involved in the accidental degeneracies. Accidental degeneracies in orbitals other than i and k can be ignored when carrying out the excitation. Obviously, with a slightly better computer program, it is possible to use symmetry-adapted basis functions and eliminate altogether this problem of accidental degeneracies by symmetry-factoring the Hückel Hamiltonian matrix.

During the UHF iteration to self-consistency the Aufbau principle cannot always be used, because the orbitals sometimes reorder after the $i \to k$ excitation has been made. It is necessary to incorporate into the SCF procedure a search process to ensure that orbitals of the desired symmetry are occupied during each cycle.

Degeneracies also occur during the spin projection of $\Psi_{i\to k}$ after self-consistency has been achieved. It is necessary to determine the charge-density natural orbitals $\{\phi\}$ and corresponding orbitals $\{a,b\}$. Harriman's expressions for calculating the density matrices of the projected states require that these orbitals satisfy the relationships in Table I. The former $\{\phi\}$ are usually obtained as eigenvectors of the total charge-density and bond-order matrix, $\mathbf{P} = \mathbf{P}^\alpha + \mathbf{P}^\beta$. The corresponding orbitals are usually obtained as eigenvectors of the product matrices, $\mathbf{P}^\alpha\mathbf{P}^\beta\mathbf{P}^\alpha$ and $\mathbf{P}^\beta\mathbf{P}^\alpha\mathbf{P}^\beta$. The eigenvalues of $\mathbf{P}$ are the occupation numbers (γ) given in Table I. The nonzero eigenvalues of $\mathbf{P}^\alpha\mathbf{P}^\beta\mathbf{P}^\alpha$ and $\mathbf{P}^\beta\mathbf{P}^\alpha\mathbf{P}^\beta$ are d_i^2, the squares of the overlap integrals defined in eq 1.

Degeneracies arise in two ways. The first has been discussed earlier and results because of the way $\Psi_{i\to k}$ is formed. Since orbitals i and k are required to have different symmetries, there is one set of natural orbitals $(\phi_i, \phi_{i'})$ for which $\langle a_i | b_i \rangle = d_i = 0$. We therefore have a limiting

TABLE II: Electronic Configuration in Lowest Excited State (B_{1u}) of Naphthalene

	α electrons	β electrons
Occupied orbitals	$1b_{3u}$	$1b_{3u}$
	$1b_{1g}$	$1b_{1g}$
	$1b_{2g}$	$1b_{2g}$
	$2b_{3u}$	$2b_{3u}$
	$2b_{1g}$	$1a_u$
Empty orbitals	$1a_u$	$2b_{1g}$
	$2b_{2g}$	$2b_{2g}$
	$3b_{3u}$	$3b_{3u}$
	$2a_u$	$2a_u$
	$3b_{2g}$	$3b_{2g}$

case of paired natural orbitals with unit occupation number. The pair $(\phi_i,\phi_{i'})$ cannot be determined solely by diagonalizing **P**; and the related a_i and b_i cannot be found solely by the process mentioned above. A variety of methods can be devised to resolve this degeneracy. Since these have been described earlier in detail,[5] however, the discussion will not be repeated here. Since the D_{2h} point group is Abelian, the excited-state molecular orbitals retain their symmetry adaptedness. It is therefore possible to simplify the determination of the self-consistent orbitals in $\Psi_{i\to k}^{u}$ by symmetry factoring the Hartree–Fock matrix. However, this does not eliminate the degeneracy problem during the projection calculation because the degenerate natural orbitals of unit occupation number are not symmetry orbitals.[5]

In the even-alternant π-electron systems of present interest, there is another source of degeneracy, which can be rationalized geometrically in terms of the Coulson–Rushbrooke (CR) pairing theorem.[10] In alternant systems, one steps through the molecule starring alternate atoms, so that each starred atom has only unstarred neighbors and vice versa. The theorem states that in the SCF ground state each bonding orbital has a complementary antibonding orbital which differs from it only in the signs associated with one set of atomic orbitals.

When the $i \to k$ excitation is performed, if orbitals i and k are complementary in the CR sense, the uniform charge distribution is maintained in the excited state, and so are the orbital pairing properties.

To see how this causes degeneracies in the natural and corresponding orbitals, let us consider the lowest excited state (B_{1u}) of naphthalene. This state is created by exciting an α electron from the 5th to the 6th orbital, giving the electronic configuration listed in Table II. These two orbitals are CR complementary, so the pairing properties are retained.

Since there is only one b_{2g} orbital occupied in the α and the β spaces, the occupied b_{2g} orbitals are also corresponding orbitals, and we have an overlap

$$\langle 1b_{2g}^{\alpha} | 1b_{2g}^{\beta} \rangle = d(b_{2g})$$

The empty b_{3u} orbitals are CR complementary to these, so we have

$$\langle 3b_{3u}^{\alpha} | 3b_{3u}^{\beta} \rangle = d(b_{2g})$$

The sets of orbitals $\{1b_{3u}^{\alpha}, 2b_{3u}^{\alpha}, 3b_{3u}^{\alpha}\}$ and $\{1b_{3u}^{\beta}, 2b_{3u}^{\beta}, 3b_{3u}^{\beta}\}$ provide two alternative definitions of the same three-dimensional space, which is illustrated in Figure 1. The two-dimensional subspace defined by the occupied orbitals $\{1b_{3u}^{\alpha}, 2b_{3u}^{\alpha}\}$ is a plane orthogonal to the empty orbital $(3b_{3u}^{\alpha})$; and the subspace $\{1b_{3u}^{\beta}, 2b_{3u}^{\beta}\}$ is a plane orthogonal to $(3b_{3u}^{\beta})$. Clearly, these two planes intersect in a line, which means that there is a pair of corresponding orbitals (a,b) of b_{3u} symmetry having unit overlap. It is also clear

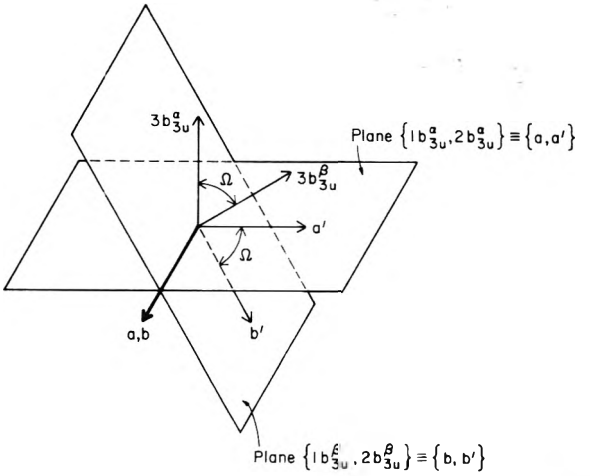

Figure 1. The three-dimensional b_{3u} space of naphthalene. $\langle a|b\rangle = 1$. $\langle a'|b'\rangle = \langle 3b_{3u}^{\alpha}|3b_{3u}^{\beta}\rangle = \cos\Omega$.

that the other set of corresponding orbitals (a',b') are separated by an angle, Ω, equal to the angle between the empty b_{3u} orbitals. Thus

$$\langle a'|b'\rangle = \langle 3b_{3u}^{\alpha}|3b_{3u}^{\beta}\rangle = d(b_{2g})$$

Therefore, when one diagonalizes $\mathbf{P}^{\alpha}\mathbf{P}^{\beta}\mathbf{P}^{\alpha}$, $\mathbf{P}^{\beta}\mathbf{P}^{\alpha}\mathbf{P}^{\beta}$, or **P** to determine the corresponding orbitals or the natural orbitals, there will be degeneracies corresponding to mixtures of the b_{2g} and b_{3u} orbitals. However, it is a simple matter to obtain the correct symmetry orbitals by using spatial symmetry projectors. This projection must be carried out in order to obtain consistent results when using Harriman's expressions for the density matrices of the projected states.

It is interesting to go a little further in this vein. The two-dimensional b_{1g} space is completely spanned by the occupied α orbitals. This guarantees that the occupied b_{1g} orbital in the β space can be perfectly matched so that we will have unit overlap of the b_{1g} corresponding orbitals, and a doubly occupied natural orbital of b_{1g} symmetry. These orbitals become degenerate with the b_{3u} orbitals with unit overlap mentioned above, but degeneracies among doubly occupied orbitals do not invalidate the Harriman expressions, so they need not be split during the calculation.

It is furthermore clear from Table II that the corresponding orbitals of zero overlap will be of b_{1g} symmetry in the α space and a_u symmetry in the β space. This knowledge makes easy the determination of those orbitals by spatial projection.

The arguments get more complicated for the larger molecules because one must work in spaces of greater than three dimensions. However the appropriate arguments can be made, and all observed degeneracies can be rationalized.

III. Results

All calculations were carried out with the usual PPP approximations of zero differential overlap and zero off-diagonal core matrix elements except between nearest neighbors. All fused benzene rings were taken to be regular hexagons with sides of length 1.40 Å. The core matrix elements between nearest neighbors were set equal to −2.395 eV. The one-center repulsion integrals were taken to be 11.13 eV and the two-center repulsion integrals were evaluated by the Mataga–Nishimoto approximation.[11] The CI calculations that were done for comparison with the projected UHF calculations included all singly excited configurations. All calculations were carried out with a slightly modified version of the Fortran program SPUHF, which has been submitted to the Quantum Chemistry

TABLE III: Unique Natural-Orbital Occupation Numbers for the Unprojected UHF States of B_{1u} Symmetry

Molecule	γ
Naphthalene	2.0, 2.0, 1.9964, 1.9964, 1.0
Anthracene	2.0, 2.0, 1.9994, 1.9994, 1.9964, 1.9964, 1.0
Naphthacene	2.0, 2.0, 1.9998, 1.9998, 1.9993, 1.9993, 1.9962, 1.9962, 1.0
Pentacene	2.0, 2.0, 1.9999, 1.9999, 1.9998, 1.9998, 1.9992, 1.9992, 1.9961, 1.9961, 1.0

TABLE IV: Wavelengths (Å) for the Ground to Excited State Transitions in Naphthalene

Excited state	Calcd: Projected UHF	Calcd: CI	Expt
$^1B_{2u}$	3137	2991	3106[a]
$^1B_{1u}$	2724	2765	2757[b]
$^1B_{3g}$	2099	2115	
$^3B_{1u}$	5006	7264	4963[b]
$^3B_{2u}$	3319	3604	3353[b]
$^3B_{3g}$	2708	4264	

[a] J. R. Platt, *J. Chem Phys.*, 18, 1168 (1950). [b] R. G. Parr, "Quantum Theory of Molecular Electronic Structure", W. A. Benjamin, New York, N.Y., 1964.

Program Exchange (QCPE No. 278). The modifications were those described above, namely, to handle the particular type of open shells used in the excited states,[5] and to split the several degeneracies when necessary.

Our group-theoretical notation is that suggested by IUPAC,[12] so that the molecules lie in the *yz* plane, the short molecular axis being the *z* direction and the long axis, *y*.

All the excitations we carried out were from the highest occupied orbital to the first three virtual orbitals of the ground state. As a result, CR-induced degeneracies only occurred during excitation to the lowest virtual orbital. In all four molecules considered, this produced states of B_{1u} symmetry. The extent to which degeneracies occurred is illustrated in Table III, which lists the unique natural-orbital occupation numbers for the unprojected UHF states. Clearly, degeneracies are quite common, and all of them can be rationalized by geometric arguments similar to those presented earlier for naphthalene. Other than those listed for the B_{1u} states, the only degeneracies were among two doubly occupied orbitals in the B_{3g} states of all molecules. It is interesting that in these cases, the degenerate doubly occupied orbitals have the same symmetries, namely, b_{3u} for naphthalene and naphthacene, and b_{1g} for anthracene and pentacene.

In all cases, the unprojected UHF states were composed of almost 50% singlet and 50% triplet character. The weights of the states with multiplicity five were about 0.3% for B_{1u} symmetry, about 1% for B_{3g} symmetry, and about 5% for B_{2u} symmetry. Much smaller, though nonvanishing contributions were also obtained for states of multiplicity seven for the larger molecules.

The calculated spectra are shown in Tables IV–VII. In most cases, there is reasonable agreement between the CI and the projected UHF results. It is interesting to note that the CI calculation generally produces appreciably lower energies for the triplet states than does the UHF treatment. However, for those cases where experimental data are available, the UHF results are in somewhat better agreement.

All preceding discussion has been devoted to open shell systems with equal numbers of α and β electrons. These are referred to as $m = 0$ states, since they have zero *z* component of spin angular momentum. These are the states that must be treated in order to obtain projected singlets and triplets from the same calculation. However, if one is primarily interested in the triplet states, it is natural to consider the $m = 1$ cases which have two more α than β electrons. We have therefore carried out the $m = 1$ calculations for all the triplet states included in Tables IV–VII. The wavelengths for excitation from the ground states to these triplets are listed in Table VIII. Comparison of these with the corresponding numbers in Tables IV–VII is rather interesting. For the B_{2u} triplets, the $m = 0$ calculations provided lower energy states than the $m = 1$ calculations except for pentacene, the largest molecule. For the B_{3g} and B_{1u} triplets, lower energies were obtained in all cases from the $m = 1$ calculations. The difference

TABLE V: Wavelengths (Å) for the Ground to Excited State Transitions in Anthracene

Excited state	Calcd: Projected UHF	Calcd: CI	Expt
$^1B_{2u}$	3713	3342	3745[a]
$^1B_{1u}$	3493	3568	3649[b]
$^1B_{3g}$	2887	2630	
$^3B_{1u}$	7921	11488	7298[b]
$^3B_{2u}$	3711	3876	
$^3B_{3g}$	3286	5468	

[a,b] See footnotes to Table IV.

TABLE VI: Wavelengths (Å) for the Ground to Excited State Transitions in Naphthacene

Excited state	Calcd: Projected UHF	Calcd: CI	Expt
$^1B_{1u}$	4239	4343	4278[b]
$^1B_{2u}$	4163	3568	3922[a]
$^1B_{3g}$	3402	3182	
$^3B_{1u}$	11802	18859	10340[b]
$^3B_{3g}$	4121	7434	
$^3B_{2u}$	3969	3899	

[a,b] See footnotes to Table IV.

TABLE VII: Wavelengths (Å) for the Ground to Excited State Transitions in Pentacene

Excited state	Calcd: Projected UHF	Calcd: CI	Expt
$^1B_{1u}$	4915	4969	5755[b]
$^1B_{2u}$	4471	3711	4167[a]
$^1B_{3g}$	4086	3696	
$^3B_{1u}$	16934	29078	
$^3B_{3g}$	5002	8622	
$^3B_{2u}$	4130	3899	

[a] Footnote *a*, Table IV. [b] E. Clar, "The Aromatic Sextet", Wiley, London, 1972.

TABLE VIII: Wavelengths (Å) for Ground to Excited Triplet States Obtained from Projected UHF Treatment of $m = 1$ Functions

Molecule	Excited state: $^3B_{1u}$	Excited state: $^3B_{2u}$	Excited state: $^3B_{3g}$
Naphthalene	6720	3148	2924
Anthracene	13393	3473	3673
Naphthacene	28788	3582	4901
Pentacene	*a*	5191	6303

[a] Triplet energy was lower than ground state RHF energy.

between the $m = 0$ and $m = 1$ energies increases with the size of the molecule, and is much greater for B_{1u} symmetry than for B_{3g}. The upshot of this is that the excitation energies for the ground state to the $^3B_{1u}$ states obtained from the $m = 1$ calculation are much too small in comparison with available experimental data. The case of pentacene is extreme in that the $^3B_{1u}$ ($m = 1$) state was found to be lower in energy than the closed shell ground state. The disparities between the $m = 0$ and $m = 1$ results can only result from differences in the effective flexibility of the basis sets.[5] Since the $m = 0$ results compare favorably with available experimental data on the whole, we must conclude that the $m = 0$ UHF basis contains comparable flexibility with that of the closed shell calculation. The effective flexibility of the basis for the $m = 1$ UHF calculations increases with molecular size and is different for different spatial symmetries, increasing in the order: $B_{3g} < B_{2u} < B_{1u}$. This order can in fact be rationalized by comparing the available virtual orbitals for naphthalene in the three calculations. However it is difficult to explain all the observed variations without a considerable amount of additional study, so further discussion of these points will be deferred.

Based on these results, as well as our earlier INDO calculations,[5] we feel that the projected UHF method is a viable alternative to CI for the calculation of excited electronic states, provided that the UHF and closed-shell RHF treatments employ basis sets with comparable effective flexibility. Experience now seems to indicate that the $m = 0$ UHF calculation satisfies this requirement in most cases. The method should become more useful in conjunction with extended basis-set ab-initio calculations, and we are presently developing computer programs to carry out such treatments.

Note should also be made of two obvious alternative methods for treating the open-shell excited states: (a) the restricted open-shell (RHF) approximation developed by Roothaan;[13] and (b) the extended Hartree–Fock (EHF) theory.[14] The RHF method is inferior to projected UHF because it employs the restriction of identical α and β orbitals in the closed-shell part of the wave function. This inferiority was shown by direct comparison at the INDO level of approximation for formaldehyde and diazomethane.[5] Even though the RHF calculations[15] included some configuration interaction, the projected UHF calculations produced lower energies for the states considered. The EHF theory is somewhat better than the present technique, since it involves energy minimization after spin projection. It also involves appreciably more work, however. Moreover, it should be noted that UHF treatment has been found to yield close to 100% of the correlation energy in some cases.[16]

References and Notes

(1) J. A. Pople and R. K. Nesbet, *J. Chem. Phys.*, **22**, 571 (1954); A. Brickstock and J. A. Pople, *Trans. Faraday Soc.*, **50**, 901 (1954).
(2) J. R. Hoyland and L. Goodman, *J. Chem. Phys.*, **36**, 12 (1962); S. Y. Chu and L. Goodman, *J. Am. Chem. Soc.*, **97**, 7 (1975).
(3) P. O. Lowdin, "Quantum Theory of Atoms, Molecules, and the Solid State," Academic Press, New York, N.Y., 1966, p 601.
(4) J. E. Harriman, *J. Chem. Phys.*, **40**, 2827 (1964); A. Hardisson and J. E. Harriman, *ibid.*, **46**, 2639 (1967).
(5) J. C. Schug, B. H. Lengsfield, and D. A. Brewer, *Int. J. Quantum Chem.*, in press.
(6) R. Pariser and R. G. Parr, *J. Chem. Phys.*, **21**, 466, 767 (1953); F. G. Fumi and R. G. Parr, *ibid.*, **21**, 1864 (1953); R. G. Parr and R. Pariser, *ibid.*, **23**, 711 (1955).
(7) A. T. Amos and G. Hall, *Proc. R. Soc. London, Ser. A*, **263**, 483 (1961).
(8) D. H. Phillips and J. C. Schug, *J. Chem. Phys.*, **61**, 1031 (1974).
(9) C. C. J. Roothaan, *Rev. Mod. Phys.*, **23**, 69 (1951).
(10) C. A. Coulson and G. S. Rushbrooke, *Proc. Cambridge Phil. Soc.*, **36**, 193 (1940).
(11) N. Mataga and K. Nishimoto, *Z. Phys. Chem.*, **12**, 335 (1957).
(12) R. S. Mulliken, *J. Chem. Phys.*, **23**, 1997 (1955).
(13) C. C. J. Roothaan, *Rev. Mod. Phys.*, **32**, 179 (1960).
(14) K. M. Sando and J. E. Harriman, *J. Chem. Phys.*, **47**, 180 (1967); I. Mayer, *Int. J. Quantum Chem.*, **8**, 363 (1975); I. Mayer and J. Kondasz, *ibid.*, **9**, 517, 527 (1975).
(15) G. A. Segal, *J. Chem. Phys.*, **53**, 630 (1970).
(16) A. Laforgue, J. Cizek, and J. Paldus, *J. Chem. Phys.*, **59**, 2560 (1973).

On the Free Volume Theory and on the Macedo–Litovitz Hybrid Equation for Diffusion in Liquids

F. P. Ricci,* M. A. Ricci, and D. Rocca

Istituto di Fisica "G. Marconi" Universita di Roma, Rome, Italy

(Received July 19, 1976)

Publication costs assisted by G.N.S.M.-C.N.R.

We compare the predictions of the Cohen–Turnbull theory with the "computer experiments" results in the case of hard spheres self-diffusions and impurity diffusions. We show the limits and the failures of the Cohen-Turnbull theory. Moreover we use such analysis to propose, for the diffusion coefficient, a new expression of the Macedo–Litovitz type which is valid also in the case of binary dilute mixtures (see eq 18). We compare our new equation with the experimental data showing a satisfactory agreement for the case of diffusions in liquid N_2 and Liquid CCl_4.

Introduction

The "computer experiments" carried out on systems of hard spheres[1-3] are very interesting and useful for many purposes. We want to use such experiments to make the first correct test of the Cohen–Turnbull (CT) theory[4] for the diffusion process. In fact such a theory has been developed quantitatively for a system of hard spheres, and therefore any test using the experimental data of the real fluids[4-6] is inconclusive. The reasons for a correct test of the CT theory are twofold: one is that it proposes very important physical ideas in a very simple mathematical context; the other is that the CT theory is the main basis for the Macedo–Litovitz hybrid expression,[7] which has been found very successful in describing the self-diffusion[8] and viscosity[9] behavior of real fluids. Moreover understanding of the limits of the CT theory can help to extend the Macedo–Litovitz expression to impurities' diffusion. We want to remark that a first crude comparison of the

CT theory using hard spheres computer experiments[17] was already reported by Turnbull and Cohen.[18] However this test is incomplete since it refers only to self-diffusion and is limited to densities near the solidification density.

Test of the Cohen-Turnbull Theory

The main idea of the CT theory is that diffusion occurs only if the local density is equal to or lower than a critical value. Therefore, in dense fluids, diffusion is driven by density fluctuations. If this situation occurs, the mass transport proceeds following a basic dynamic event; the CT theory suggests that this event is a single particle motion with a mean free path nearly equal to the diameter of the cage. For a test particle, i.e., a solute at infinite dilution, diffusing in a solvent, the two previous assumptions can be analitically expressed as

$$D_{CT}(V,T) = \int_{v^*}^{\infty} D(v,T)\, p(v)\, dv \qquad (1)$$

and

$$D(v,T) = guv^{1/3} \qquad (2)$$

where $D_{CT}(V,T)$ is the CT theoretical expression; V and T are the molar volume and the temperature, respectively; v is the free volume per molecule; $p(v)$ is the probability that the free volume per molecule is between v and $v + dv$; v^* is the value of the "critical" free volume, i.e., for $v < v^*$ the $D(v) = 0$; the only conditions that the CT theory gives for v^* are that v^* is of the same order of magnitude as V_0/N, moreover if the test particle has smaller dimensions than the solvent particle, v^* should be independent of the characteristics of the test particle; indeed diffusive transport is completed only by the jumping of the neighboring molecule into the void;[4] $u = (3RT/M_T)^{1/2}$ is the average kinetic gas velocity; R is the gas constant; M_T is the molar mass of the test particle; g is a numerical factor of the order of unity. In the case of a hard sphere fluid the redistribution of the free volumes occurs with no energy change; therefore $p(v)$ turns out to be[4]

$$p(v) = \frac{\gamma N}{V - V_0} \exp\left(-\frac{\gamma v N}{V - V_0}\right) \qquad (3)$$

where γ is a numerical factor of the order of unity; N is the Avogadro number, and V_0 is the close-packed molar volume ($V_0 = N\sigma_s^3/2^{1/2}$); σ_s is the hard sphere diameter of the solvent. V_0 depends only on the solvent properties since the concentration of the test particle is practically zero. Inserting eq 3 in eq 1 and using eq 2 we can easily obtain $D_{CT}(V,T)$ as

$$D_{CT}(V,T) = gV_0^{1/3}\sqrt{\frac{3RT}{M_T}}\left(\frac{\frac{V}{V_0} - 1}{\gamma N}\right)^{1/3} \int_{z^*}^{\infty} z^{1/3} e^{-z}\, dz \qquad (4)$$

where $z^* = \gamma v^* N/(V - V_0)$. In the range $1.5 \le V/V_0 \le 3$, eq 4 can be approximated very well by the expression

$$D_{CT}(V,T) = g'\left(\frac{V_0}{N}\right)^{1/3}\sqrt{\frac{3RT}{M_T}}\exp\left(-\frac{\gamma' v^* N}{V - V_0}\right) \qquad (5)$$

with g' and γ' numerical constants of the order of unity but, of course, different from the g and γ of eq 2 and 3. We want to remark that eq 5 does not imply making the assumption $D(v) \simeq D(v^*) = \text{constant}$[4] in eq 1. For $V/V_0 > 3$, eq 4 does not have simple analytical expression, after numerical integration. In any case since eq 3 is strictly valid only for a hard sphere fluid, a correct test of the CT theory, represented by eq 4, must be done using the experimental data of such a system. These data are now available from computer experiments.[1-3] These computer experiments have been performed in the following cases: (A) self-diffusion,[1] i.e., test particle equal to solvent particles; (B) isotopic diffusions,[2,3] i.e., the test particle having the same diameter, σ_T, as the solvent, σ_S, but different mass ($M_T \neq M_S$); (C) test particle having $M_T = M_S$ but $\sigma_T < \sigma_S$.[3]

Type A experiments allow for a check of the D dependence of V and T. Type B experiments mainly investigate the validity of the model proposed for the "basic dynamic event" (see eq 2), since the change in mass does not influence $p(v)$ as far as classical mechanics holds. Type C experiments check the dependence of v^* on the ratio $\sigma' = \sigma_T/\sigma_S$. The hard spheres data can be expressed by the general formula

$$D_{HS}\left(V,T,m = \frac{M_T}{M_S},\sigma'\right) = \frac{7.24 \times 10^{-5}}{(1+\sigma')^2}\sqrt{\frac{T}{M_T}}\, V_0^{1/3}\psi\left(\frac{V}{V_0},m,\sigma'\right) \text{ cm}^2/\text{s} \qquad (6)$$

where

$$\psi\left(\frac{V}{V_0},m,\sigma'\right) = f_{AW}\left(\frac{V}{V_0},m,\sigma'\right)\frac{V}{V_0}\frac{1}{g_{12}(\sigma_{12})}$$

$f_{AW}(V/V_0,m,\sigma')$ is the computer experiment correction to Enskog's theory and is given in ref 1–3 as D/D_E; $g_{12}(\sigma_{12})$ is the equilibrium radial distribution function at contact between the solute and the solvent;[10] $\sigma_{12} = (\sigma_T + \sigma_S)/2$.

Instead of comparing eq 4 with eq 6, we prefer to eliminate the trivial dependences on T, M_T, and V_0. Therefore we construct the quantity y as

$$y\left(\frac{V}{V_0},m,\sigma'\right) = \frac{D(V,T,m,\sigma')}{V_0^{1/3}\sqrt{\frac{T}{M_T}}} \qquad (7)$$

and we compare the y values in the cases A, B, and C.

(A) *Self-Diffusion* (i.e., $m = 1$, $\sigma' = 1$). We have

$$y_{HS}\left(\frac{V}{V_0}\right) = 1.81 \times 10^{-5} f_{AW}\left(\frac{V}{V_0},1,1\right)\frac{V}{V_0}\frac{1}{g(\sigma)} \qquad (8)$$

$$y_{CT}\left(\frac{V}{V_0}\right) = 1.87 \times 10^{-4}\, g\left(\frac{\frac{V}{V_0} - 1}{\gamma}\right)^{1/3} \int_{z^*}^{\infty} z^{1/3} e^{-z}\, dz \qquad (9)$$

All the quantities are in cgs units; $f_{AW}(V/V_0, m = 1, \sigma' = 1)$ is taken from Table I of ref 3. In Figure 1 we report y vs. $V_0/(V - V_0)$ both for the hard spheres and for the CT theory. The y_{CT} has been calculated taking the parameters $g/\gamma^{1/3} = 0.28$ and $\gamma v^* = 1.59(V_0/N)$ (which implies $g' = 0.43$ and $\gamma' v^* = 1.69\ (V_0/N)$ in eq 5); these values for the parameters are found to give the best fit to the y_{HS} data, moreover, they are quite reasonable from a physical point of view.

The most important conclusion drawn from Figure 1 is that, choosing the best values for the parameters, the CT expression for D agrees with the "experiments" only in the

TABLE I: α of Eq 15 as a Function of V/V_0 and σ'

σ'	V/V_0 = 1.6	V/V_0 = 3.0
1	0.44	0.36
3/4	0.45	0.24
1/2	0.29	0.17
1/4	0.15	0.10

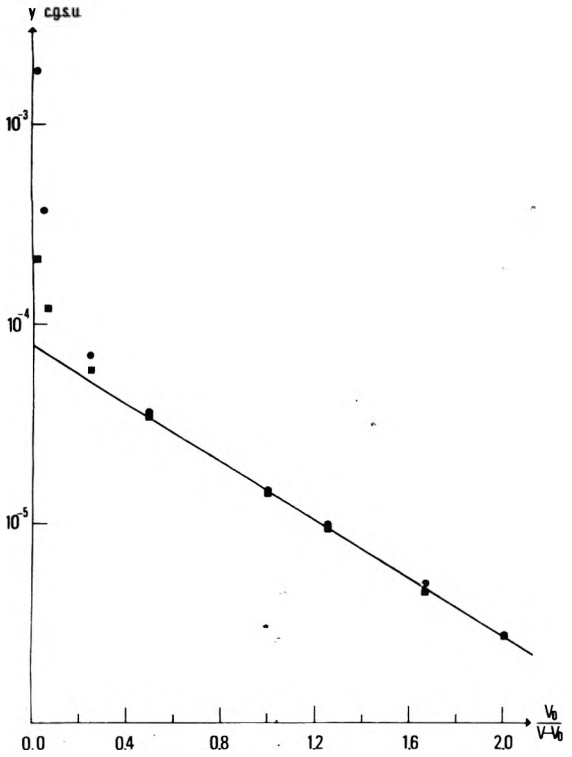

Figure 1. y vs. $V_0/(V - V_0)$: (●) values of y_{HS}; (■) values of y_{CT} numerically evaluated from eq 8 using $g\gamma^{-1/3} = 0.28$ and $\gamma v^* = 1.59(V_0/N)$; the straight line is given by $y = 8.04 \times 10^{-5} \exp\{-1.69[V_0/(V - V_0)]\}$ and is the best fit of both y_{HS} and y_{CT} in the range $1.5 \leq V/V_0 \leq 3$.

range $1.5 \leq V/V_0 \leq 3$ where both D_{CT} and D_{HS} can be expressed as

$$D(V,T) = 8.04 \times 10^{-5} V_0^{1/3} \sqrt{\frac{T}{M}} \times \exp\left(-\frac{1.69V_0}{V - V_0}\right) \text{cm}^2/\text{s} \quad (10)$$

For $V/V_0 > 3$, D_{CT} always remains lower than D_{HS}. The range $1.5 \leq V/V_0 \leq 3$ is limited on the high density side by the melting process while its low density boundary corresponds to the density region where the behavior of $(\partial\eta/\partial T)_{\rho=\text{constant}}$ vs. ρ suggests a transition from liquidlike to gaslike behavior.[11] Moreover at $V/V_0 \simeq 3$ the computer experiments[1] too show that the "cage" effect begins to become quantitatively important.

(B) *Isotopic Diffusion* (i.e., $m \neq 1$, $\sigma' = 1$). In this case we have

$$y_{HS}\left(\frac{V}{V_0},m\right) = 1.81 \times 10^{-5} f_{AW}\left(\frac{V}{V_0},m,1\right) \frac{\sqrt{\frac{m+1}{2}}}{g(\sigma)} \frac{V}{V_0} \quad (11)$$

$y_{CT}(V/V_0, m)$ remains identical with eq 9 since y_{CT} does not depend on m; $f_{AW}(V/V_0, m, 1)$ is taken from ref 2 for $m = 4$ and from ref 3 for $m \leq 1$.

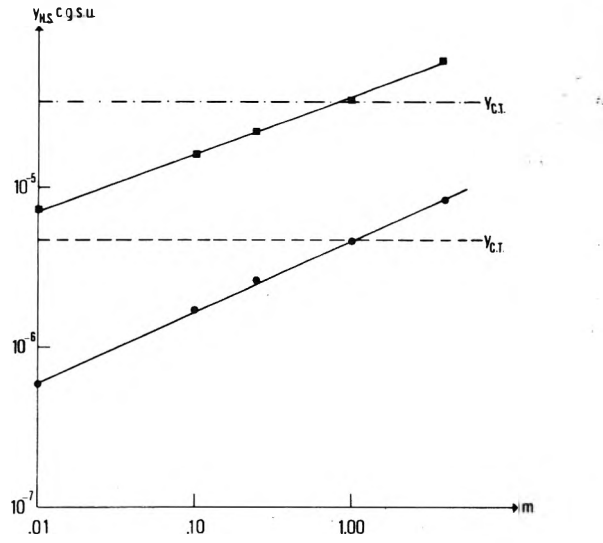

Figure 2. $y_{HS}(m)$ vs. m for $V/V_0 = 1.6$ (●) and $V/V_0 = 3$ (■). The lines - - - and – · – · – are the values of y_{CT} at $V/V_0 = 1.6$ and 3, respectively. The full lines are the equations $y = 8.04 \times 10^{-5} \exp[-1.69V_0/(V - V_0)]m^{0.44}$ for $V/V_0 = 1.6$ and $y = 8.04 \times 10^{-5} \exp[-1.69V_0/(V - V_0)]m^{0.36}$ for $V/V_0 = 3$.

The comparison between y_{HS} and y_{CT} has been made for various values of m at $V/V_0 = 1.6$ and $V/V_0 = 3$; the results are shown in Figure 2. It can be easily seen that the CT theoretical predictions strongly disagree with the "experimental" results y_{HS}. In fact y_{CT} is independent of m, while y_{HS}, for $1.6 \leq V/V_0 \leq 3$, can be represented very well by

$$y_{HS}\left(\frac{V}{V_0},m\right) = 8.04 \times 10^{-5} m^{\alpha} \exp\left(-\frac{1.69V_0}{V - V_0}\right) \quad (12)$$

where α, obtained by the best fit of Figure 2, turns out to be $\alpha = 0.44$ for $V/V_0 = 1.6$ and $\alpha = 0.36$ for $V/V_0 = 3$.

We want to stress that the failure of CT theory, in the case of isotopic diffusion, clearly demonstrates that the single particle motion underlying eq 2 is incorrect. The microscopic model from which the $D(v)$ expression is obtained must describe the motion of few correlated particles. Furthermore we think that the increase of α with density means that the number of these correlated particles increase with density; in fact $\alpha = 0$ indicates the single particle motion.

(C) *Test Particle with Different Size* (i.e., $m = 1$, $\sigma' < 1$). In this case we have

$$y_{HS}\left(\frac{V}{V_0},1,\sigma'\right) = \frac{7.24 \times 10^{-5}}{(1 + \sigma')^2} f_{AW}\left(\frac{V}{V_0},1,\sigma'\right) \frac{(V/V_0)}{g_{12}(\sigma_{12})} \quad (13)$$

while y_{CT} does not depend on σ_T if $\sigma_T < \sigma_S$ (see the discussion about v^*[4]); $f_{AW}(V/V_0, 1, \sigma')$ values are taken from Table I of ref 3. Using these data both for $V/V_0 = 1.6$ and for $V/V_0 = 3$, eq 13 can be fitted quite well by the expression

$$y_{HS}\left(\frac{V}{V_0},1,\sigma'\right) = A(\sigma') \exp\left\{-\frac{\gamma(\sigma')V_0}{V - V_0}\right\} \quad (14)$$

where $A(\sigma')$ and $\gamma(\sigma')$ are given in Figure 3a and 3b and do not depend on V/V_0. From Figure 3b we can see that

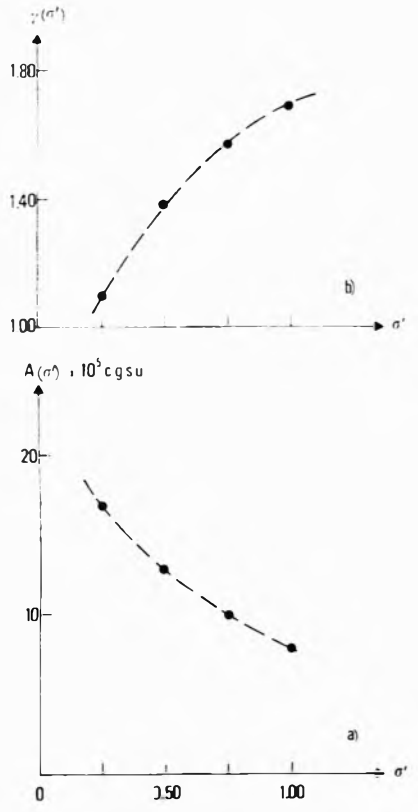

Figure 3. (a) $A(\sigma')$ vs. σ' and (b) $\gamma(\sigma')$ vs. σ'. The lines have been drawn by hand through the calculated points.

γ depends on σ' and this contradicts the predictions of the CT theory.

According to our views this failure of the CT theory indicates that v^* is dependent on σ' even if $\sigma' < 1$ and this shows again that the local dynamic event (see eq 2) is wrongly described by the CT theory.

The tests made in A, B, and C suggest the following remarks about the CT theory.

(1) The CT theory indicates that the density fluctuation is the only meaningful parameter which allows the diffusion process. This density fluctuation involves a big number of particles so that it can be regarded as a collective property. The analysis we made in A, B, and C does not contradict this basic idea since in any case the "experimental" data suggest an exponential behavior with the density and this behavior turns out to be the one predicted by the CT theory. The same conclusion was suggested in ref 18.

(2) The CT theory suggests that when we have density fluctuations "big enough", the diffusive motion proceeds like a single particle motion (see eq 2). The tests done in B and C clearly demonstrate the failure of such a picture.

The "experimental" data indicate that the basic dynamic event involves more than one particle; therefore eq 2 must be disregarded and other models must be proposed where the correlation of few particles can explain the "experimental" dependence of D on M_T and σ_T. We want to remark that the inadequacy of the model, for which the "diffusive motion" proceeds like a single particle motion, was already pointed out by Frenkel[12] with respect to diffusions of solutes having size smaller than the solvent. Frenkel stresses that the fluctuations in local free volume, which involve many particles, are responsible both for the hole formation, in which the solute molecule can jump, and for the disappearance of the void left behind by the solute.

Finally we want to indicate that if the test particle has both the mass and the size different from the solvent particles (i.e., $m \neq 1$ and $\sigma'^* \neq 1$), a generalization of eq 12 and 14 gives

$$D_{HS}\left(\frac{V}{V_0},T,m,\sigma'\right) = A(\sigma')\sqrt{\frac{T}{M_S}}\left(\frac{M_S}{M_T}\right)^{0.5-\alpha} V_0^{1/3} \times \exp\left\{-\frac{\gamma(\sigma')V_0}{V-V_0}\right\} \text{ cm}^2/\text{s} \quad (15)$$

where, as before, $V_0 = N\sigma_s^3/2^{1/2}$; $A(\sigma')$ and $\gamma(\sigma')$ are given in Figure 3; α is given in Table I as a function of V/V_0 and σ'. These α values are obtained fitting the y_{HS}, derived from ref 3 for fixed values of V/V_0 and σ', with the expression $y_{HS}(m) = \text{constant} \times m^{\alpha}$.

Extension of the Macedo–Litovitz Hybrid Expression

Macedo and Litovitz[7] pointed out that in the case of self-diffusion in real fluids, in addition to density fluctuations, energy fluctuations are important too.

Therefore the value of the transport coefficient must depend both on density fluctuations and on energy fluctuations. Following this idea they[7] write $D = Ap_E p_v$ where p_E is the probability to have "enough" energy and p_v is the probability that "enough" free volume is present so that the diffusion can occur. p_v and p_E can be evaluated[13] in a way similar to Cohen and Turnbull in eq 3.

In such hypothesis $D(V,T)$ turns out to be

$$D_{ML}(V,T) = D_0 \exp\left\{-\gamma\frac{V_0}{V-V_0} - \frac{E_v^*}{RT}\right\} \quad (16)$$

where E_v^* is the energy threshold value to allow diffusion (as v^* for the free volume); for the sake of simplicity D_0 is taken to be constant. In the density region $1 \leq V/V_{tr} \leq 2$ expression 16 has been found[8] to describe quite well the density and the temperature behavior of self-diffusion in a Lennard-Jones fluid, in CH_4, Kr, and C_6H_6, using $\gamma = 1$; V_0 and E_v^* are determined for each substance by fit. Using the value of V_0 found by the fit we can translate the condition $1 \leq V/V_{tr} \leq 2$ in $1.7 \leq V/V_0 \leq 3.4$. We want to stress that the parameters V_0 and E_v^* for the various substances result in good agreement with each other within the limits where the corresponding state theory holds.[8] The Macedo–Litovitz theory has also been found successful in the viscosity case[9] with the same limitations as concerns the density range.

We want to reconsider the Macedo and Litovitz ideas keeping in mind what we found in the previous section of this paper. First of all we can easily understand why eq 16 is successful only in this density region; we have found, in fact, in Figure 1 that the role of the density fluctuations can be represented as an exponential in terms of $V_0/(V - V_0)$ only if $1.5 \leq V/V_0 \leq 3$.

Secondly we propose expressing quantitatively the ideas of Macedo and Litovitz not by eq 16, but as

$$D(V,T) = D_{HS}(V,T)\int_{E^*}^{\infty} p(E)\,dE \quad (17)$$

where $p(E)\,dE$ is the probability that the energy per particle has the value $E \leq E \leq E + dE$. Taking for $p(E)$ the expression derived by Chung[13] we have

$$D(V,T) = CD_{HS}(V,T)e^{-E^*/RT} \quad (18)$$

where C is a numerical factor of the order of unity. Equation 18 takes a simple analytical form if we only

TABLE II: Results of the Fits of $D^* = f(V^*,T^*)$ Using Eq 16 and 19[a]

	LJ[b]	Kr[c]	CH_4[c]	C_6H_6[c]
$\chi^{2d,e}$	0.6	1.0	0.7	0.2
V_0,[d] cm³/mol	18.1 ± 1.0	22.0	24.2	62.4
E_v^*,[d] cal/mol	300 ± 43	420	364	1124
$\chi^{2e,f}$	0.5	0.5	0.95	0.67
V_0,[f] cm³/mol	15.6 ± 1.4	17.3	20.2	55.6
E_v^*,[f] cal/mol	184 ± 44	306	210	825
C^f	1.45	1.28	1.49	2.36

[a] $D^* = [D(V,T)/D(V_{tr},T_{tr})]$, $T^* = (T/T_{tr}), V^* = V/V_{tr}$ where the subscript tr represents the triple point. [b] The parameters V_0 and E^* are obtained from the fit and their uncertainties are taken such that for values outside this range $P(\chi^2) \leq 0.05$. The LJ fluid we considered has $\sigma = 3.4 \times 10^{-8}$ cm and $\epsilon/K = 120$ K. [c] The values of V_0 and E^* are obtained from the fit with the only conditions that they must be in the ranges $V_0 \pm \Delta V_0$ and $E^* \pm \Delta E^*$ where V_0 and E^* are taken from the LJ fluid values using the corresponding state idea (i.e., $V_{0,i} = V_{0,LJ}(\sigma_i/\sigma_{LJ})^3$; $E_i^* = E_{LJ}^*(\epsilon_i/\epsilon_{LJ})$ and ΔV_0 and ΔE^* must take into account both the indeterminations obtained for E_{LJ}^* and $V_{0,LJ}$ and the deviations of the ith fluid from the corresponding state behavior, i.e.

$$\left(\frac{\Delta V_0}{V_0}\right)_i = \left(\frac{\Delta V_0}{V_0}\right)_{LJ} + 3\frac{\Delta\sigma_i}{\sigma_i}; \quad \left(\frac{\Delta E^*}{E^*}\right)_i = \left(\frac{\Delta E^*}{E^*}\right)_{LJ} + \frac{\Delta\epsilon_i}{\epsilon_i}$$

We choose for $\Delta\sigma_i$ and $\Delta\epsilon_i$ the values obtained as half the differences of the parameters derived from triple and critical points. [d] Fit using eq 16, i.e.

$$D^* = \frac{e^{-V_0/(V-V_0)}e^{-E_v^*/RT}}{e^{-V_0/(V_{tr}-V_0)}e^{-E_v^*/RT_{tr}}}$$

[e] χ^2 is defined as

$$\left\{\sum_{i=1}^{N}\left(\frac{D^{(i)}_{expt} - D^{(i)}_{calcd}}{\Delta D^{(i)}_{expt}}\right)^2 \Big/ (N - p + 1)\right\}$$

where N is the number of $D^{(i)}$ values used in the fit and p is the number of free parameters in the theoretical expression for D_{calcd}. [f] Fit using eq 19, i.e.

$$D^* = \sqrt{\frac{T}{T_{tr}}}\frac{e^{-1.69V_0/(V-V_0)}e^{-E^*/RT}}{e^{-1.69V_0/(V_{tr}-V_0)}e^{-E^*/RT_{tr}}}$$

consider the density range $V/V_0 \simeq 1.5$–3. In fact recalling eq 10 we can write eq 18 as

$$D(V,T) = C \times 8.04 \times 10^{-5} \times \sqrt{\frac{T}{M}} V_0^{1/3} \exp\left[-\frac{1.69V_0}{V-V_0} - \frac{E^*}{RT}\right] \quad (19)$$

Using eq 19 we repeated the fits of the self-diffusion coefficient in the Lennard-Jones fluid, Kr, CH_4, and C_6H_6 (i.e., the same data used in ref 8), leaving V_0 and E^* as parameters to be determined by the fit.

The results are reported in Table II and we can see that, using eq 19, the agreement is as satisfactory as in the case of eq 16.

However, we want to stress that, in our opinion, eq 19 is better than eq 16 for the following reasons:

(1) It gives the same agreement as eq 16, so far as the density and temperature behavior of self-diffusion in real fluids are concerned.

(2) Equation 19 makes the connection between the hard spheres case and the real fluids very clear showing that, in the diffusion process too, the hard sphere system is a good approximation to the real fluid. It is also easy to expand D/D_{HS} vs. ϵ/KT and this expansion agrees quite satisfactorily with what was found in the case of square well fluid with respect to the hard sphere fluid.[14] On the contrary, eq 16 makes the connection with the hard sphere case looser, mainly as far as the preexponential term, D_0, is concerned.

(3) Equation 19 can be very easily extended to describe the impurity diffusion, being enough to use eq 15 instead of eq 10 for D_{HS} in eq 18 and to reconsider the meaning of E^*. On the contrary in the case of eq 16 the extension to mixtures is by no means obvious.

We want now to extend eq 19 to the case of the impurity diffusion, and therefore we want to reconsider E^*. In the case of self-diffusion E^* depends only on one type of interaction while in the case of a dilute mixture E^* must depend both on solute–solvent and on solvent–solvent interaction (solute–solute interactions are not present since the solute concentration is very low). The relative importance of the two interactions depends on the degree of cooperativity of the basic dynamic event; we can, in a first approximation, take their relative importance to be the same as the one appearing in the mass dependence. Therefore, if we only consider the density range $1.6 \leq V/V_0 \leq 3$, using eq 15 we have

$$D(V,T,m,\sigma') = CA(\sigma')\sqrt{\frac{T}{M_S}}\left(\frac{M_S}{M_T}\right)^{0.5-\alpha} V_0^{1/3} \times \exp\left\{-\frac{\gamma(\sigma')V_0}{V-V_0} - \frac{E_{mix}^*}{RT}\right\} \quad (20)$$

with

$$E_{mix}^* = \left(\frac{\epsilon_{ST}}{\epsilon_{SS}} + 2\alpha\frac{\epsilon_{SS} - \epsilon_{ST}}{\epsilon_{SS}}\right)E_S^* \quad (21)$$

where E_S^* and V_0 are the E^* and V_0 values that we have for the self-diffusion of the pure solvent, ϵ_{ij} and σ_{ij} are the Lennard-Jones parameters for $i-j$ interaction (we used the combination rules $\sigma_{ij} = (\sigma_i + \sigma_j)/2$ and $\epsilon_{ij} = (\epsilon_i\epsilon_j)^{1/2}$).

Equation 20 can be tested with the experimental data available in the literature.[6,15]

To test the density and temperature behavior we construct for each impurity diffusion in the same solvent the quantity

$$R = \frac{D(V_1,T_1,m,\sigma')}{D(V_2,T_2,m,\sigma')}$$

We report $(R_{expt} - R_{calcd})/\Delta R_{expt}$ vs. M_T in Figure 4a for the diffusions in liquid N_2[6] and in Figure 4b for the diffusions in liquid CCl_4;[15] R_{calcd} is the value calculated by eq 20 and ΔR_{expt} is the error due to the experimental errors which from ref 6 and 15 was found equal to 10% of R_{expt}.

To test the dependence of the diffusing impurity on the parameters we construct the quantity

$$S_{i,0} = \frac{D(V,T,m_i,\sigma_i')}{D(V,T,m_0,\sigma_0')}$$

where the index 0 means an impurity taken as reference; we choose CH_4 as the impurity reference. $(S_{i,0})_{calcd}$ can be easily obtained by eq 20 if we suppose that the factor C does not depend on the impurity parameters in a fixed solvent. We report $[(S_{i,0})_{expt} - (S_{i,0})_{calcd}]/(\Delta S_{i,0})_{expt}$ in Figure 5a for diffusions in N_2[6] and in Figure 5b for diffusions in CCl_4.[15,16] In Table III we report the ϵ/K and σ values we used for the various substances.

TABLE III: (ϵ/K, σ) Values Used in Figures 4 and 5[a]

Substance	ϵ/K, K	σ, Å
H_2	37	2.92
D_2	37	2.92
H_e	10.2	2.57
T_2	37	2.92
CH_4	129.5	3.62
Ne	37	2.83
N_2	90.2	3.58
A_r	120	3.43
CF_4	152.5	4.70
CCl_4	357	5.73

[a] The ϵ/K and σ values are derived from the triple point using the relationships $T_{tr} = 0.7(\epsilon/K)$ and $V_{tr} = N\sigma^3/0.85$ except for CF_4 and CCl_4 for which we used the values reported in ref 15.

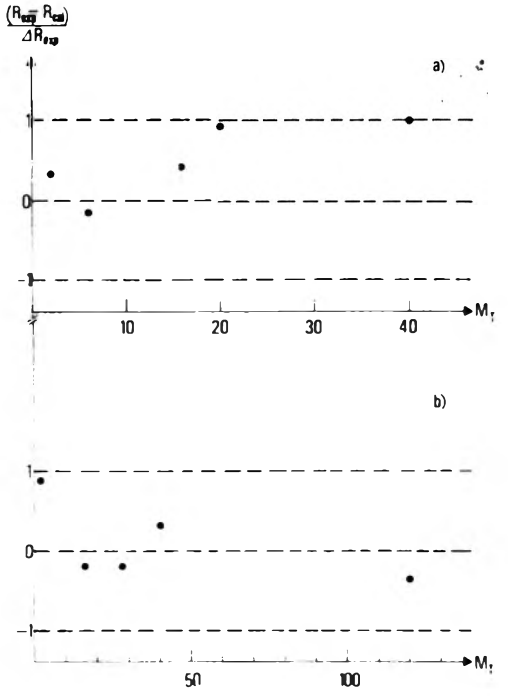

Figure 4. (a) $(R_{expt} - R_{calcd})/\Delta R_{expt}$ vs. M_T for diffusions in liquid N_2.[6] V_0 and E_S^* are translated from the LJ fluid as follows: $V_0 = 15.6 \times (32.2/27.9) = 18.0$ cm^3/mol and $E_S^* = 184 \times (63.2/84) = 138.4$ cal/mol. (b) The same as a for diffusions in liquid CCl_4.[15] $V_0 = 60$ cm^3/mol and $E_S^* = 680$ cal/mol.

As we can see from Figures 4 and 5 the agreement is satisfactory since it is well within $\pm 3\sigma$ where σ is the experimental error; this is remarkable if we consider that the diffusion coefficients we examined are differently up to a factor 7 and refer to solvents as different as N_2 and CCl_4.

Therefore we think that our generalization of the Macedo–Litovitz hybrid expression, given in eq 20, is meaningful as a first approximation. Moreover we want to remark that it makes very clear both the meaning of the so-called "activation energy" and why this "activation energy" turns out to be independent on the solute parameters as stressed in ref 6 and noted in ref 12 (see p 201).

Conclusions

In this paper we compared the hard sphere "experimental" diffusion coefficients with the predictions of the free-volume (CT) theory. This analysis shows (1) the limits of the validity of the CT theory and (2) that there is evidence of the many particle correlated motion for every diffusion step and, moreover, that the number of these particles is dependent both on the density and on the dimension of the diffusing particle with respect to the solvent particles (see the α behavior).

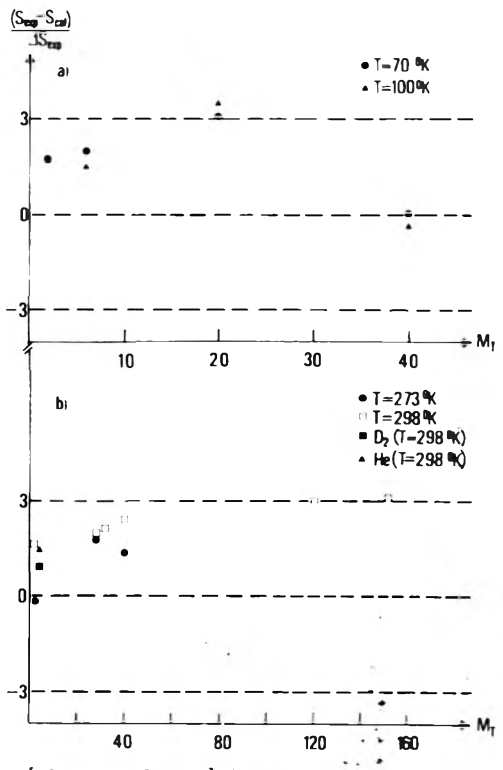

Figure 5. $[(S_{i0})_{expt} - (S_{i0})_{calcd}]/\Delta(S_{i0})_{expt}$ vs. M_T for diffusions in liquid N_2 (a) and CCl_4 (b). The values of V_0 and E_S^* are the same as in Figure 4a.

Moreover, we proposed an improved version of the Macedo–Litovitz hybrid expression. Our version, see eq 20, describes satisfactorily the experimental data of the impurity diffusions besides the ones of the self-diffusion.

In addition, eq 20 makes very clear in what sense the hard sphere fluid can be considered a good approximation to the real fluid also for the diffusion process.

From the present analysis we stress that an effort should be made to construct a model which can explain the mass dependence in the case of isotopic diffusion. It would be enough to have such a model for the hard spheres. Moreover some more "computer experiments" on the hard sphere mixture, in the region $V/V_0 \simeq 2$, would be very useful, as well as other experimental data on the real fluid mixtures, only if these experimental data were over a large density range (in the present data the density varies at most 20%) or over a large temperature range at constant density; of course the density should remain in the range $1.5 \lesssim V/V_0 \lesssim 3$ where useful comparisons can be done. In our opinion a second step would be to bridge the high density with the low density region (i.e., to go from $V/V_0 \sim 3$ to $V/V_0 \sim 100$ or higher) where the solution of the Boltzmann equation exists.

Acknowledgment. This work was supported by the Gruppo Nazionale di Struttura della Materia of the Consiglio Nazionale delle Ricerche.

References and Notes

(1) B. J. Alder, D. M. Gass, and T. E. Wainwright, *J. Chem. Phys.*, **53**, 3813 (1970).
(2) P. T. Herman and B. J. Alder, *J. Chem. Phys.*, **56**, 987 (1972).
(3) B. J. Alder, W. E. Alley, and J. H. Dymond, *J. Chem. Phys.*, **61**, 1415 (1974).
(4) M. H. Cohen and D. Turnbull, *J. Chem. Phys.*, **31**, 1164 (1959).
(5) J. Naghizadeh and S. A. Rice, *J. Chem. Phys.*, **36**, 2710 (1962).
(6) F. P. Ricci, *Phys. Rev.*, **156**, 184 (1967).
(7) P. B. Macedo and T. A. Litovitz, *J. Chem. Phys.*, **42**, 245 (1965).
(8) F. P. Ricci, M. A. Ricci, and D. Rocca, *Nuovo Cimento B*, **28**, 287 (1975).

(9) K. E. Gubbins and M. J. Tham, *AIChE J.*, **15**, 264 (1969).
(10) g(σ) values are taken from the relationship given on p 1418 and Figure 7 of ref 3.
(11) N. F. Zhdanova, *Sov. Phys. JETP*, **4**, 19 (1957); **4**, 749 (1957).
(12) J. Frenkel, "Kinetic Theory of Liquids", Dover Publications, New York, N.Y., 1955 p 200.
(13) H. S. Chung, *J. Chem. Phys.*, **44**, 1362 (1966).
(14) W. E. Alley and B. J. Alder, *J. Chem. Phys.*, **63**, 3764 (1975).
(15) M. Ross and J. H. Hildebrand, *J. Chem. Phys.*, **40**, 2397 (1964).
(16) K. Nakanishi, E. M. Voight, and J. H. Hildebrand, *J. Chem. Phys.*, **42**, 1860 (1965).
(17) B. J. Alder and T. E. Wainwright, *Phys. Rev. Lett.*, **18**, 988 (1967). This paper reports the first results of the diffusion coefficient as a functior of density in a hard spheres system. Reference 1 reports more complete data on the same subject.
(18) D. Turnbull and M. H. Cohen, *J. Chem. Phys.*, **52**, 3038 (1970).

Aqueous Solutions of Azoniaspiroalkane Halides. 3. Dielectric Relaxation

Wen-Yang Wen*

Jeppson Laboratory, Chemistry Department, Clark University, Worcester, Massachusetts 01610

and Udo Kaatze

Drittes Physikaiisches Institut der Universitaet Goettingen, D-3400 Goettingen Federal Republic of Germany *(Received August 30, 1976)*

Complex dielectric constants of aqueous solutions of azoniaspiroalkane bromides, $(CH_2)_nN^+(CH_2)_nBr^-$ (n = 4, 5, or 6) have been measured at eight frequencies in the range of 3 to 40 GHz at 25 °C by an interferometric transmission method. The observed data were fitted to the Cole function and also to a sum of Debye functions to yield the mean dielectric relaxation time in the former case and the hydration number and the reorientation time of the hydration water in the latter case. These parameters for azoniaspiroalkane bromides are compared with those of the tetraalkylammonium bromides for the purpose of gaining insight into the effect of the hydrophobic ions upon the dynamics of the surrounding water. A noteworthy result is that the dielectric relaxation times of water around the azoniaspiroalkane ions are appreciably shorter than those around the corresponding tetraalkylammonium ions.

Introduction

Previous thermodynamic investigations on the solution properties of hydrophobic ions containing either linear or cyclic alkyl groups have shown some important differences among the properties of these two types of solutes.[1-4] In view of the current wide interest toward the tetraalkylammonium ions as typical hydrophobic species,[5] it will be of interest to make a comparative study of the solution behavior of their counterpart azoniaspiroalkane ions. Since the latter type of ions have no terminal methyl groups, the study should provide information on the role of geometrical and dynamic configurational effects in the solution properties of alkyl-substituted quaternary ammonium salts.

In the previous papers of this series, enthalpies of solution,[1] apparent molal volumes, and heat capacities,[2] of azoniaspiroalkane halides have been reported. The results indicate that forming closed rings from the alkyl chains in tetraalkylammonium ions alter their thermodynamic properties and weaken the hydrophobic interaction of its hydration water considerably.

In this communication, we are reporting the results of our complex dielectric constant measurements of 1 M solutions of azoniaspiroalkane bromides at 25 °C. For one of the salts (6.6 Br) measurements were also carried out at concentrations of 0.67 and 0.33 M to study the concentration dependence. The data obtained are compared with those of the corresponding tetraalkylammonium bromides obtained by recalculating the data of Pottel and Lossen.[6] From the analysis of the dielectric data, reorientation times of water molecules surrounding these two types of hydrophobic ions have been compared and discussed.

Experimental Section

I. *Materials.* Azoniaspiroalkane bromides were synthesized by a method adapted from Blicke and Hotelling[7] and from Thomas and his co-workers.[8,9] The detailed procedures used for the purification and analysis of each product have been described in paper I.[1] The IUPAC names as well as our abbreviated names of the three compounds are as follows: (i) $(CH_2)_4N^+(CH_2)_4Br^-$, 5-azoniaspiro[4.4]nonane bromide, "4.4 Br"; (ii) $(CH_2)_5N^+(CH_2)_5Br^-$, 6-azoniaspiro[5.5]undecane bromide, "5.5 Br"; (iii) $(CH_2)_6N^+(CH_2)_6Br^-$, 7-azoniaspiro[6.6]tridecane bromide, "6.6 Br".

II. *Measurements.* The complex relative dielectric constant

$$\epsilon_{tot}(\nu) = \epsilon'(\nu) - i\epsilon''_{tot}(\nu)$$

of the solutions has been determined at eight frequencies, ν, between 3 and 40 GHz by frequency domain measurements. Five microwave interferometers of the Drittes Physikalisches Institut, Universitaet Goettingen, were used to cover the frequency range. Sample liquids were placed in the appropriate cylindrical waveguides and the propagating electromagnetic wave was transmitted through the waveguide. A receiving probe inserted in the liquid sample was shifted by a certain distance along the direction of wave propagation. The wavelength λ and the attenuation exponent $\alpha\lambda$ of the propagating wave were determined by moving the probe and by adjusting a reference signal of calibrated variable amplitude (and fixed phase) so that the probe signal and the reference signal would produce a maximum interference with zero signal. From the measured values of λ, $\alpha\lambda$, and ν, the dielectric constant was

TABLE I: Parameter Values for the Relaxation Function, $R_1(\nu)$, for the Aqueous Solutions of Azoniaspiroalkane Bromides and Tetraalkylammonium Bromides at 25 °C[a]

	c,[b] M ±0.1%	m,[b] mol (kg of H_2O)$^{-1}$ ±0.05%	c_w,[b] M ±0.1%	σ, Ω^{-1} m^{-1} ±2%	$\epsilon(\infty)$ ±0.5	$\epsilon(0)$ ±1%	τ_s, ps	h ±0.007	B_d, kg of H_2O mol^{-1} ±2%
$(CH_2)_3N^+(CH_2)_4Br^-$	1.094	1.3167	46.12	5.32	4.46	62.68	11.12 ± 0.02	0.055	0.257
$(CH_2)_5N^+(CH_2)_5Br^-$	1.008	1.2290	45.51	4.44	4.68	60.27	11.62 ± 0.02	0.052	0.333
$(CH_2)_6N^+(CH_2)_6Br^-$	0.3362	0.3478	51.66	1.85	3.00	72.99	9.35 ± 0.02	0.064	0.400
	0.6723	0.7452	48.16	3.14	4.91	63.59	10.85 ± 0.02	0.040	
	1.019	1.2882	43.89	3.91	5.03	56.44	12.49 ± 0.05	0.051	
$(CH_3)_4N^+Br^-$	0.500	0.529	52.28	3.86	5.16	71.96	8.77 ± 0.04	0.017	0.137
	1.00	1.129	49.03	6.79	5.23	66.35	9.40 ± 0.02	0.022	
	1.50	1.808	45.92	9.04	4.83	61.48	10.27 ± 0.04	0.048	
	2.00	2.592	42.70	10.58	5.54	55.89	11.21 ± 0.10	0.041	
$(C_2H_5)_4N^+Br^-$	1.00	1.204	45.97	4.64	4.58	62.21	11.82 ± 0.06	0.059	0.355
$(C_3H_7)_4N^+Br^-$	1.00	1.297	42.66	2.79	4.45	56.67	15.74 ± 0.03	0.087	0.693
$(C_4H_9)_4N^+Br^-$	0.500	0.584	47.41	1.83	4.63	64.32	12.30 ± 0.02	0.063	0.851
	1.00	1.406	39.35	2.03	4.52	51.33	$18.06^{+0.30}_{-0.10}$	0.099	

[a] The last column gives the relative molal shift of the mean dielectric relaxation time, B_d, defined according to eq 4. [b] Uncertainties of concentrations for the tetraalkylammonium solutions are greater.

calculated by the following equation

$$\epsilon_{tot}(\nu) = \left(\frac{c}{\lambda\nu} - i\frac{c(\alpha\lambda)}{2\pi\nu\lambda}\right)^2 + \left(\frac{c}{\nu\lambda_c}\right)^2$$

where c is the speed of light and λ_c is the cutoff wavelength of the empty waveguide used as the measuring cell. The frequency ν was determined and kept constant during the measurement with an uncertainty of less than 0.1%. Imperfection of the apparatus, uncertainty in measurements, and temperature fluctuation resulted in an estimated error of less than 2% in the values of ϵ' and ϵ''_{tot} obtained. A more detailed description of this interferometric transmission method and a discussion of error sources are given in ref 10.

Treatment of Data

In Figure 1 the dependence of ϵ' and ϵ''_{tot} on the frequency ν is displayed for water and for an aqueous 6.6 Br solution. In general the complex dielectric constant can be represented by the low frequency dielectric constant $\epsilon(0)$, the high frequency dielectric constant $\epsilon(\infty)$, a relaxation time distribution function $G(\tau)$, and the conductivity due to ion drift σ according to

$$\epsilon_{tot}(\nu) = \epsilon'(\nu) - i\epsilon''_{tot}(\nu) = \epsilon(\infty) + (\epsilon(0) - \epsilon(\infty)) \times \int_0^\infty \frac{G(\tau)\,d\tau}{1 + i2\pi\nu\tau} - i\frac{2\sigma}{\nu} \quad (1)$$

where $\int_0^\infty G(\tau)\,d\tau = 1$. Unfortunately (in the frequency range under consideration) the $\epsilon_{tot}(\nu)$ values reflect only weakly the fine details of $G(\tau)$. Thus it is not possible to calculate detailed properties of the relaxation time distribution function directly from the measured dependence of ϵ_{tot} on ν. So in order to get physically interpretable parameters and significant parameter values, we selected special types of $G(\tau)$ functions and fitted the corresponding relaxation functions $R(\nu)$ to the measured values. We used a non-linear least-squares fitting procedure to find the absolute minimum value of the variance given by

$$v = \frac{1}{I - 1}\sum_{i=1}^{I} |\epsilon_{tot}(\nu_i) - R(\nu_i)|^2$$

(where I is the number of frequencies of measurement). In order to avoid mathematical difficulties the frequency of measurement was treated as an exactly known independent variable in these calculations. This simplification is justified because the uncertainty of ν is much smaller

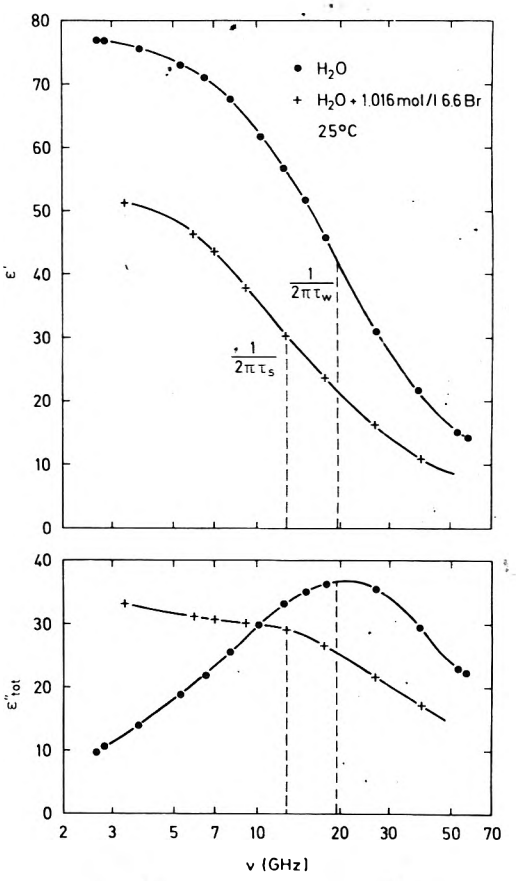

Figure 1. Real part, ϵ', and total imaginary part, ϵ''_{tot}, of the dielectric constants plotted vs. the frequency, ν, for pure water and an 1 M aqueous 6.6 Br solution at 25 °C.

than that of $\epsilon'(\nu)$ and $\epsilon''_{tot}(\nu)$ as mentioned above.

The simplest suitable relaxation function is

$$R_1(\nu) = \epsilon(\infty) + \frac{\epsilon(0) - \epsilon(\infty)}{1 + (i2\pi\nu\tau_s)^{(1-h)}} - \frac{i2\sigma}{\nu} \quad (2)$$

to which belongs a bell-shaped symmetric relaxation time distribution function $\tau G(\tau)$ ("Cole distribution function"[11]) when plotted vs. ln (τ/τ_s). Here τ_s denotes the mean relaxation time and h is a measure for the width of $G(\tau)$. The parameter values for $R_1(\nu)$ found for the different solutions are given in Table I. For comparison the corresponding values of the tetraalkylammonium bromide

solutions are included. These values were obtained by applying the fitting procedure described above to the $\epsilon_{tot}(\nu)$ data measured by Pottel and Lossen[6] in the frequency range 0.5–40 GHz. This recalculation of their data seemed necessary because Pottel and Lossen did not use the original $\epsilon_{tot}(\nu)$ values in their calculations. They measured the dc conductivity at 5 kHz in usual manner and separated the σ term from ϵ_{tot} according to

$$\epsilon(\nu) = \epsilon_{tot}(\nu) + \frac{i2\sigma(5\text{ kHz})}{\nu} = \epsilon'(\nu) - i\left(\epsilon''_{tot}(\nu) - \frac{2\sigma(5\text{ kHz})}{\nu}\right)$$

for the purpose of obtaining the dielectric constant $\epsilon(\nu)$ due to dielectric polarization processes only. However with this separation small errors of σ(5 kHz) yield large errors in $\epsilon(\nu)$. So it seems to be more suitable with highly conducting solutions to treat σ as an adjustable parameter in the fitting procedure.

Carrying out this procedure, we found the $\epsilon(0)$, $\epsilon(\infty)$, and τ_s values to be in good agreement with the respective values obtained by Pottel and Lossen who used a relaxation function slightly different from $R_1(\nu)$ to extrapolate to zero frequency and to high frequencies and to extract a mean dielectric relaxation time. The maximum deviations of their values from ours are 2% with $\epsilon(0)$, 15% with $\epsilon(\infty)$, and 1% with τ_s. In addition, within the limits of uncertainty the σ values obtained from the fitting procedure are found to be in agreement with those measured at 5 kHz. However there seems to be no indication for the existence of an additional low frequency relaxation which Pottel and Lossen assumed to be due to interactions between the ions.[6]

With regard to the function $R_1(\nu)$, the influence of the solute on the dielectric relaxation of water is expressed by a continuous spread of relaxation times τ. However, the dielectric relaxation of aqueous solutions is frequently assumed to be a superposition of a few relaxation terms, each characterized by a distinct relaxation time ("Debye" terms). Therefore, we also used the relaxation function

$$R_2(\nu) = \epsilon(\infty) + \frac{\epsilon(0) - \epsilon(\infty)}{c_w}\left[\frac{Z_h c}{1 + i2\pi\nu\tau_h} + \frac{Z_{Br}c}{1 + i2\pi\nu\tau_{Br}} + \frac{c_w - (Z_h + Z_{Br})c}{1 + i2\pi\nu\tau_w}\right] \quad (3)$$

This expression is based on the following model. The solvent water (molarity c_w) is subdivided into three subliquids: (1) the water molecules influenced by the cations ("hydration" water) with the concentration $Z_h c$ and the reorientation time τ_h ($\neq \tau_w$). (2) the hydration water of the Br^- with the concentration $Z_{Br}c$ and the reorientation time τ_{Br} (we fixed the parameter values to $Z_{Br} = 6.7$ and $\tau_{Br} = 6.2$ ps according to ref 12; (3) unperturbed water molecules between the hydration regions with the reorientation time $\tau_w = 8.25$ ps of pure water.

The reorientational motions of the different kinds of water molecules are assumed to be independent of each other. In addition, it is assumed that the water of each subliquid contributes to the static dielectric constant of the solution in proportion to its molar concentration.

We are aware that the validity of this model, when applied to the solutions under study may be questioned for the following reasons: (1) Since the solute concentration is rather high, there will be some overlaps of hydration regions. (2) As can be seen from Figure 2 the static dielectric constants of the tetraalkylammonium bromide solutions and of the azoniaspiroalkane bromide solutions are both a little smaller than those expected from nonconducting solutions. This small reduction may be due to kinetic depolarization of the water around ions caused by ion drift.[17]

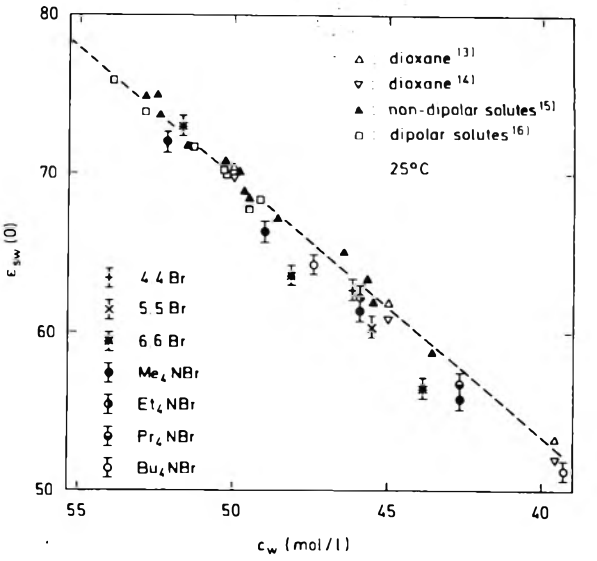

Figure 2. Static dielectric constant of the solvent water, $\epsilon_{sw}(0)$, plotted vs. the water concentration, c_w, for various types of solutes in aqueous solutions at 25 °C ($\epsilon_{sw}(0) = \epsilon(0)$ in the case of nondipolar solutes).

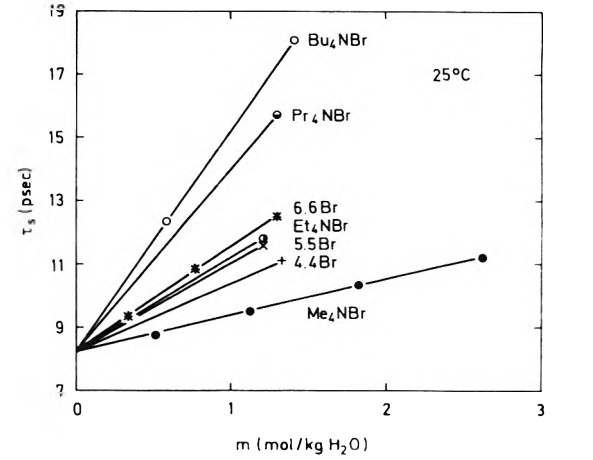

Figure 3. Mean dielectric relaxation time, τ_s, of the Cole function, $R_1(\nu)$, plotted vs. the solute molality, m, for aqueous solutions of azoniaspiroalkane bromides and tetraalkylammonium bromides at 25 °C.

In view of what we mentioned above the absolute values of τ_h and Z_h extracted from our calculations should not be overemphasized. However it seems to be of interest to compare the hydration behavior of the two series of organic ions using this model.

Results and Discussion

I. *Parameters Obtained by Fitting the Experimental Data to the Cole Function.* As shown in Figure 3, the plot of τ_s of the water in 6.6 Br solutions vs. salt molality m is a straight line which can be extrapolated back to pass through the pure water value $\tau_w = 8.25$ ps at 25 °C. For other azoniaspiroalkane bromides, we do not know their concentration dependence because we have data at only one concentration. However, since the linear dependence was also observed for Me_4NBr and Bu_4NBr, one may assume similar linear concentration dependence for 4.4 Br, 5.5 Br, as well as for Et_4NBr and Pr_4NBr. On this basis, straight lines were drawn passing through the pure water value τ_w as shown in Figure 3.

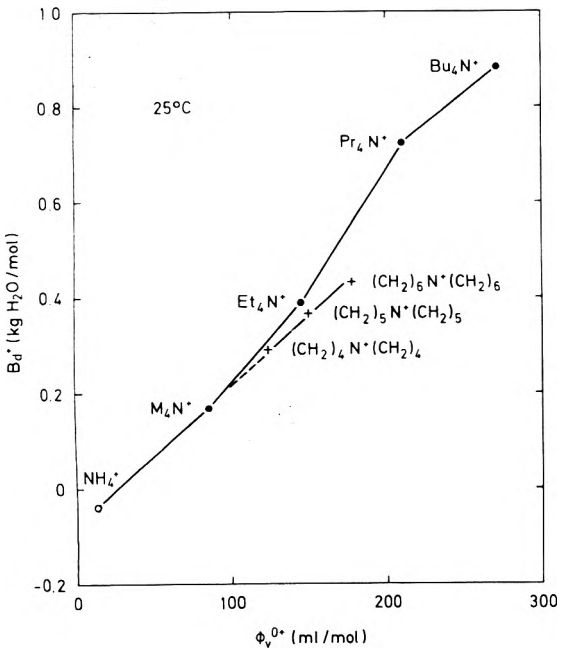

Figure 4. Relative molal shift of the mean dielectric relaxation time of the water due to the cation, B_d^+, plotted vs. the apparent molal volumes at infinite dilution, ϕ_v^{0+}, for the azoniaspiroalkane ions and the tetraalkylammonium ions at 25 °C [$\phi_v^{0+}(NH_4^+)$ from ref 18, $B_d^+(NH_4^+)$ from ref 19].

For solutions around 1 M concentration, the values of τ_s are 11.12, 11.62, and 12.49 ps for the 4.4 Br, 5.5 Br, and 6.6 Br, respectively (see Table I). These values are rather close to each other and also to the value of 11.82 ps observed for Et_4NBr, but they are considerably smaller than the value of 15.74 ps found for Pr_4NBr.

The relative molal shifts of the mean dielectric relaxation time, B_d, defined by

$$B_d = \frac{1}{\tau_w}\left(\frac{d\tau_s}{dm}\right)_{m\to 0} \qquad (4)$$

have been evaluated for the azoniaspiroalkane bromides and are given in Table I together with those for the tetraalkylammonium bromides. The values for the cations, B_d^+, obtained on the basis of the additivity rule and a B_d^- value of −0.032 kg of H_2O/mol for Br^-,[12] are plotted vs. the apparent molal volumes at infinite dilution, ϕ_v^{0+}, in Figure 4. These values of ϕ_v^{0+} are taken from paper II.[2] As to be expected, B_d^+ increases with the increase of the cationic volume for both types of hydrophobic cations. However, as shown in Figure 4, the rate of increase of B_d^+ from Et_4N^+ to Pr_4N^+ is substantially greater than the corresponding rate of increase for the azoniaspiroalkane ion series. This difference in the B_d^+ vs. ϕ_v^{0+} relations may be taken to indicate that there are factors other than the volume of hydrophobic cations which are important in influencing the value of B_d^+. These factors may include (a) presence or absence of the terminal methyl groups, and if terminal methyl groups are present, their distances from the charged nitrogen center, (b) flexibility of linear alkyl chains vs. the inflexibility of tightly packed cyclic alkyl groups, and (c) overall shape of the organic ions with respect to the arrangement of water molecules around them. These factors have been discussed in the previous papers,[1,2] and we may summarize the conclusion here as follows. The presence of flexible alkyl chains with terminal methyl groups seems to induce greater enhancement of water structure than the tightly packed cyclic alkyl groups. If this is accepted, then one may understand the reason

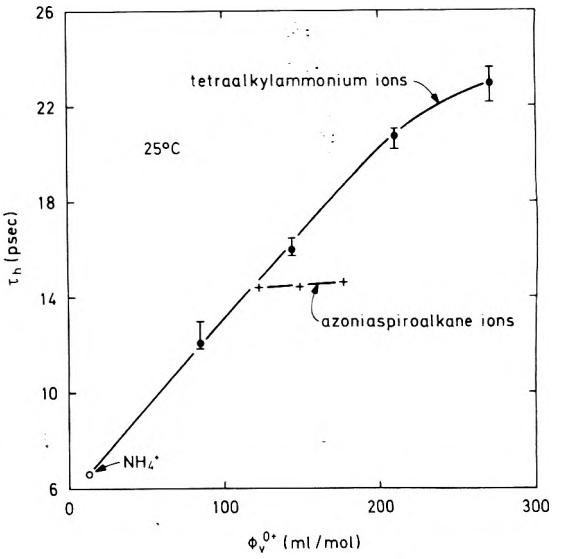

Figure 5. Reorientation time of the water around the cation, τ_h, plotted vs. the apparent molal cationic volumes at infinite dilution, ϕ_v^{0+}, for the azoniaspiroalkane ions and tetraalkylammonium ions at 1 M and 25 °C.

why B_d^+ for tetraalkylammonium ions is appreciably greater than that for azoniaspiro ions of similar volumes.

One should be aware of the fact that the solute concentrations in the present study are rather high and, consequently, there will be various ion–ion interactions (leading to cosphere overlap)[20] in addition to the ion–solvent interaction discussed above. However, in view of the observed linear dependence of the τ_s vs. m relation mentioned earlier, and in view of the fact that we are mainly interested in the comparison of two series of hydrophobic ions of similar sizes, we may ignore the complications arising from the ion–ion interactions. On the basis of these assumptions, the results of the present investigation are consistent with the results obtained from the previous thermodynamic studies carried out at very low concentrations. We conclude that the hydrophobic effect (solvent structural effect) is greater for the tetraalkylammonium ions than that for the azoniaspiroalkane ions of the similar size.

II. *Parameters Obtained by Fitting the Experimental Data to a Sum of Debye Functions.* The reorientation time of the hydration water around the cation, τ_h, at around 1 M is plotted vs. the apparent molal cationic volumes at infinite dilution, ϕ_v^{0+}, for the two types of cations in Figure 5. The values of τ_h increase steadily with ϕ_v^{0+} for the tetraalkylammonium ions, but in contrast τ_h is nearly constant for the three azoniaspiroalkane ions.

In Figure 6, the number of influenced water molecules per cation, Z_h, at around 1 M is plotted vs. the apparent molal cationic volume at infinite dilution, ϕ_v^{0+}, for the two types of cations for comparison. The rate of increase of Z_h with ϕ_v^{0+} seems to be slightly greater for the azoniaspiroalkane ions than that for the tetraalkylammonium ions. The results of our hydration model seem to imply that the increase of τ_s in the Cole function in going from $(CH_2)_4N^+(CH_2)_4$ to $(CH_2)_5N^+(CH_2)_5$, and to $(CH_2)_6N^+(CH_2)_6$ is mainly due to the increase of the hydration number Z_h and not due to any appreciable increase of the reorientation time of the hydration water, τ_h.

In conclusion, forming closed loops from the alkyl chains in the tetraalkylammonium ions has a substantial effect in decreasing the dielectric relaxation time of water surrounding them. The effect usually associated with the hydration of hydrophobic solutes is considerably reduced for the spiro ions, presumably due to their "wrong shape",

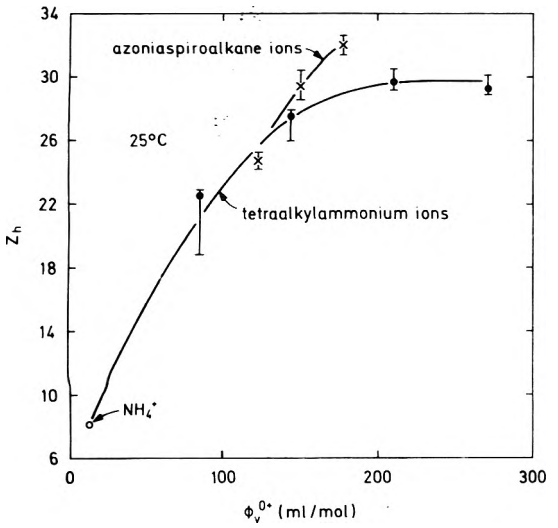

Figure 6. Number of influenced water molecules per cation, Z_h, plotted vs. the apparent molal cationic volumes at infinite dilution, ϕ_v^{0+}, for the azoniaspiroalkane ions and tetraalkylammonium ions at 1 M and 25 °C.

exposed charged nitrogen center, absence of terminal methyl groups, and lack of flexible alkyl chains.

Acknowledgment. We thank Professor R. Pottel for his interest in this work and helpful discussions. One of us (W.Y.W.) wishes to express his deep gratitude to Professor Pottel, Dr. Giese, and other people at Drittes Physikalisches Institut der Universität Göttingen for the kind assistance generously rendered to him during his stay.

References and Notes

(1) D. P. Wilson and W.-Y. Wen, *J. Phys. Chem.*, **79**, 1527 (1975). (Paper I of the series.)
(2) W.-Y. Wen, A. LoSurdo, C. Jolicoeur, and J. Boileau, *J. Phys. Chem.*, **80**, 466 (1976). (Paper II of the series.)
(3) C. Jolicoeur, J. Boileau, S. Bazinet, and P. Picker, *Can. J. Chem.*, **53**, 716 (1975).
(4) S. Cabani, G. Conti, and L. Lepori, *J. Phys. Chem.*, **76**, 1338, 1343 (1972); **78**, 1030 (1974).
(5) W.-Y. Wen, "Aqueous Solutions of Symmetrical Tetraalkylammonium Salts", in "Water and Aqueous Solutions", R. A. Horne, Ed., Wiley, New York, N.Y., 1972, Chapter 15, pp 613–661.
(6) R. Pottel and O. Lossen, *Ber. Bunsenges. Phys. Chem.*, **71**, 135 (1967).
(7) E. F. Blicke and E. B. Hotelling, *J. Am. Chem. Soc.*, **76**, 5099 (1954).
(8) J. Thomas, *J. Med. Pharm. Chem.*, **3**, 45 (1961).
(9) B. D. Roufogalis and J. Thomas, *J. Pharm. Pharmacol.*, **20**, 153 (1968).
(10) U. Kaatze, *Adv. Mol. Relaxation Processes*, **7**, 71 (1975).
(11) K. S. Cole and R. H. Cole, *J. Chem. Phys.*, **9**, 341 (1941).
(12) K. Giese, U. Kaatze, and R. Pottel, *J. Phys. Chem.*, **74**, 3718 (1970).
(13) F. E. Critchfield, *J. Am. Chem. Soc.*, **75**, 1991 (1953).
(14) G. Akerlof and A. O. Short, *J. Am. Chem. Soc.*, **58**, 1241 (1936).
(15) R. Pottel and U. Kaatze, *Ber. Bunsenges. Phys. Chem.*, **73**, 437 (1969).
(16) R. Pottel, D. Adolph, and U. Kaatze, *Ber. Bunsenges. Phys. Chem.*, 79, 278 (1975).
(17) L. Onsager, private communication.
(18) J. E. Desnoyers and M. Arel, *Can. J. Chem.*, **45**, 359 (1967).
(19) U. Kaatze, *Ber. Bunsenges. Phys. Chem.*, **77**, 447 (1973).
(20) P. S. Ramanathan, C. V. Krishnan, and H. L. Friedman, *J. Solution Chem.*, 1, 237 (1972).

V. P.
28 J
19

Volume Changes of Mixing for the System ~~*p,p'*-Di-*n*-hexyloxyazoxybenzene~~ *p,p*-Di-*n*-heptyloxyazoxybenzene + Xylene

R. A. Orwoll,* R. H. Rhyne, Jr., S. D. Christesen, and S. N. Young

College of William and Mary, Department of Chemistry, Williamsburg, Virginia 23185 *(Received July 8, 1976)*

Publication costs assisted by the Petroleum Research Fund

Volume changes of mixing for an 8.4 mol % solution of *m*-xylene in *p,p'*-di-*n*-heptyloxyazoxybenzene (PHAB) are 0.1–0.3 cm^3 mol^{-1} larger than for an 8.8 mol % solution of *p*-xylene in PHAB over the range of temperatures 75–130 °C. For solutions in the smectic and nematic mesophases the volume changes are positive; the volume change for the isotropic liquid changes from positive to negative with increasing temperature. The temperature ranges for the various phases of the solutions are reported; coexisting smectic and nematic phases and coexisting nematic and isotropic phases were observed.

Introduction

The compound *p,p'*-di-*n*-heptyloxyazoxybenzene (PHAB) is known to exist in both the smectic and nematic

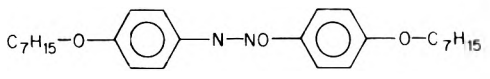

mesophases. The transition temperatures for the pure compound are[1]

crystalline solid $\xrightarrow{74.4\ ^\circ C}$ smectic (C) mesophase
$\xrightarrow{95.3\ ^\circ C}$ nematic mesophase $\xrightarrow{124.2\ ^\circ C}$ isotropic liquid

When a second, nonmesomorphic solute is mixed with this compound, the resulting solution may continue to exist in one or both of these mesophases depending on the concentration.

The molecular shape of the nonmesomorphic component can be important in determining the properties of the mesomorphic system. This was manifest in the studies of Dewar, Schroeder, and Schroeder[2] in which they measured the retention times for the meta and para isomers of xylene on a gas chromatographic column loaded with the hexyloxy analogue of PHAB in its nematic state. Their findings that *p*-xylene had a retention time 4–6% greater than the *m*-xylene were attributed to the linear *p*-xylene being more compatible with the approximately parallel arrangement of the molecules of the nematic solvent.

In this study we have examined the effect of the shape of the nonmesomorphic solute on the volume change of mixing

$$\Delta V_M = \bar{V} - (x_1 \bar{V}_1^0 + x_2 \bar{V}_2^0)$$

where $\bar{V}$ is the molar volume of the solution, $\bar{V}_1^0$ and $\bar{V}_2^0$

TABLE I: Volume Changes of Mixing for *p,p'*-Di-*n*-heptyloxyazoxybenzene with *m*- and *p*-Xylene

		ΔV_M, cm^3 mol^{-1}	
t, °C	Phase	8.4% *m*-xylene	8.8% *p*-xylene
75	Smectic	0.24 ± 0.02	0.15 ± 0.03
80	Smectic	0.30 ± 0.02	0.18 ± 0.03
95	Nematic	0.68 ± 0.02	0.52 ± 0.03
100	Nematic	0.72 ± 0.02	0.51 ± 0.03
105	Nematic	0.83 ± 0.02	0.58 ± 0.03
110	Nematic	1.02 ± 0.02	0.73 ± 0.03
125	Isotropic	0.42 ± 0.02	0.22 ± 0.03
130	Isotropic	0.23 ± 0.02	0.05 ± 0.03
135	Isotropic	0.13 ± 0.02	−0.04 ± 0.03

are the molar volumes of the pure components, and x_1 and x_2 are the mole fractions. Following Dewar et al. we have chosen the meta and para isomers of xylene for the solute. However we used the heptyoxy homologue of the *p,p'*-di-*n*-alkyloxyazoxybenzenes which is both smectogenic and nematogenic, unlike lower members of the series whose only stable mesophase is the nematic.[3]

Experimental Section

Chemicals. The *p,p'*-di-*n*-heptyloxyazoxybenzene (PHAB), obtained from Eastman Organic Chemicals, was recrystallized at least three times from a mixture of isomeric hexanes. The *m*-xylene and *p*-xylene (Eastman Organic Chemicals) were distilled once. The middle fraction used for the experiments appeared free of impurities when analyzed with a gas–liquid chromatograph.

Volume Changes of Mixing. The procedure is similar to one described previously.[4] Known amounts of PHAB and xylene were confined in a thermostated glass cell whose only outlet was the open end of a small-bore capillary. The two components, having been degassed by alternate thawing and freezing, were separated from each other initially by mercury which completely filled the remainder of the cell. The open end of the capillary was immersed in mercury which was contained by a weighing bottle. When the cell was heated, mercury was expelled into the weighing bottle; on cooling, mercury was drawn from the weighing bottle into the cell. With the components separated, the mass of mercury in the weighing bottle was found as a function of temperature by making weighings at intervals usually not exceeding 2 °C. Then the cell was tilted so as to allow the xylene to mix with the PHAB, and the measurements of the mass of mercury vs. temperature were repeated. The volume change of mixing at any temperature was obtained from the difference in the mass of mercury before and after mixing divided by the density of mercury. The observed masses were fitted to a power series equation, cubic in temperature, for the purpose of interpolating with temperature.

Temperatures were measured using a Hewlett-Packard Model 2801A quartz crystal thermometer.

The scatter in the observed mass of mercury as measured from the cubic least-squares line rarely exceeded 0.010 g for the systems reported here, in which the combined volumes of the two components were greater than 10 cm^3. Thus it was possible to measure volume changes as small as 10^{-3} cm^3, i.e., 0.01% of the volume of the system.

Results

For the purpose of comparison, measurements were made on two solutions of PHAB of nearly equal concentrations: 8.4 mol % *m*-xylene and 8.8 mol % *p*-xylene. Volume changes were computed for the range 75–135 °C at 5 °C intervals for temperatures at which the system existed in the same phase both before and after mixing. The molar volume changes ΔV_M are listed in Table I. The ratio of the observed volume changes to the sum V°_{tot} of the volumes of the PHAB[5] and xylene[6] has been plotted as a function of temperature in Figure 1.

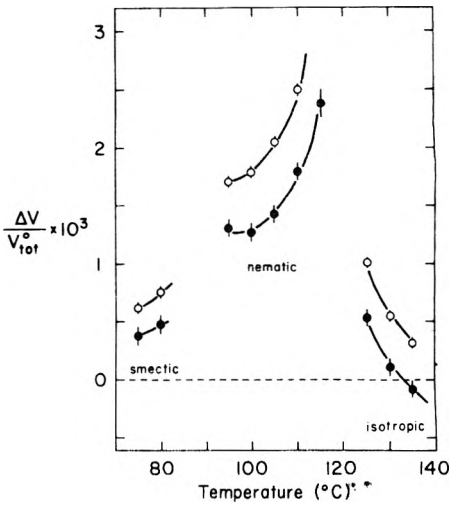

Figure 1. Relative volume changes of mixing for the system *p,p'*-di-*n*-heptyloxyazoxybenzene + xylene. The open circles designate measurements on solutions with 8.4 mol % *m*-xylene; the closed circles, 8.8 mol % *p*-xylene.

TABLE II: Temperature Ranges (°C) for the Phases

Phases present	8.4% *m*-xylene	8.8% *p*-xylene
Crystalline + smectic	<72.9	*a*
Smectic	72.9–82.7	<81.6
Smectic + nematic	82.7–85.6	81.6–86.0
Nematic	85.6–114.6	86.0–115.0
Nematic + isotropic	114.6–115.5	115.0–116.8
Isotropic	>115.5	>116.8

[a] The temperature at which crystalline PHAB disappeared was not observed.

Except at temperatures above ca. 130 °C, the values of ΔV_M were found to be positive. The solution containing the meta isomer exhibited volume changes that were 0.1–0.3 cm^3 mol^{-1} larger than the solution containing *p*-xylene.

These measurements provided an opportunity to observe the range of temperature over which each phase is stable. The observations have been recorded in Table II. Uncertainties in the values are ca. 0.5 °C.

Discussion

For all three phases the para isomer of xylene mixed with a smaller (algebraically) change in volume than the meta even though the concentration of the former slightly exceeded that of the latter. The results for the smectic and nematic systems are consistent with the interpretation[2] that because of its more nearly linear shape *p*-xylene is more compatible with the aligned molecules of the solvent. It is interesting to note that when carbon tetrachloride, toluene, benzene, or cyclohexane is the second component in solution with xylene, the system with the meta isomer exhibits a greater volume change than the corresponding one with the para.[7] However, in these other systems at comparable concentrations, the magnitude of the differences (measured in cm^3 mol^{-1}) is smaller than has been observed here with PHAB.

For both xylenes studied, the increase in volume with mixing was observed to be smaller when the system was in the smectic phase than when it was in the less dense

nematic mesophase. Perhaps the solute molecules are more readily accommodated into the smectic phase because of the possibility that disproportionately more solute mixes in the less dense regions between the layers in the smectic structure.

The volume change of mixing for the isotropic liquid changes from a positive to a negative value with increasing temperature. The temperature at which this occurs decreases with increasing concentration of xylene.[8]

For each binary system two fluid phases coexisted over ranges of temperature: at lower temperatures, the smectic and nematic phases and at higher temperatures, the nematic and isotropic. (See Table II.) Similar two-phase regions were reported many years ago by de Kock[9] on temperature–composition phase diagrams for several binary systems, one component being mesomorphic and the other nonmesomorphic. Although the existence of this two-phase region has been challenged[10] and discussed,[11,12] there can be little doubt that it exists in the PHAB + xylene system. The phase diagrams for these systems are now being determined.

Acknowledgment. Acknowledgment is made to the donors of the Petroleum Research Fund, administered by the American Chemical Society, for support of this research.

References and Notes

(1) H. Arnold, *Z. Phys. Chem. (Leipzig)*, **226**, 146 (1964).
(2) M. J. S. Dewar, J. P. Schroeder, and D. C. Schroeder, *J. Org. Chem.*, **32**, 1692 (1967).
(3) H. Arnold, *Z. Chem.*, **4**, 211 (1964).
(4) B. E. Eichinger and P. J. Flory, *Trans. Faraday Soc.*, **64**, 2035 (1968); P. J. Flory, J. L. Ellenson, and B. E. Eichinger, *Macromolecules*, **1**, 279 (1968).
(5) R. M. Stimpfle, R. A. Orwell, and M. E. Schott, *J. Phys. Chem.*, manuscript in preparation.
(6) "Selected Values of Chemical Thermodynamic Properties", National Bureau of Standards Circular 500, U.S. Government Printing Office, Washington, D.C., 1952.
(7) R. Battino, *Chem. Rev.*, **71**, 1 (1971).
(8) To be submitted for publication.
(9) A. C. de Kock, *Z. Phys. Chem.*, **48**, 129 (1904).
(10) J. S. Dave and M. J. S. Dewar, *J. Chem. Soc.*, 4616 (1954); 4305 (1955).
(11) H. T. Peterson and D. E. Martire, *Mol. Cryst.*, **25**, 89 (1974).
(12) G. W. Gray, "Molecular Structure and the Properties of Liquid Crystals", Academic Press, New York N.Y., 1962.

COMMUNICATIONS TO THE EDITOR

Compressibility of Simple Molten Salts

Sir: Reiss and his co-workers have derived the equation of state of simple fused salts based on their scaled particle theory, describing a hard sphere fluid.[1] Using in their calculations one parameter, namely, the average diameter of the anion and cation, they have obtained satisfactory agreement between the calculated and experimental values of the isothermal compressibility and surface tension of these liquids.[2,3] The theory of hard sphere fluid mixtures has been developed among other by Lebovitz, who solved the PY equation for a mixture of hard spheres of two different sizes.[4] This "compressibility" equation of state is the same as that obtained from the scaled particle theory of hard sphere mixtures[5] and can be written as

$$Z^c = [(1 + \xi + \xi^2) - 3\xi(y_1 + y_2\xi)](1 - \xi)^{-3} \qquad (1)$$

here $Z = PV/NkT$

$$\xi = \xi_1 + \xi_2 \qquad \xi_i = \frac{1}{6}\pi\rho d_i^3 x_i \qquad x_1 + x_2 = 1$$

ρ is the number density, d_i is the hard sphere diameter of the ith component, and x_i is the mole fraction of the ith component.

$$y_1 = \Delta_{12}(d_1 + d_2)(d_1 d_2)^{-1/2}$$

$$y_2 = \Delta_{12}\left[\frac{\xi_1}{\xi}\left(\frac{d_2}{d_1}\right)^{1/2} + \frac{\xi_2}{\xi}\left(\frac{d_1}{d_2}\right)^{1/2}\right]$$

$$\Delta_{12} = [(\xi_1\xi_2)^{1/2}/\xi][(d_1 - d_2)^2/d_1 d_2](x_1 x_2)^{1/2}$$

From eq 1, one can easily calculate β_T, the isothermal compressibility of such a fluid:

$$\beta_T = -[V - \pi N x_1 d_1^3/6 - \pi N x_2 d_2^3/6]^4\{[2V + \pi N x_1 d_1^3/6 + \pi N x_2 d_2^3/6 - 0.5\pi N x_1 x_2 (d_2 - d_1)^2(d_1 + d_2)][V - \pi N x_1 d_1^3/6 - \pi N x_2 d_2^3] - 3[V^2 - \pi N x_1 d_1^3 V/6 + \pi N x_2 d_2^3 V/6 + \pi^2 N^2 x_1^2 d_1^6/36 + \pi^2 N^2 x_1 x_2 d_1^3 d_2^3/18 + \pi^2 N^2 x_2^2 d_2^6/36] - 1.5\pi N x_1 x_2 (d_2 - d_1)^2[(d_1 + d_2)V + \pi N x_1 d_1^3 d_2/6 + \pi N x_2 d_1 d_2^3]\}^{-1}(VNkT)^{-1} \qquad (2)$$

It is interesting to what extent the simple uni-univalent, di-univalent, and tri-univalent molten salts may be considered as a fluid composed of hard spheres of two different sizes. Assuming that the ratios of the diameters of the ions are the same as the ratios of respective crystal radii[6] r_{1P} and r_{2P}

$$d_2/d_1 = r_{2P}/r_{1P} = n \qquad (3)$$

and substituting $x_2 = 1 - x_1 = 1 - x$, eq 2 may be written as

$$Y^4\{[x + (1 - x)n^3]^4\} + Y^3\{-4V[x + (1 - x)n^3]\} + Y^2\{6V^2[x + (1 - x)n^3]^2 - NkT\beta_T[4x^2 - 8x(1 - x)n^3 + 4(1 - x)^2 n^6 - 3x^2(1 - x)(n - 1)^2(n + 1) - 3x(1 - x)^2 n^3(n - 1)^2(n + 1) - 9x^2(1 - x)n(n - 1) - 9x(1 - x)^2 n^3(n - 1)]\} + Y\{-4V^3[x + (1 - x)n^3] - NkTV^2\beta_T[4x + 4(1 - x)n^3 - 6x(1 - x)(n + 1)(n - 1)^2]\} + \{V^4 - V^3 NkT\beta_T\} = 0 \qquad (4)$$

here $Y = \pi N d_1^3/6$. For each particular salt, one can

TABLE I: Values of the Anion and Cation Radii Computed from the Isothermal Compressibility of Simple Molten Salts

Molten salt	$10^{11}\beta_T$, $m^2\ N^{-1}$	V, cm^3	Mixture of hard spheres: Cation radius, Å	Mixture of hard spheres: Anion radius, Å Cl^-	Mixture of hard spheres: Anion radius, Å Br^-	Mixture of hard spheres: Anion radius, Å I^-	One-parameter scaled particle theory: Cation radius, Å	One-parameter scaled particle theory: Anion radius, Å Cl^-	One-parameter scaled particle theory: Anion radius, Å Br^-	One-parameter scaled particle theory: Anion radius, Å I^-
LiCl	19.4[b]	28.22[g]	0.50	1.52			0.59	1.77		
LiBr	21.3[b]	34.34[g]	0.51		1.67		0.60		1.97	
NaCl	28.7[b]	37.54[g]	0.80	1.52			0.85	1.62		
NaBr	31.6[b]	43.99[g]	0.80		1.65		0.87		1.78	
NaI	37.8[b]	54.70[g]	0.81			1.83	0.88			2.00
KCl	36.2[b]	48.80[g]	1.14	1.55			1.15	1.57		
KBr	39.8[b]	55.97[g]	1.14		1.67		1.17		1.71	
KI	46.7[b]	67.93[g]	1.14			1.86	1.19			1.93
CsCl	38.0[b]	60.31[g]	1.47	1.58			1.47	1.58		
CsBr	49.1[b]	67.93[g]	1.44		1.67		1.45		1.67	
$CaCl_2$	13.5[c]	53.35[g]	0.83	1.51			0.95	1.73		
$CaBr_2$	16.2[c]	64.14[g]	0.83		1.63		0.96		1.90	
CaI_2	19.9[c]	81.72[g]	0.83			1.82	1.00			2.18
$SrCl_2$	12.7[c]	58.16[g]	0.96	1.54			1.07	1.71		
$SrBr_2$	12.8[c]	66.74[g]	0.98		1.69		1.11		1.91	
SrI_2	16.6[c]	83.16[g]	0.97			1.86	1.13			2.15
$BaCl_2$	14.7[d]	65.61[g]	1.15	1.54			1.22	1.64		
$BaBr_2$	19.0[c]	74.34[g]	1.12		1.62		1.21		1.75	
BaI_2	19.1[c]	92.42[g]	1.15			1.84	1.27			2.03
$ZnCl_2$	41.2[c]	53.70[g]	0.60	1.46			0.73	1.80		
$ZnBr_2$	49.8[c]	64.83[g]	0.58		1.52		0.72		1.90	
ZnI_2	57.4[c]	82.30[g]	0.57			1.66	0.73			2.12
$HgCl_2$	47.2[c]	62.20[g]	0.91	1.50			1.00	1.65		
$PbCl_2$[a]	17.9[d]	57.90[g]	1.01	1.51			1.10	1.65		
$PbBr_2$[a]	21.8[d]	68.61[g]	1.00		1.64		1.11		1.79	
$CdCl_2$	26.8[e]	54.10[g]	0.77	1.44			0.89	1.65		
$CdBr_2$	40.4[e]	66.81[g]	0.75		1.51		0.88		1.77	
CdI_2	43.1[e]	83.31[g]	0.78			1.73	0.93			2.08
$BiCl_3$	38.5[f]	80.72[h]	0.79	1.50			0.95	1.79		
$BiBr_3$	36.7[f]	94.97[h]	0.80		1.63		0.98		1.99	
BiI_3	57.6[f]	126.76[h]	0.76			1.70	0.94			2.13
			Mean values	1.51 ± 0.04	1.63 ± 0.06	1.79 ± 0.08		1.68 ± 0.08	1.83 ± 0.11	2.08 ± 0.09
			Crystal radii	1.81	1.95	2.16		1.81	1.95	2.16

[a] Computed at 873 K. [b] Reference 7. [c] Reference 8. [d] Reference 9. [e] Reference 12. [f] Reference 13. [g] Reference 10. [h] Reference 11.

calculate the diameters of the anion and cation, as the hard spheres, from eq 3 and 4, substituting the experimental values of the isothermal compressibility and molar volume, and replacing values of the molar fraction by the respective values of the ionic fraction of the particular ion in the molten salt ($x = x_1 = x_2 = 0.5$ for the uni-univalent salts, $x = x_1 = x_2/2 = 0.333$ for the di-univalent salts, and $x = x_1 = x_2/3 = 0.25$ for the tri-univalent salts). The calculated values for 31 salts close to their melting points are given in Table I. The radii of the cations are satisfactorily constant in compounds with the three halides, as well as the radii of the anions in compounds with the univalent, divalent, and trivalent metals.

In molten salts the contact between ions of unlike charge predominates. This fact is emphasized in the calculations of Reiss and co-workers. In Table I a comparison between the results obtained from both uncritical application of scaled particle theory for a mixture of hard spheres and the theory of Reiss and co-workers is made (for the Latter's theory the collision parameter of the anion and cation was calculated; next the radius of the anion and the cation were computed via eq 3, respectively). It is surprising that the "stability" of the respective parameters obtained for mixture of hard spheres is better than this for a one-parameter scaled particle theory (standard deviation of chloride, bromide, and iodide radii are less for mixtures of hard spheres). It provocates a conclusion about underestimating the role of collisions between ions of the same charge (especially when the difference of the size of ions in the salt is considerable, e.g., lithium salts or in case of polyvalent salts).

References and Notes

(1) H. Reiss, H. L. Frisch, and J. L. Lebowitz, *J. Chem. Phys.*, **31**, 369 (1959).
(2) F. H. Stillinger, *J. Chem. Phys.*, **35**, 1581 (1961).
(3) H. Reiss and S. W. Mayer, *J. Chem. Phys.*, **34**, 2001 (1961).
(4) J. L. Lebowitz, *Phys. Rev. A*, **133**, 895 (1964).
(5) H. L. Frish and J. L. Lebowitz, "The Equilibrium Theory of Classical Fluids", W. A. Benjamin, New York, N.Y., 1964.
(6) R. C. Evans, "An Introduction to Crystal Chemistry", Cambridge University Press, Cambridge, 1964.
(7) J. O'M. Bockris and N. E. Richards, *Proc. R. Soc. London, Ser. A*, **241**, 44 (1957).
(8) J. O'M. Bockris, A. Pilla, and J. L. Barton, *Rev. Chim. Acad. Repub. Pop. Roum.*, **2**, 59 (1962).
(9) S. Sternberg and V. Vasilescu, *J. Chem. Thermodyn.*, **3**, 877 (1971).
(10) G. J. Janz, F. W. Dampier, G. R. Lakshminarayanam, P. K. Lorenz, and R. P. T. Tomkins, *Natl. Stand. Ref. Data Ser., Natl. Bur. Stand.*, **No. 15** (1968).
(11) F. J. Keneshea and D. Cubicciotti, *J. Phys. Chem.*, **63**, 1472 (1959).
(12) J. Galka, L. Suski, P. Tomczyk, and V. Vasiescu, *J. Chem. Thermodyn.*, in press.
(13) J. Galka, L. Suski, P. Tomczyk, and V. Vasiescu, *J. Chem. Thermodyn.*, in press.

Institute of Physical Chemistry
Polish Academy of Sciences
Molten Salts Laboratory
al. Mickiewicza 30,
30-059 Krakow, Poland

Piotr Tomczyk

Received December 22, 1975; Revised Manuscript Received September 1, 1976

Periodic Carbon Monoxide Evolution in an Oscillating Reaction

Sir: Cerium ion catalyzed oscillatory oxidation of malonic acid by bromate has been investigated by several authors.[1-5] Degn[2] has shown that there is a periodic carbon dioxide evolution during the oscillating reaction. Bornmann et al.[3] recorded the mass spectrum of the gas evolved and found it to be a typical CO_2 spectrum. This communication deals with a new method of analyzing gases evolved and, besides CO_2, we could measure a periodic evolution of carbon monoxide also. The CO gas exerts an inhibition effect.

A 1-cm^3 reaction mixture (initial reactant concentrations: malonic acid = 0.15 M, $KBrO_3 = 3.5 \times 10^{-2}$ M, $Ce(SO_4)_2 = 2 \times 10^{-3}$ M, H_2SO_4 = 3 M) was placed into a small vessel and 24 cm^3/min of hydrogen was allowed to bubble through it. A small reactor containing a nickel catalyst served for the methanization of CO_2 and CO stripped with H_2 from the reaction mixture. The methane concentration was measured by a flame-ionization detector (FID). Before the nickel reactor a selective CO_2 scrubber (soda lime) could be inserted into the gas stream or it could by-passed as well. The ionization current was measured with a Keithley-610B electrometer. The sensitivity of the FID was 50 mC/mol of carbon. According to the ionization current vs. time diagram (Figure 1) the evolving gas contains about 7% CO as an average. To check the evolution of CO in an other way CO_2 was bubbled through the oscillating mixture and the gas was collected in a gas buret containing a KOH solution. The collected gas was tested with $PdCl_2$ paper and it was found to be CO.

We have examined the effect of several gases on oscillating reactions using a bromide selective electrode. We have confirmed that N_2, H_2, and CO_2 bubbling through the reaction mixture do not disturb the oscillation, however, O_2 and especially CO have a strong inhibiting effect. The inhibition can be observed after only the first 10–12 oscillations but after 100–120 oscillations the CO completely inhibits the reaction (Figure 2). The initial reactant concentrations were the same as before.

It is known that the oscillating reaction is sensitive to stirring.[4] That fact can be explained partly by the CO evolution and its effect on the reaction and partly by the effect of atmospheric O_2.

It is interesting to note that the known inhibitors CO, O_2, Cl^-, I^-, and azide[5] can all be involved in complex-forming reactions. According to our latest investigations F^- also inhibits the oscillation.

Acknowledgment. The author is thankful to professor Dr. E. Körös and to Mr. M. Gál for the helpful discussions and to a group of students led by Mr. J. Bodiss for their assistance in the experiments.

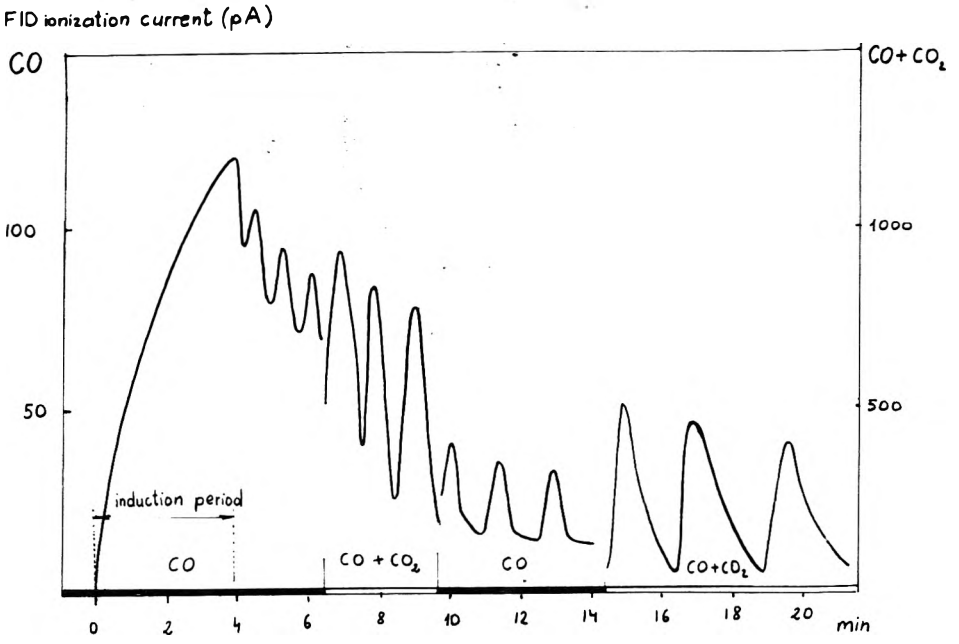

Figure 1. Periodic CO and CO + CO_2 evolution measured by FID. During the black intervals the CO_2 scrubber was inserted into the gas stream.

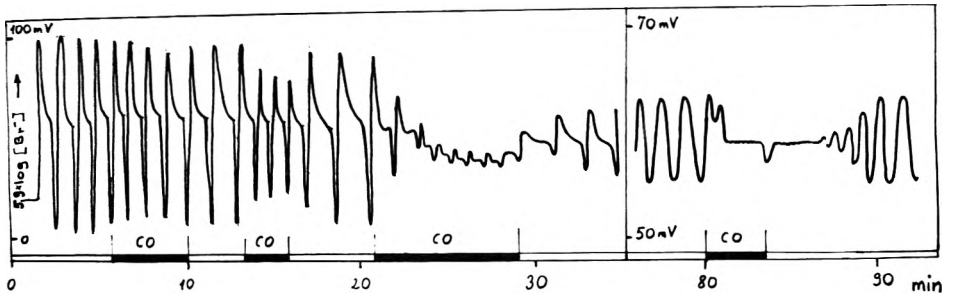

Figure 2. Potentiometric trace of the log [Br^-] oscillations (without absolute calibration) and the inhibition effect of CO. During the black intervals CO was bubbling through the reaction mixture.

References and Notes

(1) R. Field, E. Kóros, and R. Noyes, *J. Am. Chem. Soc.*, **94**, 8649 (1972).
(2) H. Degn, *Nature (London)*, **213**, 589 (1967).
(3) L. Bornmann et al., *Z. Naturforsch.*, **286**, 824 (1973).
(4) G. Kasperek and T. Bruice, *Inorg. Chem.*, **10**, 382 (1971).
(5) S. Jacobs and I. Epstein, *J. Am. Chem. Soc.*, **98**, 1721 (1976).

Institute of Physics
Department of Chemical Engineering
Technical University of Budapest
1521 Budapest, Hungary

Zoltan Noszticzius

Received June 21, 1976

Hydration Structures For Halide (−) Ions

Sir: We report the calculated hydration energies of halide (−) ions for the symmetrical hydration structures containing 1–6 waters of hydration. The method is identical with the semiempirically based electrostatic method previously used for alkali (+) ions.[1] Empirically based repulsive parameters were previously selected from alkali halide diatomic spectra and ion–rare gas beam scattering data.[2,3] These parameters have been applied to halide (−) ion hydration for the symmetrical structures including a linear dimer, a planar symmetrical trimer and tetrahedron, trigonal bipyramid, and an octahedron. The equations necessary to compute the negative ion hydration structures were included in the extensive description of the alkali (+) hydration calculations.[1] The results are given in Table I with comparisons to the experimental ΔH values of Kebarle et al.[4]

The agreement of our values with experiment has substantial deviations as the size of the hydration sphere increases. This is particularly noticeable for the F^- ion with 1–4 ligands. This disagreement shows a fundamental flaw in our previous construction of an empirical potential for negative ions and a single water molecule. As previously stated,[1] uniformly excellent experimental agreement of the alkali (+) hydration energies shows a reasonably correct radical dependence empirical potential for positive ions. The source of the halide ion difficulty is easily seen by comparison to recent SCF results for the equilibrium distance of $F^-{\cdot}H_2O$.[5,6] An SCF calculation gives the F^-–H_2O center of mass distance of 2.44 Å[6] compared to our 2.14 Å. Additional comparison to the simple algebraic form of the SCF potential[7] suggests that our interaction energy terms for halide ions would be much better represented by having the attractive ion dipole terms based closer to the H atoms rather than at the H_2O center of mass. For alkali ions the center of mass terms are similar to those implied in the SCF algebraic representation.

In summary we can conclude that the original selection of repulsive parameters[2,3] should have been based on a slightly different form of the attraction between halide ions and H_2O. This more attractive potential expression would have resulted in larger repulsive energy parameters for the H atoms of H_2O thereby yielding a larger equilibrium separation in the calculations of Table I. The availability of SCF results allows a more accurate choice of the attractive part of the halide ion–H_2O potential in the future. The use of the electrostatic method[1-3] allows an accurate representation of interaction effects in complicated clusters. As shown in ref 1, remarkable agreement with SCF results is obtained for the case of Li^+. Indeed, more recent SCF results for clusters with Li^+ and Na^+ that only contain pairwise additive terms[8] do not agree as well with experiment as the electrostatic method.[1] Large basis set SCF computations are necessary for these ions[8] to agree with experiment.

TABLE I: Energies and Distances for Symmetric Halide Ion Hydration[a]

	Hydration no. 1		2		3		4		5		6	
Ion	$-E$	R	$-E$	R	$-E$	R	$-E$	R	$-E$	R	$-E$	R
F^-	24.1 (23.3)	2.14	44.8 (39.9)	2.22	60.2 (53.6)	2.32	72.7 (67.1)	2.40	81.0 (80.3)	2.48	86.0 (−)	2.62
Cl^-	14.3 (13.1)	2.86	27.6 (25.8)	2.88	40.1 (37.5)	2.92	49.1 (48.6)	2.96	57.1 (−)	3.02	63.9 (−)	3.08
Br^-	12.6 (12.6)	3.04	24.4 (24.9)	3.08	34.8 (36.4)	3.12	43.9 (47.3)	3.16	51.4 (−)	3.20	58.0 (−)	3.24
I^-	10.5 (10.2)	3.34	20.5 (20.0)	3.36	29.4 (29.4)	3.38	37.4 (−)	3.42	44.2 (−)	3.46	50.2 (−)	3.50

[a] Energies are in kcal/mol and the equilibrium distance in angstroms is from the ion to the H_2O center of mass. The energy value enclosed in parentheses is experimental ΔH from ref 4.

Acknowledgment. Sang Hyung Kim deserves thanks for his assistance in calculating the results for halide ion binding. The author has benefited by being awarded an Alfred P. Sloan Fellowship during 1974–1976.

References and Notes

(1) K. G. Spears and S. H. Kim, *J. Phys. Chem.*, **80**, 673 (1976).
(2) K. G. Spears, *J. Chem. Phys.*, **57**, 1842 (1972).
(3) K. G. Spears, *J. Chem. Phys.*, **57**, 1850 (1972).
(4) M. Arshadi, R. Yamdagni, and P. Kebarle, *J. Phys. Chem.*, **74**, 1475 (1970).
(5) G. H. F. Diercksen and W. P. Kraemer, *Chem. Phys. Lett.*, **5**, 570 (1970).
(6) H. Kistenmacher, H. Popkie, and E. Clementi, *J. Chem. Phys.*, **58**, 5627 (1973).
(7) H. Kistenmacher, H. Popkie, and E. Clementi, *J. Chem. Phys.*, **59**, 5842 (1973).
(8) H. Kistenmacher, H. Popkie, and E. Clementi, *J. Chem. Phys.*, **61**, 799 (1974).

Department of Chemistry
Northwestern University
Evanston, Illinois 60201

Kenneth G. Spears

Received August 23, 1976

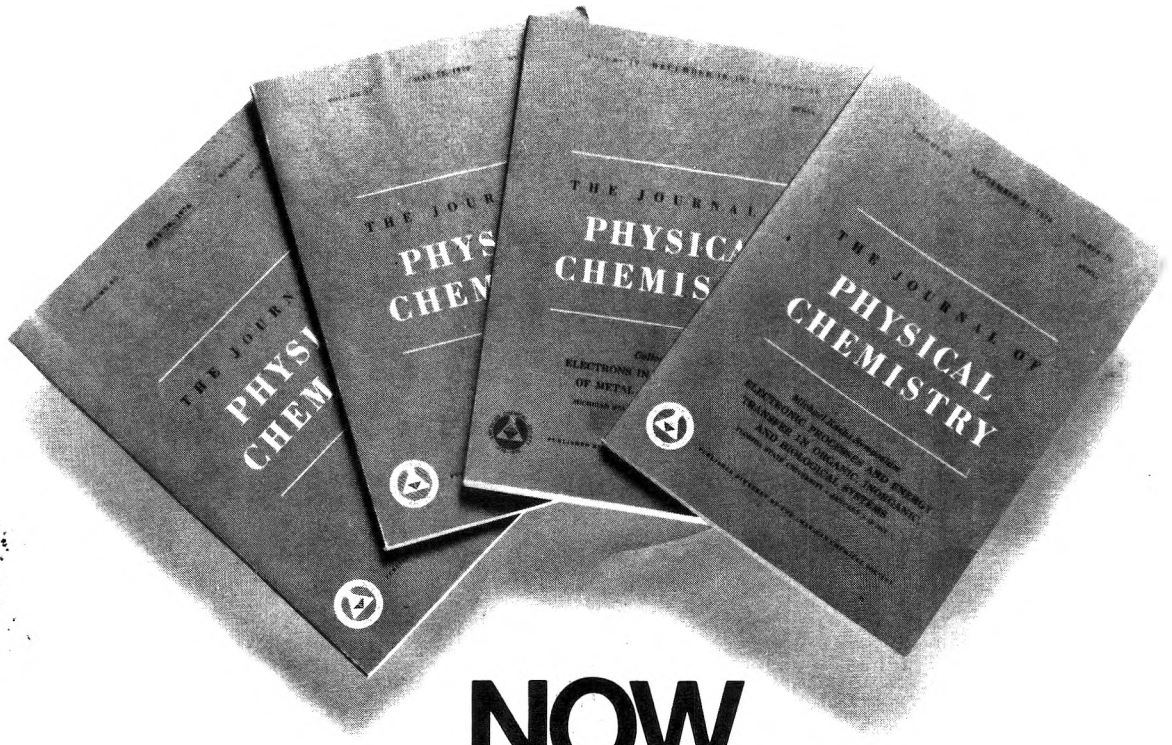

NOW you can buy all four special issues of The Journal of Physical Chemistry

and *save money on three of them.*

By buying the December 16, 1976 J. L. Franklin issue for the regular price of $4.75, you can get the **three other special issues for only $10.00!**

The Franklin issue consists of a collection of papers in theoretical and applied research, especially thermodynamics and energetics.

The other issues are:

- **Colloque Weyl IV.**
  Electrons in Fluids—The Nature of Metal-Ammonia Solutions
- **Michael Kasha**
  Symposium—Electronic Processes and Energy Transfer in Organic, Inorganic, and Biological Systems
- **Richard C. Lord**
  Issue consists of contributions from colleagues, former students, and associates of Dr. Lord. Papers are on spectroscopy and related subjects

You can order just one or two of the issues instead of all three. In that case, the price is $4.00 per issue. But please remember, it is necessary to buy the Franklin issue at the regular price before you can take advantage of the lower price.

Just fill out the form and mail it back to us today. We'll see that you receive the issue or issues of your choice just as soon as we can process your order.

MAIL WITH REMITTANCE TO:

Business Operations
American Chemical Society
1155 16th Street, N.W.
Washington, D.C. 20036

Please send me the following JOURNAL OF PHYSICAL CHEMISTRY SPECIAL ISSUES:

J. L. Franklin issue	☐ $4.75
Colloque Weyl IV. Issue	☐ $4.00*
Michael Kasha Symposium	☐ $4.00*
Richard C. Lord Issue	☐ $4.00*

*All three ☐ $10.00

I am enclosing _____.

☐ Check ☐ Money Order

Please print clearly.

NAME _____

ADDRESS _____

CITY _____

STATE/
COUNTRY _____ ZIP _____

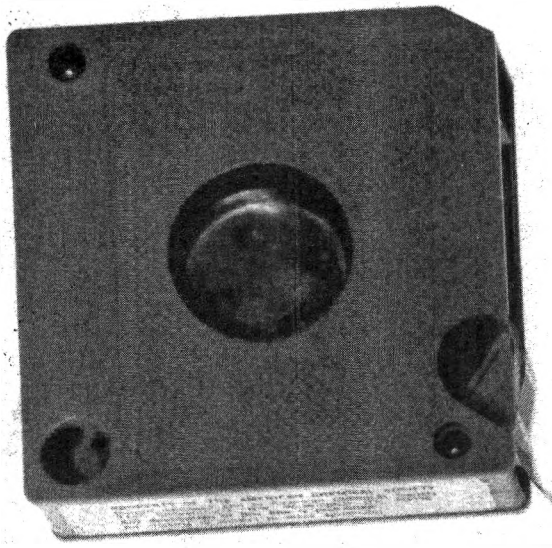

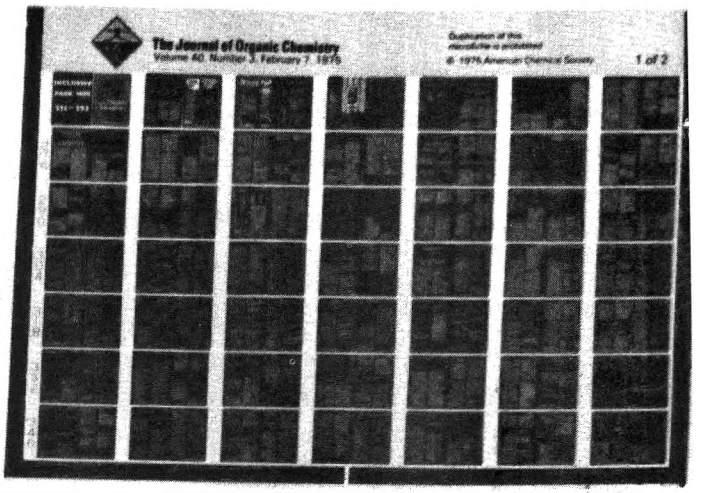

MICROFORMS

American Chemical Society publications in microform

MICROFILM OR MICROFICHE?

With the ACS microform program you can receive either, or both

Microfilm

All periodical publications back to volume one

Copying privileges included with current subscriptions

All non-print supplementary materials provided free on microfiche

Archival quality silver halide film supplied as you request; positive or negative; 16 or 35mm; cartridge, reel, or cassette.

Microfiche

Current issues of primary journals, beginning with January 1975

Individual issues or full volumes available

Supplementary materials also available on microfiche

Fiche supplied are archival quality silver halide, negative, 105 x 148mm (4" x 6"); 24x, with eye legible headers, start and end targets, and page numbers

For information about our microfilm/microfiche write:

Microform Program
Special Issues Sales
American Chemical Society
1155 16th Street, N.W.
Washington, D.C. 20036
(202) 872-4363